UNIVERSIDAD EAFIT

Engineering School
Design Engineering Research Group (GRID)

Solar beam radiation modeling for design and simulation of V-Trough photovoltaic applications

Graduation manuscript presented as partial requirement to obtain the
Master of Science in Engineering

(Draft Document: Version 22/08/2017)

AUTHOR:

Ing. Andrés Arias-Rosales

ADVISOR:

Ricardo Mejía-Gutiérrez, PhD.

July 2017

Abstract

Photovoltaic V-Troughs use simple and low-cost non-imaging optics, namely flat mirrors, to increase the solar harvesting area by concentrating the solar rays towards the photovoltaic surface. Combined with stepped manual tracking, these devices can boost the performance of regular solar cells for residential and personalized scenarios in developing countries. The geometrical set-up of a V-Trough, related to its length and angular parameters, conditions the optical phenomena that occur as the solar beam radiation dynamically interacts with the surfaces of the device. These phenomena, such as shadows and consecutive reflections, determine the solar radiation that is effectively concentrated towards the photovoltaic area. To support the design and simulation of such devices, this research project proposes a theoretical model of their effective concentration, seeking a high flexibility in the geometrical inputs, a detailed output of the optical phenomena involved and a low computational demand. The model is based on the geometrical optics of beam solar radiation and it was experimentally validated in a statistical comparison against experimental measurements performed in a laser testing platform. Based on the model, several design performance indicators were established: i) $\overline{C_e}$ (the average effective concentration); ii) $Cost$ (the cost of materials); iii) T_{sp} (the space required). Moreover, from the integration of these indicators in proportional comparisons, three multi-objective indices were proposed: a) I_{COE} ($\overline{C_e}$ versus $Cost$); b) MI_{COE} ($\overline{C_e}$ versus $Cost$ and $\overline{C_e}$ versus T_{sp} combined); c) MDI_{COE} (the same comparison as the previous one but also including the discretization effects related to the solar cells). As tools for supporting the V-Trough set-up definition process, an interactive software and a series of genetic algorithms were developed based on these indicators and indices and the modeling framework developed. The proposed software, named "VTDesign", allows a V-Trough designer to iterate and compare diverse design alternatives in real-time by means of a visualization of the optical performance, representations of the geometrical set-ups and a cost-effectiveness analysis. Among the genetic algorithms studied, a new genetic algorithm, named "GA-WA" (Genetic Algorithm - Weibull Arias), was proposed. This tool uses heuristic processes, based on biomimicry and Weibull probability distributions, in order to optimize the indicators and indices as fitness/objective functions. The intuition and the more holistic exploration of a trained engineer with VTDesign can be complemented with the broader and less biased evolutionary optimization of GA-WA. In a design case study, both VTDesign and GA-WA were implemented and found to be effective in the indices improvement, as well as efficient and flexible tools in the problem of defining the set-up of a solar V-Trough in a given personalized scenario.

Keywords: Solar Concentration, V-Trough, Manual Tracking, Modeling & Simulation, Geometrical Optics, Interactive Software, Genetic Algorithms

Acknowledgements

I would like to thank all the people who contributed, directly or indirectly, to the work of this research project and my graduate studies. I would like to express my gratitude to my advisor Ricardo Mejía–Gutiérrez for the useful comments, the support throughout my research trajectory and the freedom granted to pursue my scientific views and interests within this master's project. Also to my advisor in wind energy projects, Gilberto Osorio-Gómez, who gave me the time I needed to accomplish this research project and encouraged me in my graduate endeavors. Special thanks to Thomas Motmans and Santiago Bernal Del Río, who assisted me in experimental ventures related to my research on solar V-Troughs.

I am grateful for the funding sources that allowed me to pursue my graduate studies and research projects: to Universidad EAFIT for the postgraduate studies grant "Undergraduate research excellence scholarship". Also, special thanks to Colciencias (Colombian Administrative Department of Science, Technology and Innovation) and, again, Universidad EAFIT, who jointly sponsored the "Young Researchers and Innovators Program" in the 645-2014 and 761-2016 calls. I am also grateful to the Medellín's major and Sapiencia (Superior Education Agency) for the "Award to Outstanding Undergraduate Students for their Research Engagement", which encouraged me to pursue a research career.

Good research does not happen in isolation but in a healthy research community. Accordingly, I am deeply grateful to the Design Engineering Research Group (GRID). The casual debates, the insightful feedback, and the funny distractions all enriched my graduate experience. Special thanks to the colleagues who shared their research projects with me and who trusted me enough to ask for advice. These were some of the most intellectually stimulating challenges. Moreover, thanks to all the *"Primavera"* team and all the people who made that project possible. In a country fueled by violence, Primavera was a flag of hope. The feeling of being part of something much bigger than me inspired me to choose renewable energies as the fabric of my days. In particular, special thanks to Jorge Barrera, who encouraged me to think big and to be crazy enough to believe that I can actually change the world for better.

A graduate program such as this one is highly time intensive and thus involves considerable personal sacrifices. I am grateful to the friends and family who supported me along the way at a personal level. To Laura, whose love has empowered me to face my struggles as a team effort. Thank you for patiently listening to my unnecessarily complex philosophical daily dilemmas. To my grandfather, "Vito", who cultivated my love for engineering by teaching me how to assemble and fix all kinds of devices as a kid. To my mother, who has supported all my life decisions and made sure that everyone in the family is safe and pursues a purposeful life. You have always cultivated the creativity in me, which is nowadays my secret weapon for facing research endeavors from a different perspective. Lastly, I would like to dedicate this research project to the memory of my father, who raised me as a little scientist and made me fall in love with the quest for knowledge and a fascination for how the world works. I wish you could have known the scientist I am becoming. Perhaps in some other reality, we will discover something together.

Contents

1 Introduction **1**
- 1.1 Background . . . 1
- 1.2 Research Problem Definition . . . 7
- 1.3 Research Questions . . . 10
  - 1.3.1 General Research Question . . . 10
  - 1.3.2 Specific Research Questions . . . 11
- 1.4 Research Objectives . . . 11
  - 1.4.1 General Research Objective . . . 11
  - 1.4.2 Specific Research Objectives . . . 11
  - 1.4.3 Operationalization of the Research Objectives . . . 12
- 1.5 Research Scope . . . 12
- 1.6 Research Justification . . . 13
- 1.7 Methodological Framework . . . 13
- 1.8 Manuscript Organization . . . 15

2 State of the Art **16**
- 2.1 Beam Radiation Modeling in V-Trough Devices . . . 16
- 2.2 Interactive Tools for V-Trough Design and Engineering . . . 21
- 2.3 Optimization Methods for V-Trough Devices . . . 22

3 Proposal of a Beam Radiation Model for V-Trough devices **25**
- 3.1 Definition of the Conceptual Model . . . 26
- 3.2 Mathematical Construction of the Model . . . 35
- 3.3 Use and Interpretation of the Model . . . 41

4 Model Validation **44**
- 4.1 Experimental Design . . . 44
- 4.2 Development of the Testing Platform . . . 47
- 4.3 Results and Statistical Analysis . . . 49

5 Parameters Definition in the Design Context **55**
- 5.1 Performance Indicators and Indices in Design . . . 55
- 5.2 Interactive Tool: VTDesign Software . . . 59
  - 5.2.1 Conceptual Structure in The Design Framework . . . 59
  - 5.2.2 Interface and Usability . . . 61
- 5.3 Heuristic Optimization Tool: GA-WA Genetic Algorithm . . . 66
  - 5.3.1 Heuristics Based on the Weibull Probability Distribution . . . 67
  - 5.3.2 Proposed Scheme for GA-WA . . . 72
  - 5.3.3 Optimization of the Genetic Parameters . . . 74

6 Case Study **78**
6.1 Design Brief 78
6.2 Design Goal I: Cost 80
6.3 Design Goal II: Energy 84
6.4 Design Goal III: Space 88

7 General Analysis and Conclusions **93**
7.1 Conclusions 93
7.2 Scientific and Technological Contributions 96
7.3 Scientific Publications 96
7.4 Further Work 97

References **101**

List of Figures

1.1 (a) Sun-Earth radiation interactions. (b) Solar rays reach the Earth parallel to each other. (c) Solar elevation α. 2
1.2 Sun's apparent path and solar elevation (α). 3
1.3 Variation of the effective harvesting area of a solar panel without tracking in (a), (b) and (c); and with tracking in (d), (e) and (f). 4
1.4 Solar concentration methods. (a) Fresnel lens, (b) parabolic reflector, (c) compound parabolic reflector, (d) light-guide panel, (e) luminescent panel, and (f) V-Trough reflector. 5
1.5 Solar beam and diffuse radiation. 6
1.6 V-Trough photovoltaic devices for commercial or research use. 1.6(a) from Bahaidarah et al. (2015); 1.6(b) from Sangani and Solanki (2007); and 1.6(c)– 1.6(f) from Hermenean et al. (2009). 6
1.7 Convergence of the research context. 7
1.8 (a) Global cumulative PV installation (Fraunhofer Institute for Solar Energy Systems, ISE, 2016). (b) Global cumulative PV installation by Region in 2015 (Fraunhofer Institute for Solar Energy Systems, ISE, 2016). 7
1.9 Geometrical parameters of a V-Trough photovoltaic device. 8
1.10 An illustration of different contexts, V-Trough set-ups and tracking timings. 9
1.11 Placing research in the design context. Adapted from Imre (2007). 14
1.12 Research methodological framework. 14

3.1 Earth's tilted axis and Sun-Earth radiation interactions. 26
3.2 Solar incidence at noon affected by latitude (Φ) and declination (δ). 27
3.3 Solar paths from the perspective of a PV V-Trough located at $\phi = 23.4°$. 28
3.4 Solar incidence during summer solstice and winter solstice visualized with the analogy of symmetric cones. 29
3.5 V-Trough adjusted to counteract latitude (ϕ) and declination (δ). 29
3.6 Solar ray paths in a V-Trough and main geometrical parameters. 30
3.7 Variables describing a broad range of macro-optical phenomena in solar V-Troughs. 31
3.8 Diagram of the conceptual model. 32
3.9 Geometrical flexibility of the input parameters. 34
3.10 Illustration of variables p_L and p_R. 37
3.11 Boundary cases to consider when defining aL_{PV}. 37
3.12 Example of cases where a portion of the rays reach the PV surface after two consecutive reflections (shadowed areas). 39
3.13 Boundary cases to consider when defining aL_{RPV}. 40
3.14 Optical aperture lengths of a V-Trough and an equivalent flat panel at $\alpha = 70°$. 41
3.15 Optical aperture lengths of a V-Trough and an equivalent flat panel at $\alpha = 85°$. 42
3.16 Optical aperture lengths of a V-Trough and an equivalent flat panel at $\alpha = 120°$. 43

4.1 Visualization of the deliberately designed V-Trough set-ups for the experimental validation. . 46
4.2 Visualization of the randomly defined V-Trough set-ups for the experimental validation. . . . 47

4.3 Design of the testing platform for the experimental validation of the model. 48
4.4 Details of the real testing platform for the validation of the model. 49
4.5 Regression analysis and linear model. 50
4.6 Analysis of the regression residuals. 51
4.7 Monte Carlo test of hypothesis for the significance of the regression. 52
4.8 Bootstrapping 95% confidence intervals for (a), the slope, and (b), the Y- intercept. 52
4.9 Percentage error between predicted and measured incident (C) and effective (C_e) optical concentration. 53
4.10 Percentage error between predicted and measured incident (C) and effective (C_e) optical concentration, in function of the Measurements. 54

5.1 Diagram of a V-Trough photovoltaic device shown in two different geometrical set-ups in (a) and (b). 56
5.2 Conceptual structure where the proposed software is contextualized. 60
5.3 Conceptual scheme of the modules and sub-modules. 60
5.4 Overall distribution of the Information module. This figure is not intended for a detailed inspection of each element, but for an overview. 61
5.5 Overall distribution of the Dashboard module. This figure is not intended for a detailed inspection of each element, but for an overview. 62
5.6 Visualization curves in the Dashboard module of VTDesign. 63
5.7 Visualization of the V-Trough geometries and tracking movements in the Dashboard module of VTDesign. 64
5.8 Visualization of (a) the potential reduction in PV area, and of (b) the linear space required for the device. 64
5.9 (a) Screen-shot of the Free Input module; (c) Screen-shot of the Output Data module; and (b) illustration of informative pop-ups in the Dashboard. 65
5.10 Overall distribution of the CAD Integration module. This figure is not intended for a detailed inspection of each element, but for an overview. 65
5.11 Preliminary CAD model of a given V-Trough set-up for four solar elevations. 66
5.12 Weibull Distribution controlled by the mean (μ). (a) k values calculated for a range of $p\mu$. (b) The corresponding Weibull PDF curves adjusted for a range from 0 to $Top = 50$. 68
5.13 Weibull-distributed mutation values compared to a uniform and Gaussian distribution. 69
5.14 Weibull-distributed values for the initial population of a gene; compared to uniform and Gaussian distributions. 71
5.15 (a) Main scheme of the proposed genetic algorithm GA-WA. n is any positive integer greater than 0. (a) Scheme of a standard genetic algorithm. 73
5.16 Performance of the GA parameter combinations for (a) GAUniform, (b) GAGauss and (c) GA-WA. The combinations with the highest performance are highlighted with circles. 75
5.17 Worst and best parameter combinations for (a) GAUniform, (b) GAGauss and (c) GA-WA. . 76
5.18 Performance Box plots in function of the GA parameters for (a) GAUniform and GAGauss; and for (b) GA-WA. 77
5.19 Performance of the optimized parameter combinations for GAUniform, GAGauss and GA-WA. (a) Box plot. (b) Close-up of the evolution through the generations. 77

6.1 Real photos of the location in *Chaparral*, Colombia, for the case study. (c) presents a map of the location and the average levels of radiation; modified from Ministerio de Ambiente, Vivienda y Desarrollo Territorial, Ministerio de Minas y Energía (2005). 79
6.2 Results of the *Design Goal I* in terms of *Cost*. 81
6.3 Dynamic geometry representations of (a) $VT1_i$, (b) $VT1_{VTDb}$ and (c) $VT1_{icost}$. 82
6.4 PV area reduction of (a) $VT1_i$, (b) $VT1_{VTDb}$ and (c) $VT1_{icost}$. 82
6.5 Optical performance curves of the set-ups (a)–(b) $VT1_i$, (c)–(d) $VT1_{VTDb}$ and (e)–(f) $VT1_{icost}$. 83
6.6 (a) Preliminary CAD model and (b) realistic rendering of the fittest set-up achieved for Goal I ($VT1_{icost}$). 84

6.7 Results of the *Design Goal II* in terms of Energy. 85
6.8 Dynamic geometry representations of (a) $VT2_i$, (b) $VT2_{VTD}$ and (c) $VT2_{ce}$. 86
6.9 PV area reduction of (a) $VT2_i$, (b) $VT2_{VTD}$ and (c) $VT2_{ce}$. 86
6.10 Optical performance curves of the set-ups (a)–(b) $VT2_i$, (c)–(d) $VT2_{VTD}$ and (e)–(f) $VT2_{ce}$. 87
6.11 (a) Preliminary CAD model and (b) realistic rendering of the fittest set-up achieved for Goal II ($VT2_{VTD}$). 88
6.12 Results of the *Design Goal III* in terms of Space required. 89
6.13 Dynamic geometry representations of (a) $VT3_i$, (b) $VT3_{VTD}$ and (c) $VT3_{itsp}$. 90
6.14 PV reduction of (a) $VT3_i$, (b) $VT3_{VTD}$ and (c) $VT3_{itsp}$. 90
6.15 Optical performance curves of the set-ups (a)–(b) $VT3_i$, (c)–(d) $VT3_{VTD}$ and (e)–(f) $VT3_{itsp}$. 91
6.16 (a) Preliminary CAD model and (b) realistic rendering of the fittest set-up achieved for Goal III ($VT3_{itsp}$). 92

List of Tables

2.1 Geometrical and optical capacities of reported beam analytical models for V-Troughs. See the footnote.[1] 19
2.2 Performance indicators and indices drawn from V-Trough analytical models. See the footnote.[1] 20

3.1 Minimum and maximum values allowable for the input parameters. 34
3.2 Relevant optical variables for the V-Trough set-up in Fig. 3.14 at $\alpha = 70°$. 41
3.3 Relevant optical variables for the V-Trough set-up in Fig. 3.15 at $\alpha = 85°$. 42
3.4 Relevant optical variables for the V-Trough set-up in Fig. 3.16 at $\alpha = 120°$. 43

4.1 Input parameters of the simulated V-Trough set-ups. Those designed with "D" and those randomly defined with "S". 46
4.2 ANOVA table of the regression model. 50

5.1 Parameters for controlling GA-WA, GAGaussian and GAUniform genetic algorithms. 72
5.2 GA optimization parameters. 74

6.1 Basic consumption outline for a low-income family in *Chaparral*, Colombia. 80
6.2 Geometrical set-up parameters defined for the genes in GA-WA heuristic optimization method. 80
6.3 Results of the *Design Goal I.* 81
6.4 Results of the *Design Goal II.* 85
6.5 Results of the *Design Goal III.* 89

Chapter 1

Introduction

1.1 Background

This section contextualizes the research problem and describes the background convergence process that went from a topic of general interest to a specific context that delimits the research project. In this process, basic concepts are introduced which are essential to the understanding of the contributions of this research project.

As an opening for contextualization of the research problem, 1.2 billion people, almost one-fifth of the world's population, still lack access to electricity at a household level (He and Victor, 2017; D'Amelio et al., 2016). An additional 1.5 billion people have an unreliable electricity service (He and Victor, 2017). 99.8% of these people are from developing countries and 84% come from rural areas (Shyu, 2014). Electricity is vital for accessing information, social services such as education and health, and modern life in general. In the nowadays digital age, lacking the access to it means living in isolation and being deprived of opportunities, which is in turn linked to poverty and human under-development. Moreover, the number of people in this deplorable conditions grew between 2010 and 2012, implying that population growth is actually outpacing the expansion of the electricity coverage (Panos et al., 2016).

This acute absence of basic living conditions contrasts with the rapid rate at which developing countries are becoming industrialized with fossil-fueled economies. Unfortunately, the accelerated industrialization has not accordingly reduced the inequality between urban and rural modern energy use (Herington et al., 2017). Such scenario has taken the world to a point where "Developing nations are driving the ongoing increase in global CO_2 emissions"(MIT, 2015). This development has concentrated in dense urban areas with ever increasing emissions of gases and particulate matter which can be associated with chronic health effects in the general population (Calderón-Garcidueñas et al., 2015; Johnson et al., 2017). Moreover, the developing fossil-fueled countries are accelerating the anthropogenic climate change (Lueking and Cole, 2017; Cook et al., 2014) and they are, ironically, the most vulnerable to its projected effects (Adger et al., 2003).

Therefore, it is of utmost importance to support the development of these countries based on safer and more sustainable energy sources and which can also be deployed in rural areas. Most of the developing world is located within the tropics (Kummu and Varis, 2011), where there is higher solar insolation and hence, higher solar harvesting potential. Solar energy is one of the most promising markets for a sustainable economic growth and has the potential to mitigate greenhouse emissions and fossil fuel dependence (Sampaio and González, 2017). In particular, solar photovoltaic (PV) devices based on silicon wafers are expected to dominate the energy landscape for the next decades due to their technological maturity, cost-effectiveness and the scalability needed to displace oil on a massive scale (MIT, 2015). PV devices are suitable for decentralized energy generation and can be used to provide energy to off-the-grid rural populations at a household or community level. For instance, off-the-grid solar home systems were considered vital in the Chinese quest to reach remote users (He and Victor, 2017). Where local governments have failed to provide solar energy to off-the-grid rural communities, solutions that can be implemented at a household level are crucial for the empowerment and energy independence of entire families. Additionally, household solar

devices offer the opportunity to generate an additional income for the family in the case of energy surplus, which is a major incentive for adoption of these kinds of technologies in developing countries (Otte, 2013).

However, conventional PV technology still faces engineering challenges for a widespread adoption in the developing world. Principally, the initial capital cost of residential solar Photovoltaic (PV) devices is still prohibitive for low-income families (Bahaidarah et al., 2015; Tina and Scandura, 2012; Sindhu et al., 2016; Qureshi et al., 2017; Sampaio and González, 2017). Also, the manufacture of solar cells has a high dependence on the state of technological development of the local industry (Sampaio and González, 2017; De La Tour et al., 2011). This increases the dependence on imported products, which increases the prices further. Moreover, even though solar PV energy has a comparatively low environmental impact, it still uses some toxic materials and there is not yet the proper infrastructure for large-scale recycling or disposal of solar panels (Gupta and Anderson, 1991; Miles et al., 2005). These issues may be mitigated if the photovoltaic material, needed to fulfill a household's energy needs, is reduced. Therefore, it is crucial to develop solutions which have the potential to increase the amount of energy that can be harvested, per PV area, in a cost-effective and industrially accessible way.

The improvement of solar energy production can be approached at the level of the semiconductor material, the cell's texturing, the panel lamination or the effective harvesting area of the device. By reducing internal losses in the semiconductor materials, it might be possible to further increase the photovoltaic efficiency of silicon-based solar cells over the current record of 25.6% (Kowalczewski and Andreani, 2015). However, as the theoretical efficiency of silicon cells is around 29% (Kowalczewski and Andreani, 2015), research in this direction offers diminishing returns in the possible gains of energy production. Some of the efficiency losses in a solar panel are also caused by part of the sunlight being reflected back out from the surface. These efficiency losses can be reduced by implementing anti-reflection surfaces in the silicon cells themselves, with light-trapping nano-texturing (Salman, 2017), or in the lamination foils which are used to protect the bare silicon (Wang et al., 2017). However, the previous strategies depend on a high level of technological development in manufacturing (López, 2015) and even in nanotechnology in the case of light-trapping texturing. On the other hand, there are certain strategies which can increase the effective harvesting area of a solar panel without intervening the manufacturing of the panel itself, namely "solar tracking" and "solar concentration"; which are explained as follows.

The effective harvesting area of a solar panel, at a given time of the day, is the area of the panel projected to a plane which is perpendicular to the incident solar rays. In order to understand how the effective harvesting area is affected by the behavior of the solar rays, the Sun-Earth interactions can be considered as a reference perspective. As depicted in Figs. 1.1(a) and 1.1(b), the omnidirectional light rays emitted by the sun begin their journey so far away, that they are assumed to be parallel to each other when they reach the Earth's atmosphere (Platt et al., 2007). Fig. 1.1(c) shows how the perceived solar elevation (α) depends on the longitude and time of a given location.

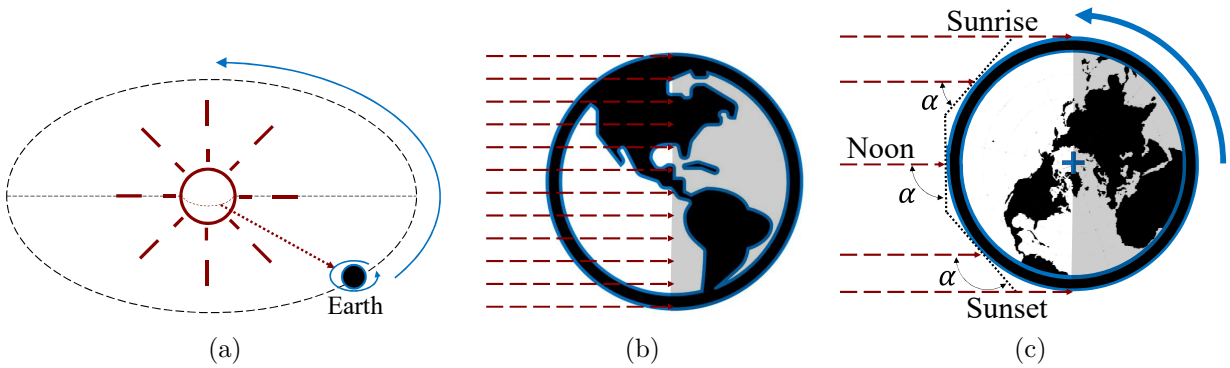

Figure 1.1: (a) Sun-Earth radiation interactions. (b) Solar rays reach the Earth parallel to each other. (c) Solar elevation α.

For instance, a horizontal plane at the rotational equator perceives a solar elevation of $\alpha = 0°$ in the

sunrise and, as the Earth spins, it reaches $\alpha = 90°$ at noon and eventually the solar angular range ends with $\alpha = 180°$ at sunset. The solar elevation, as measured from a horizontal plane, is also affected by the latitude and the declination angle caused by the tilted rotation axis of the Earth; but these two factors are not considered in this first simplified example. From the perspective of the horizontal plane, the sun is following an apparent path through the sky-dome along the day and this is directly related to the solar incidence angle to a possible PV panel, as shown in Fig. 1.2.

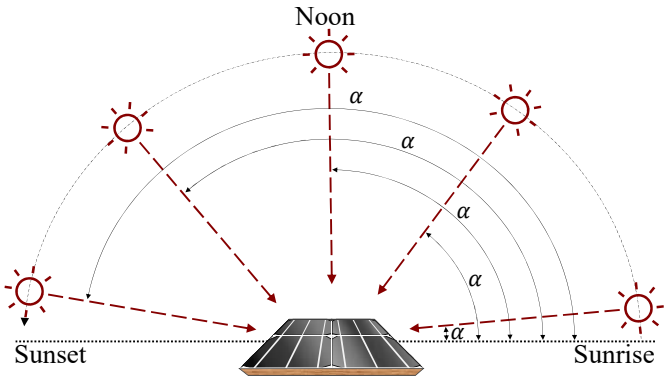

Figure 1.2: Sun's apparent path and solar elevation (α).

As the *Effective Harvesting Area* (EHA) is perpendicular to the solar rays, it might vary throughout the day with the apparent movement of the sun. Figs. 1.3(a), 1.3(b) and 1.3(c) illustrate this phenomena for a fixed horizontal solar panel. As the solar elevation differs from $\alpha = 90°$, the effective harvesting area gets reduced with the cosine of the angle of misalignment between the incoming rays and the normal to the panel (Taylor, 2000). This is crucial for energy production because a smaller effective area results in less solar radiation reaching the PV surface and thus, less electrical power can be generated.

On the other hand, Figs. 1.3(d), 1.3(e) and 1.3(f) illustrate how the inclination of a solar device (β) can be adjusted to maintain the EHA constant throughout the day. This process of adjusting the angular position of a device as a reaction to the sun's apparent movement is known as "solar tracking". Solar tracking strategies have been reported to increase the daily energy production in up to a 30-50% (Kelly and Gibson, 2009). In the case illustrated, the panel is performing a "perfect" tracking, so the solar incidence angle is 90° and the effective harvesting area is equal to the PV area.

Solar tracking can be performed by different kinds of actuation procedures, namely active, passive or manual. With active tracking the device automatically follows the sun by means of electric motors, microprocessors and electro-optical sensors (Rahimi et al., 2015). Active tracking can be performed in one (Mousazadeh et al., 2009) or two (Eldin et al., 2016; Mousazadeh et al., 2009) axis of movement, depending on the required precision. Due to the complexity and additional capital cost for an active tracking system, it might not be an appealing approach for household implementations in developing countries (Eldin et al., 2016). Passive tracking uses automatic processes based on matter re-distribution by means of evaporation (Rahimi et al., 2015; Mousazadeh et al., 2009) or progressive dripping (Foss, 2015). Seeking to favor the social adoption among non-industrialized societies, this research project focuses on manual tracking. This actuation method consists of performing manual adjustments of a device's position in one or more steps in a day or season (Lubitz, 2011; Caton, 2014). As stated by Caton (2014), "Manual tracking is feasible for a developing community and could increase ownership". Several studies have found that an actuation strategy, based on few stepped adjustments, might be enough to gain most of the tracking potential to maintain the effective area but with a simpler device (Hollands, 1971; Bannerot and Howell, 1979). However, it must be taken into account that a manual tracking strategy, at the household level, might introduce a disruption in the daily routines of the potential users.

Another way to increase the effective harvesting area is to directly escalate it with non-imaging optical elements. This approach, known as solar concentration, works by redirecting the solar rays towards a PV area which is smaller than the resulting optical area. If the optical elements cost less than the PV absorber,

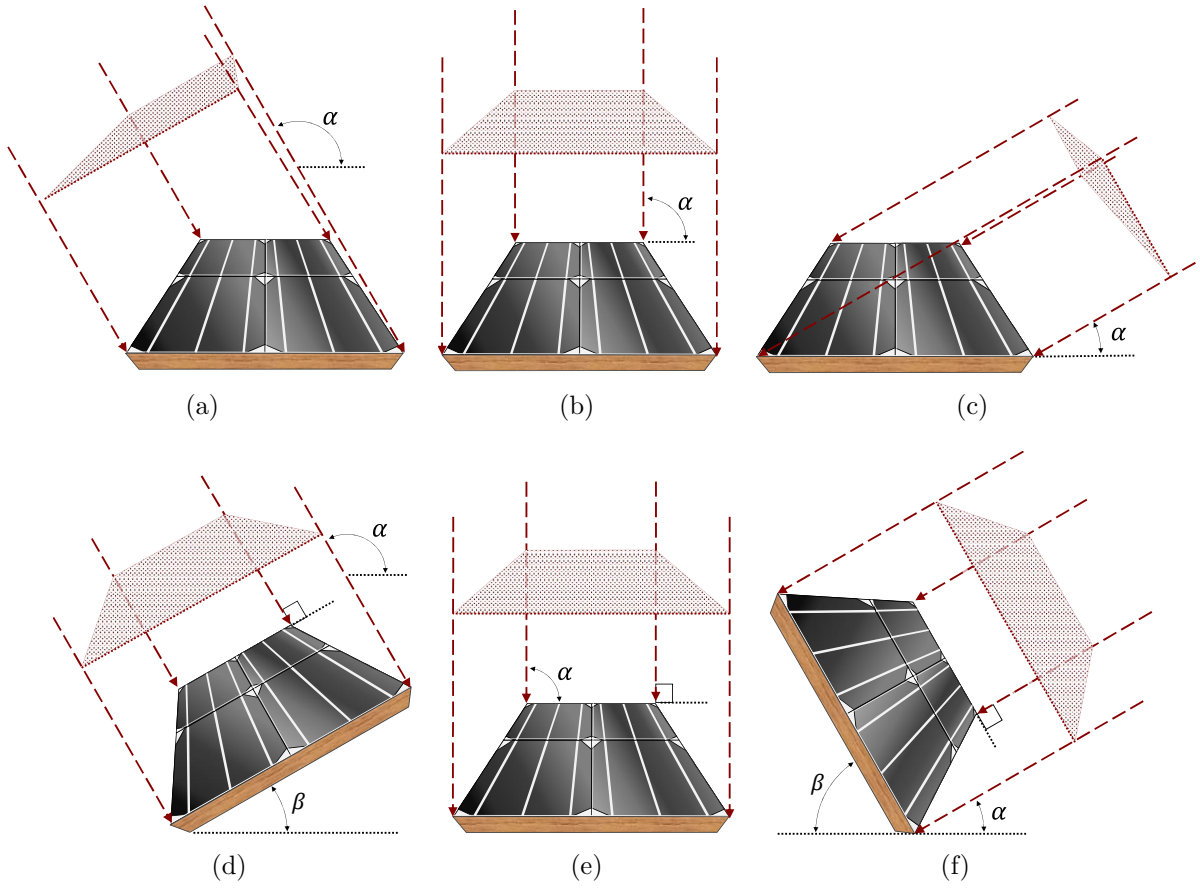

Figure 1.3: Variation of the effective harvesting area of a solar panel without tracking in (a), (b) and (c); and with tracking in (d), (e) and (f).

concentration has the potential to reduce the capital cost of the device overall (Tang and Liu, 2011, 2010). Fig. 1.4 illustrates some of the solar concentration methods and optical elements.

The Fresnel method (see Fig. 1.4(a)) uses a compact and transparent lens with grooves that refract the sun rays towards a common focal point or line (Arias-Rosales et al., 2014). The parabolic troughs or dishes (see Fig. 1.4(b)) use a specular surface, curved in a parabolic shape, that reflects the sun rays towards a focal point or line (Karathanassis et al., 2017). Similarly, the compound parabolic concentrators (see Fig. 1.4(c)) use two parabolic reflectors at the ends of a solar absorber (Jaaz et al., 2017). Morgan Solar Inc. patented (Reis and Judd, 2000) a new kind of solar concentrator, so-called Light-guide Solar Optic, which redirects sunlight to a relatively small PV absorber by means of internal reflections and refractions within a compact panel (see 1.4(d)). Also with a transparent compact panel, luminescent concentrators (see 1.4(e)) use polymer sheets doped with luminescent particles which absorb and re-emit the sunlight (Wang et al., 2011; Assadi et al., 2016). On the other hand, V-Trough devices (see 1.4(f)) use flat mirrors adjacent to the borders of a PV absorber in order to reflect the sunlight towards its surface (Arias-Rosales and Mejía-Gutiérrez, 2016).

This research project focuses on V-Trough concentrators due to their superior simplicity and ease of manufacturing, operation and maintenance, as compared to the other concentrating methods (Maiti et al., 2012; Fraidenraich, 1998, 1992; Bahaidarah et al., 2015). As stated by Tang and Liu (2011), V-Trough solar devices are “extremely easy to be constructed”. Since the flat mirrors and the additional supporting structure are usually much less expensive than an average PV panel, V-Troughs are potentially more cost-effective, more affordable in terms of their capital cost and with a more accessible technology (Maiti et al., 2012; Selçuk,

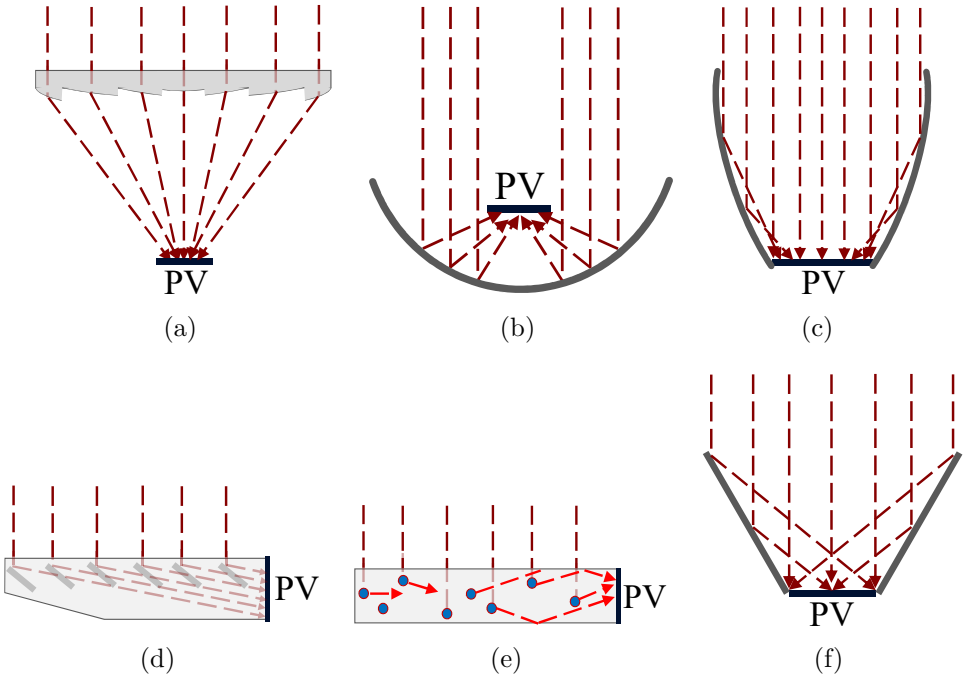

Figure 1.4: Solar concentration methods. (a) Fresnel lens, (b) parabolic reflector, (c) compound parabolic reflector, (d) light-guide panel, (e) luminescent panel, and (f) V-Trough reflector.

1979; Tang and Liu, 2011; Seitel, 1975; Bannerot and Howell, 1979; Fraidenraich, 1998, 1992). For instance, Sangani and Solanki (2007) used a V-Trough to increase the power output over 40% and reduce the cost of installed capacity by 24% as compared to a flat PV panel. V-Troughs can use regular commercial silicon cells, which contributes further to the accessibility of their technology (Tang and Liu, 2011; Maiti et al., 2012; Fraidenraich, 1998, 1992; Bahaidarah et al., 2015). Although the concentration of these devices may increase the temperature of the cells, which is detrimental for efficiency, the flat reflectors can be constructed from aluminum sheets for an effective heat dissipation (Tang and Liu, 2011). The described relative advantages of V-Troughs are crucial within the context of this research project, since the most critical barriers to the adoption of solar energy in developing countries have been reported to be the initial capital cost (Bahaidarah et al., 2015; Tina and Scandura, 2012; Sindhu et al., 2016; Qureshi et al., 2017; Sampaio and González, 2017), the reluctance of people to unfamiliar technology (Sindhu et al., 2016), technologies with reliability issues (Sindhu et al., 2016) and approaches with a high dependence on technological development (Sampaio and González, 2017).

Concentration and tracking strategies are closely related. The direction in which the solar rays are redirected, by the concentrating optical elements, depends on the solar incidence angle. This naturally generates the need to track the sun in order to keep focusing the solar rays into the PV absorber as much as possible. The higher the concentration level, the smaller the misalignment that can be tolerated (Famoso et al., 2015). Similarly, the higher the concentration level, the more the device will depend on clear weather. This is because clear skies have a greater proportion of beam solar radiation, as opposed to diffuse radiation; namely the sunlight that has been scattered by the atmosphere as shown in Fig. 1.5. Solar devices with a high concentration ratio are hence only capable of effectively using the beam radiation portion.

Conversely, V-Troughs are usually designed for a low concentration of up to three “suns”, namely the optical aperture area being three times the PV area (Bannerot and Howell, 1979). Therefore, V-Troughs can focus a considerable portion of diffuse radiation as well and hence, they are less weather-dependent (Chiam, 1981; Bannerot and Howell, 1979; Bahaidarah et al., 2015). The low concentration of V-Troughs also means that they do not need precise tracking for an effective concentration (Chiam, 1981; Bahaidarah et al., 2015).

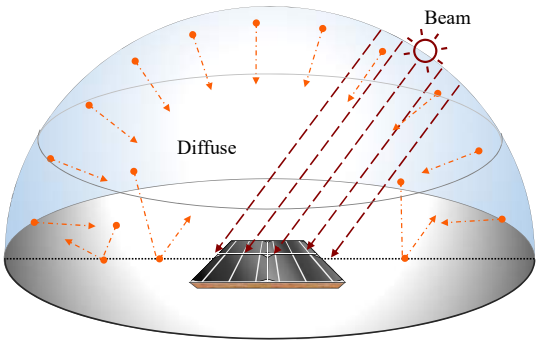

Figure 1.5: Solar beam and diffuse radiation.

Moreover, these devices do not get dangerously hot nor concentrate light in an intensely bright focal point, so they are considered to be safe for human direct manipulation. Therefore, V-Trough concentration is suitable to be combined with a stepped manual tracking, in order to increase the amount of energy per PV area, in a cost-effective and technologically simple approach. Fig. 1.6 shows photos of actual V-Trough PV devices for commercial or research use. These real-life implementations illustrate several different arranges and structures for supporting their elements and performing the tracking movements. The inherent simplicity of the main geometry of a V-Trough is evident.

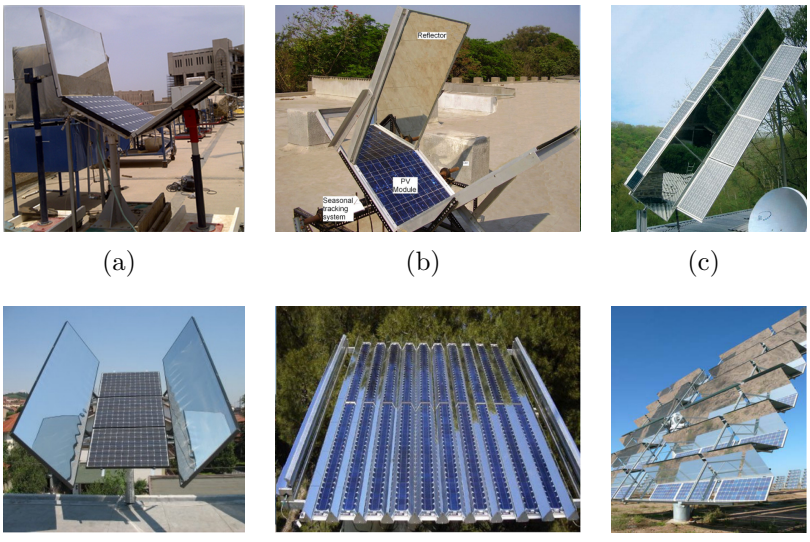

(a) (b) (c)

(d) (e) (f)

Figure 1.6: V-Trough photovoltaic devices for commercial or research use. 1.6(a) from Bahaidarah et al. (2015); 1.6(b) from Sangani and Solanki (2007); and 1.6(c)– 1.6(f) from Hermenean et al. (2009).

Fig. 1.7 synthesizes the main decisions made throughout the convergence of the research context. The background assessment went from the needs in developing countries to V-Trough devices with stepped manual tracking as an approach to cost-effectively increase the energy per PV area, at a household level, in developing countries.

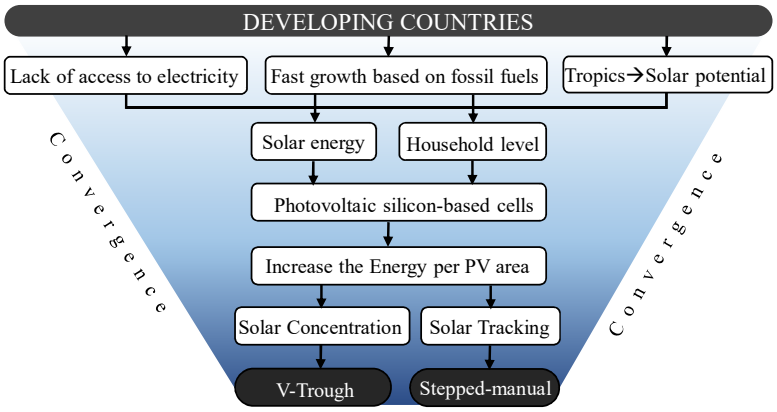

Figure 1.7: Convergence of the research context.

1.2 Research Problem Definition

In a 2015 report by Fraunhofer (see Fig. 1.8(a)) it is shown how the PV installed capacity has been growing globally at an accelerated rate. However, as also evidenced in Fig. 1.8(b), most of this installed capacity is concentrated in developed countries, such as Germany or Japan, and countries with a huge manufacturing industry, such as China. In comparison, regions of the world with a considerable proportion of developing nations, such as Africa and the Middle East, represent an almost negligible share of the market.

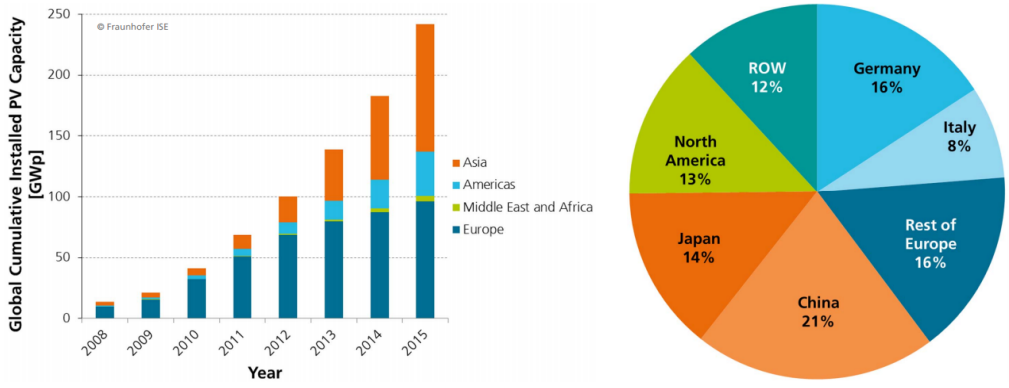

(a) (b)

Figure 1.8: (a) Global cumulative PV installation (Fraunhofer Institute for Solar Energy Systems, ISE, 2016). (b) Global cumulative PV installation by Region in 2015 (Fraunhofer Institute for Solar Energy Systems, ISE, 2016).

It is hence of utmost importance to consider the possible barriers to PV adoption in developing countries. No study has been found regarding such barriers to specifically V-Trough systems. Nevertheless, solar cookers have been assessed in this regard and they share an evident resemblance to PV V-Troughs at a household level. Despite being simple devices offering an appealing solution to a basic need, "solar cookers have not enjoyed widespread success, with low levels of successful implementation" (Otte, 2013). The most relevant barriers identified were: an initial high capital cost due to an underdeveloped market (Otte, 2013; Puzzolo et al., 2016); an inadequate or nonexistent maintenance service (Otte, 2013); the operation difficulty (Otte, 2013; Puzzolo et al., 2016); the lack of familiarity with the technology (Puzzolo et al., 2016); the inconsistencies with the daily routines of the users (Otte, 2013; Turner, 2001; Puzzolo et al., 2016); the frequently needed manual adjustments (Puzzolo et al., 2016); and the lack of a suitable place for the device to be deployed and

operated (Otte, 2013; Puzzolo et al., 2016). For solar devices in general, the lack of skilled professionals and training institutes (Sindhu et al., 2016), and the need for a relatively large area of installation (Sampaio and González, 2017), have also been found to be considerable barriers to adoption. On the other hand, if a rural family generates an energy surplus and manages to make an additional income from it, this may result in a major incentive for adoption (Otte, 2013). Likewise, if a considerable proportion of a solar device is built with local resources, the initial prices can drop and local employment can be generated (Otte, 2013). This can also increase the local availability of these devices; another barrier to adoption (Qureshi et al., 2017; Sampaio and González, 2017).

Consequently, it can be inferred that a solar PV device, for developing countries at a household level, may favor adoption if it can be adapted to the purchasing capacities of the family, the available space they have, their daily routines and if it can be built, operated and maintained mainly from local resources and with an acceptable level of technological familiarity. As described in Sec. 1.1, the simplicity and potential cost-effectiveness of V-Trough devices are an advantage when confronted with the described barriers to adoption. However, given the lack of widespread success of solar cookers as a reference perspective and the relatively small PV market in developing countries, it is reasonable to argue that more work needs to be done, from design and engineering, concerning the applicability of V-Trough PV solutions. In particular, the parameters that define the geometrical features of a V-Trough and the way in which they are to be adjusted for the manual tracking, can be tailored to the specific conditions and priorities of a given family. Such a democratization of this technology has the potential to make the most of the PV V-Trough concept in favor of a broader implementation.

In order to get a deeper insight into what would take to personalize the configuration of PV V-Troughs, Fig. 1.9 illustrates the main geometrical parameters that define their set-up:

- LPV (the length of the PV absorber)
- LL (the length of the left mirror)
- LR (the length of the right mirror)
- $Depth$ (the depth of the device)
- β (the angular position of the PV absorber)
- ψL (the angular position of the left mirror)
- ψR (the angular position of the right mirror)

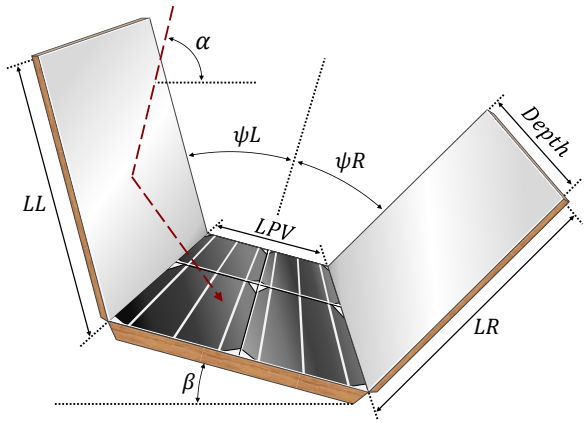

Figure 1.9: Geometrical parameters of a V-Trough photovoltaic device.

While most of the found V-Trough studies assume a symmetrical set-up, an asymmetry in the dimensions and movements can introduce a greater degree of flexibility for adapting to specific conditions (Chiam, 1982; Selçuk, 1979). Likewise, V-Trough tracking strategies are usually limited to just modifying β, but the other

parameters can also be adjustable in order to maximize the effective harvesting area by means of the tracking strategy. Therefore, the flexibility of establishing those main geometrical parameters as independently fixed or dynamic is desirable for personalized design scenarios. The design scenarios can differ, for instance, in the available space for locating the device, the allowable materials cost, the energy needs, the timing and number of manual tracking adjustments that the family is willing to perform per day, and the possible shadows at the location that may limit the available solar elevation range. Fig. 1.10 illustrates how the described flexibility can allow for different V-Trough set-ups potentially tailored to different contexts and allowable tracking strategies, such as tilting (1.10(a) and 1.10(e)) or inverting (1.10(b)) the whole device, and/or independently tilting (1.10(c)), sliding (1.10(d)) or removing (1.10(f)) the mirrors. Despite the geometrical simplicity of these devices, as the lengths and angular positions in these parameters are continuous dimensions, there is an infinite number of possible V-Trough set-ups. For a more practical perspective, if each parameter is discretized into only ten possible values, and two tracking movements are allowed, then each parameter has to be defined for three positions, in which case there would be $1E15$ (10^{15}) possible set-ups.

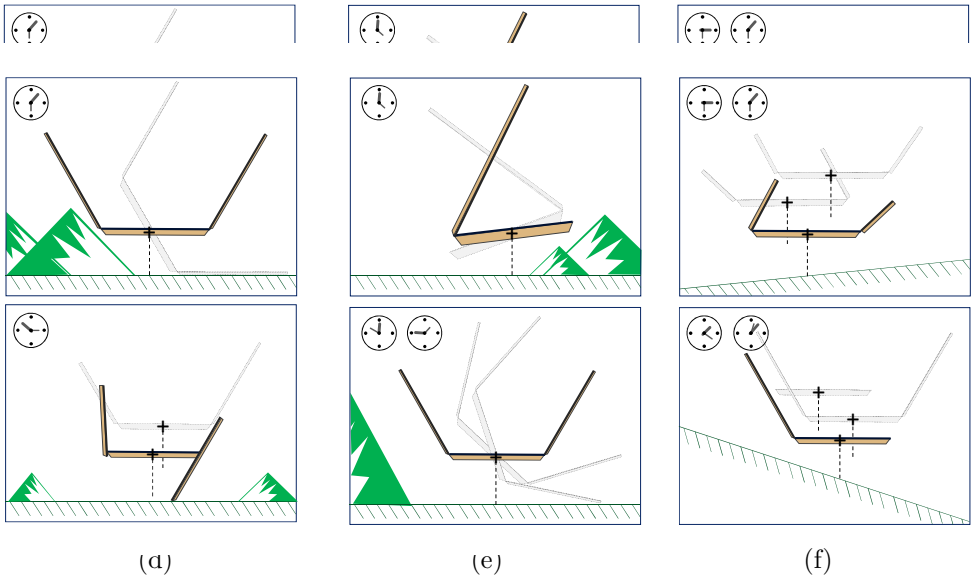

Figure 1.10: An illustration of different contexts, V-Trough set-ups and tracking timings.

Given the vast number of possible V-Trough set-ups, how to support a further exploration of these devices for their implementation in personalized scenarios at a household level? One of the most critical aspects is to enable an understanding of the relevant macro-optical phenomena that results for a given set-up. According to the Oxford Dictionary of Weather (Dunlop, 2008), an optical phenomena is "phenomena caused by diffraction, reflection, refraction, or scattering by dry particles, water droplets, or ice crystals in the atmosphere or on the ground, or by the atmosphere itself". Given the optics of V-Troughs, the term "macro-optical phenomena" will be used in this research project to refer to the reflection phenomena visible to the naked eye, such as shadows, blocked sunlight, reflected sunlight after one or two bounces off the mirrors, or the brightening of certain surfaces due to the level of concentration.

The understanding of these macro-optical phenomena can provide insight into the consequences of a given parameter for a given V-Trough's element; which in turn may empower design and engineering decisions. These phenomena can directly affect and define the effective harvesting area of a V-Trough device (see Fig. 1.3). As an indicator of the optical performance, the effective harvesting area over the PV area is referred to as the "effective concentration"; similar to other indicators found in the literature such as the "flux concentration ratio" (Selçuk, 1979) or the "area ratio" (Chiam, 1981) indicator. It is worth noting that the referred concept is different to the much more common design "concentration ratio" (Fraidenraich, 1998), which assumes that all the sunlight reaching the device will effectively be absorbed by the PV surface; thus ignoring relevant macro-optical interactions as an oversimplification.

A mathematical understanding of the macro-optical phenomena involved can lead towards the calculation of the optical performance of a V-trough device with any given set-up. Therefore, there is a need for a theoretical model that is capable of describing these phenomena and that establishes the effective concentration. This model must be geometrically flexible, as previously described, regarding the V-Trough input parameters. The geometrical flexibility and the focus on manual tracking is relevant because it demands the model to consider a broader spectrum of macro-optical phenomena which is usually ignored for more ideal conditions. For instance, if perfect continuous tracking is assumed, then there is no need to model the shadows that may be produced among the V-Trough's elements and there is no need to implement asymmetric mirrors. Hence, the more flexible the model is, in its geometrical constraints, the more comprehensive it needs to be. Furthermore, given the wide space of possible solutions, this model must present a low computational demand. This last requirement is also important in order to favor the democratization of V-Trough technology.

As V-Troughs interact with both diffuse and beam radiation (see Fig. 1.5), the macro-optical phenomena related to both kinds of solar radiation are expected to ultimately affect the effective concentration. However, diffuse radiation behaves differently to beam radiation, so they are often modeled and conceptualized independently and their effects over optical performance are then added together (Bahaidarah et al., 2015; Kostić et al., 2010; Tina and Scandura, 2012). This project focuses on the more critical problem of beam radiation, which is typically taken as 90% of the global radiation on average (Kelly and Gibson, 2009). Once this problem is solved, it could then be complemented in further work with a diffuse model as it has been reported in the literature. Moreover, some V-Trough diffuse radiation models have been found to be an extension of a more fundamental beam model (Fraidenraich, 1992).

There are several reported theoretical models of the performance of V-Trough solar devices concerning beam radiation (see Sec. 2.1). These models are developed from the perspective of geometrical optics, which describes sunlight as projected rays that propagate in a straight path and behave according to the laws derived from Fermat's "principle of least time" (Velzel, 2014; Chen et al., 2000). Geometrical optics is considered to be a practical tool for modeling the solar beam radiation since it offers a proper and comprehensive simplification of its macroscopic behavior. However, the reported models are not satisfactory in terms of their flexibility in the geometrical input parameters, the relevancy of their macro-optical considerations and/or their computational demand. Additionally, since the level of flexibility that this project proposes for V-Troughs is not yet found in the literature, there are no reported proposals, based on a theoretical model such as the one described, on how to guide the parameters definition process and effectively navigate the space of solutions.

1.3 Research Questions

1.3.1 General Research Question

The following research question is the backbone of this project:

How to model the macro-optical phenomena in photovoltaic V-Troughs with manual tracking, concerning beam radiation, to determine their effective concentration and support a flexible definition of their parameters in a personalized context at a household level?

For disambiguation, the following key terms are described as they are used in this research project:

- **Macro-optical phenomena**: It refers to the reflection phenomena visible to the naked eye, such as shadows, blocked sunlight, reflected sunlight after one or two bounces off the mirrors, or the brightening of certain surfaces due to the level of concentration.

- **Effective concentration**: As an indicator of the optical performance, this term refers to the effective harvesting area of a given solar device over its PV area. The effective harvesting area is the proportion of the area of a given device, projected to a plane which is perpendicular to the incident sunlight, that corresponds to the beam rays which manage to reach the PV surface.

- **Flexible parameter definition**: Applied to the V-Trough design problem, this refers to the possibility of independently defining each of the main geometrical parameters and establish them as fixed or as dynamic. The main geometrical parameters are the lengths and angular positions of the mirrors and the PV surface.
- **Personalized context**: It refers to design scenarios that can differ in the available space for locating the device, the allowable materials cost, the energy needs, the timing and number of manual tracking adjustments that the family is willing to perform per day, the possible shadows at the location that may limit the available solar elevation range, and the priorities in terms of the system's performance.
- **Household level**: This means that the system is intended to be deployed in or near a house, with an available clear space and operated by the family members in order to fulfill their energy needs.

1.3.2 Specific Research Questions

The following specific questions consist in a break-down of the general question. If answered satisfactorily, they are supposed to provide a solution to the general research question.

I Which are the independent and dependent variables involved?

II How are the identified variables mathematically related?

III How do the model's predictions correspond to experimental measurements?

IV How to use the model to interactively guide the definition of a V-Trough's parameters for a given personalized household context?

V How to use the model to optimize a V-Trough's parameters for a given personalized household context?

1.4 Research Objectives

1.4.1 General Research Objective

The following research objective is intended to fulfill the general research question:

To propose a theoretical model of the macro-optical phenomena of beam radiation in photovoltaic V-Troughs with manual tracking, through geometrical optics, to determine their effective concentration and support a flexible definition of their parameters in a personalized household context.

For disambiguation on "geometrical optics", refer to Sec. 1.2.

1.4.2 Specific Research Objectives

The following specific objectives consist in a break-down of the general objective. If carried out satisfactorily, they are supposed to provide a solution to the general research objective. Each specific research objective is directly aligned with the specific research question of the same number.

I To analyze the macro-optical phenomena, related to the effective concentration of beam radiation in V-Trough devices with manual tracking, in order to identify the variables involved.

II To mathematically relate the identified variables, through geometrical optics, in order to establish a theoretical model.

III To test the validity of the theoretical model by comparing it against an equivalent experimental model.

IV To propose an interactive tool, based on the theoretical model, intended to support the definition of a given V-Trough's parameters in a personalized household context.

V To propose a heuristic tool, based on the theoretical model, for optimizing a given V-Trough's parameters in a personalized household context.

1.4.3 Operationalization of the Research Objectives

According to the Oxford University (2017), to operationalize is to "Express or define (something) in terms of the operations used to determine or prove it". Accordingly, this section briefly describes variables and procedures that can be used to measure the fulfillment of the objectives. As the general research objective states, the motivation behind developing a theoretical model is to both "determine the effective concentration" and "support a flexible definition of [a V-Trough's] parameters in a personalized household context".

The effective concentration that will result from the model's calculations concerns only beam radiation. Solar beam radiation can be experimentally modeled with laser devices which, for practical matters at this scale, follow the basic principles of geometrical optics in the same way as beam radiation (Pedrotti, 2012). Also, the effective concentration comprehends, in essence, a series of geometrical relations between the PV area and certain macro-optical phenomena. Therefore, an experimental model can simulate those macro-optical phenomena with lasers, perform real measurements of their areas and/or lengths and compare them to the corresponding specific predictions drawn from the theoretical model. If the predictions are defined as a continuous independent variable and the experimental measurements are defined as a continuous dependent variable, it is possible to perform a statistical regression to assess the validity of the model. The residuals of this regression can be inspected looking for systematic deviations. If no systematic deviations are found, it can be assumed that the model does represent the relevant macro-optical phenomena involved. Furthermore, 95% prediction intervals can be calculated in order to assess the precision of the theoretical model.

The geometrical flexibility of the model parameters is a key feature of the research problem. To evaluate that this flexibility (defined in Sec. 1.3.1) is indeed achieved, it can be tested whether the model returns valid results without a human bias while selecting the values for the parameters. This can be achieved by delimiting each parameter to a reasonable range and selecting the corresponding values with a random generator algorithm. A number of V-Trough set-ups can be generated and modeled this way and then the theoretical predictions can be experimentally validated.

Once the model is tested for its validity and flexibility, there can be an exploratory evaluation of its practicality for supporting the parameters definition process for personalized household contexts. As it is stated in objectives IV and V, this will be assessed from both an interactive tool and a heuristic optimization tool. These will be evaluated in a case study, where it is possible to explore how suitable the model is for this matters in terms of: the time it takes to perform the simulations, the improvement of the performance results achieved over reference V-Trough set-ups and the convergence of results. In terms of the heuristic optimization tool, it is possible to measure its performance with the average fittest result achieved per every run of the algorithms.

1.5 Research Scope

The following points describe the limitations related to the scope of the research project.

- The performance of a real photovoltaic V-Trough is affected by the macro-optical interactions of beam and diffuse solar radiation, as well as by temperature-induced efficiency losses. However, as explained in Sec. 1.2, the theoretical focus of this project is concerned only with the more critical beam radiation. As it has been reported in the literature (see Sec. 1.2), this research project can be complemented in further research with diffuse radiation and temperature models.
- The validation of the theoretical model is performed through an experimental model of solar beam radiation with laser devices (see Sec. 1.4.3). Therefore, no V-Trough device is tested under real sunlight.
- It is assumed that the parameters regarding the manual tracking movements are carried out precisely by hypothetical users. Hence, no real potential users are analyzed in their capacity to perform such movements.
- An interactive tool and a heuristic optimization tool are proposed based on the developed model. These tools are evaluated in an exploratory hypothetical case study. Nevertheless, it is not tested

whether designers or engineers outside of the project are effectively guided by these tools in a V-Trough design scenario.

1.6 Research Justification

This section discusses the theoretical, practical and social relevance of this project.

This research project proposes a mathematical model that is new to the state of the art and transcends previously reported capacities regarding V-Trough modeling. This is the main theoretical contribution. As introduced in Sec. 1.2, there exists a knowledge gap which this project addresses, namely the capacity to model the beam effective concentration of V-Trough devices with a:

- Higher degree of flexibility in the input parameters
- Higher detail in the macro-optical phenomena considered
- Lower computational demand

The model pursued by this project, which is specifically for V-Trough solar concentrators, can also be used as a reference for developing new models for other kinds of concentrating optics. Moreover, the model can be extended, in further work, for modeling the interactions with diffuse radiation as well.

This project proposes to develop both an interactive tool and a heuristic optimization tool, based on the theoretical model, and to further explore their potential in a V-Trough design case study. Since this is the first study with such characteristics, it is in itself a theoretical contribution. The case study can provide insight into the versatile capacities that can be achieved through these tools for V-Trough design. This contribution can motivate further research in:

- An extension of the tools presented
- The introduction of new similar tools
- A study of the real impact that those tools can have in a V-Trough design process with real users
- A study to see if such tools can help democratize the V-Trough technology in a way that can push its adoption forward.

The case study proposed by this project can help to illustrate the practical advantages of flexibly exploring V-Trough set-ups for personalized contexts and performance priorities. Furthermore, this project intends to provide the needed theoretical framework and the tools to implement it. The interactive tool, complemented with the heuristic optimization tool, can be used by engineers and designers for real-life V-Trough implementations. Furthermore, the heuristic optimization tool could be developed into a portable application for automatically defining the geometrical parameters of a V-Trough without the intervention of a trained engineer.

The aforementioned theoretical and practical contributions of this research project can support a broader implementation of PV V-Trough devices in rural areas of developing countries. As presented in Sec. 1.1, this has a critical social relevance. V-Troughs can provide a clean and safe energy solution for families living in vulnerable situations. If these solutions result into a successful widespread adoption, it can favorably impact the access to electricity and empower energy independence. Also, V-Trough technology can help mitigate the anthropogenic climate change because it offers an alternative to a development based on fossil fuels.

1.7 Methodological Framework

This section presents the methodological framework proposed in this project to progressively advance towards the general research objective. This framework is based on the *Research in Design Context* methodology (Imre, 2007; Horvath, 2008). Fig. 1.11 places this reference methodology in an intermediary conceptual space between Fundamental research and industrial design; but considerably more inclined towards the former. This methodological position is related to the motivations, methods, interpretations and contributions of this

project. As stated by Imre (2007), "Contextualized research seeks to understand the semantic relationships (interplay) between the investigated phenomena, the related research variables, the concerns of design and the reflections on the concerns of design". The methodological framework of this project, as in *Research in Design Context*, is influenced by the design context in terms of the definition of the purpose of research; the circumstances in which the studied phenomena can be analyzed; the relationships that must be studied in a given context; and the interpretation of data.

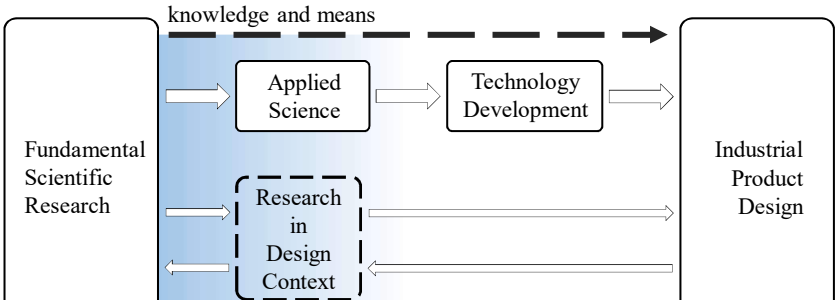

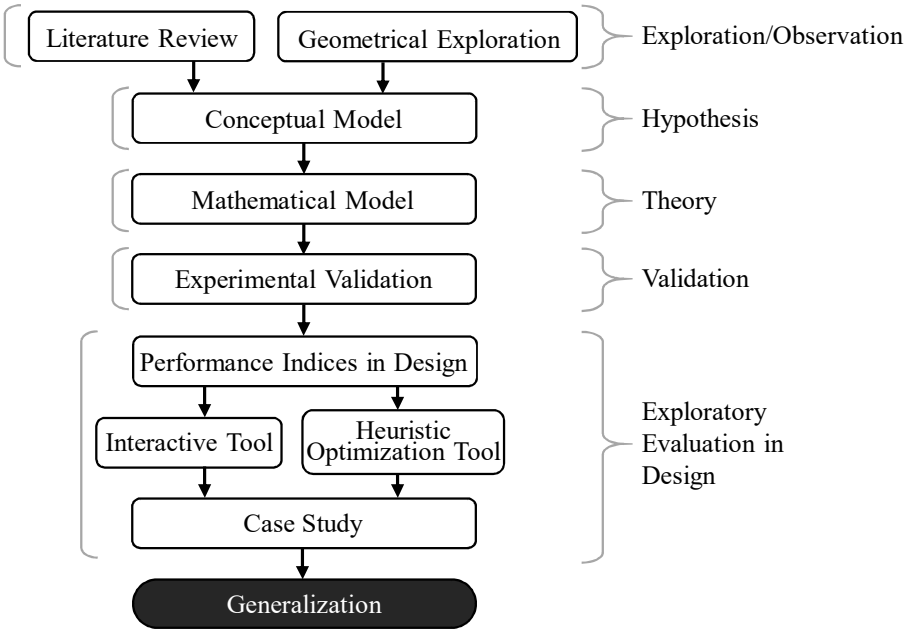

Figure 1.12: Research methodological framework.

matical model and its validation. This is the core of the research project and constitutes its main scientific contribution. This theoretical endeavor is contextualized and constrained by the design V-Trough problem and the real situation of some rural areas in developing countries. After the model is developed and experimentally tested, it is used for establishing performance indicators and indices that have a more direct use in the design decision-making process. These indicators and indices are then implemented in an interactive tool

and a heuristic optimization tool. Both approaches are used in a case study for an exploratory evaluation of their capacities to support the definition of the V-Trough's parameters in personalized design scenarios. Finally, the findings are generalized according to the theoretical and practical relevance of the project.

1.8 Manuscript Organization

As follows, Chapter 2 presents the relevant state of the art related to V-Trough modeling and different approaches that can be taken as a reference to support the parameters definition of these devices in the design context. Afterwards, Chapter 3 presents the theoretical model and its development is described in detail. The model validation procedure and its results are then presented in Chapter 4. Chapters 3-4 delimit the part of the project which is more related to fundamental research, where the priority is the mathematical understanding of the phenomena involved. Afterwards, Chapter 5 describes how the model is used to propose several performance indicators and indices which are intended to render the model's predictions more useful for the design context. This is followed, within the same chapter, by a proposal of several approaches to use these indicators and indices as a support for the definition of the V-Trough's parameters. These approaches are implemented in a case study in Chapter 6. The findings of the whole project are generalized in the conclusions, presented in Chapter 7. At the end of this manuscript, before the References, the Nomenclature is presented with a description of the variables and acronyms used in this research project.

Chapter 2

State of the Art

This section presents a review of the most relevant state-of-the-art literature concerning solar V-Trough modeling and different approaches that can be used to guide or support the process of defining the geometrical parameters of these devices. These approaches were classified into two groups, namely interactive tools and optimization methods.

2.1 Beam Radiation Modeling in V-Trough Devices

The production of solar energy is all about harvesting the solar radiation. Therefore, when designing a solar device, it is of great interest to understand how solar radiation reaches the PV absorber and which factors influence its intensity at the PV surface throughout the day. This understanding can be achieved through a theoretical model that mathematically relates the variables which best describe the phenomena involved. The Oxford English Dictionary defines a model as "A simplified description, especially a mathematical one, of a system or process, to assist calculations and predictions" (Oxford University, 2017). Accordingly, this section is interested in the different models of the optical performance of solar V-Troughs and the limitations of those models when contextualized in the background of this project.

One way to model solar radiation is as quantized discrete photons (Grynberg et al., 2010) or as a propagating wave (Arriaga et al., 2004). For instance, Penttilä and Lumme (2009) used numerical wave-optical methods to simulate light scattering in porous materials. However realistic, these simulations at the level of electromagnetic waves or photons tend to lead to unnecessarily complex and computationally intensive processes when the dimensions of the simulated objects are orders of magnitude greater than the radiation's wavelength of interest (Chen et al., 2000). As the main elements of a V-Trough are macroscopic objects with mostly smooth surfaces, there is no need to model the sunlight interactions at a quantum level. This is specially the case of this project because the ultimate objective, in terms of modeling, is the effective concentration, which relates areas and lengths pertaining to macro-optical phenomena (see 1.2).

A convenient modeling approach is hence to use geometrical optics as the conceptual and mathematical framework. Geometrical optics describes unperturbed sunlight as projected rays which propagate from a given light source in a straight path (Velzel, 2014; Chen et al., 2000). These rays, as formulated by Pierre de Fermat, follow the optical path between two points that can be traversed in the shortest time, so-called the Fermat's "principle of least time" (Velzel, 2014). From this simple principle and taking into account the refractive index of the mediums involved, it is possible to derive the main laws that describe the behavior of a light ray, namely reflection, refraction and diffraction. In general, the predicted behavior of light by geometrical optics, when interacting with macroscopic objects and structures, is consistent with the more modern wave-theory of light (Velzel, 2014).The optical laws derived from Fermat's principle can be described with basic geometry and yet provide a comprehensive simplification of the most relevant macroscopic behaviors. Therefore, geometrical optics is considered to be a practical approach for modeling the unscattered solar rays, so-called beam radiation.

Beam radiation is not the only solar radiation component to be considered, especially when the simulated

application is affected by a non-vacuum medium, such as Earth's atmosphere. Nonetheless, this project focuses entirely on beam radiation because of its major role on concentration and PV energy production in general. In the design of solar concentrators, an emphasis is often put on modeling the beam component of solar radiation (Wong and Chow, 2001). This is arguable from the fact that the proportion of direct radiation is commonly taken as 90% of the global radiation as a general approximation (Kelly and Gibson, 2009). Besides, the deterministic nature of beam radiation allows for its geometrical analysis to turn into comprehensive design insights.

The modeling of beam radiation and its interactions with solar devices can be approximated numerically with ray-tracing algorithms which, in the case of solar beam radiation, are simulated with parallel light rays, that project themselves from the direction of solar incidence and behave according to the laws of geometrical optics. Ray-tracing algorithms follow the path of a large number of solar rays in order to calculate the light intensity at the PV surface (Duffie and Beckman, 2013). For instance, Bojić et al. (2015) modeled beam radiation in sea-shell shaped solar concentrators with specular ray-tracing methods. Burkhard et al. (1978) reported that numerical Monte Carlo models have been used to calculate the concentration factor of solar V-Troughs. Similarly, Maiti et al. (2012) developed a Monte Carlo ray-tracing model in order to study the effects of the angular variations of the V-Trough's reflectors. Other studies used ray-tracing techniques to analyze the performance of asymmetrical V-Troughs with mirrors designed to be reversed twice a year for a seasonal solar tracking (Chiam, 1981; Selçuk, 1979).

Numerical models based on ray-tracing algorithms allow for a flexible exploration of the geometrical parameters of V-Troughs. The calculations are performed at the level of each singular light ray and these rays can be programmed to interact with any optical device regardless of its macroscopic shape. Nevertheless, as Collares-Pereira and Rabl (1979) stated, "a computer can produce unlimited quantities of numbers, but it provides little intuitive understanding of functional relationships". These algorithms perform a simulation and focus on reaching a final performance result, but this does not mean that there is a real understanding of the macro-optical phenomena which is affecting this result. For instance, one might put a solar cell at a given position in a urban scenario and measure its electrical power output. This test will lead towards the final performance result but it does not empower an intuitive comprehension that can provide a deep design insight into inquiries of the situation, such as: are there shadows in the surroundings blocking part of the sunlight?, is the cell's position optimal for that instant or for that day of the year?, are the nearby windows reflecting sunlight towards the PV surface? and so on. This is the kind of intuitive understanding that can empower design and engineering decisions when pursuing V-Troughs for personalized scenarios, yet numerical models are not in accordance to this.

Moreover, ray-tracing usually required from hundreds (León et al., 2011) to tens of thousands (Ha et al., 2017; Pei et al., 2012) of simulated light rays in order to provide a useful optical result from just one direction of solar incidence. The bigger the number of rays, the greater the precision. If the simulation is supposed to account for the solar apparent movement throughout the day, then this considerable amount of rays and calculations must be repeated for every solar elevation to be considered. This can be problematic and constraining, since the purpose of this project to support a flexible exploration of V-Trough geometries, means that the selected modeling approach should effectively be able to simulate potentially hundreds or thousands of geometrical set-ups. Referring to a similar situation with ray-tracing models, Collares-Pereira and Rabl (1979) stated that "even though the computing time is inconsequential for a few sample simulations, the large number of parameters to be considered will make any meaningful system optimization or comparison study costly and time consuming". Backward ray-tracing has managed to make the simulations considerably more efficient, but this technique has been reported to not work properly for concentrators with non-imaging optics (Su et al., 2012). Monte Carlo ray-tracing algorithms manage to obtain a meaningful result with fewer rays because they are projected from random positions as opposed to equally separated rays. However, for non-imaging optics, it has been reported that even millions of Monte Carlo rays may still be required (Taylor, 2000). Therefore, numerical models based on ray-tracing techniques appear to be impractical for the goals of this research project and not rich enough in terms of the intuitive understanding that can be interpreted from their simulations.

On the other hand, radiation models which are based on analytical calculations tend to be considerably less computationally expensive when it comes to simulating radiation (O'Kane et al., 2014; Sheng et al., 2013). Analytical modeling can be defined as "to seek for mathematical functions and equations that are

obtained from the closed-form (exact or approximate) solution to the original physics-governing equations" (Li, 2015a). Solving these closed-form equations usually requires several orders of magnitude fewer calculations as compared to primarily numerical models such as with ray-tracing. Even if the analytical equations require a numerical method to be solved, such as with the Bisection method (Hamming, 2012), it is very likely that there are less iterative calculations needed as opposed to the simulation of potentially millions of light rays. Analytical models are used to build behavioral models, which "are the most generic and effective forms describing the response of the system" (Li, 2015b). An analytical equation states the mathematical relations which describe the behavior of a physical entity. Consequently, the solar radiation models that are based on analytical calculations, tend to enable a deeper understanding of the causal relations in the phenomena addressed.

A plurality of analytical V-Trough models were found reported in the literature going from the pioneering studies of Hollands (1971) to the most recent variations of Bahaidarah et al. (2015). Most of these models were found to be analytical in terms of space, but numerical in terms of time. These models define analytical relations between the geometrical set-up of the device and the solar elevation. Hence, there are fully analytical expressions, which describe the optical performance at the specific time of the day, corresponding to a given solar elevation value. Therefore, the spatial relations are fulfilled analytically. However, as the sun changes its elevation angle throughout the day, the standard procedure is to evenly divide this trajectory in discrete steps and solve the spatial analytical model for every solar step. This procedure is hence a numerical solution in terms of time because the solar elevation is defined in function of discrete instances of time. This is a practical approach because it still considerably reduces the number of calculations per every spatial frame, as compared to fully numerical models, and yet conserves the mathematical simplicity. In principle, these models could otherwise be integrated for the solar elevation range in order to have a fully analytical solution in both spatial and time frames. However, it is not always possible or practical to solve the integrals defined from the V-Trough spatial models. As a general rule, the more flexible these models are, the more mathematically complex they become and hence, the more difficult it is to solve the integrals for a time range.

The modeling of the optical performance of a V-Trough is greatly dependent on the assumed or defined cardinal positions of itself and the plane where the solar path is contained. The relations between these two positions affect the angle of solar incidence. This angle is hence a three-dimensional phenomenon aligned with the solar apparent trajectory across the sky-dome. However, this trajectory can be simplified as two-dimensional if projected into two orthogonal planes: one aligned with the longitudinal axis of the V-Trough and the other plane defined as transverse to the device. The solar elevation projected into the transverse plane is key in determining the optical behavior of the device and directly conditions the macro-optical interactions. On the other hand, the solar elevation projected into the longitudinal plane is often considered to only affect the overall optical performance in a progressive magnitude variation according to the so-called "cosine effect": The effective harvesting area diminishes with the cosine of the angle of misalignment between the longitudinally projected solar elevation and the normal to the PV surface (Taylor, 2000; Bannerot and Howell, 1979; Burkhard et al., 1978). In fact, most of the reported beam models are mainly two-dimensional models because the longitudinal plane is only considered with the cosine effect, while most of the modeling emphasis is placed on the transverse plane (Bahaidarah et al., 2015; Tina and Scandura, 2012; Tang and Liu, 2011; Kostić et al., 2010; Reis et al., 2010; Hermenean et al., 2009; Sangani and Solanki, 2007; Bione et al., 2004; Fraidenraich, 1998, 1992; Burkhard et al., 1978; Mannan and Bannerot, 1978; Seitel, 1975; Hollands, 1971). This two-dimensional nature has allowed for a simpler and more intuitive mathematical modeling. Only three V-Trough studies, concerning an analytical modeling of beam radiation, were found to be essentially three-dimensional (Pucar and Despic, 2002; Garg and Hrishikesan, 1988; Taha and Eldighidy, 1980).

All the studies reviewed, except for (Pucar and Despic, 2002), assessed the tracking adjustments in axes parallel to the longitudinal plane of the device. If the V-Trough is set to perform seasonal tracking, but it remains fixed during daytime, the device is usually positioned so as to align its longitudinal axis in an East-West direction (Mannan and Bannerot, 1978; Hollands, 1971). In these cases, depending also on the latitude and the Earth's declination angles, the solar diurnal trajectory is mostly evidenced and modeled in the longitudinal plane while tracking occurs several times a year in the transverse plane. On the other hand, if diurnal tracking is assumed, then the longitudinal axis of the device is taken to a North-South direction.

Table 2.1: Geometrical and optical capacities of reported beam analytical models for V-Troughs. See the footnote.[1]

Analytical models →	[1]	[2]	[3]	[4]	[5]	[6]	[7]	[8]	[9]	[10]	[11]	[12]	[13]	[14]
Year of publication	1971	1975	1978	1978	1980	1988	1992	1998	2002	2009	2010	2010	2011	2012
Later implementations			[15]					[15][16]				[17]		
Asymmetry allowed		•			•	•			•			•		
Non-uniform at PV allowed		•			•	•	•		•			•	•	
Misalignment allowed	•	•	•	•	•	•	•	•	•	•	•	•	•	•
1 Mirror allowed		•			•	•			•			•		
2 Mirrors allowed	•		•	•		•	•	•		•	•	•	•	•
Unrestricted lengths		•			•	•								
Unrestricted Aperture		•			•	•			•			•		
1^{ry} shadows considered	•		•		•	•	•	•	•				•	
2^{ry} shadows considered														
>1 Reflection considered			•				•	•					•	
Edge losses considered					•	•			•					

In these cases, the solar diurnal trajectory is mostly evidenced and modeled in the transverse plane as well as the tracking movements.

The reported beam analytical models range in different levels of input geometrical flexibility. Depending on the particular interests of the study, these models make certain assumptions that enable a simplification of the modeling framework. The more assumptions are made, the more restricted the geometrical flexibility becomes. Also, these simplifications mean that fewer macro-optical phenomena are considered, which limits, to varying degrees, the modeling output detail and the level of richness of intuitive interpretations. Table 2.1 presents a comparison of the geometrical and optical capacities of reported beam analytical models for V-Troughs.[1] Approximately 36% of the models allow an asymmetrical configuration. These are also the same models which have an unrestricted aperture angle (traced between both mirrors). Hence, the other 64% of the models do not allow for a flexible exploration of each individual mirror. In some scenarios, a one mirror set-up might be more convenient than two. Nevertheless, the capacity to flexibly explore this possibility is only allowed by 14% of the reported models, namely the works of Garg and Hrishikesan (1988) and Kostić et al. (2010). 36% of the reviewed models allow a configuration with one mirror, while a 79% allow two mirrors; which is more usually expected for a V-Trough concentrator. All models allow for misalignments in the angle of solar incidence. This enables an exploration of tracking strategies which are not necessarily perfect in the sense of keeping the PV surface always normal to the incoming sunlight.

Half of the reviewed models assume uniform illumination throughout the PV surface for an allowed tracking misalignment range. In order to fulfill this assumption, these models impose geometrical restrictions and interrelations for the lengths of the mirrors and/or their aperture angle. Besides this assumption of uniformity, there are other reasons for restricting the lengths and the aperture angle, such as a mathematical modeling of a narrow range of optical scenarios. This is why only three models, the 21%, allowed both unrestricted lengths and aperture angle. Also, only four models, the 29%, considered the possible effects of more than one consecutive reflection between the mirrors. 8 models, more than half, considered the primary shadows that can be caused by any of the mirrors over the PV surface. However, no reviewed model makes a comprehensive study of the secondary shadows, such as the ones caused by one mirror over the other one for the first incoming rays of after a reflection, or the shadows that the PV surface may create over one of the mirrors in more unconventional positions. Three models are three-dimensional in nature and, this way, they manage to account for the edge reflection losses that may have an effect when there is a misalignment in the longitudinal orientation; namely the models reported by Taha and Eldighidy (1980); Garg and Hrishikesan

[1] [1] Hollands (1971); [2] Seitel (1975); [3] Burkhard et al. (1978); [4] Mannan and Bannerot (1978); [5] Taha and Eldighidy (1980); [6] Garg and Hrishikesan (1988); [7] Fraidenraich (1992); [8] Fraidenraich (1998); [9] Pucar and Despic (2002); [10] Hermenean et al. (2009); [11] Reis et al. (2010); [12] Kostić et al. (2010); [13] Tang and Liu (2011); [14] Tina and Scandura (2012); [15] Sangani and Solanki (2007); [16] Bione et al. (2004); [17] Bahaidarah et al. (2015).

(1988); and Pucar and Despic (2002). The other models rely on the "cosine effect" (described above) in order to account for the longitudinal misalignment but ignore the possible edge losses.

The analytical model presented by Garg and Hrishikesan (1988) was found to be the most comprehensive in terms of its geometrical and optical capacities and considerations. Nonetheless, even this complex three-dimensional model is ignoring the possible secondary shadows and double reflections. The broad and flexible exploration of the V-Trough geometries, intended by this research project, would hence be directly constrained or lead towards misleading results if the modeling were to be performed with any of the analytical models found in the literature. Also, the reported analytical models are not satisfactory in terms of the detail of their outputs concerning the macro-optical phenomena. While they consider several of these phenomena in the overall calculations and certain geometric inflection points, they do not provide explicit expressions to interpret the role of each phenomenon involved. For instance, the only reference that Burkhard et al. (1978) make regarding shadows is "Discontinuities in the slopes of the curves correspond to the onset of shadowing". Their model hence considers shadows but they do not provide the expressions to directly address this macro-optical phenomenon that could very well support the decision making process. Consequently, it was found that none of the found analytical models are satisfactory in terms of their flexibility in the geometrical input parameters, nor in the extent to which they address the macro-optical phenomena involved. Moreover, numerical models based on ray-tracing techniques are not practical due to their computational demands. Nor are they rich enough in terms of the limited intuitive insights that can be drawn from their simulations. The statement of French (2002) highlights the importance of this matter: "Progress [in a design problem] depends on the related tasks of recognizing the key issues and developing insight into the problem, both of which demand work on the engineering science".

Simulating a detailed optical performance can empower design insights. Performance indicators and indices can condense these results and offer an objective perspective for comparing set-up alternatives. Table 2.2 presents a classification of the performance indicators and indices drawn from the analytical modeling of V-Trough devices in reported studies. It can be seen that "Effective concentration" is the most used indicator, present in 53% of the studies; followed equally by "Absorbed|output power" and "Absorbed|output energy", each present in 29% of the studies.

Table 2.2: Performance indicators and indices drawn from V-Trough analytical models. See the footnote.[1]

Analytical studies →	[1]	[2]	[3]	[4]	[15]	[5]	[6]	[7]	[8]	[16]	[9]	[10]	[11]	[12]	[17]	[13]	[14]]
Geometrical concentration				•				•	•								
Effective concentration	•		•		•				•	•			•	•		•	•
Enhancement vs. ref						•					•						
Incident power|irradiance											•	•		•		•	
Absorbed|output power		•				•	•						•		•		
Incident energy											•	•				•	
Absorbed|output energy		•				•	•		•				•				
Energy efficiency														•		•	
Cost per aperture area									•								
Cost of energy									•								

These studies do not necessarily use the indicators and indices with the exact presented terms, but they do fall into narrow categories:

- **Geometrical concentration**: A ratio of the aperture area over the PV area. As seen in both tables 2.2 and 2.1, none of the studies using this indicator allowed for asymmetry. Therefore, this ratio, combined with the aperture angle, characterize the V-Trough geometry and suggest a rough estimate of the resulting harvesting area.
- **Effective concentration**: A ratio of the expected irradiance at the PV surface over the irradiance at the aperture of the device before being concentrated. It can also be defined as the effective harvesting area over the aperture area or over the PV area. Regardless of the variations found, this indicator measures the optical effectiveness of a given set-up for harvesting the solar radiation, particularly the

beam component. This indicator can be presented as instantaneous or as an average for a range of time or solar elevations.

- **Enhancement vs. ref**: Describes the gain in optical performance, instantaneous or averaged, of a given V-Trough set-up as compared to a reference set-up. The reference is usually a flat panel with the same inclination or in a horizontal disposition.
- **Incident power|irradiance**: A direct calculation of the instantaneous solar power $[W]$ or irradiance $[W/m^2]$ expected to reach the PV surface.
- **Absorbed|output power**: This indicator goes further than the previous one by also considering the capacity that a given PV surface has to absorb the incident radiation and convert it into electrical energy.
- **Incident energy**: A direct calculation of the solar energy $[Wh]$ expected to reach the PV surface in a given period of time.
- **Absorbed|output energy**: This indicator goes further than the previous one by also considering the capacity that a given PV surface has to absorb the incident radiation and convert it into electrical energy.
- **Energy efficiency**: A ratio of the energy reaching the PV surface over the energy reaching the aperture area. It can also be calculated with the electrical output energy.
- **Cost per aperture area**: The capital cost of the device per aperture area. It considers the cost of the main materials, reported in area cost indices, and can also consider the cost of a reference solar tracker.
- **Cost of energy**: A relation between the capital cost of the device and the cost of the electrical energy that the device is expected to produce during its entire lifespan.

A V-Trough is not a cost-effective strategy if the chosen set-up increases the materials cost more than it increases the effective harvesting area. Several simple cost-effectiveness analysis were found in the literature which compare the proportional gain in solar harvesting with the proportional increase in capital cost due to the materials needed for the mirrors and additional supporting structure (Sangani and Solanki, 2007; Tina and Scandura, 2012; Kostić et al., 2010; Lo et al., 2015). Among the studies reviewed, only Fraidenraich (1998) proposed an index, drawn from analytical modeling, which directly addresses this. The cost calculations are based on the basic geometry of the device and reported area costs $[USD/m^2]$ of the main materials involved. However, this index was specifically tied to the beam radiation model he proposed, which is not considered satisfactory for the aims of this research project.

The described indicators and indices serve as a valuable reference for this research project in order to determine how to support the definition of the V-Trough parameters. Aligned with the scope of this research project, some of the reviewed studies used performance indicators and indices directly drawn from the modeling of beam radiation (Hollands, 1971; Hermenean et al., 2009; Tang and Liu, 2011). The other studies based their indicators and indices also on the modeling of diffuse radiation.

2.2 Interactive Tools for V-Trough Design and Engineering

Product design is a complex endeavor and, in the case of solar devices, it can be better guided with the support of tools that enable the designer/engineer to explore the consequences of new product configurations in an insightful and straightforward manner. An ever increasing use of simulation and modelling tools throughout the design process is a clear trend in product design and engineering (Fischer and Coutellier, 2006; Vergnano et al., 2015; Savio et al., 2013). In accordance with the *Interactive Design* theoretical framework, these tools may be used to actively support the designer in the preliminary design phase, allowing for a greater insight into the implications of early decisions (Fischer and Nadeau, 2011). As described in Sec. 1.2, there

is a vast number of possible V-Trough set-ups when a further geometrical flexibility is allowed. In order to help navigate the space of possible solutions, an interactive tool may make use of the intuition of a trained engineer and the visualization of the optical performance. Moreover, in the pursue to democratize the exploration and adoption of the V-Trough technology for personalized scenarios, such a tool should be intuitive and practical in terms of the knowledge needed and computational demands.

Accordingly, reported interactive tools which are relevant to that matter are discussed as follows. Design interactive tools can be classified as either generative or evaluative (Shaviv, 1999). Generative tools are meant to guide in the definition of the main geometry of a possible design solution. They require little input data regarding the design scenario and hence are of particular use in the early design stages. On the other hand, evaluative tools are meant for a thorough performance analysis of a given detailed design proposal in a detailed scenario. Thus, evaluative tools are directed towards more advanced design stages. Generative tools are hence of special interest because this research project is contextualized in the early design stages and the desired output is a general geometrical set-up.

Several interactive softwares were found which can be used to support the development and exploration of photovoltaic devices. For instance, PVsyst® is a widespread software used to support the development of new solar projects by guiding the user, in early stages, in the definition of general parameters of the system (Kumar and Sudhakar, 2015). Nevertheless, it is too limiting in terms of tracking and concentration exploration for new devices. Other softwares offer more design flexibility by focusing on a detailed simulation of the optical performance of a solar device by means of ray-tracing methods. RaySim6® is a graphical user interface which can be used to perform a ray-tracing analysis of "glass static concentrators" (Cotter, 2005). However, it is not directly useful for V-Trough geometries and a typical simulation reportedly requires an average of 10 million trace operations. Radiance® is a suite of programs, for the analysis and visualization of lighting in design, that might be used for V-Troughs since it can deal with specular reflections (Compagnon, 1997). However, this is an evaluative tool which requires a highly detailed previously defined geometry of the context and the object of interest. Similarly, Photopia® has been reported to produce comprehensive performance evaluations for non-imaging optical designs and has already been used in a study for a solid dielectric compound parabolic concentrator in a combined PV and daylighting application (Yu et al., 2014). This is also an evaluative tool for detailed CAD (Computer Aided Design) based simulations. Yew et al. (2015) used a comparable evaluative tool, so-called LightTools®, in a study with compound parabolic concentrators as secondary optics. Other powerful tools, such as TracePro® (Sun et al., 2016) and SolTrace® (Le Roux, 2016), were found as suitable in terms of visualization and geometrical capacities for solar concentrators with tracking.

Some of the interactive tools reviewed are satisfactory in terms of geometrical flexibility and intuitiveness in the visualization of the optical performance. However, the tools which were suitable in that regard, were evaluative tools for a more advance design stage. Also, these tools were based on CAD three-dimensional models and ray-tracing numerical algorithms, which is not a practical solution for an effective exploration of a broad space of solutions. A simpler and more effective approach could be a V-Trough dedicated interactive software based on an analytical core.

2.3 Optimization Methods for V-Trough Devices

This section seeks to address what has been done in literature concerning the optimization of V-Trough solar devices. Heuristic optimization methods are presented as a suitable approach, in particular Genetic Algorithms (GAs). As follows, there is hence a review on GAs implementations in solar matters and specific genetic heuristics which are of interest for this study. As defined by Pearl (1984), "heuristics stand for strategies using readily accessible information to control problem-solving processes in man and machine". Neth and Gigerenzer (2015) stated that "people routinely rely on heuristics not because they are irrational, but because they have to make decisions under uncertainty". Applying this concepts to optimization, metaheuristics can be seen as a general algorithmic framework that selects among different heuristic strategies and can be applied to a wide set of different design/engineering problems (Dorigo et al., 2010).

In the majority of the V-Trough studies found, the optimization process is based on performance curves obtained numerically (Selçuk, 1979; Tang and Liu, 2011; Fraidenraich, 1998; Bione et al., 2004; Chiam,

1982; Mannan and Bannerot, 1978; Kostić et al., 2010; Bannerot and Howell, 1979; Chiam, 1981; McDaniels et al., 1975). A given geometrical parameter is iterated within an allowable range while leaving the other parameters fixed. An analytical model is then successively recalculated. This way, it is possible to generate families of performance curves, or nomograms (Bannerot and Howell, 1979), where the optimum points are usually evidently distinguishable. Conversely, Maiti et al. (2012) assessed a V-Trough based on a numerical Ray-Tracing model, which they iterated in order to find an optimum value for the inclination of the mirrors. Nevertheless, the previous work does not specify how the iteration was performed or how it led towards an optimum. By means of these iterative methods, parameters such as the aperture angle (Tang and Liu, 2011) and the inclination of each mirror (Selçuk, 1979; Chiam, 1982, 1981; McDaniels et al., 1975), or of the solar absorber (Tang and Liu, 2011; Bannerot and Howell, 1979), have been effectively optimized. Satisfactory results can be achieved in highly constrained case studies, where the iteration process can be limited to only one or two parameters varying within narrow ranges. However, this approach may be unpractical or too restrictive for a more flexible set-up exploration. It is not possible to simply find the optimum value of one parameter and then continue with the next one because the optimum value of every parameter is in function of the others. For instance, the best inclination for the left mirror depends on its length, as well as on the disposition of the other elements relative to that mirror and the solar rays.

On the other hand, Taha and Eldighidy (1980) explored the angular position of the solar absorber and one adjacent mirror with Pattern Search, an optimization metaheuristic. This method allows for a progressive variation, of multiple parameters, in the direction of improvement. Nevertheless, the nature of Pattern Search makes it vulnerable to getting stuck in a local optimum.

A genetic algorithm metaheuristic may offer a way to perform a broader and more unbiased exploration of the solution space. When more traditional methods are not applicable, genetic algorithms can be an effective way to navigate an extensive space of possible configurations looking for an optimal (or near-optimal) solution in design and engineering matters (Roupec, 2011; Randall, 1995; Shiffman et al., 2012; Hilbert et al., 2006; Eremia et al., 2016). Genetic algorithms are based on the biomimicry of Darwinian evolution principles (Shiffman et al., 2012). Following this biological metaphor, V-Trough devices can be regarded as animals whose DNA (genetic information) determines the geometrical parameters of their mirrors and the PV absorber and the way in which they move in reaction to the solar apparent movement. Within a genetic algorithm, these "V-Trough beings" would be arranged in a diverse population where every individual may have a different physiology (set-up). Through a series of processes, inspired by sexual reproduction and biological mutation, this population can evolve throughout a given amount of generations. The evolutionary progress seeks to converge into the best explored solution in terms of a given objective function. Genetic algorithms offer the opportunity to overcome possible design biases, find non-intuitive solutions and even to effectively and consistently converge for personalized scenarios.

GAs have already been used for solar applications. Khlaichom and Sonthipermpoon (2006) used a GA to actively fine-tune the tracking position of a solar panel. Similarly, Chen et al. (2005) optimized the installation angle of a fixed solar panel with a GA. Still, no study has been found in the literature in which genetic algorithms are used to optimize solar V-Troughs. This is relevant because the efficacy and efficiency of genetic algorithms is highly problem-dependent (Roupec, 2011; Brest et al., 2006). Moreover, GAs can use different heuristics for each of the evolutionary steps; heuristics which are themselves more or less effective depending on the problem and the other complementing heuristics within the GA.

Several heuristics have been reported to improve the performance or the adaptability of a GA. For instance, with Elitism, a proportion of the best performing individuals passes to the next generation as part of the offspring (Chen et al., 2005). Elitism can speed up the convergence process and avoid losing the best solutions of a given generation (Deb et al., 2002). Mutation, which introduces diversity and reduces the premature-convergence tendency, can also be implemented from different heuristics (Hermawanto, 2013). One interesting heuristic approach is the "non-uniform mutation", where the mutation values progressively become smaller in order to advance from a wide exploration to a local search (Zhao et al., 2007). The mutation values are usually determined through uniform randomness, where any value within an allowable range has the same probability of occurring (Khlaichom and Sonthipermpoon, 2006; Magalhães-Mendes, 2013). As with biological mutation, this is not always reasonable, since large mutations are commonly unlikely. To address this issue, mutations have reportedly been controlled by probability distributions. The most common is the Gaussian distribution, but Lee and Yao (2004) found that the Cauchy distribution may

result in a superior performance in certain problems where bigger mutation values are beneficial. Given the success of this alternative control for mutation, it is desirable to pursue further flexibility in how such distributions can adapt towards different levels of mutability. However, the heuristics reported in this regard are still too restrictive.

It can be therefore stated that there is a need for an assessment of genetic algorithms, with different heuristics, as tools for determining the geometrical parameters of solar V-Troughs. Additionally, there are certain heuristic procedures, for flexibly controlling mutation, which could benefit the GAs performance in this assessment but which are missing in the reviewed literature.

Chapter 3

Proposal of a Beam Radiation Model for V-Trough devices

The objective of this section is to propose a theoretical model of the macro-optical phenomena of beam radiation in photovoltaic V-Troughs with manual tracking. The main purpose of this model is to determine the effective concentration of a given V-Trough set-up in a way which can support a flexible definition of its parameters in a personalized household context. Therefore, given the vast number of possible V-Trough set-ups, the model was determined to be mainly analytical, as opposed to the more computationally demanding numerical models (explained in Sec. 2.1). As detailed in Sec. 1.2, this model should also allow a flexible definition of each of the main geometrical parameters as independently fixed or dynamic. In order to favor this flexibility in the geometrical input parameters of the model, the relevant macro-optical phenomena should be identified, modeled and presented in a way that can develop insight into the design/engineering problem. For reasons described in Sec. 1.2, the model follows the mathematical tools and theoretical simplifications of geometrical optics. This section provides a solution to the specific objectives I and II: The relevant modeling variables are identified in Sec. 3.1 and the mathematical relations among them are established in Sec. 3.2.

Not only was the model developed for interactive design purposes, but it was also itself produced through a process aided by interactive design tools. The model was developed in a parallel and systematic approach, where:

- The modeling problem was divided into smaller and simpler optical interaction phenomena, for which corresponding variables were assigned.
- For every variable, an analytical equation was developed, through a geometrical assessment of the particular phenomenon being addressed, in order to achieve the capacity to predict it.
- By using Microsoft Excel®, each new equation was added to the previous ones and then numerically solved for a whole range of solar elevations. This way, it was possible to simulate its behaviour throughout a solar day.
- The numerical data-set obtained with these simulations was directly inspected in search of mathematical errors and possible inconsistencies. The data-set was then visualized through Microsoft Excel® graphs, where a first interpretation of its behaviour took place and inflection points were inspected.
- Several static scenarios (for a given solar elevation) where selected from points of interest in the graphs and then further visualized in a three-dimensional space by means of SolidWorks®, a Computer Aided Design Software (CAD).
- The SolidWorks® Sketch module was used to verify the predicted values for the variable being addressed. This is possible because the specific predictions of the theoretical model can be interpreted as geometrical dimensions and ratios. The verification process was performed by modeling the light rays with CAD sketch lines defined to behave according to the laws of geometrical optics.

The described process was carried out until all the identified variables were mathematically described, visualized, verified and added to the main model. Through this systematic approach, aided by the integration of interactive design tools, it was possible to make intuitive sense of every variable being modeled and the geometrical implications and detailed causes of the model's predictions.

In the following subsections, a conceptual model is defined by delimiting the addressed phenomena and schematically interrelating the main variables to be considered in accordance with the beam radiation interactions. The geometrical construction of the model is then described, comprising an analytical framework. Afterwards, as an example of how to use and interpret the model, the optical beam performance of a given V-Trough set-up is analyzed for three different solar elevations.

3.1 Definition of the Conceptual Model

This section presents the geometrical exploration of the macro-optical phenomena involved; how it resulted in the definition of the conceptual model; and the assumptions and constrains of the modeling framework. A conceptual model "involves all processes, which could be relevant for the studied system" (Holzbecher, 2012). Conceptual models can be also taken as "expressed mental models that can be defined as an accurate, reasonable representation of natural phenomena" (McNeal et al., 2008).

The optical performance of a V-Trough is greatly dependent on the relative angle between its elements and the incident solar rays. Therefore, in order to develop a conceptual model of this, it is necessary to understand the phenomena that affect the angle of solar incidence in relation to a V-Trough's positioning. The behavior of the solar apparent trajectory across the sky-dome determines the solar elevation as measured from a horizontal plane. The solar path for a given day is contained in a plane. However, this plane is not always perpendicular to a horizontal plane. Therefore, the solar elevation throughout the day can not be entirely described only from one plane which is orthogonal to the horizontal plane. This is caused by two geometrical entities described as follows, namely the latitude and the declination angle.

The declination (δ) is the angle between the incident solar rays and the plane containing the Earth's equator circle (Maatallah et al., 2011). As depicted in Fig. 3.1, the Earth's rotation axis is tilted 23.45° (Maatallah et al., 2011) from the Celestial North (CN). CN is a vector that is normal to the celestial plane, which contains the Earth's orbit trajectory around the Sun.

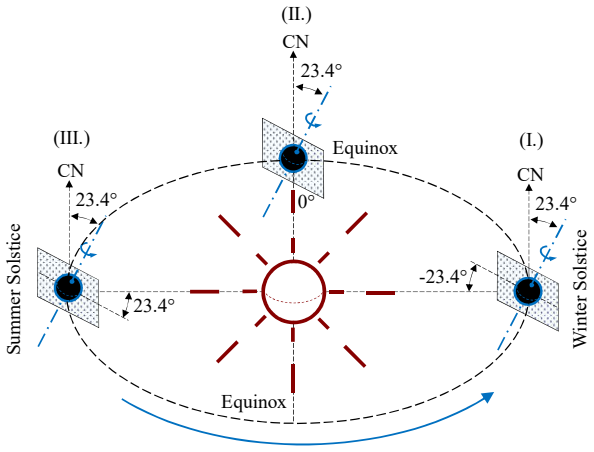

Figure 3.1: Earth's tilted axis and Sun-Earth radiation interactions.

From a perspective as shown in the figure, the Earth's axis remains tilted in the same direction as it moves around the sun. Since the inclination of the equatorial plane is fixed, but the direction of solar incidence is not, the declination changes throughout the year. As shown, the winter solstice represents the time of the year when the axis is most tilted away from the incident solar rays and hence δ reaches its lowest

possible value; while the summer solstice represents the opposite. During the two yearly equinoxes, the solar incident rays are aligned with the Earth's equatorial plane, so $\delta = 0°$.

Fig. 3.2 illustrates how declination (δ) and latitude (ϕ) can affect the solar incidence (θ) on a given surface during the key yearly moments, i.e., (I.) winter solstice, (II.) equinox and (III.) summer solstice. In

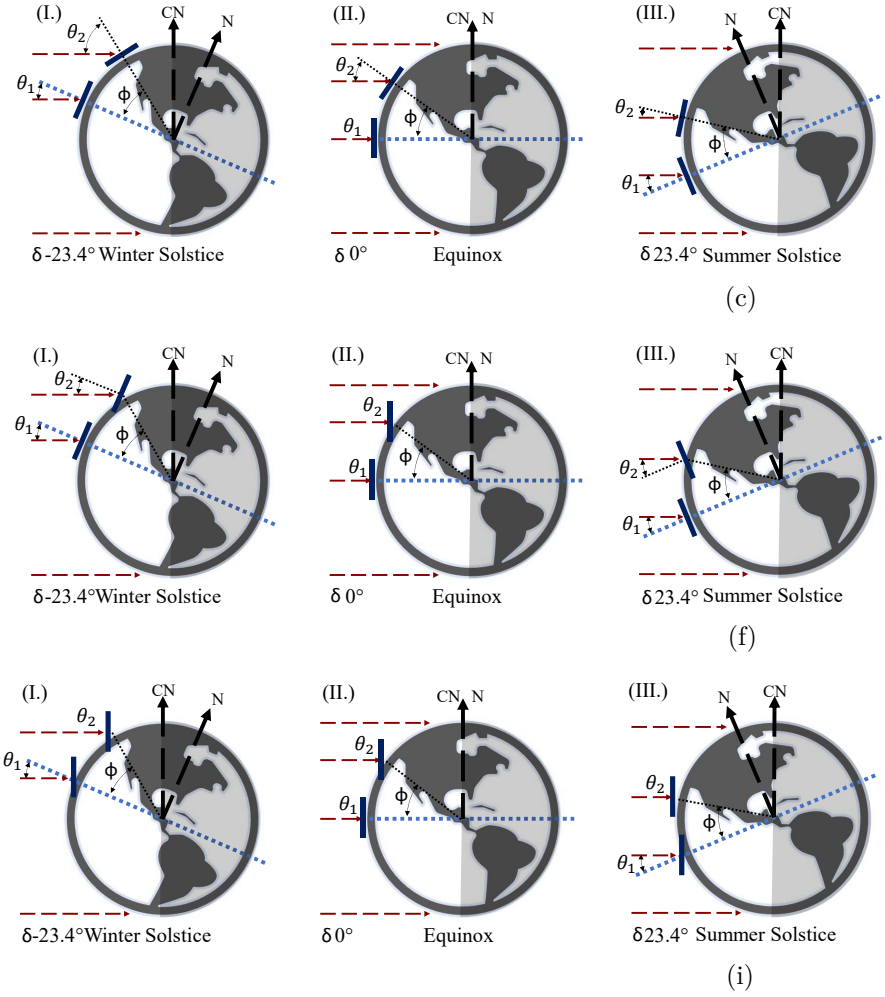

Figure 3.2: Solar incidence at noon affected by latitude (Φ) and declination (δ).

Figs. 3.2(a)–3.2(c) two flat surfaces are positioned horizontally according to their latitude. It can be seen that, for the equatorial ($\phi = 0°$) surface at noon, θ is affected only by δ. On the other hand, the θ in the other surface is affected both by δ and ϕ. Figs. 3.2(d)–3.2(f) illustrate the effect of tilting the upper surface as to counteract its latitude. In this case, $\theta = \delta$ for both surfaces as they become parallel to the Earth's rotation axis (N). The misalignment is opposite but symmetrical in the summer solstice (III.) as compared to the winter solstice (I.). It is worth highlighting that, even after a counter-latitude adjustment at noon, the solar rays will only be perpendicularly incident during the equinoxes (II.). Figs. 3.2(g)–3.2(i) show what is necessary for receiving the solar rays perpendicular to a given surface every noon, namely to adjust the angular position for both latitude and the Earth's declination at that particular day of the year.

Fig. 3.3 illustrates the previous phenomena from the perspective of a PV V-Trough located at $\phi = 23.4°$. This latitude is relevant to the focus of this research project because it is the maximum latitude that can be reached within the tropics ($-23.45° \leq \phi \leq 23.45°$), where most of the developing world is located (Kummu and Varis, 2011). It can be seen that the three key solar paths (winter solstice, equinoxes and summer

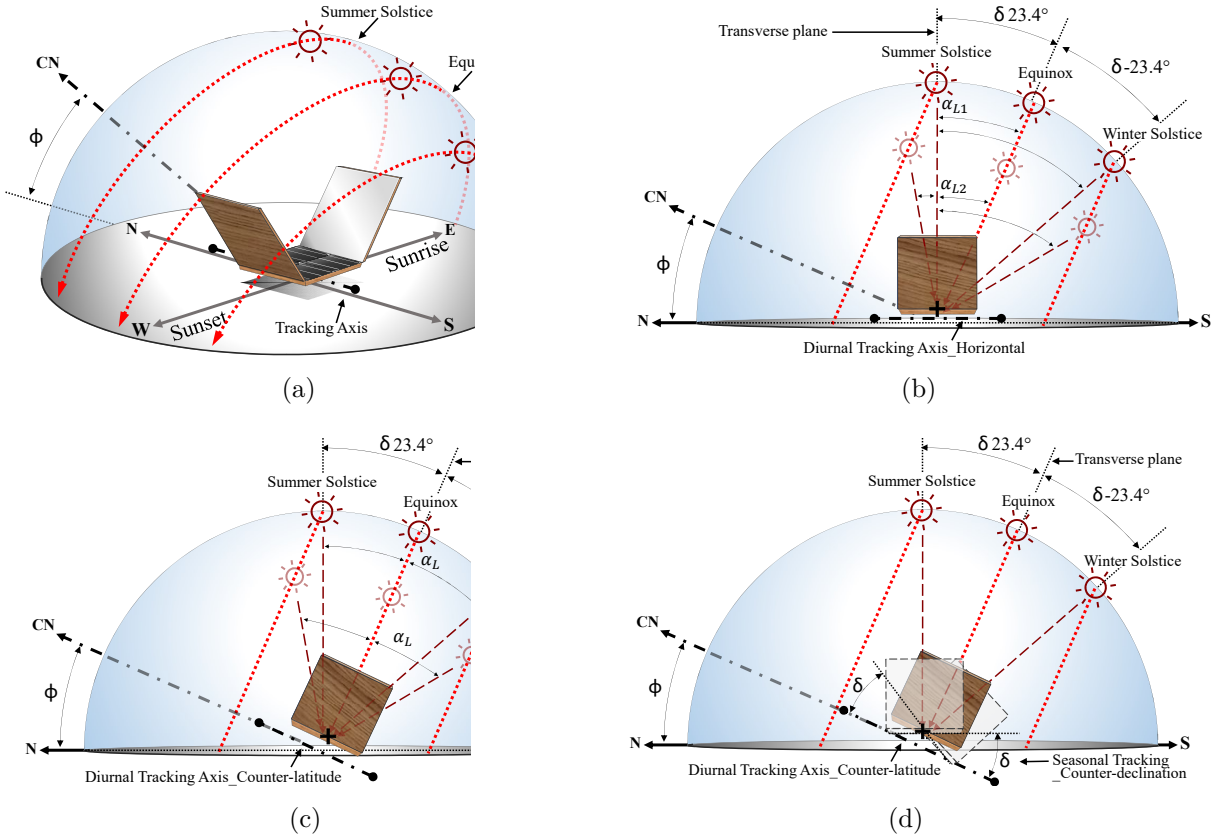

Figure 3.3: Solar paths from the perspective of a PV V-Trough located at $\phi = 23.4°$.

solstice) follow a trajectory which is radially equidistant to the Celestial North (CN); not to the Earth's North (N). Figs. 3.3(a) and 3.3(b) correspond to a horizontally placed V-Trough with its longitudinal axis aligned in a North-South direction. This V-Trough will receive solar rays perpendicularly only at noon during the summer solstice. At any other time of the year, the rays will have a longitudinal misalignment (α_L). In this case, α_L varies with the declination δ, which changes every day, and with the time of the day; so $\alpha_{L1} \neq \alpha_{L2}$. In Fig. 3.3(c) the V-Trough's longitudinal axis is tilted as to counteract the latitude of its location. This way, the magnitude of $\alpha_L = \delta$. Since δ is approximately constant during a given day, the longitudinal misalignment α_L is considered to be constant throughout the diurnal solar path across the sky-dome. This can be better visualized in Fig. 3.4, where the trajectory of the solar incidence during the solstices is depicted as two conic surfaces which are symmetric with respect to an equinox plane. If a V-Trough is positioned as in Fig. 3.3(c), its transverse plane aligns with the equinox plane. As a conic geometry implies, these rays will hence maintain their α_L as they revolve around their axis of symmetry, namely CN.

On the other hand, Fig. 3.3(d) illustrates the case of a V-Through with a tracking strategy that counteracts the effects of both latitude and declination. The latitude is neutralized by tilting the diurnal tracking axis in the same magnitude. In order to counteract the declination, the device must also be tilted away from its diurnal tracking axis, as shown in the figure. If this inclination is readjusted every day in a magnitude δ with respect to an axis for diurnal tracking which is itself tilted a magnitude ϕ, then it is possible to maintain $\alpha_L = 0°$ throughout the year. This is illustrated in detail in Fig. 3.5, where the longitudinal and transverse planes are shown. With this tracking procedure, the solar incidence can be fully described by a solar elevation α in the transverse plane.

For other configurations with diurnal tracking that do not counteract the latitude and declination,

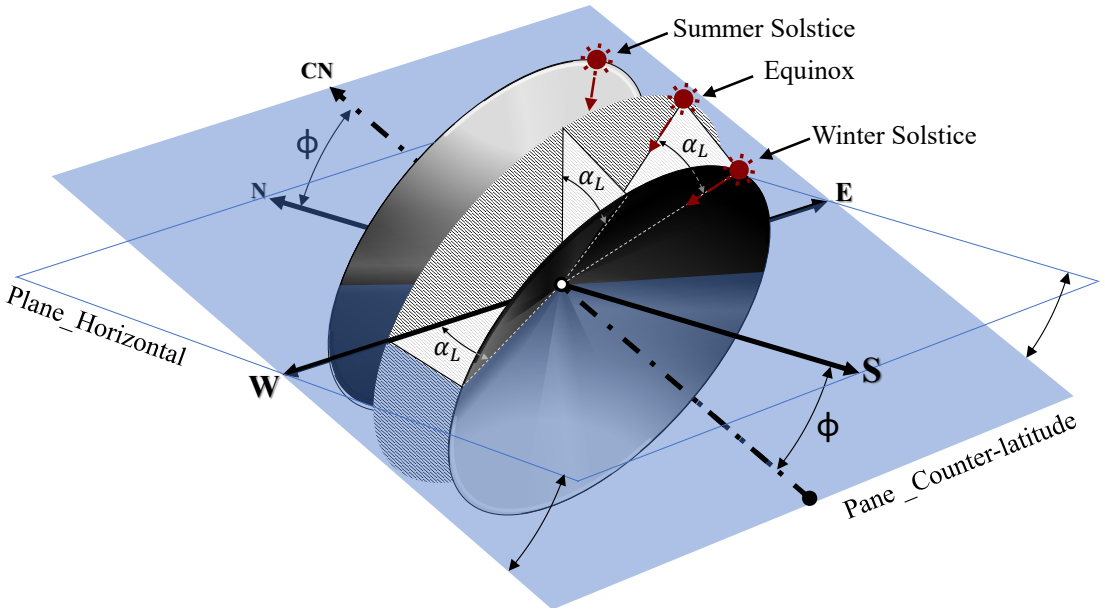

Figure 3.4: Solar incidence during summer solstice and winter solstice visualized with the analogy of symmetric cones.

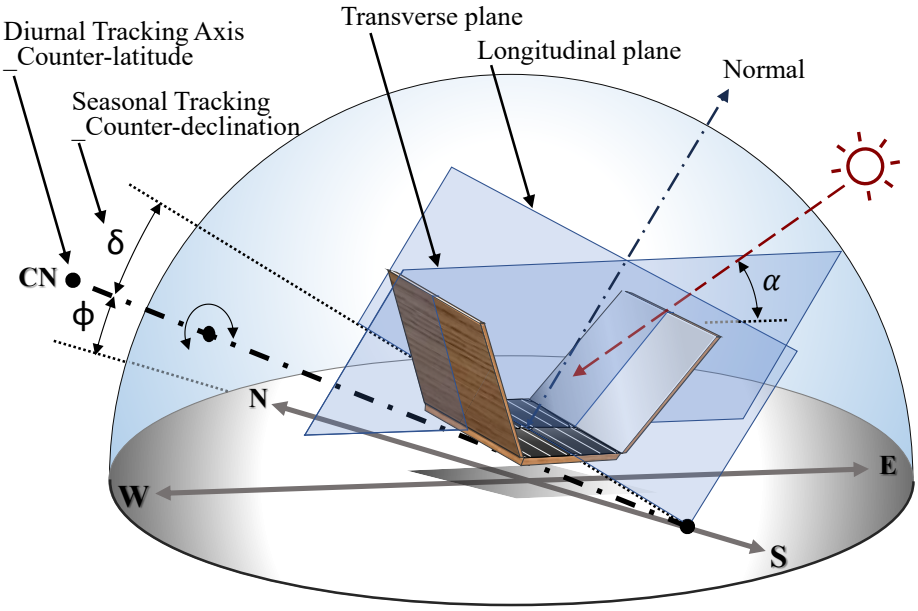

Figure 3.5: V-Trough adjusted to counteract latitude (ϕ) and declination (δ).

the impact of the longitudinal misalignment α_L on the optical performance can be modeled according to the "cosine effect" (Bahaidarah et al., 2015; Tina and Scandura, 2012; Tang and Liu, 2011; Kostić et al., 2010; Reis et al., 2010; Hermenean et al., 2009; Sangani and Solanki, 2007; Bione et al., 2004; Fraidenraich, 1998, 1992; Burkhard et al., 1978; Mannan and Bannerot, 1978; Seitel, 1975; Hollands, 1971). Hence, the more complex optical modeling can be focused on the transverse plane according to α. The focus of this research project involves diurnal tracking with the device pivoting around a North-South longitudinal axis. Conversely, if the intention is to model a V-Trough with seasonal tracking only, then its longitudinal axis would have an East-West alignment. In this case, the diurnal solar elevation α would be modeled with the

cosine effect in the longitudinal plane and the α_L misalignment would be modeled in the transverse plane. Either way, the modeling efforts are mainly focused on the geometrical interactions in the transverse plane.

The previous geometrical exploration provides a conceptual framework for the model to focus its assessment of the macro-optical phenomena in a two-dimensional analysis in the transverse plane. Any longitudinal misalignment will be considered only through the cosine effect. Additionally, the conceptual modeling is based on the geometrical parameters illustrated in Fig. 3.6:

- LPV (the length of the PV absorber)
- LL (the length of the left mirror)
- LR (the length of the right mirror)
- $Depth$ (the depth of the device)
- β (the angular position of the PV absorber)
- ψL (the angular position of the left mirror)
- ψR (the angular position of the right mirror)

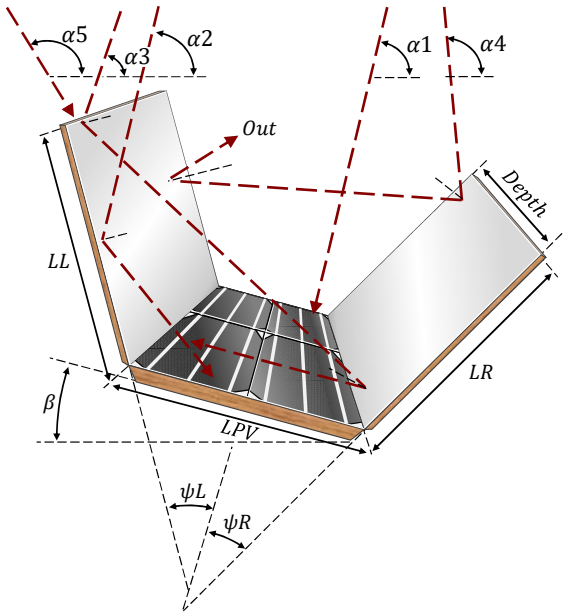

Figure 3.6: Solar ray paths in a V-Trough and main geometrical parameters.

Fig. 3.6 shows a series of solar rays, in different positions and with different solar elevations, corresponding to different macro-optical phenomena:

- At $\alpha 1$, the ray directly reaches the PV surface
- At $\alpha 2$, the ray reaches the PV surface after one bounce off a mirror
- At $\alpha 3$, the ray reaches the PV surface after two subsequent bounces off the mirrors
- At $\alpha 4$, the ray bounces twice and then heads outwards
- At $\alpha 5$, the ray is blocked by the left mirror which, from that solar elevation, produces a shadow over the PV surface (Primary Shadow) and over a lower portion of the right mirror (Secondary Shadow)

This first exploration illustrates the importance of considering a range of macro-optical phenomena that is broader than what is considered in most of the analytical models in the state-of-the-art (see Sec. 2.1). Fig. 3.7 shows a deeper geometrical exploration of the macro-optical phenomena involved and presents variables that can be defined in order to describe their behavior. The conceptual model considers the main variations in the effective harvesting area related to angles of incidence, reflections and shadows (primary and secondary; see Sec. 2.1). These phenomena can be described as sections of the device's area as projected in a plane which is perpendicular to the incident solar rays. Due to the way in which the V-Trough's geometries interact with the incoming rays, the macro-optical phenomena are expected to all share the same *Depth* dimension. Hence, they can be mainly described by their two-dimensional projection in the transverse plane. Accordingly, the model describes the interactions with beam radiation in terms of lengths, or apertures, perpendicular to the incident sunlight. These aperture lengths are directly proportional to corresponding areas that extend in a depth-wise third dimension (see Fig. 3.6).

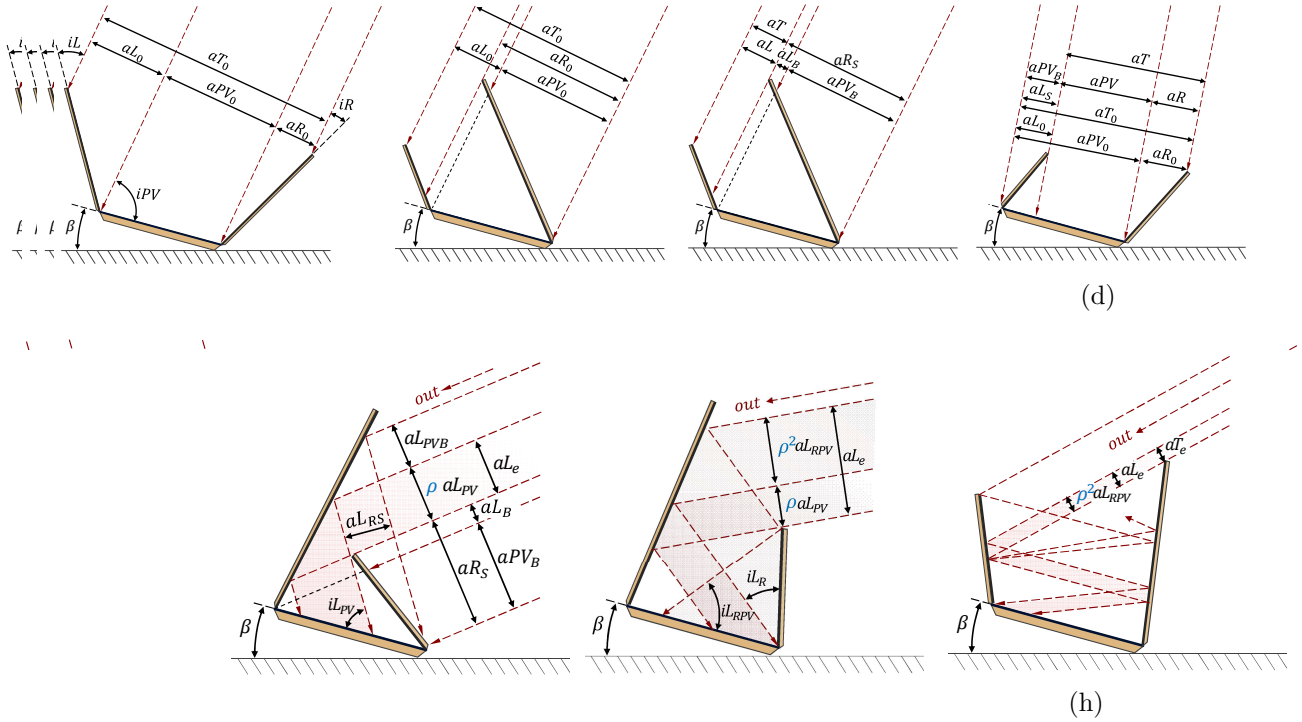

Figure 3.7: Variables describing a broad range of macro-optical phenomena in solar V-Troughs.

Fig. 3.7(a) shows the apertures lengths of *Geometrical Incidence* for every V-Trough's element. These variables (aL_0, aPV_0, aR_0 and the total aT_0) correspond to the lengths of these elements projected into a plane which is perpendicular to the sunlight. Hence, these projections must be dependent on the angles between these elements and the incoming solar rays (iL, iR and iPV). Fig. 3.7(b) presents a case where the right mirror does not contribute to the total aperture of *Geometrical Incidence*. In Fig. 3.7(c) it is shown how certain elements can produce shadows over the others. In this case, the right mirror produces a shadow (aR_S) that blocks a portion of the rays which were heading towards PV (aPV_B) and the left mirror (aL_B). In a similar case, Fig. 3.7(d) shows a left mirror producing a shadow (aL_s) which blocks a portion of the rays heading directly towards PV (aPV_B). The figure also shows the corresponding *Real Incidences* (aPV, aR and the total aT), namely the portion of rays which directly reach the PV surface or the reflective surfaces of the mirrors. In Fig. 3.7(e), a one mirror set-up illustrates how the PV surface can also generate shadows (aPV_S) over the other elements.

In the case of the mirrors, the previous variables considered only the rays that managed to reach their reflective surface, but not what happens afterwards. Fig. 3.7(f) presents an interesting case where the right

mirror causes a shadow for the directly incoming rays (aR_S) and another shadow (aL_{RS}) that blocks a portion of the rays that were heading towards PV after being reflected by the left mirror (aL_{PVB}). Here, the only rays reaching PV are the ones described by aL_{PV} after one bounce off the left mirror. For every reflection, a conceptual ray loses power according to the index of reflection (ρ) of the mirrors. Also, it is depicted how the rays reaching the left mirror over aL_{PVB} would be reflected outwards and lost. The set-up of Fig. 3.7(g) also presents a contribution of the left mirror after one reflection (aL_{PV}) and another contribution after two reflections (aL_{RPV}). The variables describing the macro-optical phenomena after reflections must be dependent on the angles between the V-Trough's elements and the reflected solar rays, such as iL_{PV}, iL_R and iL_{RPV}. Fig. 3.7(h) illustrates a case where the only effective contribution is a portion of rays which are reflected from the left mirror and then from the right one (aL_{RPV}). As shown, the rays reaching the left mirror over the height of aL_{RPV} will eventually be lost by being reflected outwards after several reflections.

The cases conceptually analyzed in Fig. 3.7 serve as an illustration of the diversity of macro-optical phenomena that can arise if the V-Trough geometry is allowed to be flexibly defined. Similar geometrical explorations were performed exhaustively and systematically, seeking to identify the relevant macro-optical phenomena and the variables related to them. Fig. 3.8 shows the conceptual scheme of the proposed model for a given solar elevation angle α. Each V-Trough's element (left mirror, PV surface and right mirror) is

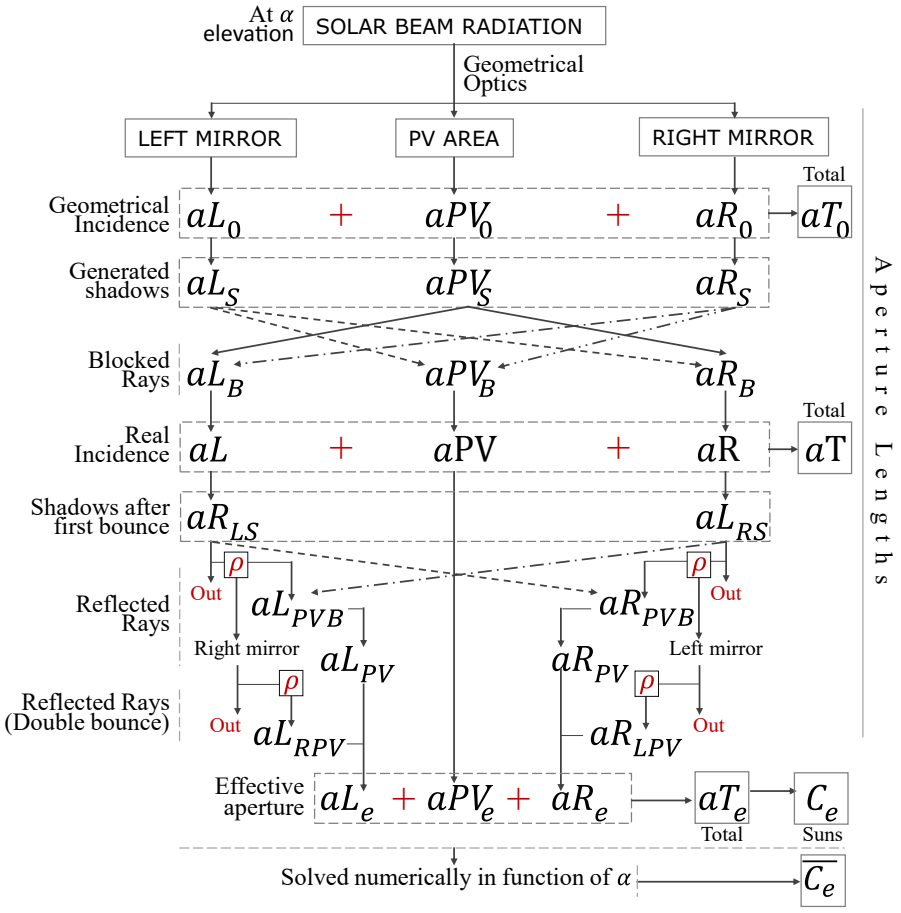

Figure 3.8: Diagram of the conceptual model.

conceptually examined separately for a more detailed description. First, the geometrical projection of each element is assessed normal to the incident beam radiation, namely the *Geometrical Incidence* aperture (aL_0, aPV_0 and aR_0). Then, the direct *Generated Shadows* that each element may cause are calculated (aL_S, aPV_S and aR_S). These shadows are used to find the *Real Incidence* aperture of each element (aL, aPV and

aR) by subtracting the *Blocked Rays* (aL_B, aPV_B and aR_B) from the *Geometrical Incidence* of each element. After the rays directly reach each mirror, they will either bounce (be reflected) out of the device, reach the reflective surface of the other mirror, be blocked (aL_{PVB} and aR_{PVB}) by the other mirror's generated second shadows (aR_{LS} and aL_{RS}), or they may be directly reflected towards the PV area (aL_{PV} and aR_{PV}). After an aperture section is reflected from a mirror, it must be proportionally reduced according to the index of reflection (ρ) of the mirrors. The rays that reach the other mirror after the first bounce, may then either bounce out of the device or reach the PV area after the second bounce (aL_{RPV} and aR_{LPV}). In the last case, the corresponding aperture section gets reduced once again by ρ. Afterwards, the *Effective aperture* of the mirrors (aL_e and aR_e) can be calculated. In the case of the PV area, the *Real Incidence* aPV is equal to its *Effective aperture* aPV_e. Finally, the added *Effective aperture* of these three contributions corresponds to the *Total Effective aperture* aT_e.

When aT_e is multiplied by the *Depth* of the V-Trough, it represents the section of the harvesting area, perpendicular to the incident beam radiation, which effectively reaches the PV surface after the relevant macro-optical phenomena are considered; namely the *Effective Harvesting Area* (EHA). Conceptually, a V-Trough set-up with a given EHA, for a given α, would harvest the same amount of solar power as a flat PV panel, positioned perpendicularly to the sunlight, with a surface area equal to EHA.

Comparing aT_e against aT_0 and aT can provide an insight into the overall optical performance of the device for a given α. aT_0 is the *Total Geometrical Incidence* and aT is the *Total Real Incidence*, namely the section of rays that reach PV or the reflecting surfaces of the mirrors. Hence, aT_0 versus aT, is related to the proportional radiation losses due to the direct shadows generated by any of the V-Trough's elements. Moreover, a aT versus aT_e comparison, is related to the proportion of rays that reach the reflecting surfaces but which are then blocked or reflected outwards. The ratio between aT_e and LPV results in the total *Effective Concentration* (C_e). The same ratio is obtained between EHA and the PV area. Furthermore, C_e can be calculated numerically for a range of solar elevations in order to find an *Average Effective Concentration* ($\overline{C_e}$).

Expression 3.1 shows that $\overline{C_e}$ is modeled in function of α and the geometrical parameters of the V-Trough. This expression implies that the geometrical parameters are constants (fixed) that can be independently defined by the user of the model and that the solar elevation α varies in function of time. This level of flexibility is already a modeling advantage over most of the models discussed in the state of the art (see Sec. 2.1). Expression 3.2 goes further by establishing each geometrical parameter as a dynamic variable in function of the solar elevation. By considering both expressions within the capabilities of the model, a user can deliberately define any of those parameters to be static or dynamic. Therefore, this allows for V-Trough set-ups in which any of its geometrical parameters can have a solar tracking dynamic response. In accordance with personalized tracking constraints, the user can then define any control function relating the dynamic parameters to the solar elevation.

$$\overline{C_{e\left(\alpha_{(t)},\beta,\psi L,\psi R,LPV,LL,LR,\rho\right)}} \tag{3.1}$$

$$\overline{C_{e\left(\alpha_{(t)},\beta_{(\alpha)},\psi L_{(\alpha)},\psi R_{(\alpha)},LPV_{(\alpha)},LL_{(\alpha)},LR_{(\alpha)},\rho\right)}} \tag{3.2}$$

Table 3.1 delimits the ranges allowed for each input parameter. These ranges comprise all reasonable values for any practical purpose and therefore, they support the geometrical flexibility sought in this project. Any unit of measurement can be used for the lengths (LPV, LL and LR), as long as there is consistency among all the length parameters and the results interpretations. For the sake of simplicity, the PV length can be defined as a dimensionless 1 ($LPV = 1$) and the other lengths can then be established as a proportion of LPV. After the optical performance results are modeled, the lengths can be scaled to their real dimensions.

Fig. 3.9 illustrates the geometrical flexibility implied by Table 3.1. According to the shadows in a given personalized context (see Fig. 3.9(a)), the solar elevation range can be defined from a starting value (α_f) to a ceiling limit (α_c). Fig. 3.9(b) shows how the angular position of the whole device, controlled by β, is allowed to reach any value within one revolution. Fig. 3.9(c) shows how each mirror can be tilted to any angular position that is equal or over the PV surface plane. It is evidently not reasonable to tilt any mirror further than this range. Lastly, Fig. 3.9(d) shows how each mirror can independently adopt any positive length; even zero.

Table 3.1: Minimum and maximum values allowable for the input parameters.

	α	β	ψL	ψR	LPV	LL	LR	ρ
Min	0	$-\pi$	$-\pi/2$	$-\pi/2$	0	0	0	0
Max	π	π	$\pi/2$	$\pi/2$	∞	∞	∞	1

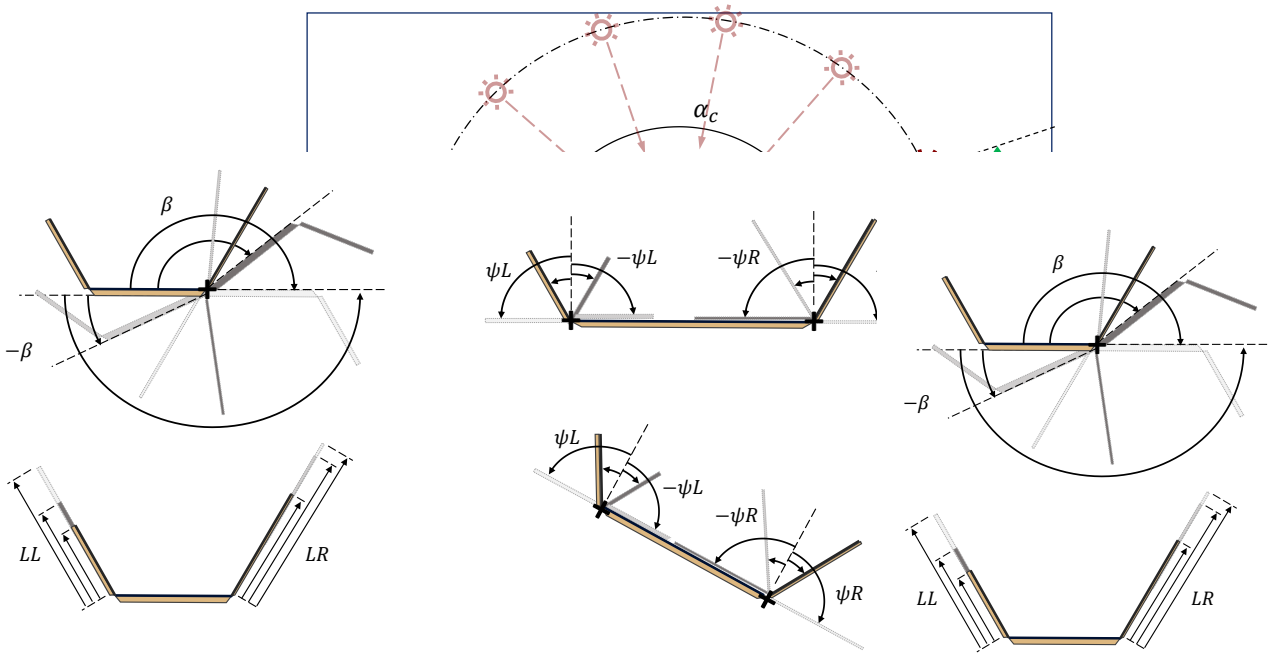

(c) (d)

Figure 3.9: Geometrical flexibility of the input parameters.

As follows, the assumptions corresponding to the modeling framework are described:

- Only beam solar radiation is considered for calculating the effective concentration for reasons explained in Sec. 1.2 and Sec. 2.1.
- The main analytical modeling corresponds to the radiation which effectively reaches the PV surface but which is not necessarily transformed into electricity completely. In further modeling steps, the results from this model can include the photovoltaic efficiency and temperature losses in order to calculate electrical power. However, that is not the focus of this research project.
- As in all analytical models discussed in the state of the art, Sec. 2.1, the mirrors are assumed to generate specular reflections. Also, the optical efficiency of these reflections is assumed to be independent of the angle of incidence and to correspond to a constant index of reflection ρ.
- In order to simplify the model, without losing considerable accuracy or relevancy, the model considers up to two consecutive mirror reflections per solar ray. During the geometrical exploration, it was found that the cases with more than two consecutive bounces are uncommon in V-Trough devices with low concentration factors and this does not usually play a considerable role in the total effective suns.
- The model is mainly two-dimensional in the transverse plane. The effect of the longitudinal misalignment on the optical performance is modeled according to the reported "cosine effect". However, no

border losses are considered due to this misalignment. As it was discussed in Sec. 2.1, this is also the case in most of the other reported analytical models. The role that this possible effect can have over the effective concentration can be minimized if the V-Trough is assumed to have an infinite *Depth*, if the length-to-width ratio is high, or if the mirrors are assumed to have a longitudinal overhang (Garg and Hrishikesan, 1988).

- As part of the aim of this model to support the development of V-Trough solutions for personalized scenarios, the shadows that may arise in the context are considered. These shadows are conceptually assumed as limitations in the solar elevation (α) range. Particularly, shadows like mountains in the context, that appear in the East or West direction, can be modeled as a modification in the initial and final α values in the solar elevation range for the analytical model to be iterated.

3.2 Mathematical Construction of the Model

The analytical model was developed by following the conceptual model and the variables it defines as shown in Figure 3.8. In the model's equations, expressions of absolute value ("|...|") are used as a tool to correctly handle lengths that result negative. Additionally, several conditionals are used to handle boundary conditions.

The first step is to define the angle of incidence between the direct rays and the PV absorber (iPV), the left mirror (iL) and the right mirror (iR); as described by Eqs. 3.3, 3.4 and 3.5 respectively (see Fig. 3.7(a)).

$$iPV = \alpha + \beta \tag{3.3}$$

$$iL = \psi L - \alpha - \beta + \frac{\pi}{2} \tag{3.4}$$

$$iR = \psi R + \alpha + \beta - \frac{\pi}{2} \tag{3.5}$$

Eqs. 3.6, 3.7 and 3.8 are used to calculate the aperture lengths of the *Geometrical Incidence* for each V-Trough's element, i.e. the PV absorber (aPV_0), the left mirror (aL_0) and the right mirror (aR_0) respectively. The previous results are then used to calculate the aperture length of the *Total Geometrical Incidence* with Eq. 3.9. It is worth clarifying that these apertures do not consider shadows yet. Figs. 3.7(a)-Fig. 3.7(e) illustrate these variables for different V-Trough set-ups. When the PV surface or the reflective surfaces of any of the mirrors are facing the incoming solar rays from the opposite direction, the corresponding *Geometrical Incidence* results negative from Eqs. 3.6–3.8. This behavior is used by Eq. 3.9, which nullifies the negative results by means of the expressions of absolute value.

$$aPV_0 = LPV * \sin(iPV) \tag{3.6}$$

$$aL_0 = LL * \sin(iL) \tag{3.7}$$

$$aR_0 = LR * \sin(iR) \tag{3.8}$$

$$aT_0 = \frac{1}{2}\left(|aPV_0| + |aL_0| + |aR_0| + aPV_0 + aL_0 + aR_0\right) \tag{3.9}$$

Considering all the shadows that each element could generate over the other ones and the portion of rays that could be blocked accordingly, Eqs. 3.10, 3.11 and 3.12 respectively define the aperture length of the *Real Incidence* for the PV absorber, the left mirror and the right mirror. For aPV, Eq. 3.10 considers the *Blocked Rays*, if any, by subtracting the geometrical incidences of the mirrors only when they result negative. Negative results here mean that a given element is producing a shadow equal in magnitude to its *Geometrical Incidence*. Similarly, in the case of aL and aR, Eqs. 3.11–3.12 consider the shadow that could be produced by the PV absorber, only when its *Geometrical Incidence* is negative. Also, these equations consider the *Generated Shadows* by the opposite mirror, only when such shadows surpass the length of aPV_0.

Figs. 3.7(c)–Fig. 3.7(e) illustrate these variables.

$$aPV = aPV_0 - \frac{1}{2}\left(|aL_0| + |aR_0| - aL_0 - aR_0\right) \tag{3.10}$$

$$aL = aL_0 - \frac{1}{2}\left(\left|aPV_0 - \frac{|aR_0| - aR_0}{2}\right| - aPV_0 + \frac{|aR_0| - aR_0}{2}\right) \tag{3.11}$$

$$aR = aR_0 - \frac{1}{2}\left(\left|aPV_0 - \frac{|aL_0| - aL_0}{2}\right| - aPV_0 + \frac{|aL_0| - aL_0}{2}\right) \tag{3.12}$$

Eq. 3.13 defines the aperture length of the *Total Real Incidence* (aT). aT represents the portion of incoming beam radiation which reaches the V-Trough's reflective surfaces or the PV absorber. As with aT_0, this aperture aT considers only the contributions that result positive.

$$aT = \frac{1}{2}\left(|aPV| + |aL| + |aR| + aPV + aL + aR\right) \tag{3.13}$$

The *Incident Concentration* (C) is defined by Eq. 3.14. C relates to the proportion of beam radiation that reaches the "useful" surfaces of the device as a whole, regardless of whether these rays ultimately reach the photovoltaic surface.

$$C = \frac{aT}{LPV} \tag{3.14}$$

In order to consider the macro-optical phenomena that may occur after the incoming rays are reflected from the mirrors, it is necessary to calculate the angles between the reflected rays and the V-Trough's elements. iL_R, in Eq. 3.15, is the angle between the rays reflected from the left mirror and the surface of the right mirror; iR_L, in Eq. 3.16, is the angle between the rays reflected from the right mirror and the surface of the left mirror; iL_{PV}, in Eq. 3.17, is the angle between the rays reflected from the left mirror and the PV surface; and iR_{PV}, in Eq. 3.18, is the angle between the rays reflected from the right mirror and the PV surface. Several of these angles are illustrated in Figs. 3.7(f)–Fig. 3.7(g).

$$iL_R = \psi R + 2\psi L - \alpha - \beta + \frac{\pi}{2} \tag{3.15}$$

$$iR_L = \psi L + 2\psi R + \alpha + \beta - \frac{\pi}{2} \tag{3.16}$$

$$iL_{PV} = -2\psi L + \alpha + \beta \tag{3.17}$$

$$iR_{PV} = \pi - 2\psi R - \alpha - \beta \tag{3.18}$$

As seen in Fig. 3.7(f), when rays go through their first reflection and head towards the PV plane, they may be blocked by the back part of the opposing mirror. Eq. 3.19 is the length of the shadow, if any, generated by the back part of the left mirror with respect to the rays reflected from the right mirror. Conversely, Eq. 3.20 is the length of the shadow generated by the back part of the right mirror with respect to the rays reflected from the left mirror. These shadows may block the portion of reflected rays, completely or partially, and keep them from reaching the PV absorber. When the reflected rays face the back part of one of the mirrors, the corresponding angle (iL_R or iR_L) results negative. Therefore, the corresponding shadow's length (aR_{LS} or aL_{RS}) results negative, indicating that there is indeed a shadow being generated.

$$aR_{LS} = LL * \sin\left(iR_L\right) \tag{3.19}$$

$$aL_{RS} = LR * \sin\left(iL_R\right) \tag{3.20}$$

The following step is to calculate the aperture lengths within which any ray that reaches the reflective surface of a given mirror will be reflected towards the PV surface. Variables p_L and p_R are respectively defined by Eqs. 3.21 and 3.22 and are illustrated in Fig. 3.10. These apertures consider the shadows after one reflection (aR_{LS} and aL_{RS}) but not the shadows before the first reflection (aR_S and aL_S), as can be seen in Fig. 3.10(b). Also, as seen in Fig. 3.10(a), these apertures do not depend on the length of the corresponding mirror; they can extend to a virtual point which exceeds the mirror. This figure illustrates a

virtual ray, defined to delimit p_L, which bounces off a virtually extended surface. The grey areas represent the apertures of p_L and p_R, so they do not necessarily correspond to real rays reaching the PV surface.

$$p_L = LPV * \sin(iL_{PV}) - \frac{|aL_{RS}| - aL_{RS}}{2} \tag{3.21}$$

$$p_R = LPV * \sin(iR_{PV}) - \frac{|aR_{LS}| - aR_{LS}}{2} \tag{3.22}$$

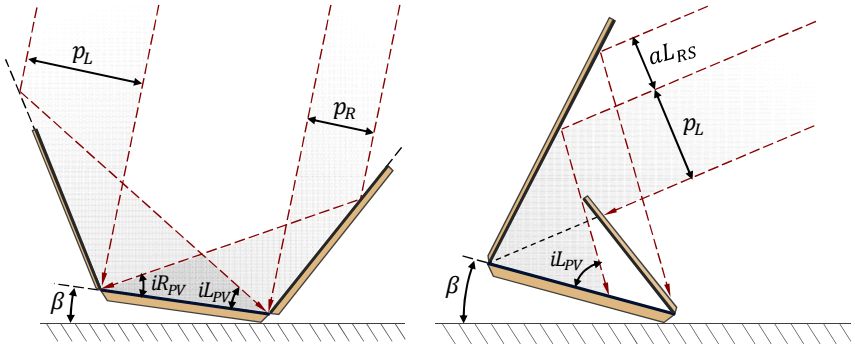

(b)

Figure 3.10: Illustration of variables p_L and p_R.

The entities represented by p_L and p_R interact with the *Geometrical Incidence* (aL_0 and aR_0) and with the *Real Incidence* (aL and aR) of the mirrors in order to determine the aperture length of the rays that reach the PV surface after only one reflection from the left mirror (aL_{PV}) or the right mirror (aR_{PV}). By geometrically exploring the possible interactions and effects of these variables, three boundary cases were found. These cases are illustrated in Fig. 3.11 and exemplified with the reflections from the left mirror. The areas which are more intensely shadowed correspond to aL_{PV}; if any. It is worth noting that the rays that may reach the PV surface after two reflections are not considered yet. Fig. 3.11(a) presents the case where

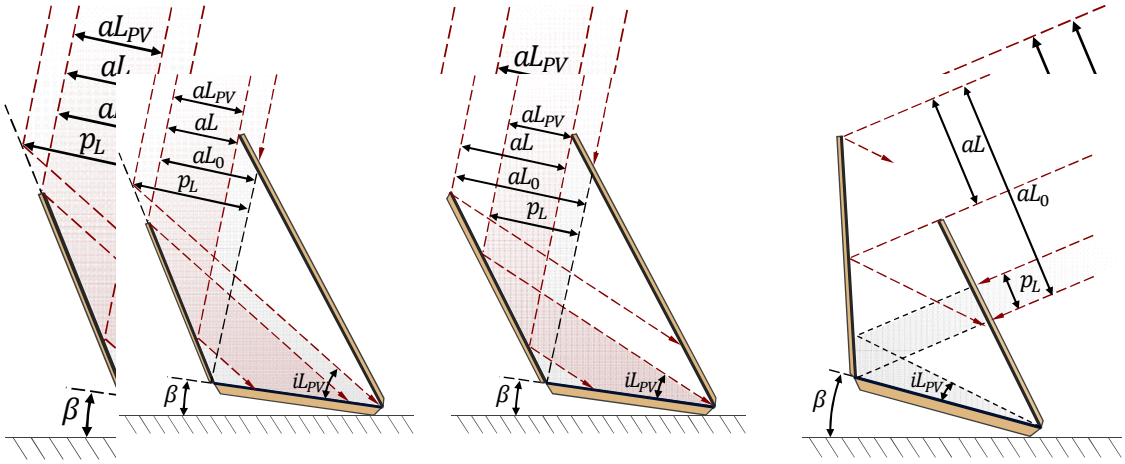

(c)

Figure 3.11: Boundary cases to consider when defining aL_{PV}.

the allowable aperture p_L is larger than the geometrical incidence aL_0. In this case, all rays represented by

the real incidence aL are expected to reach the PV surface directly afterward. In Fig. 3.11(b), the length of aL_{PV} is limited by the upper boundary of p_L and the lower boundary of the real incidence aL. In Fig. 3.11(c), there is no overlap between the allowable aperture p_L and the real incidence aL. Therefore, none of the rays that get reflected from the left mirror are expected to reach the PV surface after only one reflection. The same optical behavior of these cases can happen for the reflections of the right mirror.

The angles between the rays reflected from both mirrors (only one reflection) and the PV surface must be considered as well. When these angles, namely iL_{PV} and iR_{PV} described by Eqs. 3.17–3.18, are ≤ 0, the reflected rays will not intercept the PV surface in their direction of advance. Also, if the geometrical incidence of a given mirror is ≤ 0, no rays are expected to even reach the mirror directly. Another special case is when $(aL_0 - p_L - aL) = 0$ or $(aR_0 - p_R - aR) = 0$. Here, the lower limit of the real incidence meets with the upper limit of the allowable aperture (p_L or p_R), but there is no overlap yet, so no ray is expected to reach the PV surface after one reflection from the corresponding mirror. These cases and boundary conditions are all considered in Eqs. 3.23–3.24, which respectively define aL_{PV} and aR_{PV}.

$$\begin{aligned} aL_{PV} =& \frac{(|aL_0 - p_L| - 2aL + aL_0 - p_L)}{4\,(aL_0 - p_L - aL)} * (|aL_0 - p_L - aL| - aL_0 + p_L + aL) \\ =& \begin{cases} 0, \text{if} & iL_{PV} \leq 0 \\ 0, \text{if} & aL_0 \leq 0 \\ 0, \text{if} & (aL_0 - p_L - aL) = 0 \end{cases} \end{aligned} \tag{3.23}$$

$$\begin{aligned} aR_{PV} =& \frac{(|aR_0 - p_R| - 2aR + aR_0 - p_R)}{4\,(aR_0 - p_R - aR)} * (|aR_0 - p_R - aR| - aR_0 + p_R + aR) \\ =& \begin{cases} 0, \text{if} & iR_{PV} \leq 0 \\ 0, \text{if} & aR_0 \leq 0 \\ 0, \text{if} & (aR_0 - p_R - aR) = 0 \end{cases} \end{aligned} \tag{3.24}$$

In certain scenarios, the rays may reach the PV surface after two reflections (Double bounce). The analytical formulations needed to assess this are similar to the previously described definition of aL_{PV} and aR_{PV}. Figs. 3.12(a) and 3.12(c) show two different such scenarios. Several variables are established in order to account for all the ways in which these phenomena can happen. iL_{RPV}, defined in Eq. 3.25, corresponds to the angle between the PV surface and a ray that was first reflected by the left mirror and then by the right mirror. Conversely, Eq. 3.26 defines iR_{LPV}, which is the angle between the PV surface and a ray coming from the left mirror after a Double bounce. The aperture length m_{LR} in Eq. 3.27, depicted in the same figures, corresponds to the incoming rays which have access to the reflecting surface of the left mirror and which do not get directly reflected towards the PV surface. Conversely, m_{RL} in Eq. 3.28 corresponds to the same phenomenon but for the right mirror. Similar to p_L and p_R, p_{LR} and p_{RL} represent the aperture lengths within which any ray that reaches the reflective surface of a given mirror, after a previous first reflection, will be reflected towards the PV surface; Eqs. 3.29–3.30. f_{LR} (Eq. 3.31) corresponds to an aperture, normal to the rays of the first bounce, which starts from the vertex of the right mirror and ends in the projected length of the left mirror. Conversely, f_{RL} in Eq. 3.32 corresponds to the same phenomenon but for the rays which are first reflected by the right mirror. The calculations of f_{LR} and f_{RL} require the intermediate step of defining the diagonals D_{LR} and D_{RL} with Eqs. 3.33–3.34. Fig. 3.12(b) shows the geometrical disposition of D_{LR} as an example. Also, aL_{RS} and aR_{LS}, from Eqs. 3.19–3.20, can be used here to represent the length of a given mirror projected normal to the rays that were previously reflected by the opposite mirror. m_{LR}, m_{RL}, p_{LR}, p_{RL}, f_{LR}, f_{RL}, aL_{RS} and aR_{LS} are all aperture lengths which are normal to the rays that were already reflected once.

$$iL_{RPV} = -2\psi L - 2\psi R + \alpha + \beta \tag{3.25}$$

$$iR_{LPV} = \pi - 2\psi R - 2\psi L - \alpha - \beta \tag{3.26}$$

$$m_{LR} = aL - aL_{PV} \tag{3.27}$$

$$m_{RL} = aR - aR_{PV} \tag{3.28}$$

$$p_{LR} = LPV * \sin\left(iL_{RPV}\right) \tag{3.29}$$

$$p_{RL} = LPV * \sin\left(iR_{LPV}\right) \tag{3.30}$$

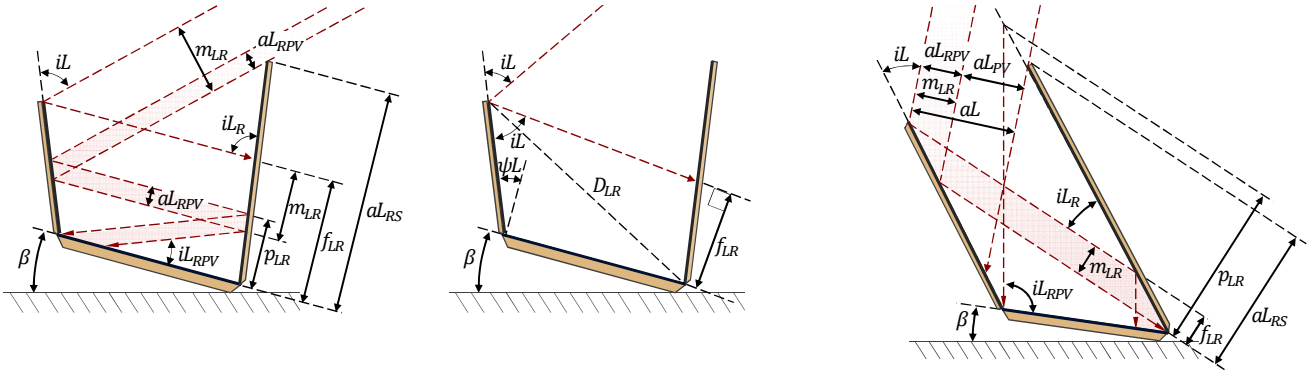

(c)

Figure 3.12: Example of cases where a portion of the rays reach the PV surface after two consecutive reflections (shadowed areas).

$$f_{LR} = D_{LR} * \sin\left(iL - \arcsin\left(\frac{LPV * \cos(\psi L)}{D_{LR}}\right)\right) \tag{3.31}$$

$$f_{RL} = D_{RL} * \sin\left(iR - \arcsin\left(\frac{LPV * \cos(\psi R)}{D_{RL}}\right)\right) \tag{3.32}$$

Where

$$D_{LR} = \sqrt{LL^2 + LPV^2 + LL * LPV * 2\sin(\psi L)} \tag{3.33}$$

$$D_{RL} = \sqrt{LR^2 + LPV^2 + LR * LPV * 2\sin(\psi R)} \tag{3.34}$$

Fig. 3.13 illustrates the most interesting boundary cases to consider in order to properly define the aperture lengths corresponding to the rays that reach the PV absorber after a second bounce (aL_{RPV} and aR_{LPV}). The figure exemplifies cases for rays that are first reflected from the left mirror. The phenomenon of interest of these figures, namely aL_{RPV}, is highlighted with colored shadows.

Figs. 3.13(a) and 3.13(e) show cases in which the aperture of interest is limited in the upper boundary by p_{LR}. On the other hand, in Figs. 3.13(d) and 3.13(f), the upper boundary is defined by the length of the right mirror projected normal to the direction of the first reflection (aL_{RS}). For Figs. 3.13(b) and 3.13(c), $aL_{RPV} = 0$ because either p_{LR} or aL_{RS} is too small to overlap with m_{LR}. Lastly, Fig. 3.13(g) corresponds to a case where all the rays that do reach the reflective surface of the right mirror, after the first reflection, are expected to reach the PV surface.

It was found that the phenomena aL_{RPV} and aR_{LPV} fall within the corresponding aperture lengths m_{LR} and m_{RL} and are limited in the upper boundary by the minimum value among the corresponding $[aL_{RS}, f_{LR}, p_{LR}]$ or $[aR_{LS}, f_{RL}, p_{RL}]$. Moreover, in order for these phenomena to be ≥ 0, m_{LR} or m_{RL} (depending on the mirror being analyzed) must overlap with both the corresponding p_{LR} or p_{RL} and aL_{RS} or aR_{LS}. The previously described behaviors are considered in Eqs. 3.35–3.36, which respectively define aL_{RPV} and aR_{LPV}.

$$\begin{aligned} aL_{RPV} =& \frac{1}{2}\left(|m_{LR} - f_{LR} + min\left[aL_{RS}, f_{LR}, p_{LR}\right]| + m_{LR} - f_{LR} + min\left[aL_{RS}, f_{LR}, p_{LR}\right]\right) \\ =& \begin{cases} 0, \text{if} & iL_{RPV} \leq 0 \\ 0, \text{if} & m_{LR} = 0 \\ 0, \text{if} & p_L \geq aL_0 \end{cases} \end{aligned} \tag{3.35}$$

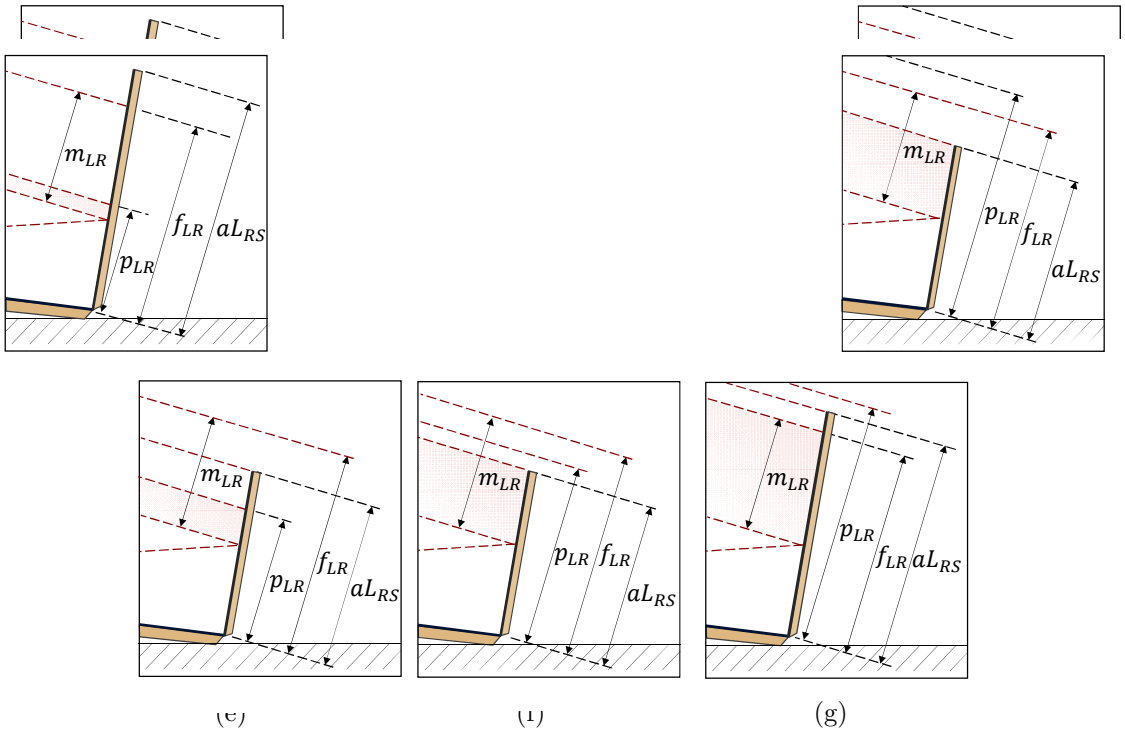

Figure 3.13: Boundary cases to consider when defining aL_{RPV}.

$$\begin{aligned} aR_{LPV} =& \frac{1}{2}\left(|m_{RL} - f_{RL} + min\left[aR_{LS}, f_{RL}, p_{RL}\right]| + m_{RL} - f_{RL} + min\left[aR_{LS}, f_{RL}, p_{RL}\right]\right) \\ =& \begin{cases} 0, \text{if} & iR_{LPV} \leq 0 \\ 0, \text{if} & m_{RL} = 0 \\ 0, \text{if} & p_R \geq aR_0 \end{cases} \end{aligned} \tag{3.36}$$

Subsequently, the *Effective Aperture* lengths of the three main elements of a V-Trough, namely the PV absorber, the left mirror and the right mirror, can be respectively calculated with Eqs. 3.37-3.39. The mirror contributions after one reflection are reduced by the index of reflection ρ, while the mirror contributions after two reflections are reduced by ρ^2.

$$aPV_e = \frac{|aPV| + aPV}{2} \tag{3.37}$$

$$aL_e = \rho * aL_{PV} + \rho^2 * aL_{RPV} \tag{3.38}$$

$$aR_e = \rho * aR_{PV} + \rho^2 * aR_{LPV} \tag{3.39}$$

Afterwards, the *Effective Concentration*, considering only the beam radiation that reaches the PV surface, can be calculated with Eq. 3.40.

$$C_e = \frac{aPV_e + aL_e + aR_e}{LPV} \tag{3.40}$$

C_e is a variable that can be hence solved analytically for any given solar elevation α and an established V-Trough geometry. It is a dimensionless indicator because it is defined as a proportion of the length of the PV absorber LPV. Since all the macro-optical phenomena and surfaces in a V-Trough are assumed to share a common *Depth*, C_e is also the ratio of the *Effective Harvesting Area* (EHA) over the PV area. As a reference for interpretation, a flat PV panel without concentrating mirrors and placed perpendicularly to the incident solar rays, results in $C_e = 1$ proportional suns of beam radiation. As explained in Sec. 3.1, this indicator of optical performance must be adjusted for any longitudinal misalignment with the "cosine effect".

3.3 Use and Interpretation of the Model

As follows, a given V-Trough set-up is analyzed, from results obtained through the proposed method, in order to show the level of detail in which its optical performance can be described in terms of beam solar radiation. The analysis is performed for three different solar elevations as an example of how to use and interpret the proposed model and its optical results.

Fig. 3.14 illustrates some of the most relevant (in this case) optical variables for the chosen set-up of this example at $\alpha = 70°$. The lengths and angular positions are specified in the figure and the index of reflection is taken as $\rho = 0.85$. All lengths, including the aperture results presented in Tables 3.2-3.4, are defined as proportions of LPV. The optical apertures allow for a quantification of the macro-optical phenomena expected to occur at the given solar elevations.

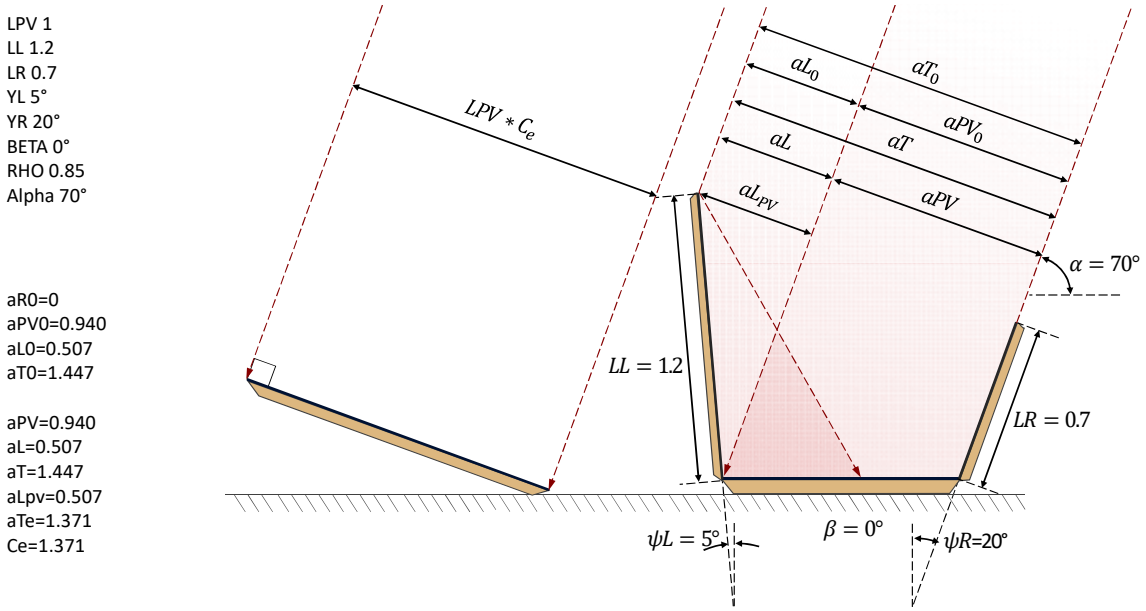

Figure 3.14: Optical aperture lengths of a V-Trough and an equivalent flat panel at $\alpha = 70°$.

Table 3.2: Relevant optical variables for the V-Trough set-up in Fig. 3.14 at $\alpha = 70°$.

aR_0	aPV_0	aL_0	aT_0	aPV	aL	aT	aL_{PV}	aT_e
0	0.94	0.507	**1.447**	0.94	0.507	**1.447**	0.507	**1.371**

At this solar elevation, the incident rays become parallel to the right mirror, so it can not directly contribute for the concentration of beam radiation. As shown in Table. 3.2, the *Geometrical Incidence* of the right mirror (aR_0) is hence 0. On the other hand, there are no shadows generated, so $aPV_0 = aPV$ and $aL_0 = aL$. The PV surface contributes to 65% of the *Total Geometrical Incidence* (aT_0) and the left mirror contributes to the other 35%. Since there are no shadows at this solar elevation, and none of the V-Trough's elements are opposing the incoming rays, the *Total Geometrical Incidence* is the same as the *Real Geometrical Incidence* (aT). All the rays that reach the left mirror are directly reflected towards the PV surface, so aL_{PV} becomes the only effective contribution of this mirror. The resulting *Total Effective Aperture* (aT_e) is 5.3% less than aT_0 and aT. This optical loss is due to ρ, which proportionally reduces the contribution of the left mirror. The *Effective Concentration* is $C_e = 1.371$. This implies that this set-up, at $\alpha = 70°$, can harvest the same solar power as a flat solar panel perpendicular to the incident solar rays and

with 137.1% of the PV area used in the V-Trough; such panel is depicted in Fig. 3.14. In other words, the V-Trough can harvest the same amount of solar radiation with a PV area 27.1% smaller than the described flat panel. Interestingly, even though the right mirror is not contributing, this is the solar elevation for which C_e is maximized in this set-up.

Fig. 3.15 shows an optical analysis for the same set-up at $\alpha = 85°$. The macro-optical phenomena here are similar to the previous analysis but the right mirror is now contributing in a similar proportion as the longer left mirror.

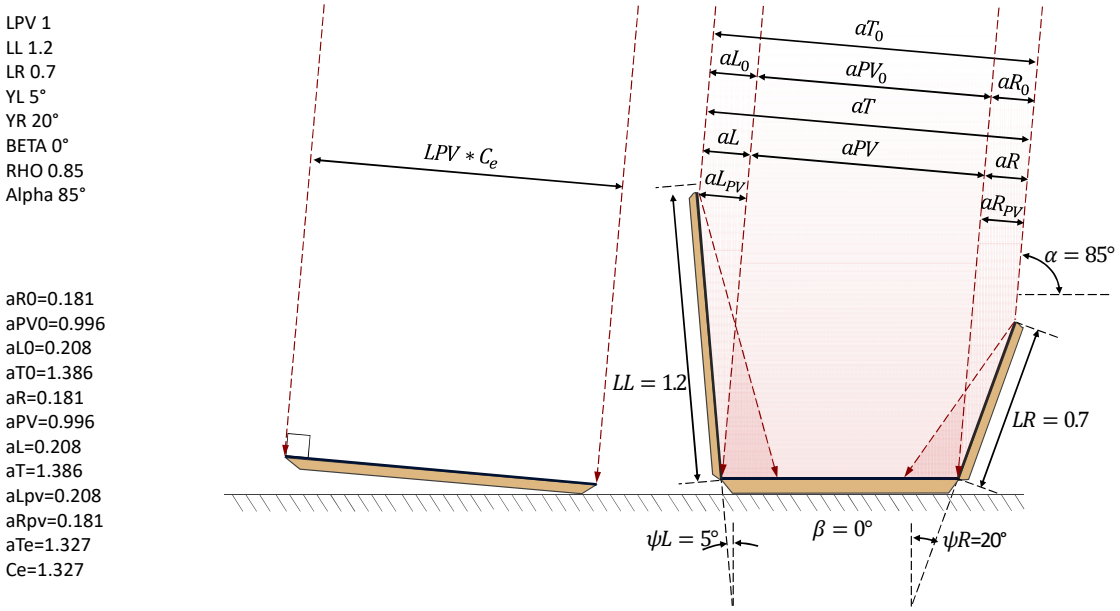

Figure 3.15: Optical aperture lengths of a V-Trough and an equivalent flat panel at $\alpha = 85°$.

Table 3.3: Relevant optical variables for the V-Trough set-up in Fig. 3.15 at $\alpha = 85°$.

aR_0	aPV_0	aL_0	aT_0	aR	aPV	aL	aT	aL_{PV}	aR_{PV}	aT_e
0.181	0.996	0.208	**1.386**	0.181	0.996	0.208	**1.386**	0.208	0.181	**1.327**

At this solar elevation, all *Geometrical Incidences* are equal to the corresponding *Real Incidences*, as seen in Table. 3.3. This means that all rays reaching the device manage to make contact with "useful" surfaces, namely the reflective faces of the mirrors or the PV upper surface. The right mirror, the PV absorber and the left mirror respectively contribute to 13.1%, 71.9% and 15.0% of aT. The contributions of both mirrors happen after only one reflection. The resulting aT_e is 4.3% less than aT due to the ρ optical losses. With an *Effective Concentration* of $C_e = 1.327$, this device is harvesting the same solar radiation as a flat panel perpendicular to sunlight with 132.7% of the PV area used in the V-Trough; as depicted in Fig. 3.15. The optical efficiency has hence dropped, as compared to $\alpha = 70°$, but the mirrors are still producing a favorable concentration indicator.

Fig. 3.16 illustrates an optical analysis for the same set-up at $\alpha = 120°$; with the most relevant results presented in Table. 3.4. The PV surface contributes to 61.8% of the *Total Geometrical Incidence*, while it only contributes to 40.1% of the *Total Real Incidence* due to the shadow produced by the left mirror (aL_S). There is no obstruction for accessing the right mirror, so $aR_0 = aR$. The aperture area which manages to reach the useful surfaces ($aT * Depth$) is 36.2% less than the area of the whole device as seen from the incident solar rays ($aT_0 * Depth$). In other words, 36.2% of the rays that reach the device as a whole are blocked.

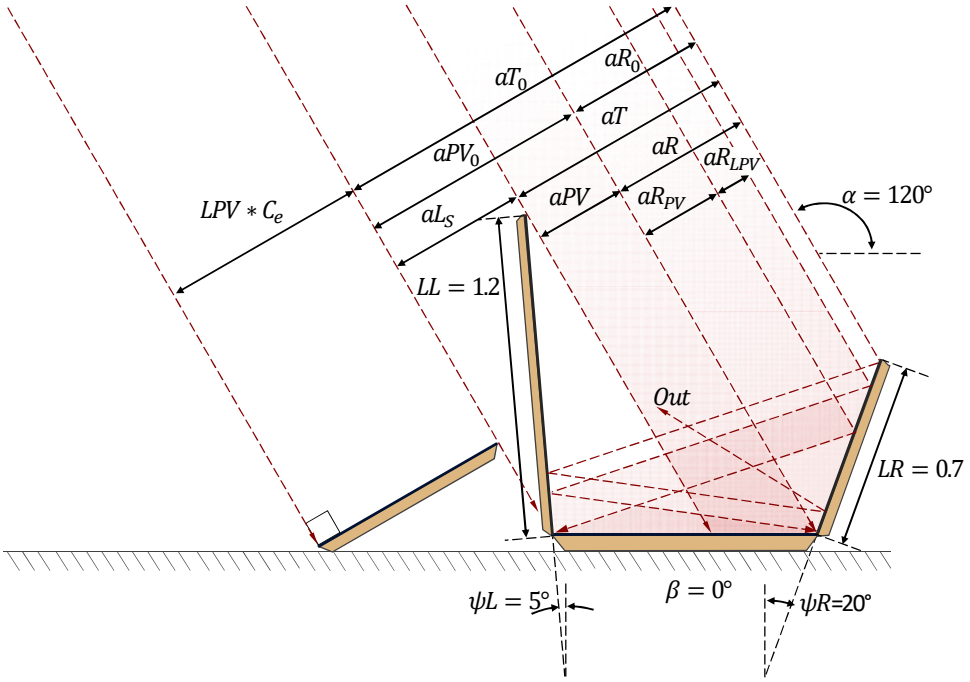

Figure 3.16: Optical aperture lengths of a V-Trough and an equivalent flat panel at $\alpha = 120°$.

Table 3.4: Relevant optical variables for the V-Trough set-up in Fig. 3.16 at $\alpha = 120°$.

aR_0	aPV_0	aL_S	aT_0	aPB_B	aPV	aR	aT	aR_{PV}	aR_{LPV}	aT_e
0.536	0.866	0.507	**1.402**	0.507	0.359	0.536	**0.895**	0.342	0.174	**0.775**

There are three contributions to the *Total Effective Aperture*, i.e., the rays which directly reach the PV surface ($aPV = aPV_e$), the rays that reach the PV surface after being reflected once from the right mirror (aR_{PV}), and the rays that reach the PV surface after being reflected from the right mirror and then from the left one (aR_{LPV}). These contributions correspond respectively to 46.3%, 44.1% and 22.5% of the total rays which are effectively harvested. The *Effective Harvesting Area* ($aT_e * Depth$) is 13.4% less than the aperture area that manages to reach the useful surfaces ($aT * Depth$). This difference can be explained from the effect of the index of reflection (ρ) reducing the mirror contributions and from the fact that 2.2% of the rays corresponding to aT are reflected back out after they bounce twice.

From the presented aT_e and considering that $LPV = 1$ in this example, it can be established that the *Effective Concentration* is $C_e = 0.775$. This means that, for this given set-up and solar elevation, the V-Trough can harvest the same solar radiation as a flat panel perpendicular to the incident solar rays and with 77.5% of the PV area used in the V-Trough. Such a panel is shown on the left side of the figure. Accordingly, at this solar elevation, the mirrors are no longer favoring the energy harvesting efficiently. This highlights the importance of performing tracking adjustments along the day. The example also illustrates how the macro-optical phenomena can vary, in magnitude and qualitative nature, as the solar elevation progresses. The detailed results empower a deep understanding of what affects the *Effective Concentration* and provide insight into possible solutions for improvement. The use of the proposed model for design/engineering matters is further explored in Sec. 6.

Chapter 4

Model Validation

The proposed model calculates the *Effective Concentration* based only on the beam radiation that is expected to reach the PV surface. Therefore, the model does not directly define the electrical output of a given V-Trough device; a calculation that should also consider electrical losses at the level of the semiconductor material, thermal losses and the macro-optical phenomena related to diffuse radiation. However, as explained in Secs. 1.2–1.1, a beam radiation model addresses the most critical aspects for the performance assessment of a V-Trough device. Consequently, it is crucial to validate the proposed model within its conceptual focus. This section presents the development of an experimental procedure to validate the model's capacity to accurately account for the *Effective Concentration*, of beam radiation, in a given V-Trough PV device.

Since the validation aim is related only to beam radiation, an experimental model based on laser devices is used for challenging a series of geometrical predictions obtained from the mathematical model. In order to perform the experiment, a testing platform was developed to carry out the measurements and to adopt the geometries and movements of a V-Trough device. Subsequently, the experimental results are statistically compared to the model's predictions and the interpretations of the results are then presented.

This section provides a solution to the specific objective III: "To test the validity of the theoretical model by comparing it against an equivalent experimental model".

4.1 Experimental Design

The proposed direct radiation model calculates and relates a series of proportional lengths in order to produce a final concept of effective optical concentration. The central concept of this experimental validation is that these calculated lengths, dependent on a given set of geometrical input parameters, are specific predictions that can be compared against real laser measurements of those same lengths in an equivalent experimental model. These experimental measurements were defined to be performed in a testing platform capable of adopting the same geometries as the ones in the theoretical V-Trough simulations. If the model is correctly defined, the predicted values are expected not to diverge significantly from the measured values, as long as the geometrical input parameters respect the allowable ranges established in Table 3.1. Also, the experimental procedure is designed for the possible detection of relevant macro-optical phenomena that were ignored, if any, in the conceptual framework of the model.

The experimental design is based on procedures used by the National Renewable Energy Laboratory (Freeman et al., 2013) to validate solar radiation models against experimental measurements. For this project, the model's predictions and the measurements are both defined as continuous variables, namely optical aperture lengths as proportions of LPV. The measurements can be arranged in function of the predictions in corresponding couples, which are then plotted for a regression analysis. This procedure allows inspecting how well the measurements coincide to the predictions along the magnitude range of these variables. If the model is correct, there should appear a clearly linear relationship between both variables with an equation tending to $Y = X$. Also, systematic errors can manifest in this analysis as a significant deviation from the line $Y = X$; as several simultaneous line patterns; or as residuals which are not randomly

aligned around the linear trend.

The measured and predicted variables are both dependent on the combination of geometrical inputs, i.e. α, β, ψL, ψR, LPV, LL and LR. The index of reflection ρ can be estimated for any mirror with methods which are not within the scope of this research project. Therefore, ρ is taken as 1 for the validation comparisons.

For the previous procedure to be performed, a data-set of predictions must first be generated. For this, 11 V-Trough set-ups were defined and for every set-up, there were four α values selected to perform aperture length calculations. Furthermore, for every α value selected, the aperture lengths that were considered were aPV_e, aL, aR, aL_{PV}, aR_{PV}, aL_{RPV} and aR_{LPV}. Therefore, there were 308 aperture length predictions, which were correspondingly compared against 308 experimental measurements.

All V-Trough set-ups were defined with a dynamic β parameter in order to simulate stepped solar tracking. Eq. 4.1 can be used to determine β. The expression "$\lfloor ... \rfloor$" means that the term inside must be rounded–down to the next integer.

$$\begin{aligned}\beta_{(\alpha,\beta_i,\beta_{\alpha s},\beta_s)} =& \beta_i + \beta_s * \left\lfloor \frac{\alpha}{\beta_{\alpha s}} \right\rfloor \\ =& \begin{cases} \pi, \text{if} & \beta > \pi \\ -\pi, \text{if} & \beta < -\pi \end{cases}\end{aligned} \tag{4.1}$$

With β_i = Initial β inclination, $\beta_{\alpha s}$ = Step variation of α needed for every variation in β, and β_s = Step variation of β every tracking movement. Accordingly, β starts at β_i and it varies a magnitude β_s every $\beta_{\alpha s}$ variation in the solar elevation α. The first function shown in expression 4.1 may lead towards a β value which exceeds the allowable range $[-\pi, \pi]$ even if the parameters of the function do respect the range. This can unnecessarily lead towards inaccurate calculations from the model. Therefore, the second section of the expression performs a trim in the progression of β in order to remain within the allowable range. This is a situation that may easily arise when defining any of the input angular parameters as dynamic, but may as easily be corrected by procedures as the one used in Eq. 4.1 for β.

While Eq. 4.1 allows for a simple control of β, it stops the tracking movement once the allowable range is exceeded. In the definition of the set-ups for the experimental validation, Eq. 4.2 was used instead, which is a modification of the former. This expression allows for a V-Trough which can conceptually revolve freely without its motion being stopped. Whenever the revolving motion leads to $\pi < \beta < -\pi$, this expression replaces β by a value which is equivalent but within the allowable range.

$$\begin{aligned}\beta_{(\alpha,\beta_i,\beta_{\alpha s},\beta_s)} =& \beta_i + \beta_s * \left\lfloor \frac{\alpha}{\beta_{\alpha s}} \right\rfloor - 2\pi \left\lfloor \frac{\beta_i + \beta_s * \left\lfloor \frac{\alpha}{\beta_{\alpha s}} \right\rfloor}{2\pi} \right\rfloor \\ =& \begin{cases} -2\pi + \beta, \text{if} & \beta > \pi \\ 2\pi + \beta, \text{if} & \beta < -\pi \end{cases}\end{aligned} \tag{4.2}$$

From the 11 defined V-Trough set-ups, 6 were defined by an algorithm that randomly selected values for every input parameter within the allowable ranges; named as "S1,...,S6". The parameters were defined randomly to avoid possible bias and with the expectation that more unconventional and counterintuitive set-ups could be more challenging for the predictions of the model. The other 5 set-ups were deliberately designed in other to address more realistic and representative V-Trough strategies; names as "D1,...,D5". Among those 5 set-ups, some were defined with other dynamic parameters in function of solar elevation, besides β, such as with the individual lengths and inclinations of the mirrors. Since the lengths are set as proportional to the PV absorber's length, the latter was defined for all the set-ups as $LPV = 1$. Also, for the sake of practicality in experimental measurements, the lengths of the mirrors were limited to maximum $LL = LR = 1.5 * LPV$. A summary of the set-up parameters is presented in Table 4.1; with lengths given as dimensionless proportions of the PV length, angles given in radians and dynamically defined parameters shown as variables in function of α.

Figs. 4.1–4.2 provide a visualization of the 11 V-Trough set-ups defined for the experimental validation. Each sub-figure specifies the four solar elevations chosen, for every set-up, to perform the optical predictions and the corresponding measurements.

Table 4.1: Input parameters of the simulated V-Trough set-ups. Those designed with "D" and those randomly defined with "S".

Set-Up	LPV	LL	LR	ψL	ψR	β_i	$\beta_{\alpha s}$	β_s
D1	1	1	1	$2\pi/15$	$2\pi/15$	$\pi/3$	$\pi/3$	$-\pi/3$
D2	1	1	1	$\psi L_{(\alpha)}$	$\psi R_{(\alpha)}$	$\pi/4$	$\pi/2$	$-\pi/2$
D3	1	1	1	$\psi L_{(\alpha)}$	$\psi R_{(\alpha)}$	0	0	0
D4	1	$LL_{(\alpha)}$	$LR_{(\alpha)}$	0	0	0	0	0
D5	1	1.5	0.5	$\psi L_{(\alpha)}$	$\psi R_{(\alpha)}$	$\pi/4$	$\pi/2$	$-\pi/2$
S1	1	0.9	1.35	$-6\pi/23$	$5\pi/36$	$\pi/14$	$3\pi/20$	$-14\pi/29$
S2	1	0.4	0.7	$-\pi/35$	$5\pi/22$	$2\pi/9$	$\pi/12$	$-36\pi/41$
S3	1	0.65	0.95	$-5\pi/31$	$36\pi/79$	$\pi/3$	$\pi/26$	$-9\pi/29$
S4	1	0.85	0.7	$-\pi/90$	$3\pi/11$	$14\pi/37$	$\pi/35$	$-13\pi/14$
S5	1	1	1.3	$\pi/90$	$13\pi/33$	$11\pi/46$	$45\pi/89$	$-2\pi/17$
S6	1	0.65	1.45	$3\pi/20$	$\pi/14$	$-13\pi/33$	$2\pi/21$	$-5\pi/23$

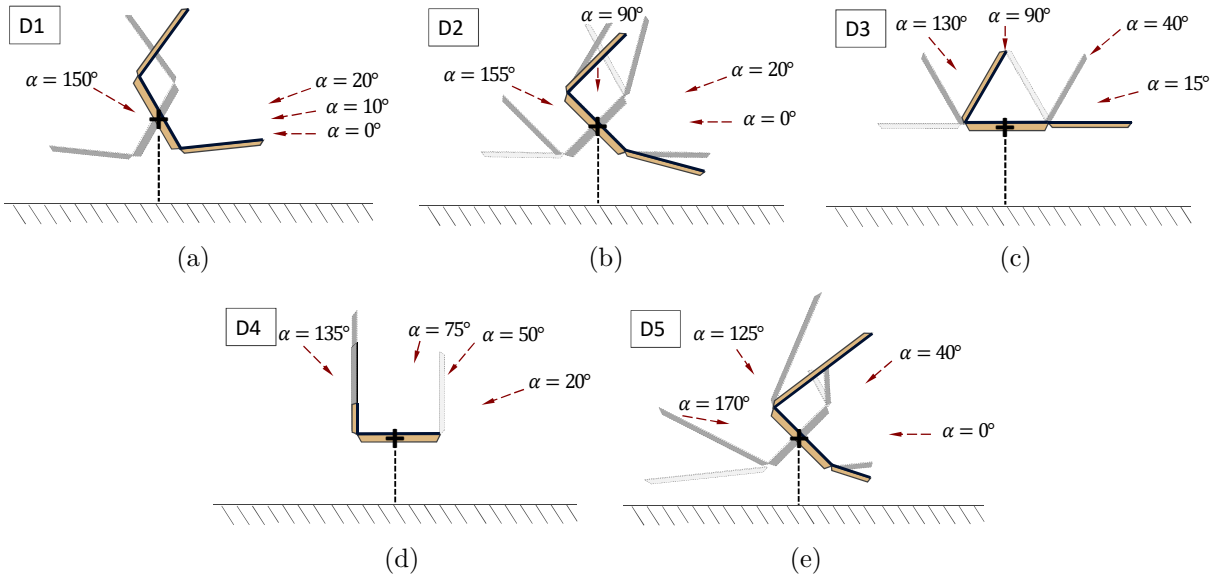

Figure 4.1: Visualization of the deliberately designed V-Trough set-ups for the experimental validation.

Set-up D1, Fig. 4.1(a), corresponds to a device with fixed mirrors and a β tracking strategy of two steps or adjustments per day; therefore the device adopts three positions. D2, in Fig. 4.1(b), has a β tracking strategy of one step and the mirrors are continually re-adjusting their angular position along the day. D3, in Fig. 4.1(c), has a fixed β and the mirrors change their angular position in two steps (three positions) along the day. D4, in Fig. 4.1(d), also has a fixed β but tracks the sun by means of continuously adjusting the length of its mirrors. D5, in Fig. 4.1(e), has a β tracking strategy of one step and its mirrors are continuously adjusting their angular position. D5 differs from D2 in that all its elements have different fixed lengths. On the other hand, the randomly defined set-ups shown in 4.2(a)–4.2(f), all have fixed mirrors and perform the

tr

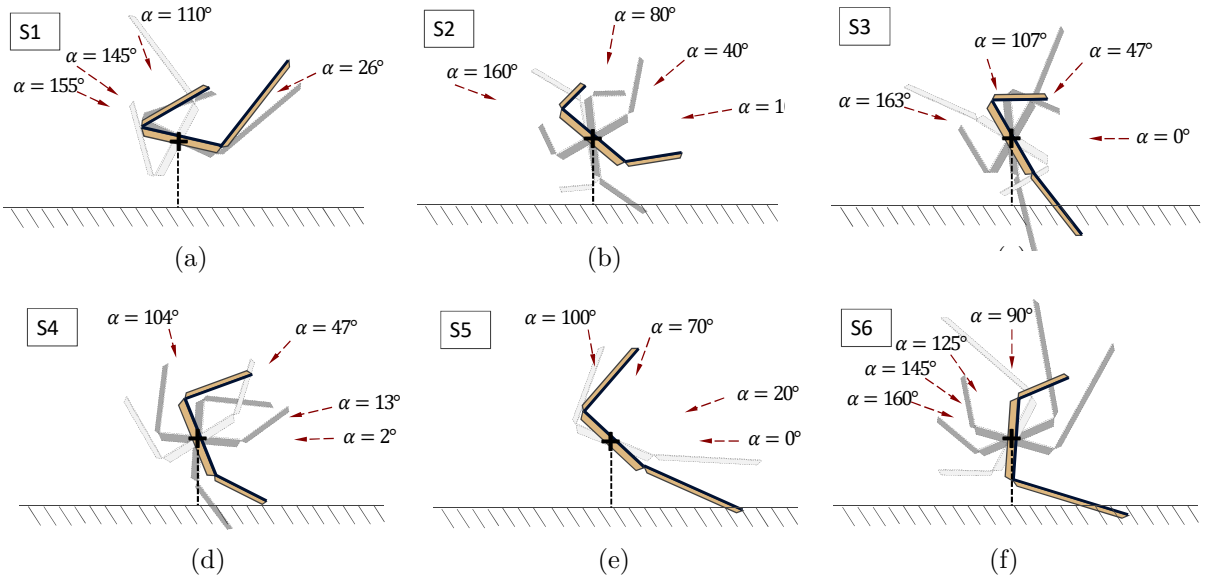

Figure 4.2: Visualization of the randomly defined V-Trough set-ups for the experimental validation.

4.2 Development of the Testing Platform

Laser beams, for practical matters at this scale, follow the basic principles of geometrical optics in the same way as beam radiation (Pedrotti, 2012). Correspondingly, laser devices may be used to experimentally model and corroborate specific predictions of the proposed theoretical model.

A testing platform was developed in order to validate the previously described (Sec. 4.1) 308 predictions related to the 11 V-Trough set-ups defined. The concept behind the testing platform is a device capable of experimentally measuring the aperture lengths that correspond to the macro-optical phenomena considered by the model. Fig. 4.3(a) shows the detailed computational design of the testing platform. This platform is designed to accurately adopt all geometries needed to test the 11 set-ups and explore in detail the interactions between beam radiation and the V-Trough's elements by means of a pair of sliding lasers.

Instead of leaving a V-Trough on the ground facing the sky-dome, this device directly simulates the relative incidence between the experimentally modeled beam rays and the V-Trough's surfaces. Hence, the lasers maintain their aiming direction, while the V-Trough adjusts its angular position θ, as shown in Fig. 4.4(a), in order to account for both the modeled solar elevation α and the β of the PV surface. θ is defined by Eq. 4.3

$$\theta = \beta + \alpha - \pi/2 \tag{4.3}$$

Since the modeled aperture lengths are defined as perpendicular to the incident solar rays, the testing platform performs length measurements perpendicularly to the laser beams. With the platform, it is possible to identify where the start and end of a given macro-optical phenomenon happen. The difference between the locations of these two events determines the experimental length of the corresponding phenomenon. Figs. 4.3(b)–4.3(d) illustrate this procedure for experimentally measuring aR and aR_{PV} for a given V-Trough set-up. The lasers slide, as shown in the figures, until it is visually detected that both aR and aR_{PV} start occurring. The location is marked and then the lasers keep sliding until the phenomena are not detected anymore, which delimits their individual length. With this same procedure, it is possible to measure the aperture lengths chosen in the experimental design (Sec. 4.1), namely aPV_e, aL, aR, aL_{PV}, aR_{PV}, aL_{RPV} and aR_{LPV}. These experimental measurements are then defined as proportions of the length of the PV

surface used for the test. Afterwards, the measured proportions can be compared against the corresponding theoretical predictions.

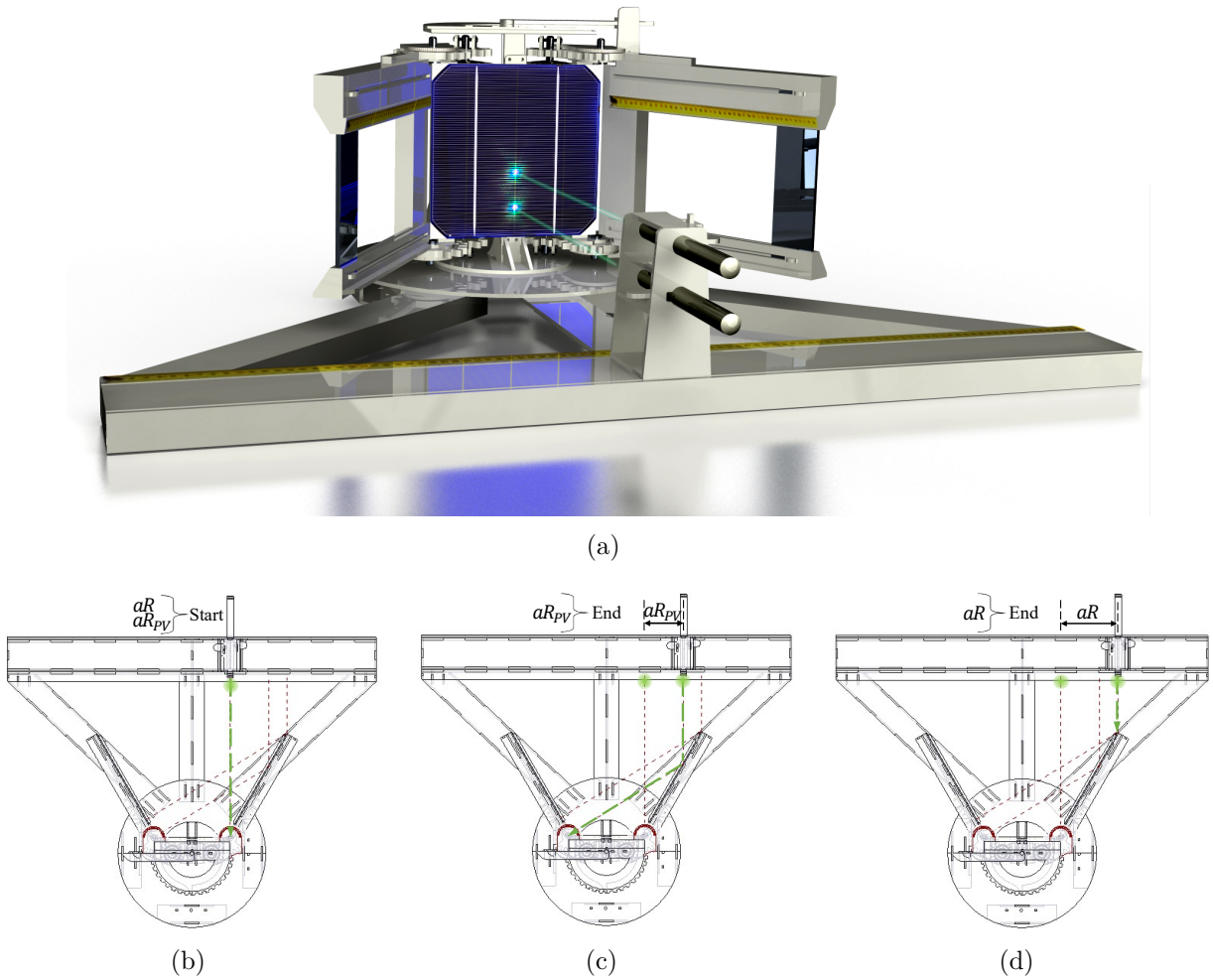

Figure 4.3: Design of the testing platform for the experimental validation of the model.

The testing platform was computationally calculated and designed with Creo Parametric ®; a Computer Aided Design Software (CAD). Seeking to maximize the geometrical accuracy in the final assembly, the majority the pieces were manufactured by Computer Numerical Control (CNC) laser cutting. After the pieces were assembled, the mechanisms were fine-tuned and the lasers carefully calibrated. Fig. 4.4 presents photos of the real testing platform. As illustrated in Fig. 4.4(a), the V-Trough in the platform can adjust its θ and the angular position of its mirrors (ψL and ψR). Also, the reflective surface of each mirror can slide in order to adjust for the given mirror lengths of the set-ups. As pointed in Fig. 4.4(b), the testing platform includes CNC-built tools for measuring the angular positions of all the V-Trough's elements. Additionally, as also shown in Fig. 4.4(b), a series of laser-cut jigs were manufactured for accurately guiding the geometrical disposition of the V-Trough for every set-up.

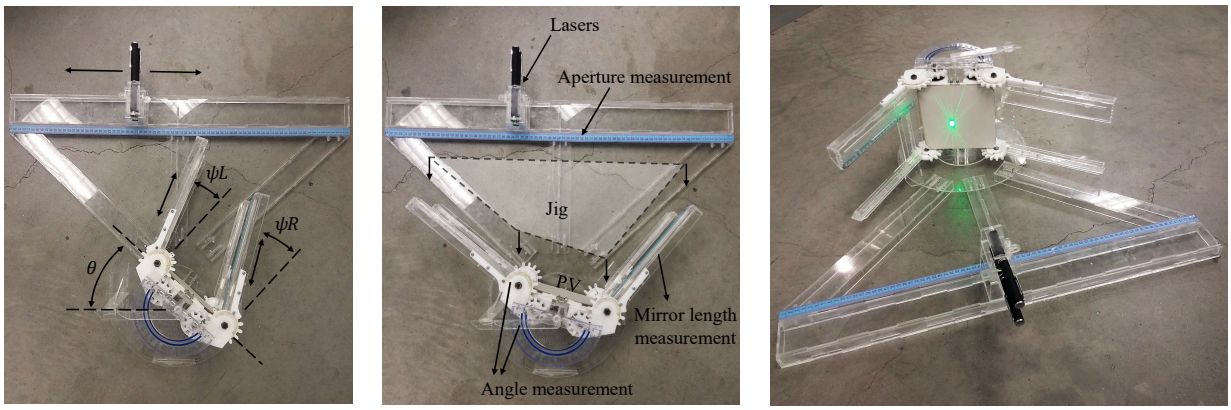

(a) (b) (c)

Figure 4.4: Details of the real testing platform for the validation of the model.

4.3 Results and Statistical Analysis

The results of the experiment were analyzed through a linear regression of the measured values in function of the model predictions. The points for the regression are in fact specific model predictions coupled with the corresponding experimental measurements. If the predictions relate well to the real measurements, the expected result of the regression is a straight line with a slope tending to 1 and a Y-intercept tending to 0.

Fig. 4.5 presents the performed linear regression analysis and the equation of the obtained linear model of the data. This line equation resulted in a highly satisfactory slope of 0.9931 and a Y-intercept of 0.0007. The coefficient of determination $R^2 = 0.9977$ resulted considerably high, implying that 99.77% of the variation in the variable *Measurements* is predictable from the variation in the variable *Model Predictions*.

The residual standard deviation, so-called *Standard Error of estimate* (SE), was calculated to be $SE = 0.0157$. Hence, it can be interpreted that the linear model of the regression has an average accuracy within 1.57% of the PV area.

Fig. 4.5 also shows the 95% *Prediction Interval*. Given a new specified value in the *Model Predictions* variable, the corresponding experimental measurement is 95% likely to fall within this range. This 95% interval can be taken as an estimate of the expected accuracy for future aperture lengths predicted by the V-trough model. The procedure used to define this interval is specified later in this section.

Even if the regression analysis suggests an evidently linear relationship between the predictions and the measurements, statistical analysis can address the following questions more objectively:

- How likely is it that the observed linear response is mainly due to randomness?
- Are there signs of a systematic error?
- How are the residuals arranged around the linear model?
- Is the obtained linear model statistically equivalent to the ideal $X = Y$ response?

The first question can be addressed by testing the "significance of the regression". For this purpose, a parametric statistical analysis was performed and its results are summarized in Table 4.2. According to the shown P-value the regression is, by convention, "extremely statistically significant". This means that it is extremely unlikely that randomness alone could have been the causal reason for the observed linear behavior. Therefore, the null hypothesis of random causality is rejected and, in terms of regression, it is thus accepted that the variable *Model Predictions* is of use in explaining the variability in the variable *Measurements*.

In order to be confident on the results shown in Table 4.2, it is necessary to test the parametric assumptions related to the residuals, i.e., normality and homoscedasticity. Fig. 4.6(a) shows a scatter-plot of the standardized residuals, namely the residuals divided by the standard deviation. There is not an evident systematic pattern within the residuals, which suggests that the regression model fits the data properly.

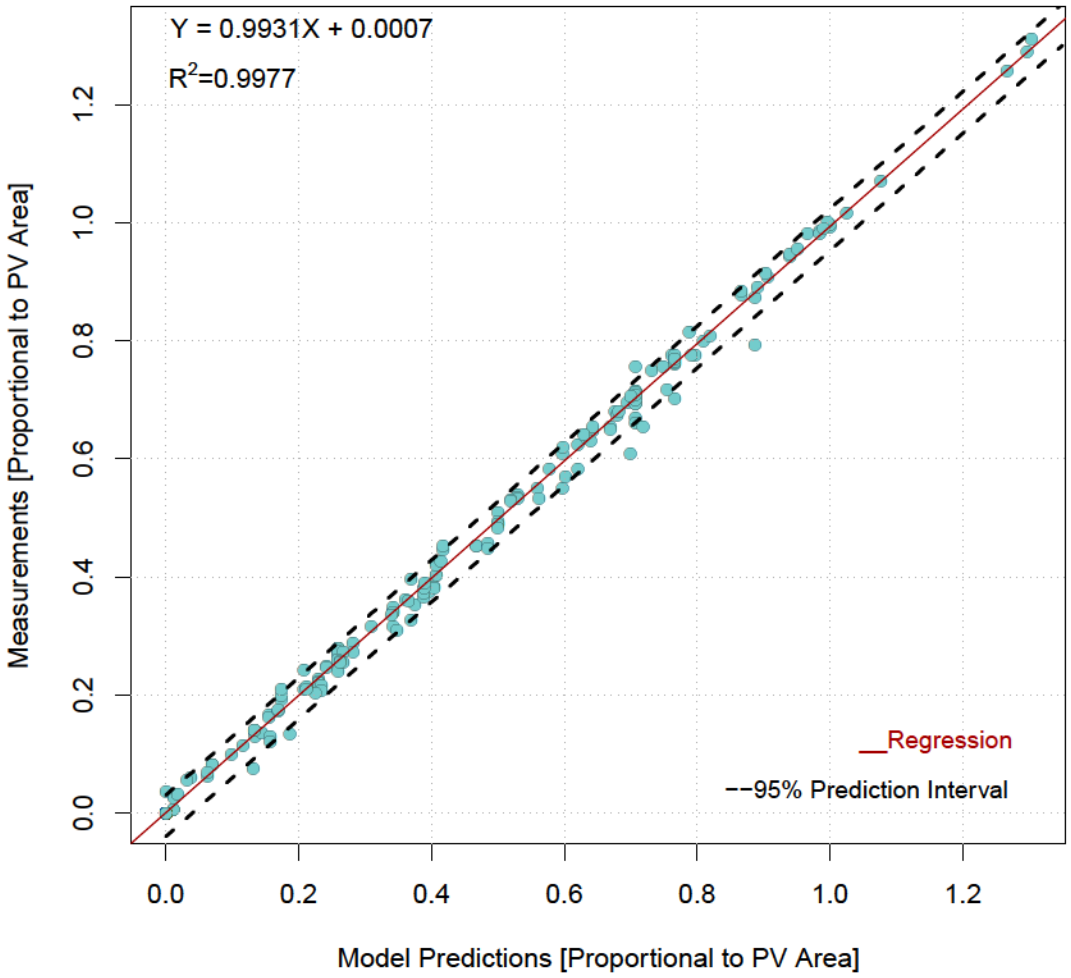

Figure 4.5: Regression analysis and linear model.

Table 4.2: ANOVA table of the regression model.

Source	*DF*	*SS*	*MS*	$F-value$	$P-value$
Regression	1	33.29	33.29	135512	$< 2e-16 * **$
Residuals	306	0.08	0.00025		

Fig. 4.6(b) presents a histogram of the residuals. In this histogram there are evident violations to the normality assumption. The residuals are not normally distributed, tending more towards zero in a so-called state of "thin-tails" distribution. The appreciation about non-normality was corroborated with Shapiro-Wilk and Anderson-Darling normality tests, which resulted significant with P-values $< 2.2e-16$ for both tests. This means that it is very unlikely that the differences between the distribution of the residuals and the normal distribution are solely due to randomness. Several standard transformations of the data were implemented, i.e., $(1/y)$, $ln\,(y+1)$, $log_{10}\,(y+1)$, $\sqrt{y}$ and arcsin; but none of the transformations could satisfy the parametric assumptions for the residuals.

According to Reis and Judd (2000), "thin-tail violations of normality are generally benign". In this case, this normality violation means that the differences between the experimental values and the predicted values tend to 0 more than expected; which is not problematic for the accuracy of the model. However, significant

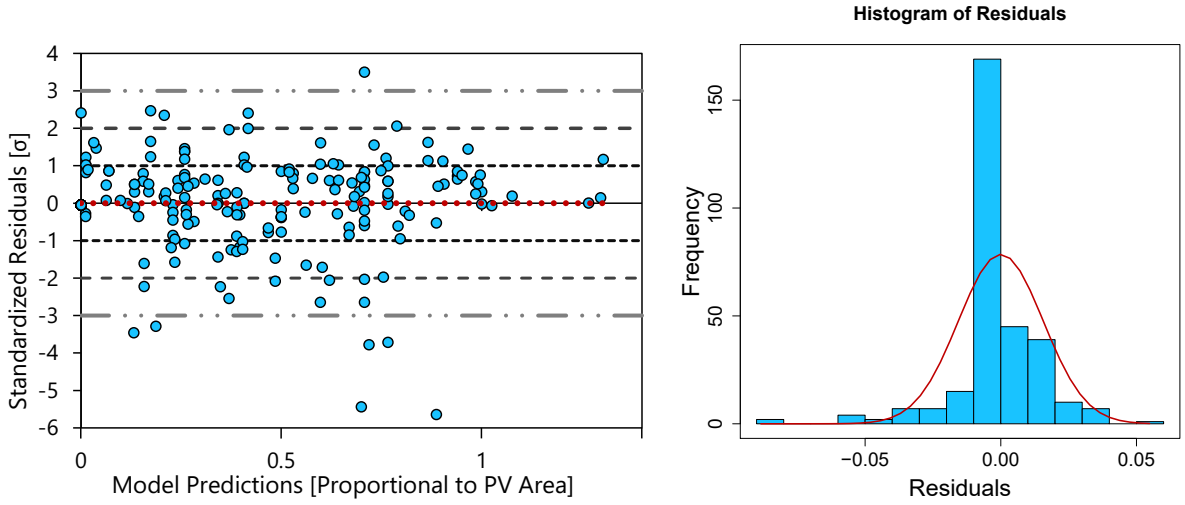

(a) (b)

Figure 4.6: Analysis of the regression residuals.

violations of normality may affect the validity and precision of inferences made from parametric tests of statistical hypothesis, confidence intervals and prediction intervals. Therefore, it was defined to further analyze the experimental results with non-parametric methods, i.e., Monte Carlo randomization hypothesis test and Bootstrapping intervals, and see if the non-parametric results differ from the parametric analysis summarized in Table 4.2.

As indicated by Gotelli and Ellison (2013), the "significance of the regression" was tested by means of a Monte Carlo randomization analysis. As opposed to comparing the data-set with the expected behavior of a normal distribution, this analysis directly simulates the effect of randomness by randomly re-arranging the data many times and recalculating the regression line. After 100000 Monte Carlo simulations, the number of times that a randomly simulated regression slope was equal or greater than the observed slope of the model was 0. The previous result implies, in accordance with the parametric results, that the regression is extremely statistically significant with a P-value tending to 0. Fig. 4.7 illustrates the Monte Carlo method implemented, where a histogram is shown of the simulated slopes calculated from every reshuffling of the data. From this figure it is evident that the randomness effect is far from reaching the slope obtained by the original regression.

Even though the significance of the regression is now evident, it is also of great interest to test if the slope of the regression is statistically equivalent to 1, which is the value expected from an ideal $X = Y$ correspondence between the model predictions and the respective measurements. To test this hypothesis, it is necessary to analyze if the effect of randomness could have been the major cause of the delta between the slope of the regression model and an ideal slope of 1. This delta resulted in $\Delta m = 0.0068$. Within the Monte Carlo simulations, 90324 was the number of times that this observed delta Δm was matched or exceeded by simulated slopes with their delta calculated from the mean slope of the Monte Carlo simulations. Therefore, the significance level for the regression's Δm, from a slope 1, corresponds to a high P-value $= 0.90324$. From the previous result, it can be stated that the slope achieved by the regression model is statistically equivalent to the ideal 1, since it is very likely that the observed Δm could have been caused mainly by randomness. It is also of interest to test a similar hypothesis for the Y-intercept. Since the ideal regression line for this case has a Y-intercept $b = 0$, does the observed Y-intercept differs significantly from 0?; with that difference referred to as the delta Δb. With the same Monte Carlo method, it was found that the significance level for the regression's Δb, from a Y-intercept of 0, corresponds to the P-value $= 0.96171$. As with the slope significance analysis, from the previous result it can be inferred that the Y-intercept of the regression model is statistically equivalent to 0. Consequently, it can be assumed that the regression model as a whole is statistically equivalent to the ideal expected model, where $Y \approx X$; so *Model Predictions* $\approx$ *Experimental Measurements*.

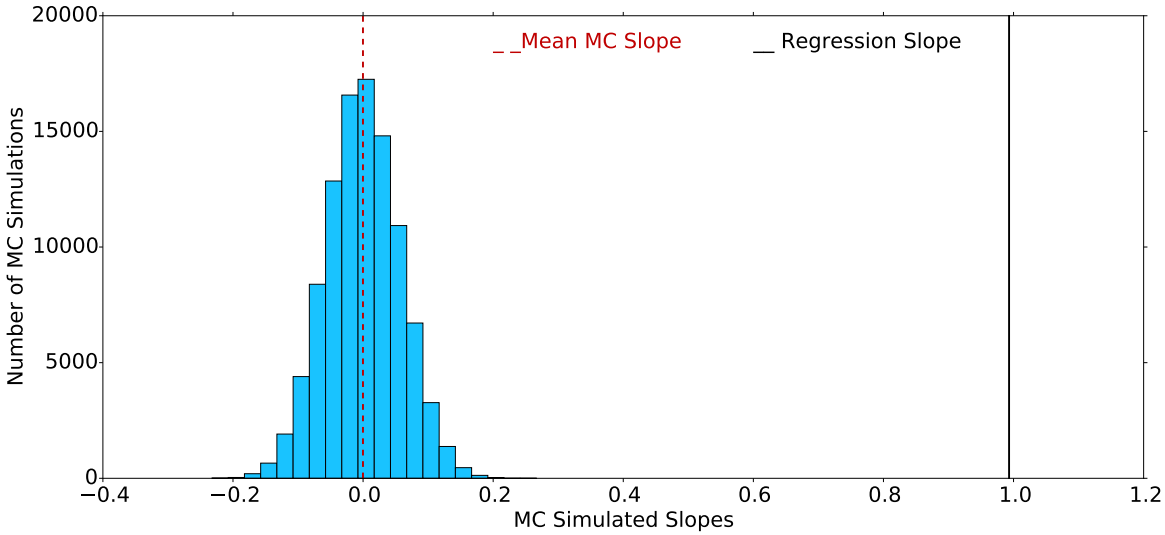

Figure 4.7: Monte Carlo test of hypothesis for the significance of the regression.

The performed regression analysis proposes a linear model for a population of data but based only on a sample data-set. Therefore, *Confidence Intervals* are a useful way of estimating the likely ranges for the real linear parameters of the whole population of possible data. Since the residuals cannot be assumed to be normally distributed, a non-parametric method, so-called Bootstrapping (Lins et al., 2015), can be used to estimate such intervals. Fig. 4.8 shows the frequency distribution of the simulated Bootstrapping slopes with Fig. 4.8(a) and the simulated Bootstrapping Y-intercepts with Fig. 4.8(b). For the distribution of every statistic calculated, 100000 Bootstrapping reshuffling simulations were performed.

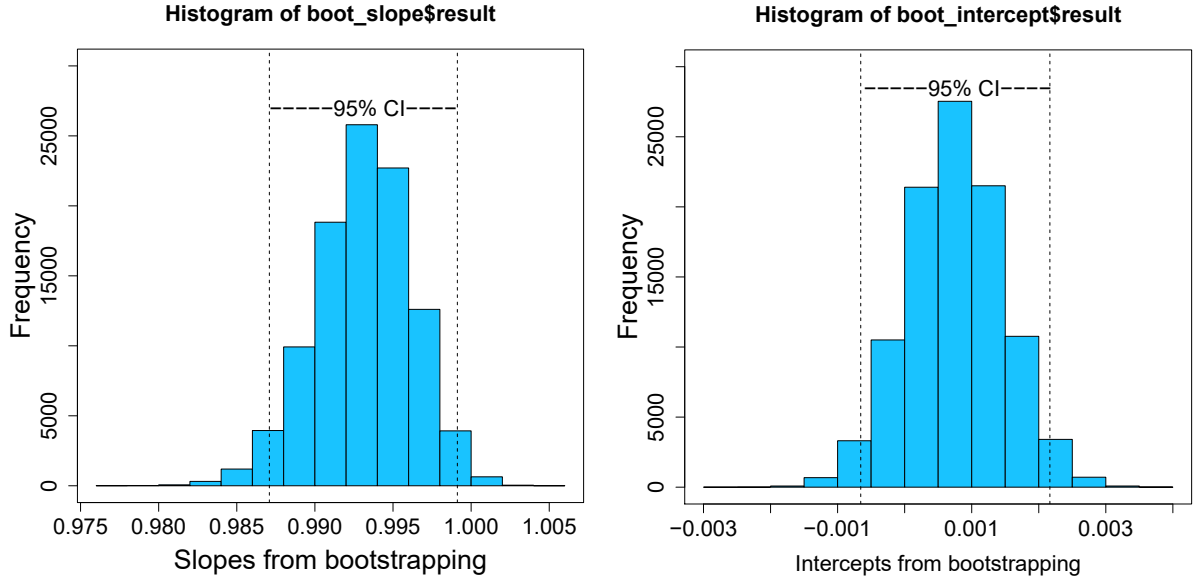

(a) (b)

Figure 4.8: Bootstrapping 95% confidence intervals for (a), the slope, and (b), the Y- intercept.

Through Bootstrapping it was possible to estimate the 95% confidence intervals for the slope and Y-intercept. There is hence a 95% confidence in that the interval $[0.987, 0.999]$ contains the real slope drawn from the whole population of data related to the *Model Predictions* versus *Experimental Measurements*.

Similarly, there is 95% confidence in that the interval $[-0.00065, 0.00216]$ contains the real Y-intercept. Those narrow 95% confidence intervals imply favourable expectations in terms of how accurately the regression model represents the whole scenario of *Model Predictions* versus *Experimental Measurements*. Even the boundaries of those intervals, with a high confidence that they contain the real values, are still virtually identical to the ideal values.

A Bootstrapping Monte Carlo method was also used to estimate the 95% prediction interval; shown in Fig. 4.5. The average ceiling for this prediction interval was 0.03 higher than the estimated response variable (*Experimental Measurements*) and the average floor of the interval was 0.041 below the estimated response variable. This result implies that, if the current regression model is applied to new data, it is expected that 95% of the times the real values would fall within an interval than would, in the worst case, underestimate a given optical entity in 3% of the PV length or overestimate it in a 4.1%.

The most critical optical results that can be predicted by the theoretical model are the *Incident Concentration* (C) and the *Effective Concentration* (C_e). In order to assess the accuracy implications of the model, a comparison was made between those variables calculated from the model's predictions against the same variables calculated directly from the experimental measurements. On average, the *Model Predictions* led to a C that is 0.56% less than the same entity calculated from the *Experimental Measurements*. Also, the *Model Predictions* led to a C_e that is, on average, 0.31% greater than the experimentally calculated value. Fig. 4.9 presents, for all the tested V-Trough set-ups, the percentage errors between modelled and measured C, with EC, and between modelled and measured C_e, with EC_e. The figure also shows the corresponding average percentage errors with $\overline{EC_e}$ and $\overline{EC}$.

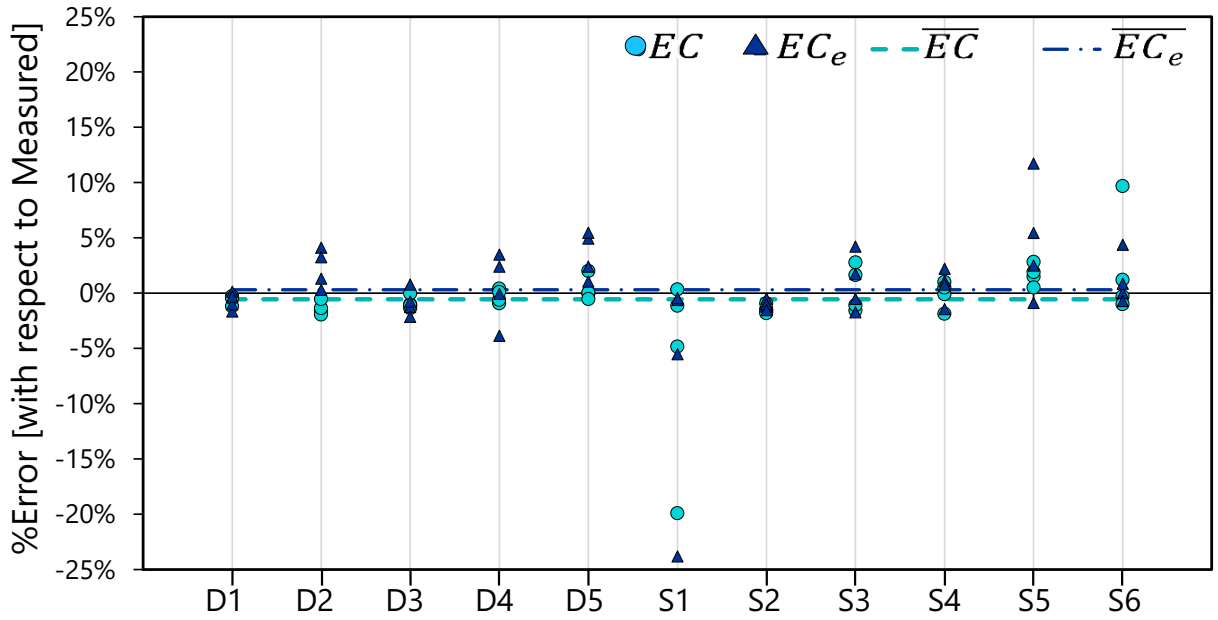

Figure 4.9: Percentage error between predicted and measured incident (C) and effective (C_e) optical concentration.

Fig. 4.10 explores the behavior of EC and EC_e plotted against the *Experimental Measurements*. Two linear regressions were performed, for EC with $R(EC)$ and for EC_e with $R(EC_e)$. The equations of these regression lines are presented in the figure. Both regressions show a tendency for the percentage errors to decrease as the magnitude of *Experimental Measurements* increases. This suggests that the errors between the compared optical variables are not proportional to the magnitude of the measurements, but rather homogeneous in magnitude themselves. Therefore, in accordance with the results, the same average magnitude of relative errors is expected to have a proportionally greater impact when the measurements are smaller in magnitude; and vice-versa. Considering the nature of the experiment and the way it was performed with the described testing platform, this behavior makes intuitive sense: It is reasonable to suggest that small

and, on average, homogeneous errors could have been caused by geometrical imprecision in the assembly of the testing device and in the measuring procedure. This imprecision is not proportionally linked to the aperture length being measured because what is actually being measured are the locations of the start and end points for a given macro-optical phenomenon.

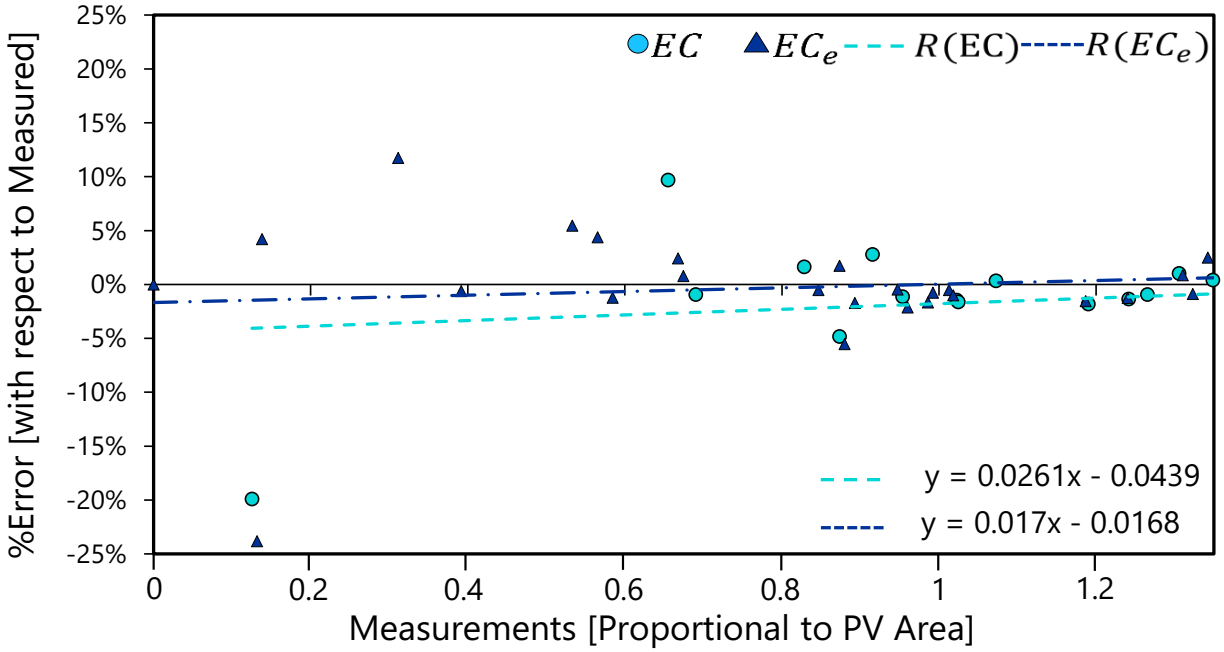

Figure 4.10: Percentage error between predicted and measured incident (C) and effective (C_e) optical concentration, in function of the Measurements.

Considering the results of the statistical analysis, in particular the behavior of the residuals, it is reasonable to support the hypothesis that most of the errors between the model's predictions and the experimental measurements, however small, correspond to random errors in the measurement process, either due to the imprecision in detecting the optical events or due to structural imprecision in the testing platform. Even so, the results are statistically equivalent to the ideally expected behavior and the proposed theoretical model is considered to have been satisfactorily corroborated.

Chapter 5

Parameters Definition in the Design Context

With the geometrical flexibility in V-Troughs pursued by this project, a vast number of possible fixed and dynamic set-ups (combinations of parameters) becomes available for a given designer/engineer. Accordingly, how to guide the parameters definition process and support an effective navigation of the space of solutions? In this section, a series of performance indicators and indices are proposed to extend the implications of the theoretical model into the design context. These indicators and indices are intended for guiding the parameters definition process when implemented through two new tools: an interactive tool, named "VTDesign", and and a heuristic optimization tool, named "GA-WA". By proposing these tools, this section addresses the specific objectives I and II.

5.1 Performance Indicators and Indices in Design

As the general objective states (Sec. 1.4), one of the main purposes to develop the theoretical model that is proposed in this project is to "support a flexible definition of their [V-Trough devices] parameters in a personalized household context". As reviewed in Sec. 2.1, it is desirable to generate performance indicators and indices, based on a core analytical model, in order to better guide design/engineering decisions. This section presents a series of such performance indicators that measure the performance of a V-Trough in the design context:

(i) $\overline{C_e}$ (the average effective concentration)

(ii) $Cost$ (the cost of materials)

(iii) T_{sp} (the space required)

Moreover, from the integration of these indicators in proportional comparisons, three multi-objective indices were proposed:

(a) I_{COE} ($\overline{C_e}$ versus $Cost$)

(b) MI_{COE} ($\overline{C_e}$ versus $Cost$ and $\overline{C_e}$ versus T_{sp} combined)

(c) MDI_{COE} (the same comparison as the previous one but also including the discretization effects related to the solar cells)

These indices support the specific objectives IV and V because they are used in the proposed interactive tool (Sec. 5.2) as well as in the proposed heuristic optimization tool (Sec. 5.3).

It is worth emphasizing that these indicators and indices are dependent on the same assumptions made for the core analytical model (Sec. 3.1). In particular, the optical performance is solely based on the solar beam radiation interactions and no temperature losses are considered. It is well understood that these

assumptions limit the direct applicability of these indicators and indices in real design/engineering scenarios. However, this research project is contextualized in the early design stages, where it has been reported (Sec. 2.1) that similar indicators and indices can be used for an early comparison of V-Trough strategies. Moreover, these indicators and indices can be complemented, in further work, with other reported models of diffuse radiation and temperature losses for a more realistic performance estimation.

As depicted in Figs. 5.1(a)–5.1(b), not all the solar rays that reach the device manage to make contact with the PV absorber. Several optical phenomena can affect the *Effective Concentration* (C_e), such as shadows or rays that are reflected back out after one or two bounces off the mirrors. The mathematical

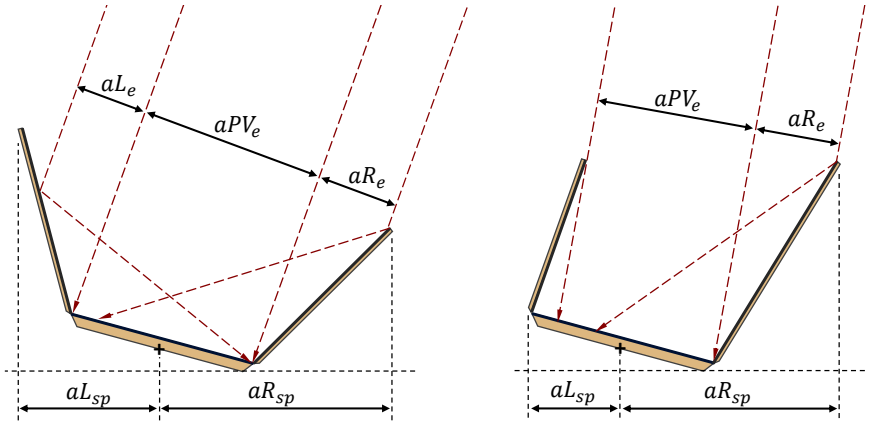

(b)

Figure 5.1: Diagram of a V-Trough photovoltaic device shown in two different geometrical set-ups in (a) and (b).

model presented in Sec. 3.2 provides the detailed equations to assess this phenomena and estimate the optical effective contributions from each V-Trough's elements (aPV_e, L_e and aR_e). The sum of these contributions results in the *Total Effective Aperture* (aT_e), which is related to C_e in Eq. 5.1. Since the phenomena related to aT_e and the PV length (LPV) share the same *Depth*, C_e can be considered as the ration of the *Effective Harvesting Area* (EHA) over the PV area.

$$C_e = \frac{aT_e}{LPV}. \tag{5.1}$$

While C_e is useful for assessing the optical performance of a given set-up, it is related to only one given solar elevation α. In order to obtain an indicator of the optical effectiveness of the device throughout the day ($\overline{C_{e(\alpha f,\alpha c)}}$), Ce is averaged over an angular α range, as presented in Eq. 5.2. This range goes from a "floor" α_f to an angular "ceiling" of α_c and advances in angular discrete steps of magnitude α_s. As explained in Sec. 3.1 and shown in Fig. 3.9(a), α_f and α_c can be defined so as to account for possible shadows in a personalized context. For the same photovoltaic area, the greater $\overline{C_e}$ is, the greater the solar energy that can be harvested throughout the given α range. Hence, this indicator can be used in early design stages to compare different V-trough set-ups through the perspective of average optical (beam) effectiveness.

$$\overline{C_e} = \frac{\sum_{i=0}^{\left[\frac{\alpha_c-\alpha_f}{\alpha_s}\right]} C_{e(\alpha_f+i*\alpha_s)}}{\frac{\alpha_c-\alpha_f}{\alpha_s}+1} \tag{5.2}$$

Although a V-Trough can increase the optical concentration of a solar absorber, it can also increase the amount of materials required due to the mirrors and additional supporting structure. For a V-Trough to be preferable over a flat solar panel, it must at least increase the effective harvesting area in a greater proportion than it increases the cost of materials. The indicator $\overline{C_e}$ is of great use to compare V-Trough alternatives with equivalent or similar mirror area. However, when comparing alternatives with considerable differences

in the mirrors as proportions of the PV area, $\overline{C_e}$ alone may be misleading for design decisions. For instance, a given V-Trough set-up may be able to double the $\overline{C_e}$ of a PV absorber, but if it also triplicates the capital cost of the device due to the additional materials required, then such set-up would not be cost-effective. In such a case, it would be more cost-effective to just use the available budged to acquire a bigger area of regular flat PV panels. Therefore, a new cost-effectiveness index (I_{COE}) is proposed to address this proportional comparison in early design stages of a V-Trough system. I_{COE} can be used to assess the performance of V-trough set-ups by contrasting the gain of incident energy, due to resulting $\overline{C_e}$, against the added materials cost due to the mirrors and extra supporting structure.

It is worth noting that it is not the intention of this research project to offer an all-encompassing index to take final decisions of cost-effectiveness, since that would imply taking into account the interactions with diffuse radiation and the losses due to temperature and non-uniform illumination, among others. Moreover, the proposed index does not take into account the tracking costs, since it focuses on manual tracking and other simple tracking actuation methods, such as water dripping. I_{COE} is based on other simple cost-effectiveness assessments reported in the literature (see Sec. 2.1). It is intended as a practical index for broad first comparisons within the limitations of the model proposed. I_{COE} may be complemented with other factors in further work.

In order for the index I_{COE} to be more intuitive, it is defined in proportion of a reference set-up, which consists in a fixed PV absorber with no concentrating mirrors. This way, if $I_{COE} > 1$, it suggests that the alternative being assessed has a better cost-effectiveness than the reference. Conversely, if $I_{COE} < 1$, it may imply that it is not worth employing the V-Trough set-up being analyzed, since it probably would perform worse than a simpler fixed PV absorber with no mirrors.

Eq. 5.3 defines the proposed cost-effectiveness index, which must also be calculated for a given (αf,αc) range. Accordingly, $\overline{C_e}$ and $\overline{C_{eRef}}$ are also stated in function of the same solar elevation range and correspond respectively to the average effective concentration of the V-Trough set-up being analyzed and to the reference set-up described. The index λ is defined in Eq. 5.4 and can be interpreted as the proportion of the area costs related to the mirror surfaces over the area costs related to the PV absorber.

$$I_{COE(\alpha f,\alpha c)} = \left(\frac{\overline{C_{e(\alpha f,\alpha c)}}}{\overline{C_{eRef(\alpha f,\alpha c)}}} \right) * \left(\frac{LPV}{LPV + \lambda\,(LL + LR)} \right) \tag{5.3}$$

Where

$$\lambda = \frac{CO_s + CO_m}{CO_s + CO_{pv}} \tag{5.4}$$

With CO_{pv} = Area cost $\left[\mathrm{USD}/m^2\right]$ of the PV absorber, CO_m = Area cost $\left[\mathrm{USD}/m^2\right]$ of the mirrors and CO_s = Area cost $\left[\mathrm{USD}/m^2\right]$ of the supporting structures. These area cost values may vary according to the country, the year and if the implementation is either for a household or utility scale. However, the following values are suggested as a useful reference. Mirror CO_m and supporting structures CO_s area costs can be taken from Sangani and Solanki (2007) as 13.33 $\left[\mathrm{USD}/m^2\right]$ and 62.23 $\left[\mathrm{USD}/m^2\right]$, respectively. From MIT (2015) it was estimated that the area cost of a residential PV panel of 15% efficiency is approximately 600 $\left[\mathrm{USD}/m^2\right]$. Therefore, a suggested λ that can be taken as a reference is $\lambda = 0.114$.

I_{COE} can hence be used as a multi-objective index. Its maximization implies maximizing $\overline{C_e}$, while minimizing the proportional cost of materials. However, even under the same previously described assumptions, not always the V-Trough set-up with the highest I_{COE} results in the lowest cost in terms of materials. For instance, a given design case study may aim at minimizing the materials cost of a V-Trough device for a given daily energy need. In this case, a number of solar cells will be arranged according to the chosen V-Trough set-up. Solar cells are discrete units with discrete areas and, therefore, they can not always be arranged in a solar panel so as to precisely fulfill a given energy demand. This discretization effect of the solar cells can be considered in a more detailed cost comparison. For this purpose, the minimum number of solar cells required (N_{pvc}) is first calculated, for a daily energy need [Wh] (E_{day}), with Eq. 5.5.

$$N_{pvc} = \left\lceil \frac{E_{day}}{\overline{I} * \overline{C_e} * \eta_{pv} * \eta_s * A_{pvc} * H_{sun}} \right\rceil, \text{ where } H_{sun} = \frac{\alpha c - \alpha f}{15} \tag{5.5}$$

With $\overline{I}$ = Average solar irradiance $[W/m^2]$, η_{pv} = Photovoltaic efficiency, η_s = Electric efficiency of the system, A_{pvc} = Area $[m^2]$ of a single solar cell, and H_{sun} = Hours of exposure to sunlight. It is worth noting that N_{pvc} must be rounded-up in order to account for the discretization of the solar cells. The cost of materials ($Cost$ in USD), for a given energy need, can then be calculated with Eq. 5.6. $Cost$ can be used as a performance indicator, similar to I_{COE}, but considering also the discretization of the PV surface into individual solar cells.

$$Cost = N_{pvc} * A_{pvc} \left[CO_{pv} + CO_s + \left(\frac{LL + LR}{LPV} \right) * (CO_s + CO_m) \right] \tag{5.6}$$

The space required for a V-Trough system can also be considered a priority for taking design decision. This space depends on the geometrical disposition of the device, as shown in Figs. 5.1(a)–5.1(b). For this calculation, it is useful to assume that β changes by means of a pivot at the center of the LPV length. It is also assumed that the V-Trough's elements have no thickness. The linear space can then be calculated to the left of the pivot (aL_{sp}), with Eq. 5.7, and to the right of the pivot (aR_{sp}), with Eq. 5.8.

$$aL_{sp} = max \left[\left(\frac{aPV_{sp} + |aLL_{sp}| + aLL_{sp}}{2} \right), \left(\frac{|aLR_{sp}| - aLR_{sp} - aPV_{sp}}{2} \right) \right] \tag{5.7}$$

$$aR_{sp} = max \left[\left(\frac{aPV_{sp} + |aLR_{sp}| + aLR_{sp}}{2} \right), \left(\frac{|aLL_{sp}| - aLL_{sp} - aPV_{sp}}{2} \right) \right] \tag{5.8}$$

Where,

$$aPV_{sp} = LPV * cos\beta \tag{5.9}$$

$$aLL_{sp} = -LL * sin\,(\beta - \psi L) \tag{5.10}$$

$$aLR_{sp} = LR * sin\,(\beta + \psi R) \tag{5.11}$$

The previous equations were geometrically derived and then verified in multiple set-ups with Creo Parametric®; a Computer Aided Design Software. In order to calculate the *Total Linear Space Required* (aT_{sp}), aL_{sp} and aR_{sp} must be calculated for every change in position of the V-Trough along the day. As stated in Eq. 5.12, the maximum linear spaces for left and right are then independently identified and added together. It is worth noting that $max\ aL_{sp}$ and $max\ aR_{sp}$ do not have to happen at the same solar elevation. aT_{sp} can be used as an indicator for comparing different set-ups in terms of the linear space required. If the minimum number of cells (N_{pvc}) is known, the *Total Area Required* $[m^2]$ (T_{sp}) can then be calculated with Eq. 5.13. T_{sp} can be used as a performance indicator for the same purpose of aT_{sp}, but also considering the discretization effects of the solar cells in the term N_{pvc}.

$$aT_{sp} = max\ aL_{sp} + max\ aR_{sp} \tag{5.12}$$

$$T_{sp} = \left(\frac{aT_{sp}}{LPV} \right) * N_{pvc} * A_{pvc} \tag{5.13}$$

While I_{COE} considers both harvesting energy gain and material costs, it might be useful to have a multi-objective index which also considers the space required for the device. In this research project, two new such indices are proposed, namely MI_{COE} and MDI_{COE}. Both address and weight the following two questions:

- How does the energy harvested by a given V-Trough compare to the energy that could be harvested if the same cost of materials were used for a reference panel?
- How does the energy harvested by a given V-Trough compare to the energy that could be harvested if the same space were used to allocate a reference panel?

In essence, these indices address the problem of cost-effectiveness from the perspectives of both monetary cost and the space needed.

The *Multi-Index of Cost-Effectiveness* (MI_{COE}), presented in Eq. 5.14, allows to compare the relative impact of any given V-Trough set-up in terms of the optical performance, the cost of materials and the

linear space needed. A weight $W1$ is assigned as the relative importance of monetary capital cost and $W2$ as the relative importance of space required. As Eq. 5.15 establishes, for a more intuitive interpretation, it is suggested that both weights fulfill the equality. $W1$ and $W2$ are subjective and must be assigned by the user of the MI_{COE} index according to his/her priorities and the case studio at hand. MI_{COE} can be used as a multi-objective performance index seeking to simultaneously maximize the average effective concentration, minimize the cost of materials and minimize the linear space needed.

$$MI_{COE(\alpha f,\alpha c)} = \left(\frac{\overline{C_{e(\alpha f,\alpha c)}}}{\overline{C_{eREF(\alpha f,\alpha c)}}} \right) * \left[W1 \left(\frac{LPV}{LPV + \lambda\,(LL + LR)} \right) + W2 \left(\frac{LPV}{aT_{sp}} \right) \right] \tag{5.14}$$

$$W1 + W2 = 1 \tag{5.15}$$

The *Multi-Discrete-Index of Cost-Effectiveness* (MDI_{COE}), presented in Eq. 5.16, differs from MI_{COE} in that it considers the discretization effects related to the solar cells. $Cost_{REF}$ and T_{spREF} are, respectively, the cost of materials and the total area, needed for a given energy need, in the case of a reference horizontal and flat solar panel.

$$MDI_{COE(\alpha f,\alpha c)} = W1 \left(\frac{Cost_{REF}}{Cost} \right) + W2 \left(\frac{T_{spREF}}{T_{sp}} \right) \tag{5.16}$$

The presented performance indicators and indices, namely $\overline{C_e}$, I_{COE}, $Cost$, aT_{sp}, T_{sp}, MI_{COE} and MDI_{COE}, are hence presented in order to support the definition of V-Trough parameters in the design context.

5.2 Interactive Tool: VTDesign Software

This section presents the conceptual structure, the interface design and the usability considerations of VT-Design, a new interactive generative tool. VTDesign is intended to support the early design stages of a given V-Trough system in personalized scenarios. It was developed to guide a designer/engineer through the process of defining the parameters of such devices by means of real-time iterations and the visualization of their dynamic geometries and their optical performance. The optical calculations are based on the model proposed in Sec. 3. Furthermore, some of the most critical performance indicators and indices, presented in Sec. 5.1, are used in the software seeking to allow a greater insight into the implications of early decisions.

5.2.1 Conceptual Structure in The Design Framework

Fig. 5.2 contextualizes the role and conceptual procedures related to VTDesign in the design framework. According to the specific given design scenario, there are several initial conditions to consider, such as an α range limited by shadows or the number of tracking steps defined from technical or human limitations. As explained in Sec. 1.1, a manual tracking strategy, at the household level, might introduce a disruption in the daily routines of the potential users. There may also be limited resources in terms of the budget for the capital cost, the space to allocate the device or the number of solar cells available.

Regarding the goals behind the engineering of the V-Trough system, they may be classified from two perspectives. The first is to maximize the energy harvesting potential, or the broad cost-effectiveness (I_{COE}), within constraints given by the initial conditions. The second one is to meet a given daily energy need, while minimizing the materials cost, the PV area required or the space occupied.

From the initial conditions and a stated design goal, the software intends to interactively guide the designer throughout the process of defining the static and dynamic geometrical parameters of the device. Several performance indicators and indices provide a quantitative assessment of the performance resulting from the geometrical parameters explored by the user. Based on the theoretical model presented in this research project, curves of the optical performance also support this assessment. Moreover, these curves contrasted with a visualization of the dynamic geometry of the device, are intended to provide a qualitative insight into the optical behavior. After successive iterations, the user proceeds for a more detailed inspection of the device under exploration in a three-dimensional preliminary CAD model. After further iterations, the

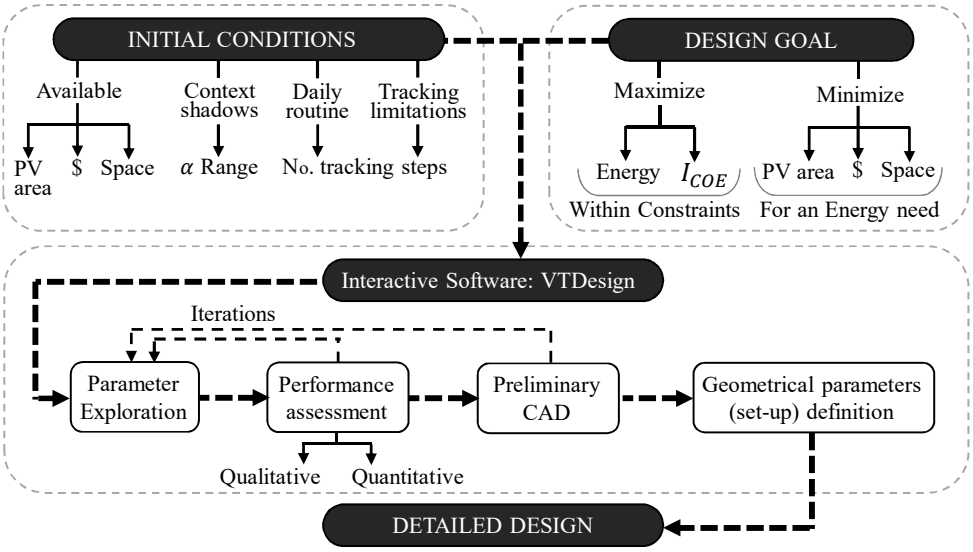

Figure 5.2: Conceptual structure where the proposed software is contextualized.

user determines the desired parameters comprising the set-up of the V-Trough system. This lays the foundation for the subsequent detailed design stages, which may include more realistic optical simulations. The output of VTDesign is a preliminary V-Trough set-up and the numerical results of these initial performance simulations. VTDesign is hence a "Generative interactive tool", which results can then be further analyzed with "Evaluative tools" such as the ones discussed in Sec. 2.2.

Fig. 5.3 presents the structure of modules and sub-modules defined to accomplish the stated role of the software.

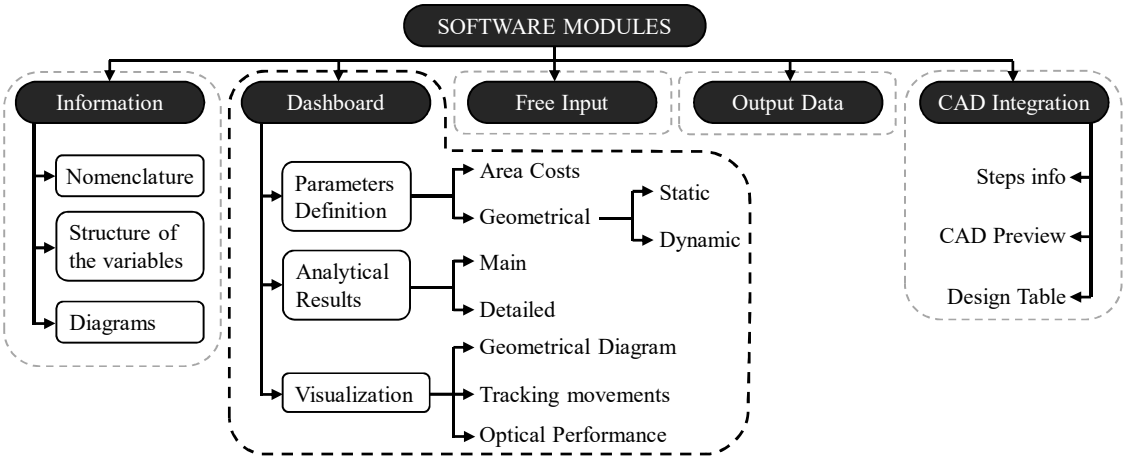

Figure 5.3: Conceptual scheme of the modules and sub-modules.

The "Information" module is intended to guide non-expert users before or during their exploration of potential V-Trough parameters. The Oxford English Dictionary defines a non-expert as "A person without professional or specialized knowledge in a particular subject" (Oxford University, 2017). The main module is the "Dashboard", where the user can define the main geometrical parameters while visualizing the V-Trough's proportions, movements and performance in terms of optics and cost-effectiveness. For more advanced users, the dynamic parameters can be freely entered as lists for the whole α range in the module "Free Input". Also, the module "Output Data" provides a detailed table with all the optical entities calculated for every

solar elevation of interest. Lastly, in the module "CAD Integration", the parametric exploration process is integrated with the CAD software SolidWorks® for a three-dimensional visualization of the geometries and tracking movements.

5.2.2 Interface and Usability

The structure presented in Fig. 5.3 served as a guide to design in detail the features of each module and their interactions. The user interface application was developed in Microsoft Excel®. Also, several functional features, such as the integration with SolidWorks®, were programmed in Visual Basic.

Fig. 5.4(a) shows the Information module's interface structured into functional and graphical sections. The final design and overall distribution is shown in Fig. 5.4(b). The conceptual structure uses the previously discussed Fig. 3.8 in order to show how the main optical variables are causally interrelated. The Diagrams section provides several depictions of the V-Trough parameters and how they relate to some of the most critical optical aperture lengths. The nomenclature section provides a full description of the variables involved: N.1 defines the most important variables; N.2 defines the prefixes and suffixes used in the nomenclature; N.3 defines the optical angles which are not entered by the user, but calculated by the model; N.4 defines the variables of area costs; and N.5 defines all aperture length variables.

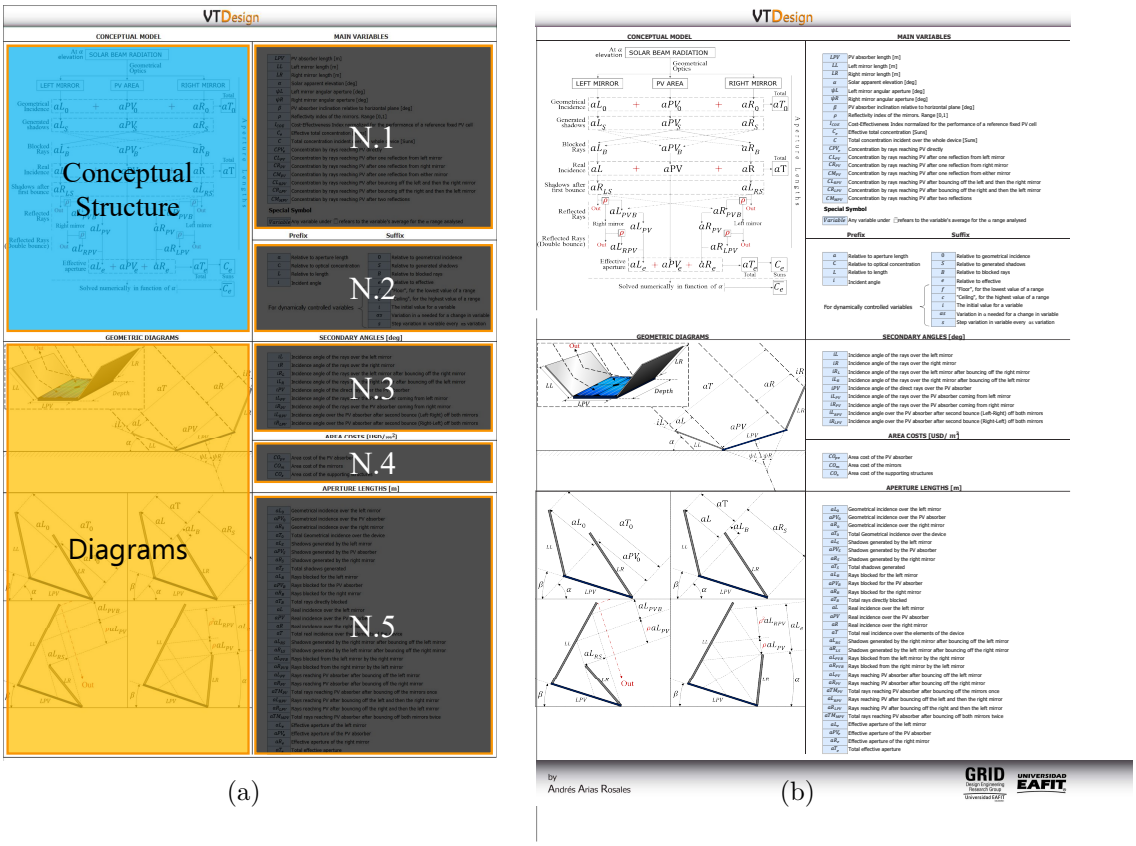

Figure 5.4: Overall distribution of the Information module. This figure is not intended for a detailed inspection of each element, but for an overview.

Fig. 5.5(a) presents the functional and graphical sections of the Dashboard module. The interface is divided into sub-modules of Parameter Definition (PD), visualization (V) and Results analysis (AN). First, the user defines the α range in PD.1 and the geometrical parameters which are set to be fixed in PD.2. If β, ψL or ψR are desired to be set as dynamic for tracking purposes, their parameters can be defined in PD.3 and PD.4. Lastly, the user enters the area costs in PD.5.

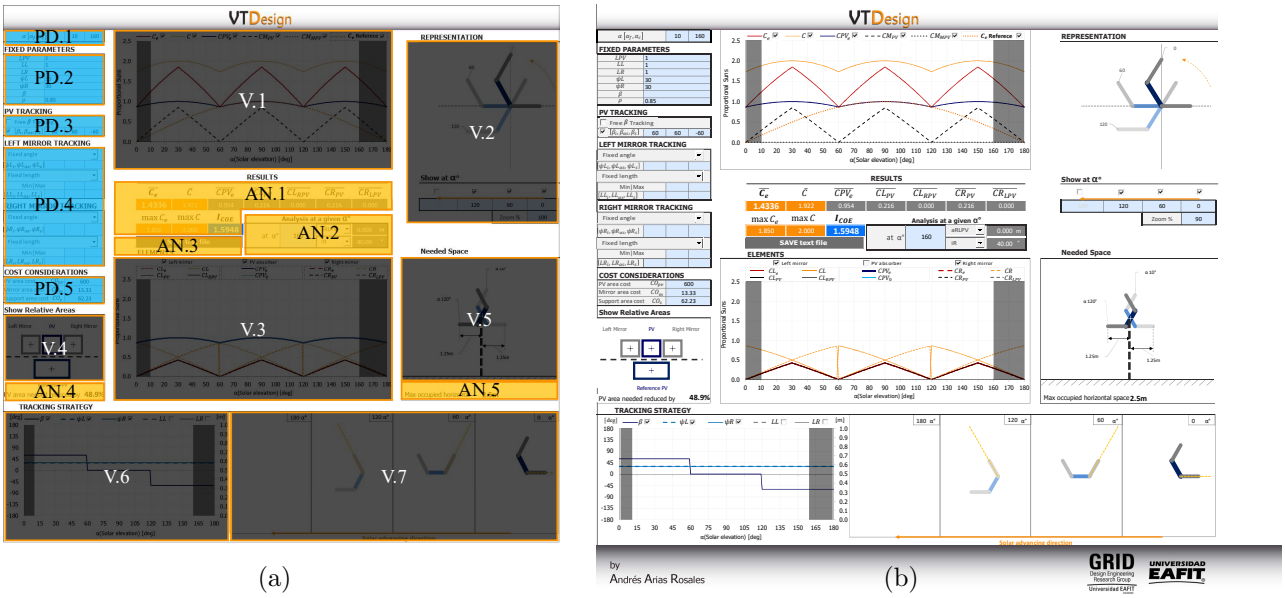

Figure 5.5: Overall distribution of the Dashboard module. This figure is not intended for a detailed inspection of each element, but for an overview.

The performance related to the user-defined parameters can be first viewed in AN.1 with the indicator *Average Effective Concentration* ($\overline{C_e}$) and *Index of Cost-Effectiveness* (I_{COE}). Other useful variables are presented in the same section: maximum Effective Concentration (max C_e), Average Real Incidence Concentration ($\overline{C}$), maximum Real Incidence Concentration (max C), Average Effective Concentration coming only from the PV direct contributions ($\overline{CPV_e}$), Average Effective Concentration coming only from the left mirror after one reflection ($\overline{CL_{PV}}$), Average Effective Concentration coming only from the left mirror after two reflections ($\overline{CL_{RPV}}$), Average Effective Concentration coming only from the right mirror after one reflection ($\overline{CR_{PV}}$), and Average Effective Concentration coming only from the right mirror after two reflections ($\overline{CR_{LPV}}$). These variables allow the user to gain quantitative insight into the contributions of each V-Trough element after one and two reflections and to compare the maximum values achieved against the averages. The section AN.2 allows for a deeper inspection. The user can define a specific solar elevation of interest and then look for any optical angle or aperture length by selecting the desired variable from two drop-down lists. The *Linear Space Required* (aT_{sp}) is presented in AN.5 and AN.4 presents in what percentage the PV area required may be reduced. Moreover, there is a button in AN.3 with which the user can obtain a text file, for further analysis, with all the detailed results from the performed simulation.

All visualization sub-modules (V.1–V.7) are shown in greater detail in Figs. 5.6–5.8. The exemplified set-up, used for showing these charts as features of the software, is limited in the Parameters Definition Section to a α solar elevation range from 10° to 160°. In order to favor a more intuitive interpretation of the performance curves, they show shadowed areas according to the α range; as seen in the four charts of Fig. 5.6. Fig. 5.6(a) presents a chart with the main performance curves: Effective Concentration (C_e), Real Incidence Concentration (C), Effective Concentration coming only from the PV direct contributions (CPV_e), Effective Concentration coming from both mirrors after one reflection (CM_{PV}), Effective Concentration coming from both mirrors after two reflections (CM_{MPV}), and Effective Concentration corresponding to a reference fixed solar panel without mirrors. As shown in the figure, the user can inspect the chart by means of a check-box for every one of those performance curves. Similarly, the chart shown in Figs. 5.6(c)–5.6(d) groups the performance curves by each V-Trough element. For the left mirror: Effective Concentration after both one and two reflections (CL_e), Effective Concentration after one reflection (CL_{PV}), Effective Concentration after two reflections (CL_{RPV}), and Real Incidence Concentration (CL). For the PV absorber: Effective Concentration (CPV_e) and Geometrical Incidence Concentration (CPV_0). For the right mirror: Effective

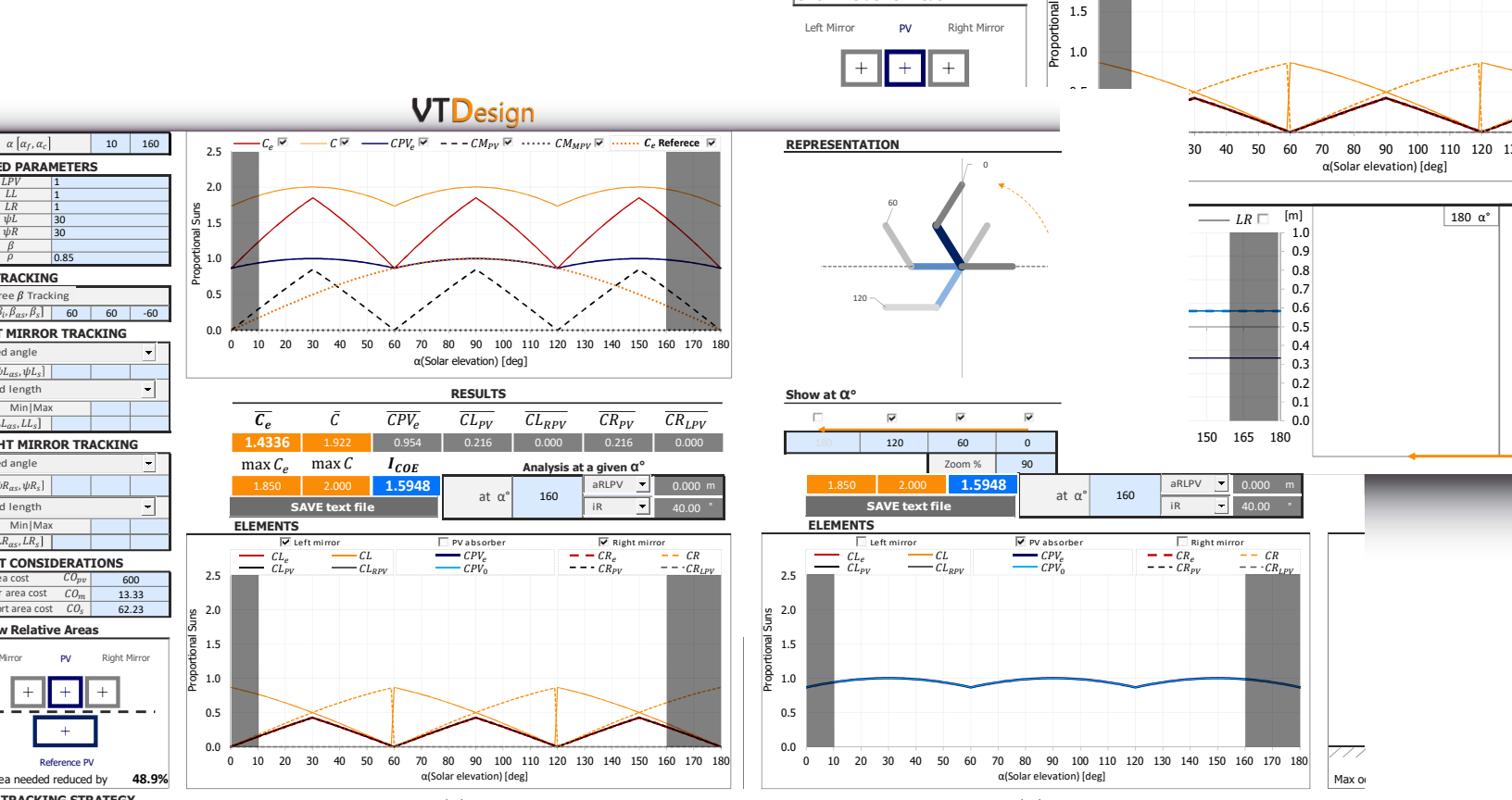

Figure 5.6: Visualization curves in the Dashboard module of VTDesign.

Concentration after both one and two reflections (CR_e), Effective Concentration after one reflection (CR_{PV}), Effective Concentration after two reflections (CR_{LPV}), and Real Incidence Concentration (CR). All these curves are presented for empowering the user to explore, to a great detail, the optical behavior of his/her proposed V-Trough set-up. The chart in Fig. 5.6(c) has the two check-boxes corresponding to the mirrors activated, while the same chart in Fig. 5.6(d) has only the check-box of the PV absorber activated. This functionality pursues a better usability of the performance curves.

The chart in Fig. 5.6(b) is intended for understanding the tracking adjustments. Any of the geometrical parameters β, ψL, ψR, LL or LR can be defined by the user as dynamic in function of α. This chart is useful for understanding the tracking motion that results from the input parameters. Figs. 5.7(a) and 5.7(b) present two additional visualization features of the Dashboard. As can be seen in Fig. 5.7(a), the user enters up to four solar elevations of special interest for a deeper geometrical visualization. According to the check-boxes selected, the V-Trough is depicted in the position and with the geometry corresponding to the entered α values.

Fig. 5.8(a) provides a visualization of the result shown in the section AN.4 of the Dashboard, namely in what percentage the PV area required may be reduced as compared to a reference fixed and flat solar panel. The proportional areas of the mirrors are also shown. The main motivation for implementing a V-Trough system is to reduce the amount of expensive Photovoltaic materials needed by means of inexpensive mirrors and manual tracking. Therefore, this visualization is critical for an intuitive understanding of the V-Trough set-up being explored by the user.

Fig. 5.8(b) is a visualization, presented in the Dashboard module, of the linear space required for the device. The position that occupies the largest linear space is shown for the left and the right side of the tracking pivot. Their corresponding lengths are also presented. Also, this visualization indicates the α values when these positions first happen. With this diagram, a user of the software can develop intuitive insight into the space needed in the floor to allocate the device and how this relates to the geometries and tracking strategies of the system.

Fig. 5.9 presents several features developed in VTDesign to extend the functionality and guide the usability of the software. Fig. 5.9(a) shows a screen-shot of the Free Input module. A table appears with blank spaces for the parameters β, ψL, ψR, LL and LR for all possible α solar elevations. An advanced

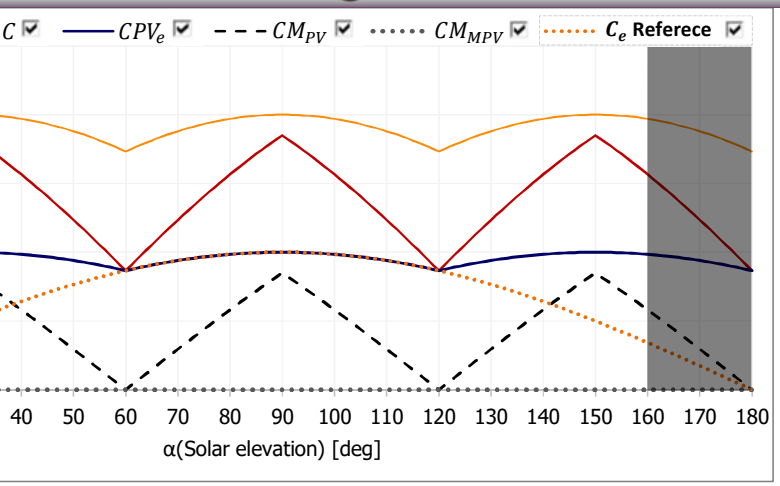

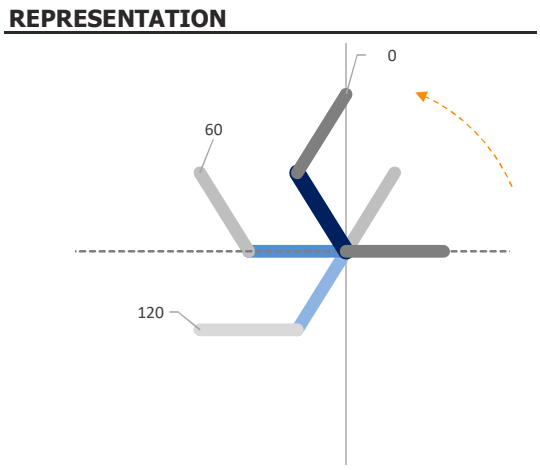

RESULTS

$\bar{C}$	$\overline{CPV_e}$	$\overline{CL_{PV}}$	$\overline{CL_{RPV}}$	$\overline{CR_{PV}}$	$\overline{CR_{LPV}}$
.922	0.954	0.216	0.000	0.216	0.000

ax C	I_{COE}	Analysis at a given α°			
.000	1.5948	at α°	160	aRLPV	0.000 m
text file				iR	40.00 °

Show at α°

180	120	60	0
		Zoom %	90

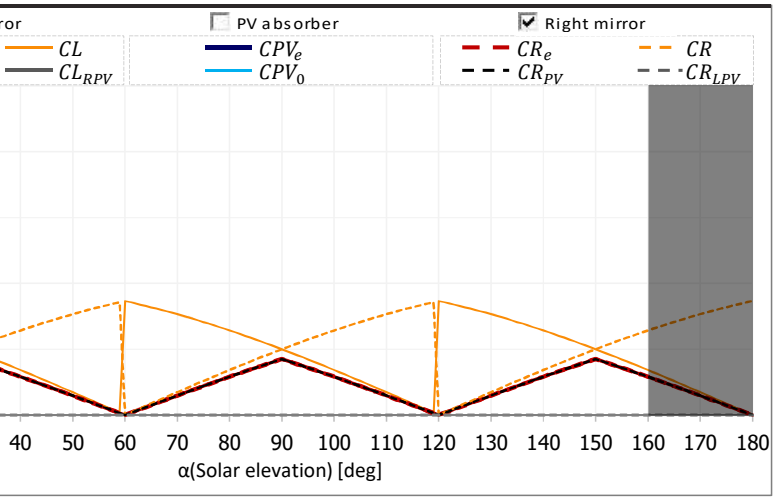

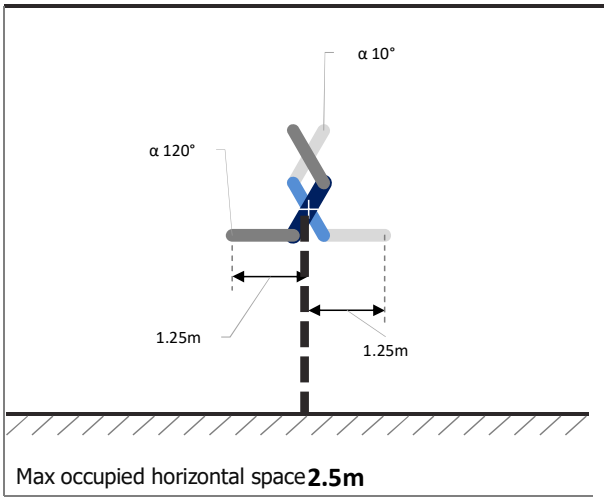

(b)

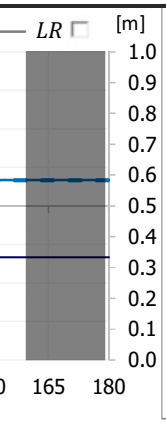

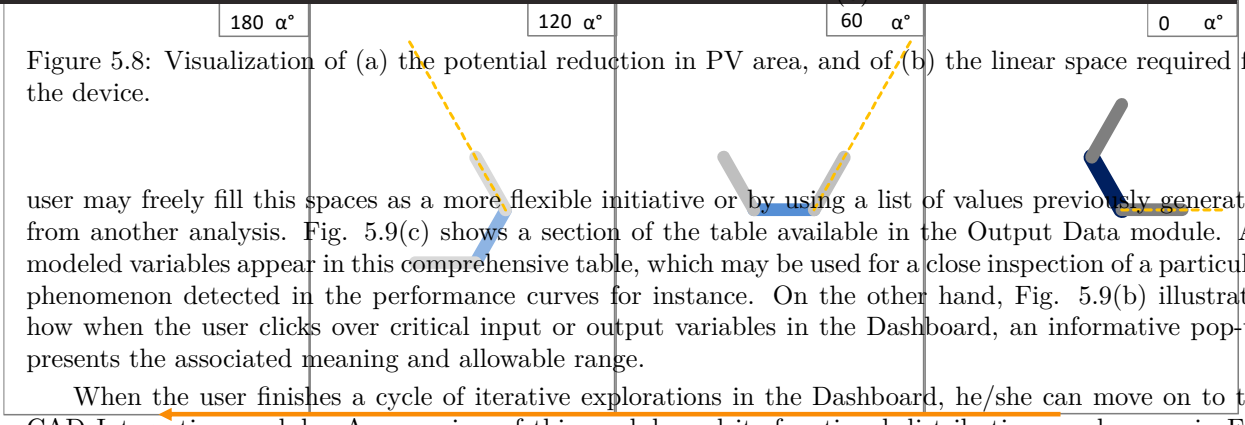

Figure 5.8: Visualization of (a) the potential reduction in PV area, and of (b) the linear space required for the device.

user may freely fill this spaces as a more flexible initiative or by using a list of values previously generated from another analysis. Fig. 5.9(c) shows a section of the table available in the Output Data module. All modeled variables appear in this comprehensive table, which may be used for a close inspection of a particular phenomenon detected in the performance curves for instance. On the other hand, Fig. 5.9(b) illustrates how when the user clicks over critical input or output variables in the Dashboard, an informative pop-up presents the associated meaning and allowable range.

When the user finishes a cycle of iterative explorations in the Dashboard, he/she can move on to the CAD Integration module. An overview of this module and its functional distribution can be seen in Fig. 5.10. The module includes a design table in which the user can define parameters for three-dimensional considerations, such as thickness of the surfaces and depth dimensions. The interface provides a description of the recommended steps for integrating the set-up being explored with the CAD functionalities. When the user fills the design table, the "Update" button must be pushed in order for the CAD model in SolidWorks®

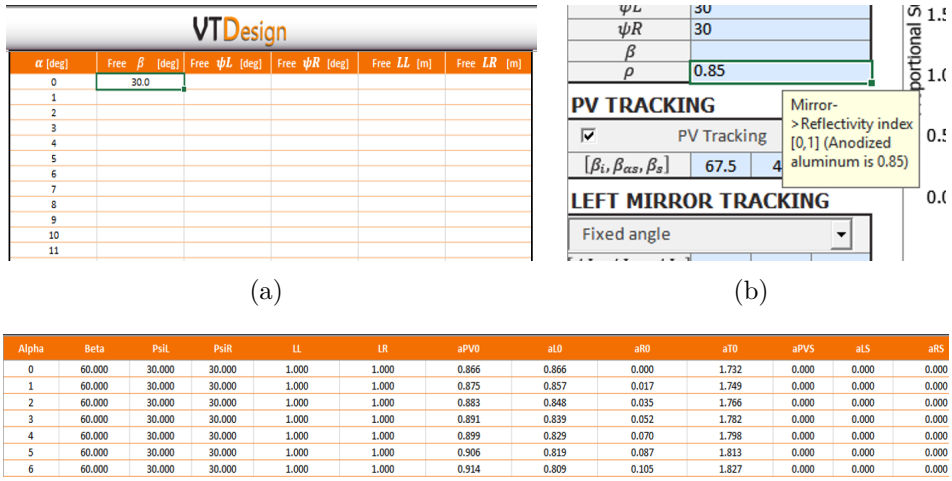

(a) (b)

Alpha	Beta	PsiL	PsiR	LL	LR	aPV0	aL0	aR0	aT0	aPVS	aLS	aRS
0	60.000	30.000	30.000	1.000	1.000	0.866	0.866	0.000	1.732	0.000	0.000	0.000
1	60.000	30.000	30.000	1.000	1.000	0.875	0.857	0.017	1.749	0.000	0.000	0.000
2	60.000	30.000	30.000	1.000	1.000	0.883	0.848	0.035	1.766	0.000	0.000	0.000
3	60.000	30.000	30.000	1.000	1.000	0.891	0.839	0.052	1.782	0.000	0.000	0.000
4	60.000	30.000	30.000	1.000	1.000	0.899	0.829	0.070	1.798	0.000	0.000	0.000
5	60.000	30.000	30.000	1.000	1.000	0.906	0.819	0.087	1.813	0.000	0.000	0.000
6	60.000	30.000	30.000	1.000	1.000	0.914	0.809	0.105	1.827	0.000	0.000	0.000

(c)

Figure 5.9: (a) Screen-shot of the Free Input module; (c) Screen-shot of the Output Data module; and (b) illustration of informative pop-ups in the Dashboard.

to adopt the geometry of the set-up proposed by the user. The integration with the CAD software allows for a detailed exploration of the dynamic geometry of a given V-Trough in four different configurations, corresponding to four solar elevations defined for visualization. An illustration of this functionality is shown in Fig. 5.11. This preliminary CAD can be used merely for an early visualization or it can be used as the base for a detailed CAD model in further design phases.

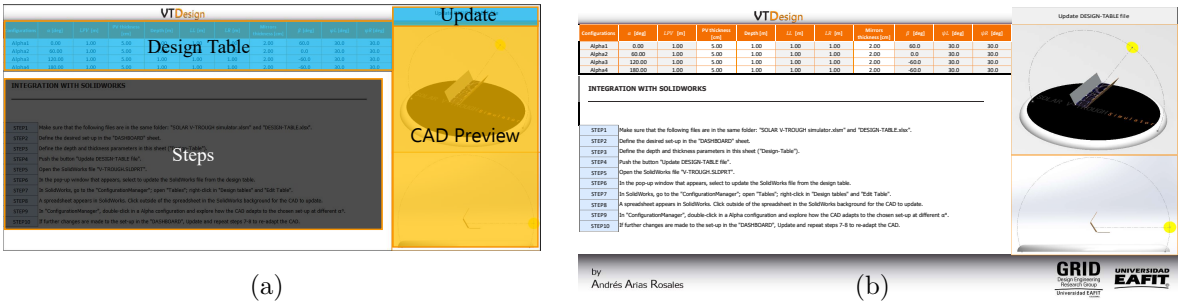

(a) (b)

Figure 5.10: Overall distribution of the CAD Integration module. This figure is not intended for a detailed inspection of each element, but for an overview.

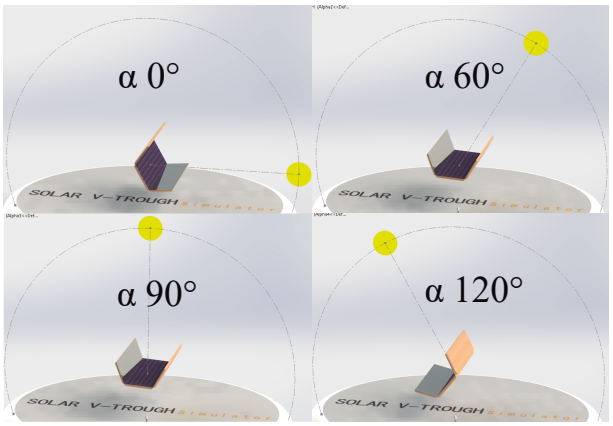

Figure 5.11: Preliminary CAD model of a given V-Trough set-up for four solar elevations.

5.3 Heuristic Optimization Tool: GA-WA Genetic Algorithm

This section studies genetic algorithms as a tool to determine V-Trough geometrical set-ups for specific conditions (refer to Sec. 2.3 for an introduction on heuristic methods for optimization and genetic algorithms). From another perspective, this study provides a solution to the same inquiry that VTDesign addresses (Sec. 5.2), namely how to guide the parameters definition process and support an effective navigation of the space of solutions? As opposed to the interactive exploration pursued by the VTDesign approach, the study in this section implements heuristic optimization methods intended to automatically converge to an optimal (or near-optimal) set-up solution without human intervention. The capacity to achieve satisfactory set-ups for personalized scenarios, without requiring a deep understanding of the optical phenomena behind the simulations, may favor a widespread exploration and implementation of V-Trough technology. In a following section (Sec. 6), a case study compares both VTDesign and the heuristic optimization tools discussed here to address how they differ from one another and how they can be used to complement each other.

The simulations performed by the genetic algorithms developed are based on the proposed theoretical model (Sec. 3). Genetic Algorithms (GAs) are used to optimize a given fitness (objective) function. Accordingly, the performance indicators and indices presented in Sec. 5.1 were used as different possible fitness functions. The GAs here can hence work from different objective modalities: Maximization of the Average Effective Concentration ($\overline{C_e}$); minimization of the materials cost ($Cost$) or the space required for the whole device (T_{sp}); or maximization of any of the multi-objective indices of cost-effectiveness (I_{COE}, MI_{COE} and MDI_{COE}).

The implementation of genetic algorithms as tools for defining the parameters of PV V-Troughs, for various fitness functions, has not been reported in the literature as discussed in Sec. 2.3. Moreover, pursuing a greater control of the random procedures within the GAs and an expanded functionality, a new genetic algorithm is proposed based on Weibull frequency distributions. The new metaheuristic is named as "GA-WA" (Genetic Algorithm - Weibull Arias) and it is believed to be of special use for the V-Trough case study. However, GA-WA can be used to address all kinds of design-engineering problems when a flexible control of the random processes is desired. GA-WA is a general-purpose genetic algorithm and, therefore, it can be used in other design-engineering problems besides V-Trough devices. Consequently, the GAs presented in this section, as well as their evaluation in Sec. 6, are a contribution to the state of the art.

As follows, the development of the new heuristic procedures is described. The general scheme of GA-WA is then presented and compared against two other reference GAs. Lastly, the parameters controlling the heuristic procedures of the three GAs are optimized.

5.3.1 Heuristics Based on the Weibull Probability Distribution

The lack of flexibility for mutation control, described in section 2.3, was approached in this section with the development of new heuristic processes. These were found useful for controlling other random or semi-random processes, besides mutation, in other stages of the evolution scheme. In this research project, a semi-random process, variable or parameter, is one which is bounded by randomness with a given probabilistic bias which may differ from a uniform or Gaussian distribution.

Genetic algorithms are inspired by biological evolution. Hence, many of their internal heuristics result from direct biomimicry of natural processes translated into code. Among these, the heuristics related to the random or semi-random processes are of special interest. Randomness introduces variability and diversity, which ultimately allows a GA to navigate the wide solution space. As explained in section 2.3, probability distributions have been used for a more reasonable control of randomness, as opposed to uniform randomness. For the first time, this research project proposes the Probability Density Function (PDF) of Weibull (Bowden et al., 1983) as a more flexible and adaptable approach. The Weibull distribution has already been used in GAs for fitness (objective) functions related to reliability (Coit and Smith, 2002) and Wind modeling (Arabali et al., 2013). However, to the best of the author's knowledge, the Weibull PDF has not been used before in heuristics for controlling the random or semi-random processes within a GA.

This distribution function was selected because it can adopt a wide range of different shapes by being controlled by its two parameters, i.e., shape (k) and scale (c). In fact, the Weibull distribution is the general form of other widely used distributions, such as the exponential and Rayleigh distributions. At a given k, the Weibull PDF can also resemble a Gaussian distribution. Therefore, by manipulating k and c, a GA user can have a high degree of control over several kinds of genetic steps involving randomness. Nevertheless, k and c are not intuitive parameters. If the distribution is to be adjusted to a given range and shaped towards a desired bias, there are no obvious k and c corresponding values. Consequently, the following method was developed in order to control a Weibull distribution from a more intuitive parameter, namely the mean (μ).

Eq. 5.17 presents the Weibull probability density in function of x, k and μ.

$$f_{(x)} = \frac{k\Gamma\left(1+1/k\right)}{\mu}\left(\frac{x\Gamma\left(1+1/k\right)}{\mu}\right)^{k-1} * e^{-\left(\frac{x\Gamma(1+1/k)}{\mu}\right)^{k}} \tag{5.17}$$

The intention is to constrain the distribution to a range from 0 to a maximum allowed value (Top). k can be defined in order to make it highly unlikely for a value greater than Top to occur, as stated in expression 5.18.

$$\frac{k\Gamma\left(1+1/k\right)}{\mu}\left(\frac{Top*\Gamma\left(1+1/k\right)}{\mu}\right)^{k-1} * e^{-\left(\frac{Top*\Gamma(1+1/k)}{\mu}\right)^{k}} \leq 0.0002 \tag{5.18}$$

It was found that a satisfactory k value remains the same for equal proportions of $p\mu = \mu/Top$, regardless of the Top magnitude. Hence, seeking a more general analysis, expression 5.18 was normalized to Top, making $Top = 1$ and $\mu = p\mu$. The resulting inequality was solved for k in the range $0.15 \leq p\mu \leq 0.5$ in steps of 0.01, as shown in Fig. 5.12(a). When $p\mu < 0.15$, a $k < 1$ would result. However, a Weibull PDF with a $k < 1$ approaches the vertical axis asymptotically, which is problematic for the intention of clearly delimiting the PDF to a given allowable range. Therefore, $k = 1$ is assigned whenever $p\mu < 0.15$. Additionally, the search was limited to $p\mu \leq 0.5$ for a symmetry to be further created in the range $p\mu > 0.5$. From the points shown in Fig. 5.12(a), a polynomial regression (see Eq. 5.19) was obtained with a sample standard error of 0.0038.

$$k = 15.8749972991 * p\mu^3 - 6.46861529214 * p\mu^2 + 5.93130385328 * p\mu + 0.185331693521 \tag{5.19}$$

With this equation, it is possible to directly calculate the k value for a given $p\mu$ in the stated range. The Weibull PDF can then be traced with Eq. 5.17. With this procedure, Fig. 5.12(b) shows the PDF curves corresponding to various desired $p\mu$ values (shown in vertical dashed lines) and adjusted to a range $0 \leq X \leq 50$. These curves illustrate how the probability distribution of a semi-random variable can be flexibly shaped, within a given range, with the proposed procedure.

When $p\mu = 0.5$ and $3 < k < 4$, the Weibull PDF tends to be symmetrical and resembles the shape of a Gaussian distribution. However, PDFs with $k > 4$ do not present a mirrored behavior of PDFs with $k < 3$. Such a symmetrical behavior would be beneficial for a more intuitive control of the semi-random variables.

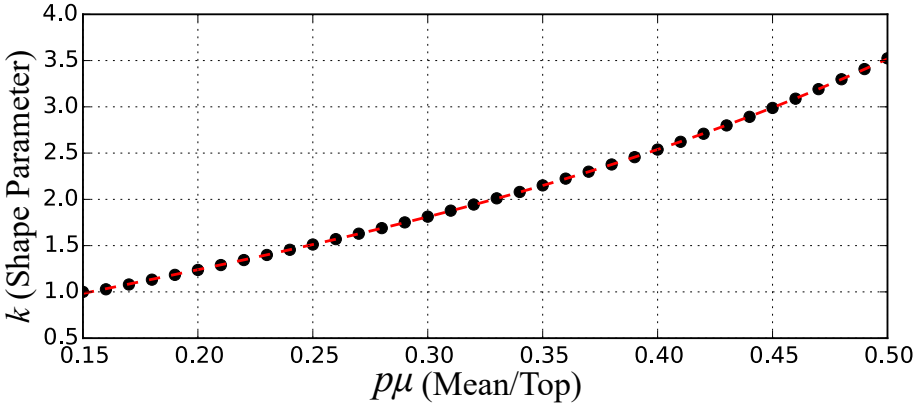

(a)

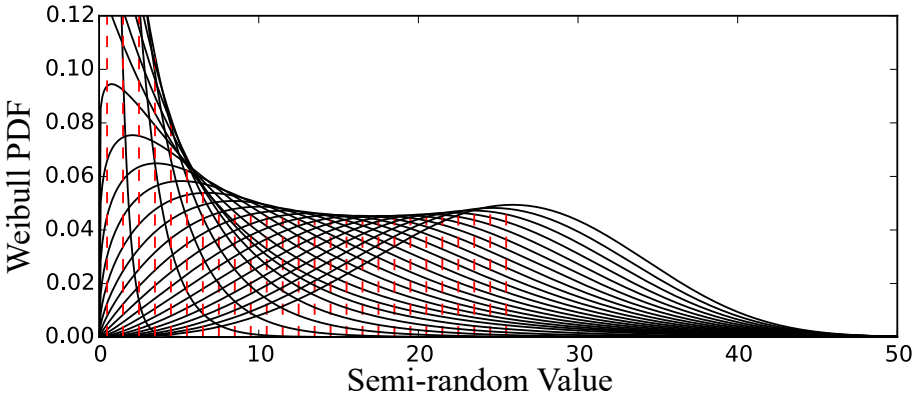

(b)

Figure 5.12: Weibull Distribution controlled by the mean (μ). (a) k values calculated for a range of $p\mu$. (b) The corresponding Weibull PDF curves adjusted for a range from 0 to $Top = 50$.

For instance, a $p\mu = 0.8$ should present a PDF with an inverse, yet proportionally equivalent, shape as when $p\mu = 0.2$. Therefore, expression 5.20 presents the necessary steps required to generate the symmetry desired: first the mean is flipped to its proportional inverse (μ'). Then the mean-to-Top proportion is calculated based on the flipped mean ($p\mu'$), which is used to find k' with Eq. 5.19. A number of values V' must be generated by satisfying a PDF calculated in function of the flipped shape (k') and mean (μ') parameters. Finally, the values V are obtained by flipping back each V' value.

$$\begin{aligned} \text{if } p\mu > 0.5\text{: } & \mu' = Top - \mu; \\ & p\mu' = \mu'/Top; \\ & k'_{(p\mu')}; \\ & \text{values } V' \text{ following } f'_{(k',\mu')}; \\ & V = Top - V'. \end{aligned} \tag{5.20}$$

The previous procedures allow for a Weibull distribution which is adjusted for a given range and shaped with a bias towards the desired mean value. This capacity was used in the following heuristic processes that differentiate GA-WA from the rest of the genetic algorithms; heuristics related to mutation control, elitism, stagnation strategies and the initialization of the first population.

5.3.1.1 Mutation Control and Elitism

Promoting mutations in a population of possible solutions is in itself a heuristic, inspired by biological evolution, for introducing diversity. This greater diversity is meant for reducing the tendency for the algorithm to get stuck in a local optimum and keep looking for different approaches as opposed to just an incremental progression in the direction of improvement. Mutation, as in nature, is a process linked to randomness. As explained in section 2.3, a procedure to control a probabilistic bias for this randomness in mutation may be beneficial. The heuristics within the mutation evolutionary step must provide an answer to the following questions: How many mutations per generation?, Which individuals will be mutated?, which genes will mutate?, by how much (magnitude) and in which direction will every mutation change a gene? The following heuristic process addresses these decisions based on the Weibull procedures described at the beginning of section 5.3.1.

I The user of the GA must define the mean proportion of individuals who will suffer a mutation, per generation; a parameter that will be known as $\mu pMut$. From the desired mean and defining $Top = 1$, a Weibull distribution can be determined. A number of values is generated by following this Weibull distribution. Each generation, one of those values is randomly selected as the proportion of individuals who will suffer a mutation.

II Following the selected proportion, the individuals are randomly chosen from the offspring of every generation. For every chosen child, one of its genes is randomly selected to be mutated.

III The user of the GA must define the mean mutation magnitude (μMut) for every gene, as well as the maximum (Top) and minimum (Min) values that will be allowed for every gene. A Weibull distribution is determined for every gene with the corresponding μMut values and adjusted from 0 to $0.5*(Top - Min)$. A number of values is generated and stored in a list, for every gene, by following the defined Weibull distributions. Every time a gene is selected for mutation, a value is randomly chosen, as the mutation magnitude, from the corresponding Weibull-distributed list.

IV The direction of mutation is defined from randomly selecting between "+" and "-". The mutation is then implemented to every chosen gene. If a mutated gene surpasses one boundary (Min or Top) of the allowable range, the value of the gene must be replaced by the value of the concerning boundary.

Fig. 5.13 illustrates various possible ways in which the mutation values could be distributed for a range $-1 \leq V \leq 1$ from Weibull, Gaussian and Uniform PDFs. The curves correspond to different Weibull distributions calculated for the shown μ values. As the mutation values might be added or subtracted, the curves are shown as symmetrical to a vertical axis at 0. In the background, a random-uniform distribution shows how every sub-range of values has approximately the same frequency and probability of occurrence. In order to address the mutation distribution with a Gaussian distribution, as also seen in the figure, the mean is set to 0 and the standard deviation (SD) is adjusted for the allowable range. Following the "68-95-99.7 rule" of the Gaussian distribution (Jiang et al., 2013), it can be calculated that approximately 99.95% of the values will be within the $3.5*SD$ range. Therefore, the standard deviation can be calculated as $SD = 0.5 * (\text{Top-Min})/3.5$.

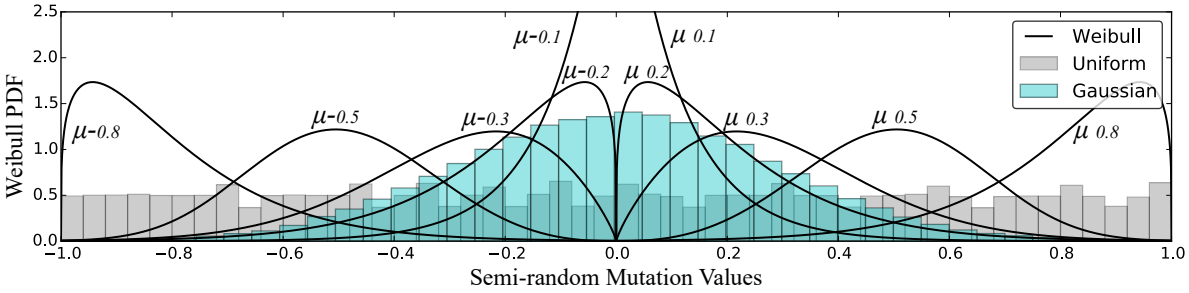

Figure 5.13: Weibull-distributed mutation values compared to a uniform and Gaussian distribution.

On the other hand, elitism is also controlled by a heuristic process. These heuristics must address the questions: What proportion of the population will be selected as elites? can elites mutate? how many will mutate and by how much? Regarding the first decision, there is no obvious proportion of elites which would benefit the GA performance in any case study. In some situations, it may be beneficial to have an elite portion as small as possible in order to maximize the diversity that the non-elites may introduce. Conversely, some situations may get a better performance from a wider elite portion by increasing the reproduction among elites. Therefore, the proportion of elites could be better defined by a probabilistic Weibull distribution biased towards a reasonable mean proportion. In this way, while the mean introduced by the user is fulfilled overall, some generations will explore a wider range of possibilities regarding the elite proportion. Hence, the GA user must initially define a mean proportion of elites (μn_e). Then, by following the same procedure of step I for mutation, the proportion of elites is to be determined for every generation from Weibull-distributed values.

Mutation should not necessarily be the same for the elites. For instance, a shark's DNA presents a much slower rate of accumulated mutations compared to other animals such as mammals (Martin et al., 1992). Given the high degree of adaptation that sharks have already achieved in their environment, this can be interpreted as a biological way of preserving a highly effective solution, namely the shark's phenotype. Biomimicry of this can be translated into the elite portion of the population mutating less often or in smaller magnitudes. Therefore, the mutation of elites follows the same heuristic process (steps I-IV) but with different GA parameters unique for the elites: mean proportion of elites to suffer mutations ($\mu pMut_e$) and a mean mutation magnitude (μMut_e).

5.3.1.2 Stagnation

For the kinds of problems where GAs are implemented, there are usually different suitable solution approaches. Each approach can be fine-tuned to the best of its potential, but one of them is usually superior. Each of those different approaches, after fine-tuning, would be a local maximum. Additionally, one (or more) of those local maximums would also be a global maximum. When a GA finds the hill of a local maximum, it may focus the evolution resources towards reaching the best of its local potential instead of looking whether there is a global maximum hill which has not been explored yet. In other words, the GA is stuck or stagnated in a local maximum. Mutation is used to reduce the tendency towards this premature-convergence. However, sometimes regular mutation is not capable of introducing the variability needed to escape from a local maximum. Therefore, this research project proposes a heuristic process to increase the chances of reaching a global maximum:

I The user defines the number of generations ($Gstuck$), without fitness improvement, before considering the GA as stuck. A counter must be programmed in order to keep track of the generations without historic fitness improvement.

II When the counter reaches a multiple of $Gstuck$, the GA first assumes that the evolution might be approaching a global maximum. Given this assumption, the elites are prioritized and the mutations are intensified in occurrence but decreased in magnitude. For this generation, the elites are cloned, doubling their influence and the chances of them having offspring and reproducing with other elites. Mutation is temporarily set to occur twice as often and with half the mean magnitude: 2*$\mu pMut$, 2*$\mu pMut_e$, 0.5*μMut and 0.5*μMut_e.

III If the previous strategy did not improve the historic fittest value, then the GA assumes that it is stuck in a local maximum. The strategy is then to keep the mutation occurrence doubled, but to double as well the mean mutation magnitude as compared to the normal parameters: 2*μMut and 2*μMut_e. Additionally, the population is temporarily doubled by means of new individuals whose genes have been randomly initialized.

IV If one of the previous strategies manages to improve the historic fittest value, then the stuck counter is set back to 0 and the GA parameters are set back to normal. Otherwise, if both strategies have been implemented without improvement, the stuck counter is left counting and the parameters are set back to normal until the counter reaches another multiple of $Gstuck$.

5.3.1.3 Initialization from Intuition

Initialization is the first stage of a GA. During this phase, the individuals of the first generation are created with randomly defined genes. These genes are usually generated with uniform randomness within an allowable range $[Min, Top]$ defined by the GA user for every gene. This way, the evolution starts unbiased and broadly spread throughout the solution space. However, in some cases, it is of interest to initialize the population with a distribution which is biased towards an intuitive value of the genes. These initial gene values could be set not necessarily from intuition, but from a previous parameters definition process. This capability is of great use for this research project, as there was a previous exploration of the V-Trough parameters with the interactive software VTDesign. Based on the Weibull procedures described at the beginning of section 5.3.1, the following heuristic process is proposed to address a population initialization around intuitive or influential values:

I The range for the Weibull distribution must be calculated for every gene going from 0 to Top'; with $Top' = Top - Min$. This makes the Weibull variation range to have the same absolute size as the allowable range of every gene, but starting at 0. The intuitive value for the gene (μi) must also be displaced in order to calculate the Weibull desired mean; with $\mu i' = \mu i - Min$. A Weibull distribution, which satisfies Top' and $\mu i'$, can then be determined. A number of values (V') is generated by following the defined Weibull distribution. The values are then adjusted with $V = V' + Min$. The result is a Weibull distribution adjusted for the range $[Min, Top]$ of a given gene and with a mean μi.

II The number of non-elite individuals is calculated and their genes are randomly selected from the Weibull distributed and adjusted values.

III The elite individuals are directly initialized with their genes being μi, namely the intuitive value which the user defined for every gene.

Fig. 5.14 shows a series of different ways in which a population could be distributed, from Weibull, Gaussian and Uniform PDFs, in a range [-50,50] concerning one gene. The population is shown in the background with a random uniform distribution and a Gaussian distribution with mean 0 and a SD adjusted to the range. These two options are highly restrictive, since the uniform randomness can not be biased or reshaped and the Gaussian PDF is symmetrical, which is not always reasonable or desired. On the other hand, the curves of the figure show some of the various ways in which the population could be flexibly Weibull-distributed with the procedures described in this section. Each curve is related to a desired intuitive value (μi) as the mean and they comprise only the non-elite individuals of a first generation. The curve of the middle (which is thicker) corresponds to a Weibull distribution calculated for $p\mu = 0.5$, namely for a mean which is half the distribution range. It is evident how this curve resembles the Gaussian distribution in the background.

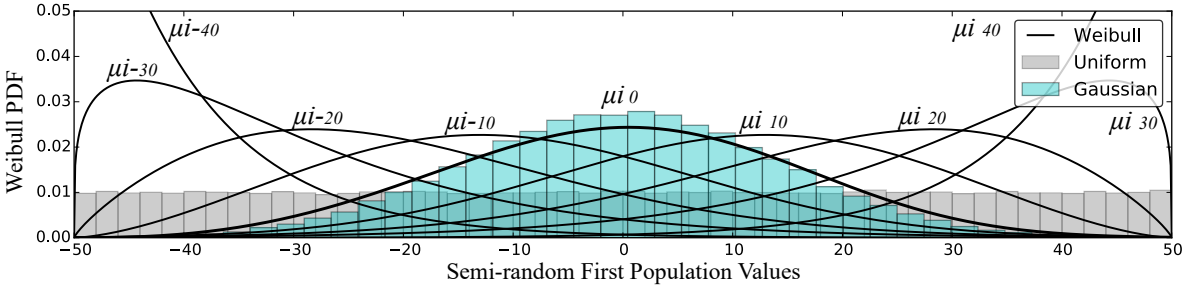

Figure 5.14: Weibull-distributed values for the initial population of a gene; compared to uniform and Gaussian distributions.

Pursuing a further flexibility in the initialization stage of GA-WA, it was made possible for some genes to be distributed around an intuitive value, while the others can be determined with uniform randomness as usual. This level of flexibility is important when there is not the same initial amount of information about every gene.

5.3.2 Proposed Scheme for GA-WA

A new genetic algorithm, GA-WA, is proposed by integrating the heuristic processes described in Sec. 5.3.1. The main scheme of this algorithm is presented in Fig. 5.15(a). It is worth noting that this scheme is designed for maximizing a given fitness function. If, on the contrary, the objective is to minimize a given function, the same scheme may be used with its reciprocal (1/Fitness). Also, it is shown how three genetic processes are controlled by Weibull probability density functions: The initialization of the first population regarding a gene for which an "intuitive" starting value (μi) has been provided; the establishment of the proportion of top individuals, for every generation, who will be considered elites; and the mutation procedures in both non-elites and elites.

Every time the highest fitness of a generation (Fittest-G) is not an improvement over the highest historic fitness of the Run (Fittest-Run), a counter (Stuck) is increased by one. When Stuck becomes a multiple of $Gstuck$, the first stagnation strategy is activated. If this "Possible Global Maximum" strategy does not result in an improvement for the next generation, a second strategy increases variability. This "Possible Local Maximum" strategy is implemented as a subsequent resource because it is more risky that the first stagnation strategy. The increased magnitudes of mutation may cause the best solutions to be lost, but this increased variability may also allow the population to escape from a local stagnation. The parent selection is performed with the "Roulette wheel" method and the sexual reproduction process swaps the genes at a randomly defined single point (Magalhães-Mendes, 2013).

The parameters needed to control the heuristic processes of GA-WA are described in Table 5.1. The ones shown with (*) are mutually exclusive, so the user of the algorithm must choose whether to control the mean mutation magnitude, for elites, at the general or the gene level. If $fMut_e$ is chosen, the mean mutation magnitude of the elites would be defined relative to the mean mutation magnitude of the non-elites. This approach can be more straightforward and intuitive. For instance, the user may want the elites to mutate, on average, half the magnitude of the non-elites ($fMut_e = 0.5$). Additionally, the parameter μi is optional and can be defined only for the genes that have an intuitive or pre-defined value.

Table 5.1: Parameters for controlling GA-WA, GAGaussian and GAUniform genetic algorithms.

Parameter	Level	Genetic Algorithm	Description
nG	General	all	No. of generations
$Gstuck$	General	GA-WA	No. of generations, without improvement, for stagnation
nP	General	all	No. of individuals in the population
μn_e	General	GA-WA	Mean proportion of elites
n_e	General	GAUniform,GAGauss	Fixed proportion of elites
$\mu pMut$	General	GA-WA	Mean proportion of non-elites who will mutate
$\mu pMut_e$	General	GA-WA	Mean proportion of elites who will mutate
$fMut_e$	General*	GA-WA	Elite mutation factor. $fMut_e = \mu Mut_e/\mu Mut$
μMut	Genes	GA-WA	Mean mutation magnitude for a gene in non-elites
μMut_e	Genes*	GA-WA	Mean mutation magnitude for a gene in elites
μi	Genes	GA-WA	Desired intuitive value for a gene; Optional
Top	Genes	all	Maximum value allowed for a gene
Min	Genes	all	Minimum value allowed for a gene
$pMut$	Genes	GAUniform,GAGauss	Probability for any given gene to mutate

For comparison purposes, two other genetic algorithms with standard heuristic processes are described, i.e., GAGaussian and GAUniform. Fig. 5.15(b) illustrates the scheme which both follow. The initial population is always defined with uniform randomness and the elites are selected according to a fixed proportion (n_e). Also, there is no stagnation strategy. These reference genetic algorithms differ only in the mutation phase. Their procedure for distributing the mutation magnitude is illustrated in Fig. 5.13 and described in Sec. 5.3.1.1. A parameter $pMut$ is entered as the probability that any given gene mutates.

Any of the performance indicators and indices presented in Sec. 5.1 can be defined as the fitness function for GA-WA or for the two GAs used as references. These potential fitness functions all depend on a set of

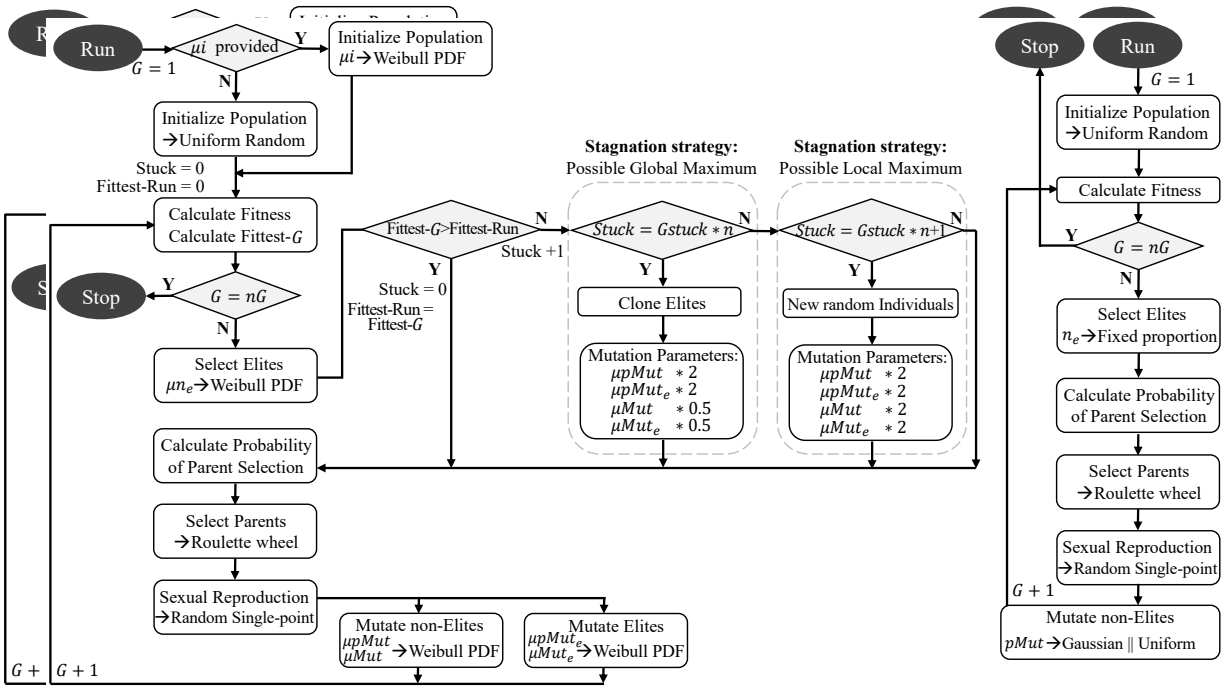

(b)

Figure 5.15: (a) Main scheme of the proposed genetic algorithm GA-WA. n is any positive integer greater than 0. (a) Scheme of a standard genetic algorithm.

parameters/variables which can be assigned to one of two categories, namely the needs and constrains of a given case study, or the geometrical set-up of a V-Trough device. The latter is the category of interest to be iterated, by the genetic algorithms, in the optimization process. These variables, which define the geometrical set-up, are the lengths LL, LR and LPV; and the angular positions ψL, ψR and β. Seeking to simplify the optimization problem, LPV can be set as 1 and the other lengths would then be defined as a proportion of LPV. Therefore, a solution obtained with the genetic algorithms should fully define the behavior of the five geometrical variables: LL, LR, ψL, ψR and β. Additionally, each of those variables can be defined as a fixed value or as a value which dynamically varies in function of the solar elevation (α). Then, depending of how each variable is defined, they must be translated into genes which can feed the evolutionary process. The following modalities are proposed for defining each of these five geometrical variables:

- **DF**: The variable is defined as a fixed value entered by the user. No genes are assigned to this variable.
- **DL**: The variable is defined as a list entered by the user. The values of the list define the value of the variable for every α value to be considered in the calculations. No genes are assigned to this variable.
- **RF**: The variable is defined as a random fixed value to be specified by the GA. Since it is fixed, it does not depend on the solar elevation α. One gene is assigned to this variable.
- **RD**: The variable is defined as a random dynamic value, to be specified by the GA, according to a user-defined list of α tracking points. The user must specify a list with an arbitrary number of n solar elevations α, for which the variable will change to a new position. $(n + 1)$ genes are assigned to this variable, corresponding to the positions which the variable will adopt in function of α.
- **RRD**: The variable is defined as a random dynamic value without a user-defined list of α tracking points. The user must specify the number n of α tracking points where the variable should change

its position. $(2 * n + 1)$ genes are assigned to this variable, corresponding to the positions which the variable will adopt in function of α, as well as the α tracking points themselves.

- **RRDsame**: The variable is defined in the same way as in **RRD**. However, if there are several **RRDsame** variables, they will share the same α tracking points as soon as they are defined by the GA genes.

These different modalities allow for the degree of geometrical flexibility pursued by this research project in terms of V-Trough exploration. Since each geometrical variable can be independently defined as fixed or dynamic, the set-ups may very well include asymmetric mirrors, as well as mirrors which can tilt and/or slide in order to track the sun. This kind of flexibility was not found in other V-Trough studies, as discussed in Sec. 2.3.

5.3.3 Optimization of the Genetic Parameters

The effectiveness and efficiency of a GA can be greatly affected by the tuning of the parameters which control its heuristic processes (Shiffman et al., 2012). Therefore, this section presents the results of a partial optimization of the genetic parameters for GA-WA and both reference algorithms, i.e., GAUniform and GAGauss.

The most relevant GA parameters were selected and their variation was constrained to three discrete levels [0.1, 0.5, 0.9], corresponding to a subjective interpretation of [low, intermediate, high]. Although those are originally continuous parameters, they were discretized in order to reduce the computational expense and for a more practical initial optimization. Consequently, it was possible to explore all possible combinations of the discretized GA parameters and run each combination 10 times. The performance of each combination was measured according to the fitness function I_{COE} in a simple and common scenario for V-Trough devices.

Table 5.2 defines the optimization scenario. The GA parameters control the heuristic processes, while the set-up parameters control how the genetic algorithms explore the V-Trough geometry. The parameters marked with (*) are the ones which were partially optimized in discrete levels. There are hence nine possible combinations (two parameters with three levels each) for GAUniform and GAGauss. In the case of GA-WA, there are 243 combinations (five parameters with three levels each). Within the GAs, there were seven genes iterated in the evolution process: four genes defined the RF length and angular position of each mirror; and three genes defined the RD β angular positions which changed according to the provided α tracking-point positions $[60°, 120°]$. In order to calculate I_{COE} as the fitness function, other needed fixed parameters were defined as $LPV = 1, \rho = 0.85, \alpha f = 0°, \alpha c = 180°, CO_{pv} = 600 USD/m^2, CO_m = 13.33 USD/m^2$ and $CO_s = 62.23 USD/m^2$ (Arias-Rosales and Mejía-Gutiérrez, 2016).

Table 5.2: GA optimization parameters.

GA Parameters	Genetic Algorithm	Definition
nG, nP	all	100
$Gstuck$	GA-WA	5
μn_e, $\mu pMut$, $\mu pMut_e$, $fMut_e$	GA-WA	*Levels [0.1, 0.5, 0.9]
$fMut$	GA-WA	*Levels [0.1, 0.5, 0.9]; μMut =$(Top/4)$*$fMut$
n_e, $pMut$	GAUniform,GAGauss	*Levels [0.1, 0.5, 0.9]
Set-up Parameters	Genetic Algorithm	Definition
LL, LR	all	RF. $Top = 2.5$, $Min = 0$. 2 Genes
ψL, ψR	all	RF. $Top = 90°$, $Min = -90°$. 2 Genes
β	all	RD. $Top = 180°$, $Min = -180°$, α $[60°, 120°]$. 3 Genes

Fig. 5.16 shows the performance of all the GA parameter combinations for the three genetic algorithms. Three different curves appear, corresponding to different perspectives for measuring the performance of a GA. "Fittest/Combination" considers only the highest fitness achieved during the 10 runs of each combination; "Mean Fittest/Run" averages among the highest fitness achieved for every run; and "Mean Fittest/G" averages among the highest fitness achieved for every generation of the evolutionary process. Unlike the

others, the latter is affected not only by the end result of each run, but also by how fast the GA converges throughout the generations. For GAUniform and GAGauss, combination 2 ($n_e = 0.5$ and $pMut = 0.1$) achieved the highest performance in "Fittest/Combination", while combination 1 ($n_e = 0.1$ and $pMut = 0.1$) performed better in "Mean Fittest/Run" and "Mean Fittest/G". In the case of GA-WA, combination 208 ($\mu n_e = 0.5$, $\mu pMut = 0.9$, $\mu pMut_e = 0.9$, $fMut = 0.1$ and $fMut_e = 0.1$) performed better in "Fittest/Combination", combination 175 ($\mu n_e = 0.1$, $\mu pMut = 0.9$, $\mu pMut_e = 0.5$, $fMut = 0.1$ and $fMut_e = 0.5$) performed better in "Mean Fittest/Run" and combination 183 ($\mu n_e = 0.1$, $\mu pMut = 0.9$, $\mu pMut_e = 0.9$, $fMut = 0.9$ and $fMut_e = 0.1$) performed better in "Mean Fittest/G".

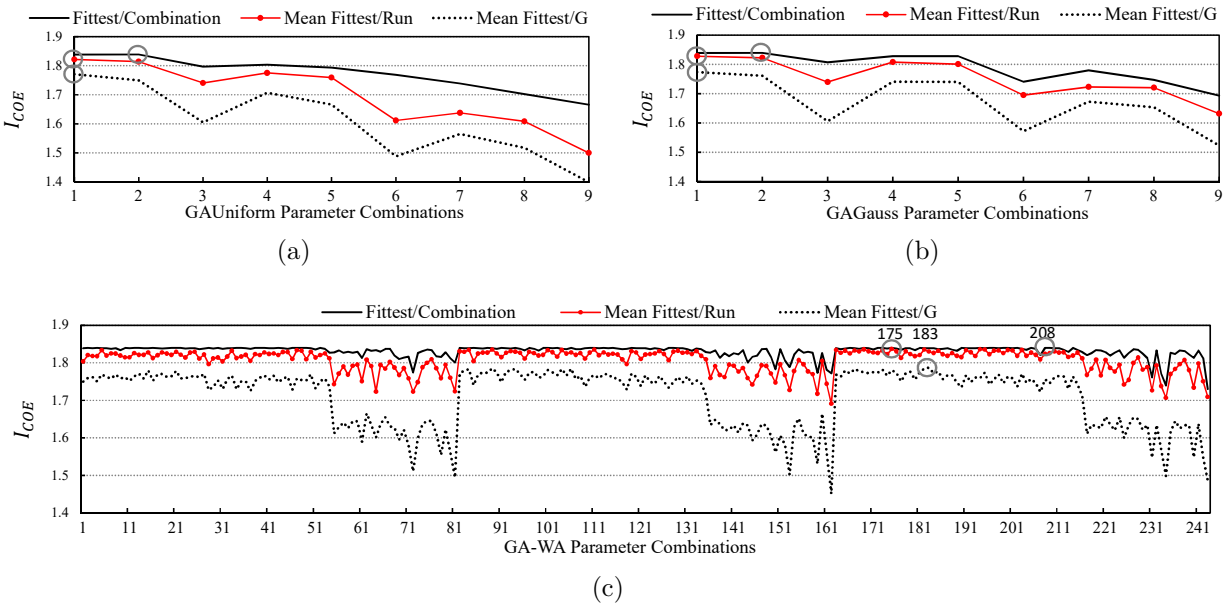

Figure 5.16: Performance of the GA parameter combinations for (a) GAUniform, (b) GAGauss and (c) GA-WA. The combinations with the highest performance are highlighted with circles.

Fig. 5.17 illustrates the importance of tuning the GA parameters. The graphs here show the highest I_{COE} fitness, achieved for every generation, for the worst and best (optimized) combinations of the three algorithms. Every curve corresponds to the progression of a GA for one run. The so-called "worst" (combination 9 for GAUniform and GAGauss and combination 162 for GA-WA) present evolutionary paths which are more dispersed, converge to different points and the highest fitness tends to be smaller in comparison.

As there are random processes involved in the performance of any GA, it is worth analyzing the results from a statistical point of view: are the differences between the three GAs and the effects of their parameters significant? The residuals of the obtained data presented clear violations to normality and homogeneity of variance. Several transformations of the data were implemented, i.e. $(1/y)$, $ln\,(y+1)$, $log_{10}\,(y+1)$, $\sqrt{y}$ and arcsin; but none could satisfy the parametric assumptions for the residuals. Therefore, the Kruskal-Wallis rank sum test was used as a non-parametric approach for discrimination of stochastic dominance, namely "The probability that a randomly drawn observation from one group will be greater than a randomly drawn observation from another" (Dinno, 2015).

With Kruskal-Wallis tests, it was possible to verify that the combination of the GA heuristic parameters had a highly significant effect on the "Fittest/Run" in GAUniform, with P-value = 1.39E-12, in GAGauss, with P-value = 4.15E-13, and in GA-WA, with P-value <2.2E-16. It is therefore highly unlikely that the variations in GA performance, shown in Fig. 5.16, were caused by randomness alone and it is hence assumed that the combinations had a real effect over the measured GA performance.

The combinations involve a selection of values for various parameters. It is also of interest to explore the isolated overall effect of each of those parameters. Fig. 5.18 presents how the "Fittest/Run" results are

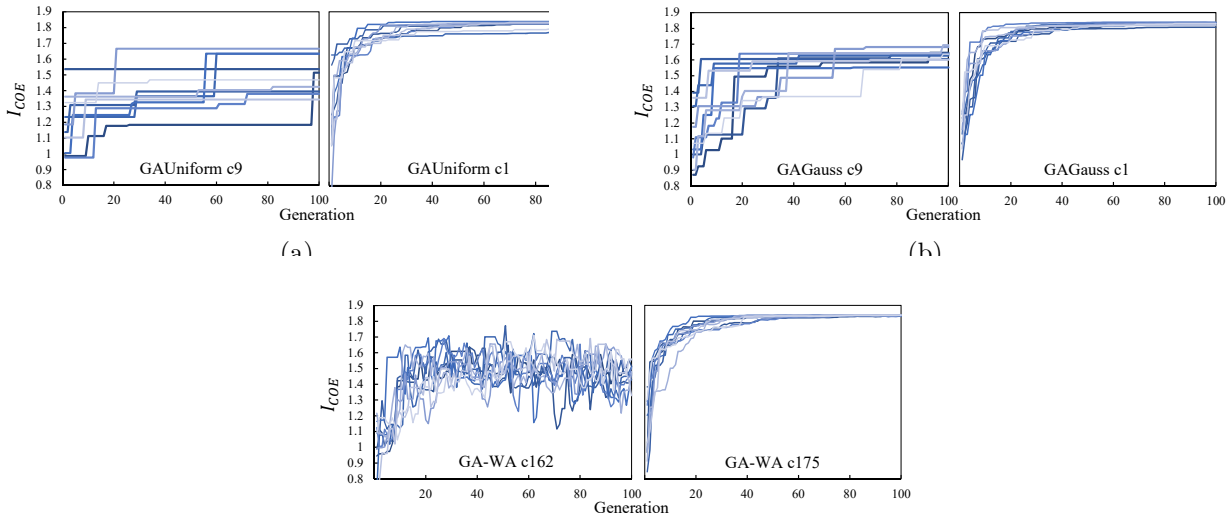

Figure 5.17: Worst and best parameter combinations for (a) GAUniform, (b) GAGauss and (c) GA-WA.

distributed for every GA and for every level of the GA heuristic parameters. In GAUniform, the parameters n_e and $pMut$ both had a significant effect with P-values 1E-4 and 5.75E-12, respectively. Likewise, in GAGauss, the parameters n_e and $pMut$ both had a significant effect with P-values 2.31E-8 and 4.13E-9, respectively. In GA-WA, the parameters μn_e, $fMut$ and $fMut_e$ had a significant effect with P-values <2.2E-16, 1.49E-4 and 1.56E-4, respectively. On the other hand, the parameters $\mu pMut$ and $\mu pMut_e$ did not have a significant effect, with P-values 6.1E-2 and 7.7E-2. Going further, Dunn's test, with the Benjamini–Hochberg adjustment (Dinno, 2015), was used as a non-parametric pairwise comparison of the levels of each parameter. The pairs of level-groups that presented a significant difference are highlighted in the figure with (*).

The "Mean Fittest/Run" performance is the most decisive perspective for comparing different GAs because it indicates the fitness at which a GA will tend to converge after every time that it is used. From this perspective and considering only the optimized combinations of parameters, was GA-WA significantly superior to the reference GAs? The comparison of how the results of these three GAs are distributed are shown in Fig. 5.19(a). With the adjusted Dunn's test, it was found that GA-WA (combination 175) presented a significant superiority when compared to both GAUniform (combination 1) and GAGauss (combination 1). Moreover, there was no significant difference in the case of GAUniform when compared to GAGauss. Fig. 5.19(b) shows a close-up of their evolutionary progression throughout the generations. These curves illustrate how GA-WA converges most of its evolutionary progressions towards a narrower range at the top.

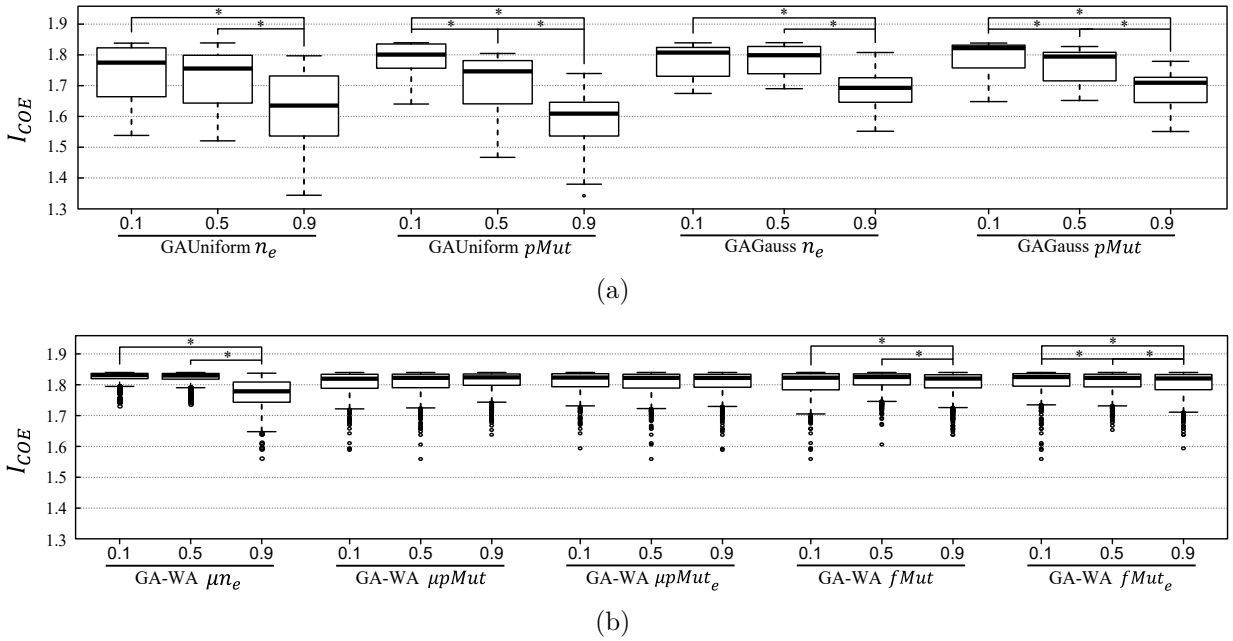

Figure 5.18: Performance Box plots in function of the GA parameters for (a) GAUniform and GAGauss; and for (b) GA-WA.

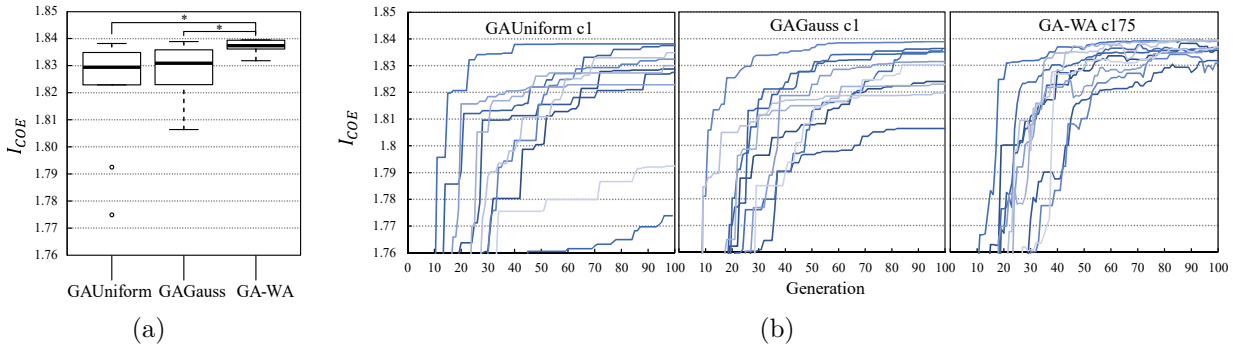

Figure 5.19: Performance of the optimized parameter combinations for GAUniform, GAGauss and GA-WA. (a) Box plot. (b) Close-up of the evolution through the generations.

Chapter 6

Case Study

Secs. 5.2 and 5.3 respectively introduced a new interactive tool, VTDesign, and a new heuristic optimization tool, GA-WA. This section presents a case study for an exploratory theoretical evaluation of their capacities to support the definition of the V-Trough's parameters in personalized design scenarios. This section provides an insight into the versatile capacities that can be achieved through these tools. Moreover, the results of the case study can help to illustrate the practical advantages of a flexible exploration of V-Trough set-ups for personalized contexts and for a set of performance priorities. Through this section, the specific objectives IV and V are hence concluded.

The case study is approached from three different design goals. In the following sections, each goal is addressed from both VTDesign and GA-WA and the best resulting V-Trough set-ups are compared. GA-WA is implemented with the heuristic parameters that were found in Sec. 5.3.3 to have the best performance: $\mu n_e = 0.1$, $\mu pMut = 0.9$, $\mu pMut_e = 0.5$, $fMut = 0.1$ and $fMut_e = 0.5$.

6.1 Design Brief

The case study was designed around a rural Colombian family seeking to fulfill their daily energy demand by means of a V-Trough system. The people, their context and their needs are based on real facts taken from a series of exploratory field trips performed during 2014. Therefore, the family of this case study is defined as to represent a typical scenario for a rural and low-income household in a developing country. The case study is located in the region *Chaparral*, in the Colombian *Antioquia* Department. This rural location was chosen because, according to the people who were interviewed there, their homes had been connected to the public electrical grid in the previous five years. Therefore, the people in *Chaparral* were aware of the implications of living off-the-grid. Fig. 6.1(a) shows a photo of an actual household in this location that serves as the particular context for this analysis. Fig. 6.1(b) shows their surrounding open space, where a V-Trough system could be deployed and manipulated.

Fig. 6.1(c) locates *Chaparral* on a map that also shows different levels of solar radiation in terms of the multi-year mean daily solar incident energy. The map with the levels of solar radiation was modified from Ministerio de Ambiente, Vivienda y Desarrollo Territorial, Ministerio de Minas y Energía (2005), who used real measurements and interpolation methods for its construction. According to this solar map, a household in *Chaparral* is expected to receive an average irradiance of $\overline{I} = 354.17 W/m^2$ during daylight hours. The instantaneous irradiance is in fact expected to considerably vary according to the time of the day, the day of the year, which affects the declination angle, and the particular daily weather, which can affect the amount of blocked solar rays and the proportion of beam solar radiation (see Sec. 3.1). It is not the interest of this case study to perform a realistic simulation of an specific location, but to assess the capacities of the developed tools for a generic situation. Therefore, a representative day is defined for this analysis with a constant $\overline{I} = 354.17 W/m^2$ throughout the average 12h of sunlight. Also, the whole $\overline{I}$ is assumed to behave as beam radiation, in terms of V-Trough interactions, because diffuse radiation is out of the scope of this research project.

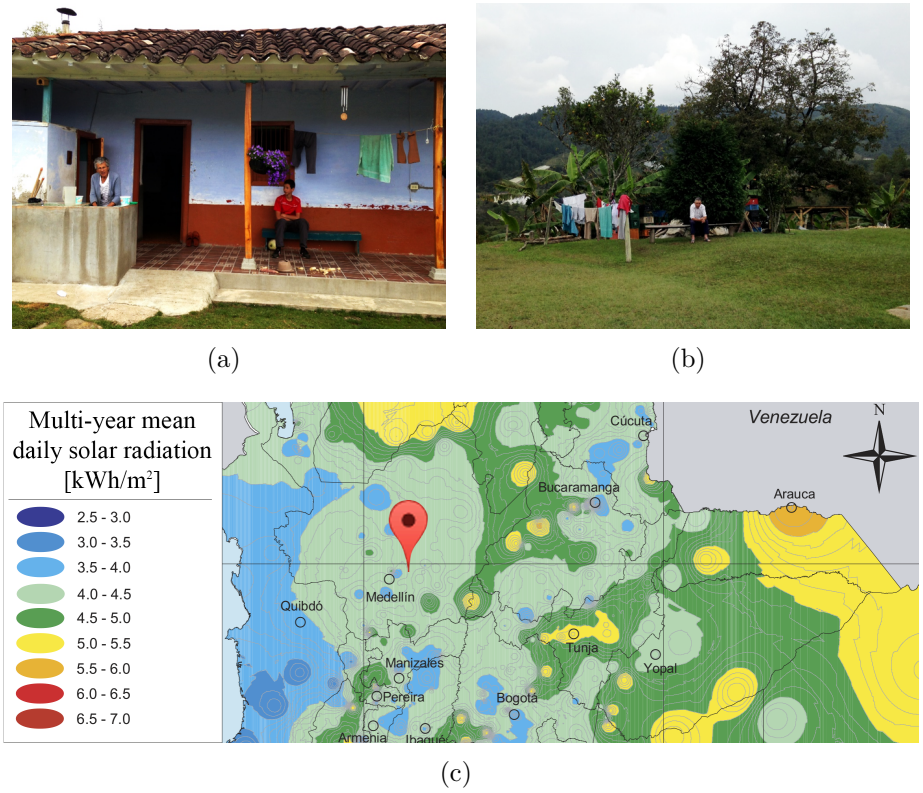

Figure 6.1: Real photos of the location in *Chaparral*, Colombia, for the case study. (c) presents a map of the location and the average levels of radiation; modified from Ministerio de Ambiente, Vivienda y Desarrollo Territorial, Ministerio de Minas y Energía (2005).

Table 6.1 presents a basic consumption outline for this representative family. According to this outline, the V-Trough system should generate $1495.4 Wh/day$ in order to fulfill their energy needs with a 20% margin. Since their solar exposure is not particularly privileged, the family wants to maximize the performance of their harvesting system as compared to a regular fixed and flat solar panel. They do not desire the complexity and additional capital cost of an automatic tracking system. However, they are willing to manually adjust the position of the system twice a day, i.e., at 10 a.m. ($\alpha = 60°$) and at 2 p.m.($\alpha = 120°$). In the afternoon, the sun gets blocked in the horizon by a mountain, so they have an available solar elevation range of $0° \leq \alpha \leq 160°$. They have access to regular silicon photovoltaic cells with an efficiency of $\eta_{pv} = 15\%$ and a cell area of $A_{pvc} = 0.024 m^2$. Based on the specifications of their power inverter, a system efficiency of $\eta_s = 84\%$ is assumed.

From Sangani and Solanki (2007), the reflection index is taken as $\rho = 0.85$, corresponding to anodized aluminum reflectors. As suggested in Sec. 5.1, the area costs are defined as follows: $CO_m = 13.33 \left[\text{USD}/m^2\right]$, $CO_s = 62.23 \left[\text{USD}/m^2\right]$ and $CO_{pv} = 600 \left[\text{USD}/m^2\right]$. The geometrical exploration was constrained to a V-Trough with: fixed mirrors, in terms of length and angular position; and a tracking strategy performed by adjusting β twice a day (at $\alpha = 60°$ and $\alpha = 120°$). Table. 6.2 defines the previous scenario as the inputs needed for the genes in GA-WA.

Table 6.1: Basic consumption outline for a low-income family in *Chaparral*, Colombia.

Household appliance	Consumption [W]	No.	Use [h/day]	Energy [Wh/day]
Halogen light	11	4	4	176
90 liter fridge	38.18	1	12	458.16
Cell Phone charger	4	3	1	12
Small stereo	30	1	3	90
TV	100	1	3	300
Laptop	70	1	3	210
			Total	1246.16
			Total +20%	1495.4

Table 6.2: Geometrical set-up parameters defined for the genes in GA-WA heuristic optimization method.

Geometrical set-up Parameters	Definition
LL, LR	RF. $Top = 2.5$, $Min = 0$. 2 Genes
ψL, ψR	RF. $Top = 90°$, $Min = -90°$. 2 Genes
β	RD. $Top = 180°$, $Min = -180°$, α $[60°, 120°]$. 3 Genes

Regarding an energy production system such as the one of this case study, the design/engineering priorities can vary according to the specific constraints and expectations of the potential users; as previously described in Fig. 5.2. Therefore, the design/engineering problem of satisfying the energy needs of this theoretical family is approached from three different design goals:

- ***Design Goal I (Cost):*** To minimize the cost of the system, in terms of materials, while fulfilling the given energy need.
- ***Design Goal II (Energy):*** To maximize the daily energy to be harvested by the V-Trough within a given available space for the device and a given number of solar cells to allocate.
- ***Design Goal III (Space):*** To minimize the space needed to allocate the device while fulfilling the energy need.

Focusing of the modeling priorities of this research project, this case study assumes a theoretical performance based only on beam radiation. No temperature losses are modeled and no longitudinal misalignments are considered.

6.2 Design Goal I: Cost

The goal is to minimize the cost of the system, in terms of materials, while fulfilling the energy need of $1495.4 Wh/day$. This goal was approached from both VTDesign and GA-WA. The optimizations with GA-WA were performed with several Performance Indicators and Indices used as fitness functions. For each fitness function used, the genetic algorithm converged into a particular V-Trough set-up. The following are the set-ups that resulted from the exploration with both tools (VTDesign and GA-WA):

- $VT1_i$: An intuitive set-up established as a starting point.
- $VT1_{VTDa}$: The fittest set-up, in terms of I_{COE}, achieved through the exploration with VTDesign.
- $VT1_{VTDb}$: The fittest set-up, in terms of $Cost$, achieved through the exploration with VTDesign.
- $VT1_{icoe}$: The fittest set-up achieved through the optimization with GA-WA by using the index I_{COE} as fitness function.

- $VT1_{cost}$: The fittest set-up achieved through the optimization with GA-WA by using the indicator *Cost* as fitness function.
- $VT1_{icost}$: The fittest set-up achieved through the optimization with GA-WA by using the indicator *Cost* as fitness function and with the first population distributed around the intuitive set-up $VT1_i$.

The geometrical parameters of the previous set-ups are presented in Table. 6.3. LL and LR are defined as proportions of LPV; ψL, ψR and β are given in [deg]; T_{sp} in $[m^2]$; *Cost* in [USD] and E_{day} in $[Wh]$. The table also shows the performance results of each set-up in terms of the indicators and indices: $\overline{C_e}$, I_{COE}, MI_{COE}, T_{sp}, *Cost*, MDI_{COE} and E_{day}. The results in terms of *Cost* are highlighted in the table because this is the most relevant indicator according to the *Design Goal I*. This is shown in Fig. 6.2 as well. Also, the indices MI_{COE} and MDI_{COE} are calculated with the weights $W1 = 0.9$ and $W2 = 0.1$. These weights prioritize the monetary cost over the space implications.

The set-up $VT1_i$ is considered an intuitive starting point for cost-effectiveness because the mirrors have the same length as the PV absorber, they are symmetrically arranged and their angular position is such that all solar rays should reach the PV surface, directly or after only one reflection, if they are perpendicular to the device ($iPV = 90°$). The strategy for the exploration with VTDesign was to start iterating different variations of $VT1_i$ by identifying the changes that increased the Cost-Effectiveness Index (I_{COE}). The two set-ups with the highest I_{COE}, after this interactive process, were $VT1_{VTDa}$ and $VT1_{VTDb}$. Interestingly, even though $VT1_{VTDa}$ achieved higher $\overline{C_e}$ and I_{COE} indicators, the set-up $VT1_{VTDb}$ resulted in a lower *Cost* with a 3.7% cost reduction as compared to the intuitive set-up. This can be explained from the discretization effect of the solar cells described in Sec. 5.1. The required solar cells in $VT1_{VTDa}$, being discrete units, are forced to include an excess of PV material that results in $12.74Wh$ more than needed.

Table 6.3: Results of the *Design Goal I*.

	Geometrical set-up					Performance Indicators and Indices						
Set-up	LL	LR	ψL	ψR	β	$\overline{C_e}$	I_{COE}	MI_{COE}	T_{sp}	*Cost*	MDI_{COE}	E_{day}
$VT1_i$	1	1	30	30	[60,0,-60]	1.409	1.659	1.575	5.597	**1821**	1.571	1501.4
$VT1_{VTDa}$	1	1	24	27	[59,2,-55]	1.463	1.723	1.634	5.466	**1761.6**	1.623	1508.1
$VT1_{VTDb}$	0.8	0.8	25	25	[60,4,-52]	1.403	1.716	1.64	4.778	**1753.4**	1.642	1495.4
$VT1_{icoe}$	1.01	1	23.55	25.31	[59.13, -0.42, -51.87]	1.471	1.73	1.641	5.441	**1743.9**	1.639	1499.5
$VT1_{cost}$	0.90	1	25.43	25.74	[60.61, 1.13, -47.66]	1.451	1.726	1.639	5.277	**1744.4**	1.641	1496.1
$VT1_{icost}$	1.04	0.96	21.73	27.33	[57.55, -3.97, -51.62]	1.468	1.728	1.639	5.429	**1742.5**	1.64	1496.1

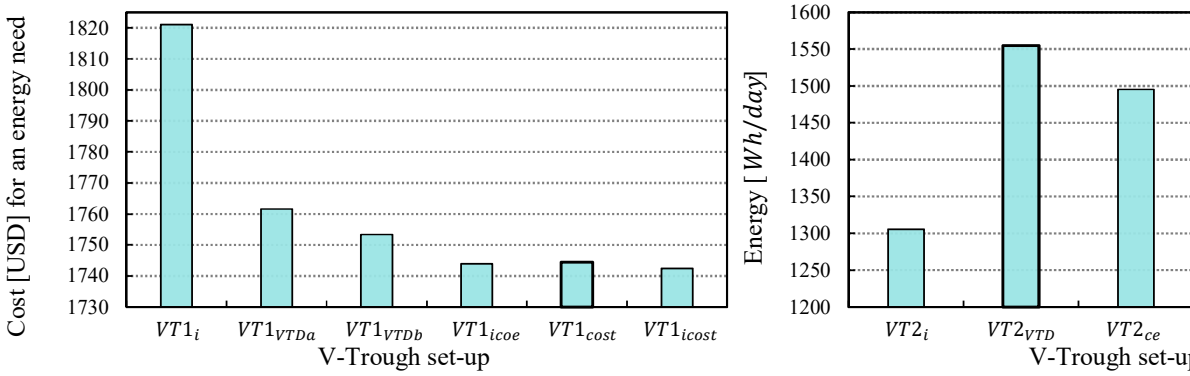

Figure 6.2: Results of the *Design Goal I* in terms of *Cost*.

For approaching this problem from GA-WA, the heuristic optimization algorithm was run in three different ways. The fittest set-ups obtained are: $VT1_{icoe}$, $VT1_{cost}$ and $VT1_{icost}$. The intention was to

see if different set-ups resulted from considering the discretization effects with *Cost* and if an intuitively-distributed initial population presented an evolutionary advantage for this particular goal and scenario. As shown in Fig. 6.2 and detailed in Table 6.3, the three different runs with GA-WA converged into similar set-ups and with almost equivalent costs in terms of materials; differing in less than $2USD$.

The set-up $VT1_{icost}$ achieved the lowest cost in terms of materials. This set-up presented a cost reduction of 4.3% as compared to the intuitive $VT1_i$ and 0.6% as compared to the fittest from VTDesign ($VT1_{VTDb}$). Moreover, the *Cost* with $VT1_{icost}$ is 42.2% less than the reference flat and fixed horizontal solar panel; a considerable gain in cost-effectiveness. There is an evident convergence between the results obtained directly from intuition, from VTDesign and GA-WA in its three runs. The fine-tuning of the intuitive $VT1_i$ was performed almost in the same way by interactive exploration in $VT1_{VTDb}$ and heuristic optimization in $VT1_{icost}$. This convergence may imply that the results achieved are close to a global maximum in the space of possible solutions.

For a visualization of the geometries involved and the corresponding performance curves, all resulting set-ups were inspected in VTDesign; including the ones obtained through GA-WA. Fig. 6.3 illustrates the most relevant dynamic geometries, at $\alpha = 0°$, $\alpha = 60°$, $\alpha = 90°$ and $\alpha = 120°$, for the set-ups (a) $VT1_i$, (b) $VT1_{VTDb}$ and (c) $VT1_{icost}$. In these figures, two α values are linked to one same V-Trough illustration. This means that the V-Trough has maintained the same position for both solar elevations. Fig. 6.4 illustrates the PV area reduction, as compared to a reference flat and fixed solar panel, achieved by these same set-ups from calculations of $\overline{C_e}$. The PV area reduction helps to intuitively explain how the corresponding set-ups manage to reduce the cost of materials.

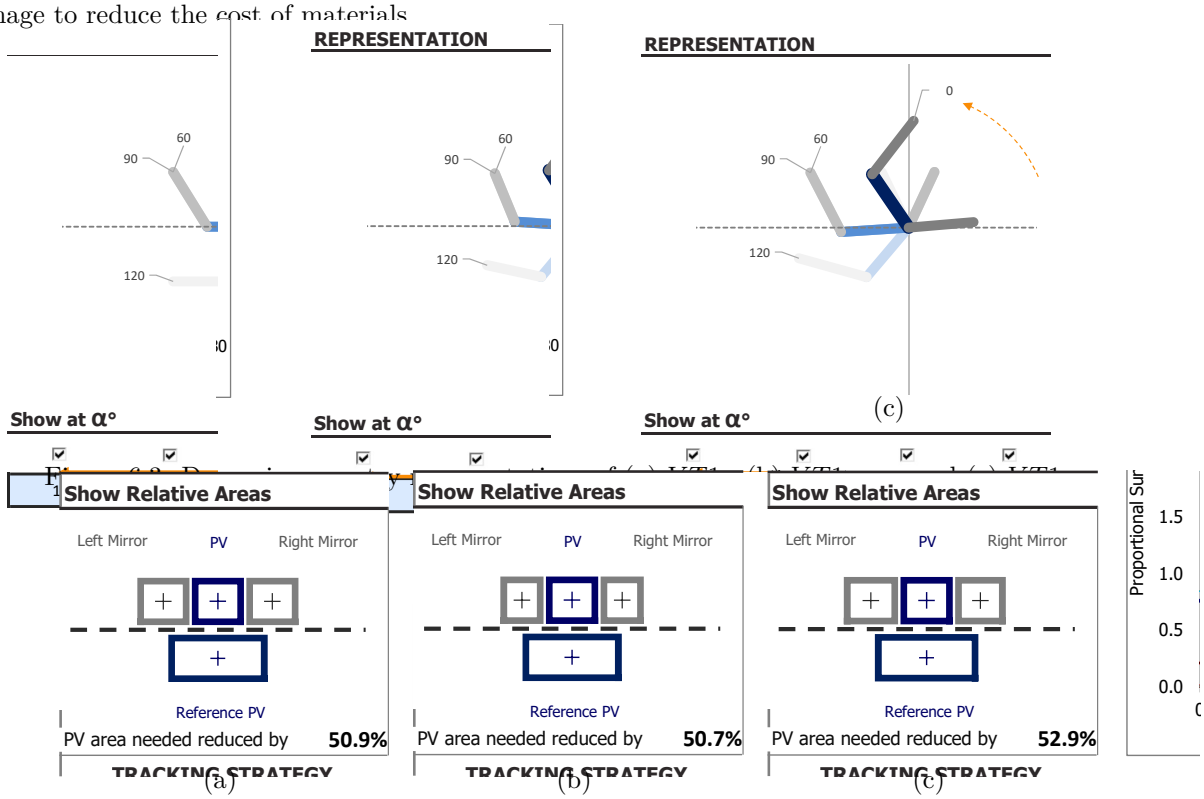

Figure 6.4: PV area reduction of (a) $VT1_i$, (b) $VT1_{VTDb}$ and (c) $VT1_{icost}$.

Fig. 6.5 presents the optical performance charts, directly obtained from VTDesign, for the set-ups $VT1_i$ (6.5(a)–6.5(b)), $VT1_{VTDb}$ (6.5(c)–6.5(d)) and $VT1_{icost}$ (6.5(e)–6.5(f)). The differences in these curves are evident even between such similar geometrical set-ups. For instance, the C_e curve of $VT1_i$ has three equal peaks corresponding to the three positions that the V-Trough adopts. On the other hand, the C_e curves of $VT1_{VTDb}$ and $VT1_{icost}$ present three peaks each that may not rise as high as the ones of $VT1_i$, but that manage to accumulate a larger area under the curve throughout the α range. For the three set-ups, all

contributions correspond to the rays that reach the PV surface directly or after only one reflection. In $VT1_i$, the effective contributions of both mirrors (CL_e and CR_e) behave exactly in the same way. In $VT1_{VTDb}$, these contributions do not converge to a same curve but are symmetrical to a midpoint between tracking positions. Similarly, these contributions do not fall in the same curve for $VT1_{icost}$ and here, the contributions of the left mirror (CL_e) are greater. The slight difference between the curves CPV_e and CPV_0, for both $VT1_{VTDb}$ and $VT1_{icost}$, reveal that there are shadows being generated over the PV surface in narrow α ranges around the points when the V-Trough has adopted a new tracking position. Remarkably, the optical performance of $VT1_i$ is worse overall even with a smoother progression in the C_e curve, a total symmetry in the three detected peaks and with no shadows generated.

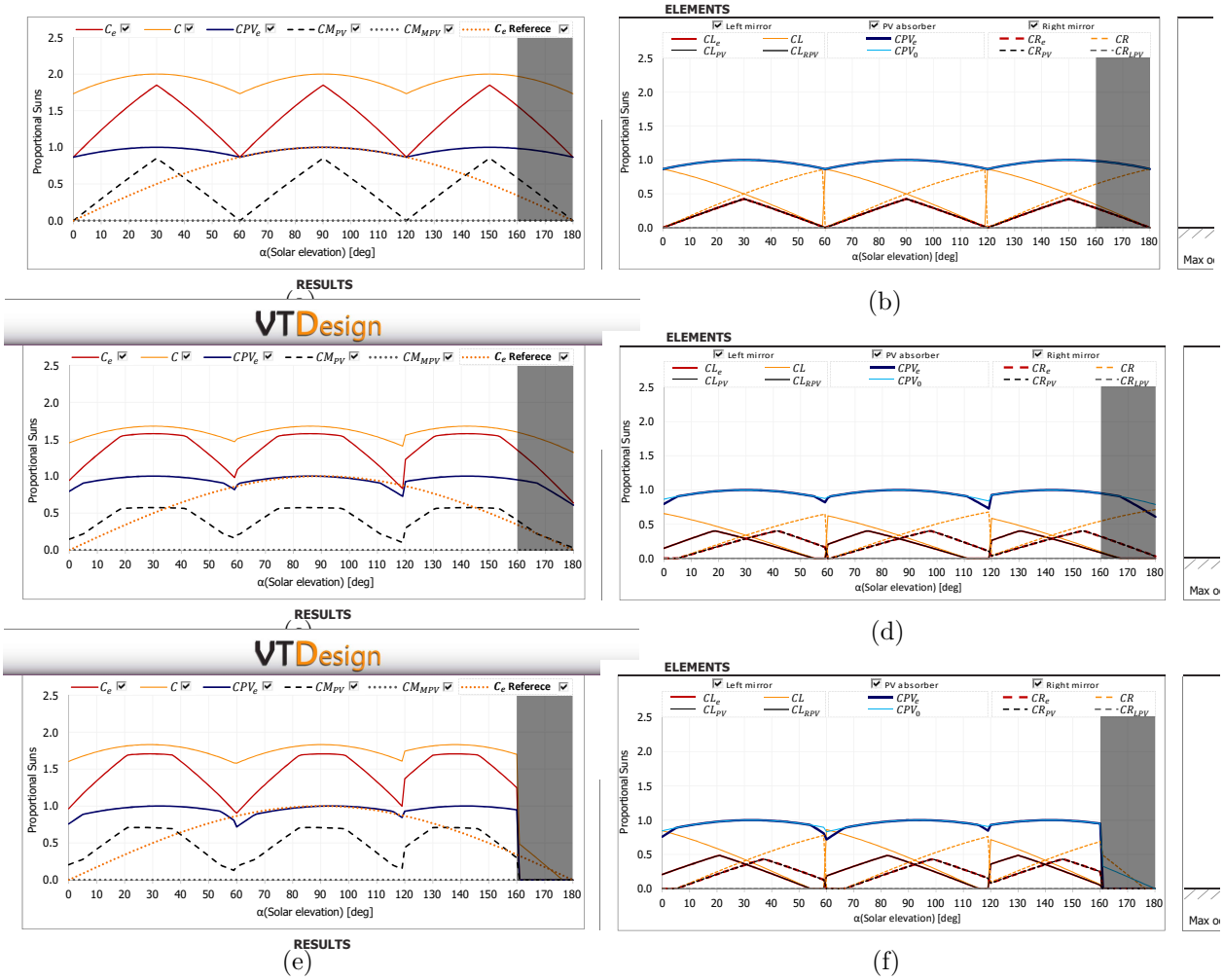

Figure 6.5: Optical performance curves of the set-ups (a)–(b) $VT1_i$, (c)–(d) $VT1_{VTDb}$ and (e)–(f) $VT1_{icost}$.

Fig. 6.6(a) presents the preliminary CAD model of the fittest set-up achieved for the *Design Goal I* ($VT1_{icost}$); obtained from the automatic integration between VTDesign and SolidWorks®. Fig. 6.6(b) illustrates the same geometrical set-up developed in a more detailed design and contextualized in the real scenario of the case study. The 88 solar cells, required by this set-up, are distributed in 4 rows and 22 columns of cells in the PV surface.

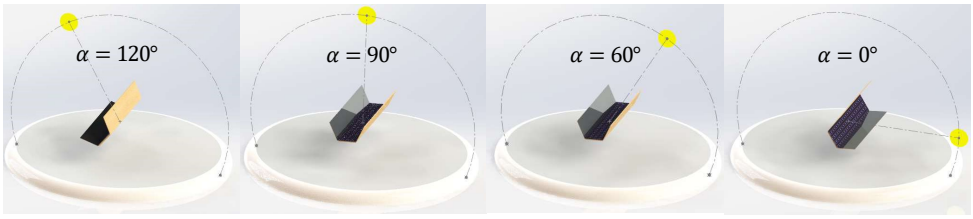

(a)

(b)

Figure 6.6: (a) Preliminary CAD model and (b) realistic rendering of the fittest set-up achieved for Goal I ($VT1_{icost}$).

6.3 Design Goal II: Energy

The goal is to maximize the daily energy to be harvested by the V-Trough within a given available space for the device and a given number of solar cells to allocate. The available space was defined as $10m^2$ based on the observations performed during the field trips to the location of this case study. The available number of solar cells was arbitrarily defined as 80. This goal was approached from both VTDesign and GA-WA. The following are the set-ups that resulted from the exploration with both tools (VTDesign and GA-WA):

- $VT2_i$: An intuitive set-up established as a starting point according to the *Design Goal II*.
- $VT2_{VTD}$: The fittest set-up, in terms of $\overline{C_e}$, achieved through the exploration with VTDesign.
- $VT2_{ce}$: The fittest set-up achieved through the optimization with GA-WA by using the indicator $\overline{C_e}$ as fitness function.
- $VT2_{micoe}$: The fittest set-up achieved through the optimization with GA-WA by using the index MI_{COE} as fitness function.
- $VT2_{ice}$: The fittest set-up achieved through the optimization with GA-WA by using the indicator $\overline{C_e}$ as fitness function and with the first population distributed around the intuitive set-up $VT2_i$.

The geometrical parameters of the previous set-ups are presented in Table. 6.4. LL and LR are defined as proportions of LPV; ψL, ψR and β are given in [deg]; T_{sp} in [m^2]; $Cost$ in [USD] and E_{day} in [Wh]. The table also shows the performance results of each set-up in terms of the indicators and indices: $\overline{C_e}$, I_{COE}, MI_{COE}, T_{sp}, $Cost$, MDI_{COE} and E_{day}. The results in terms of E_{day} are highlighted in the table because this is the most relevant indicator according to the *Design Goal II*. Also, the indices MI_{COE} and MDI_{COE} are calculated with the weights $W1 = 0.9$ and $W2 = 0.1$.

The intuitive set-up $VT2_i$ shares the same geometrical parameters of $VT1_i$. Even though the goal is to maximize energy, the lengths of the mirrors for this intuitive set-up were not defined larger because this *Design Goal* includes also a restriction in the total area available for the device. The strategy for the exploration with VTDesign was to start iterating different variations of $VT2_i$ by identifying the changes that increased the Effective Concentration ($\overline{C_e}$) and subsequently verifying that all the available 80 solar cells could be used without exceeding the available space for the device ($10m^2$).

Table 6.4: Results of the *Design Goal II*.

	Geometrical set-up					Performance Indicators and Indices						
Set-up	LL	LR	ψL	ψR	β	$\overline{C_e}$	I_{COE}	MI_{COE}	T_{sp}	$Cost$	MDI_{COE}	E_{day}
$VT2_i$	1	1	30	30	[60,0,-60]	1.409	1.659	1.575	4.867	1583.5	1.806	**1305.6**
$VT2_{VTD}$	2.35	2.35	20	20	[60,4,-52]	1.678	1.58	1.469	9.943	1980.7	1.415	**1554.8**
$VT2_{ce}$	2.5	2.5	8.19	31.85	[46.44, -13.47, -63.23]	1.699	1.564	1.454	9.964	1923.6	1.456	**1495.4**
$VT2_{micoe}$	0.94	0.56	17.86	33.09	[52.15, -10.39, -59.19]	1.38	1.704	1.632	3.962	1509.7	1.911	**1278.6**
$VT2_{ice}$	2.5	2.5	19.45	21.06	[60.67, 0.71, -52.41]	1.697	1.563	1.452	9.987	1923.6	1.456	**1494.3**

The fittest set-up found with this procedure was $VT2_{VTD}$ (see Fig. 6.7), which even managed to harvest more energy (E_{day}) than all the results obtained with GA-WA. $VT2_{VTD}$ increased E_{day} by 19.1%, as compared to the intuitive $VT2_i$, and by 142.7%, as compared to a reference fixed and flat solar panel with 80 cells. The success of this set-up can be explained from the fact that it managed to considerably increase the Effective Concentration, while at the same time using all 80 solar cells and almost perfectly matching the available space of $10m^2$.

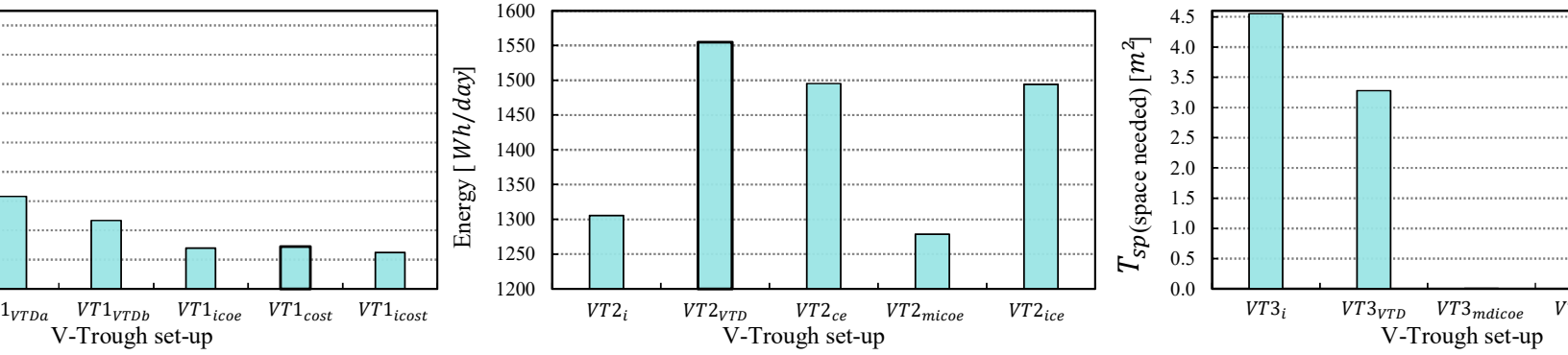

Figure 6.7: Results of the *Design Goal II* in terms of Energy.

For approaching this problem from GA-WA, the heuristic optimization algorithm was run in three different ways. The fittest set-ups obtained are: $VT2_{ce}$, $VT2_{micoe}$ and $VT2_{ice}$. The intention was to see if different set-ups resulted from considering only the maximization of the harvesting area, with $\overline{C_e}$, or from also considering the space required with the index MI_{COE} ($W1 = 0.9$ and $W2 = 0.1$).

The set-ups $VT2_{ce}$ and $VT2_{ice}$ converged into similar geometries and energy results; differing in less than $2Wh$. Even though they achieved the highest $\overline{C_e}$ values, they are surpassed in terms of energy by $VT2_{VTD}$ because they can only use 76 solar cells without exceeding the available space for the device. This fact allows $VT2_{VTD}$ to generate 4% more energy as compared to the fittest GA-WA set-up, namely $VT2_{ce}$.

On the other hand, $VT2_{micoe}$, considering also the space minimization, achieved the highest I_{COE}, MI_{COE} and MDI_{COE} indices. Being more compact, $VT2_{micoe}$ could have allocated up to 201 cells and surpass the E_{day} of all the other set-ups; but the 80 cells limit greatly restricted its energy performance. Overall, the different results show more divergence as compared to the *Design Goal I*.

Fig. 6.8 illustrates the most relevant dynamic geometries, at $\alpha = 0°$, $\alpha = 60°$, $\alpha = 90°$ and $\alpha = 120°$, for the set-ups (a) $VT2_i$, (b) $VT2_{VTD}$ and (c) $VT2_{ice}$. In these figures, two α values are linked to one same V-Trough illustration. This means that the V-Trough has maintained the same position for both solar elevations. From Fig. 6.8, it can be seen that a configuration with proportionally bigger mirrors resulted form both GA-WA and VTDesign explorations. Also, from these three, the fittest GA-WA set-up was the only one with asymmetric mirrors in terms of angular position. Fig. 6.9 illustrates the PV area reduction, as compared to a reference flat and fixed solar panel, achieved by these same set-ups from calculations of $\overline{C_e}$. The set-up $VT2_{\ldots}$ is the most successful in this regard.

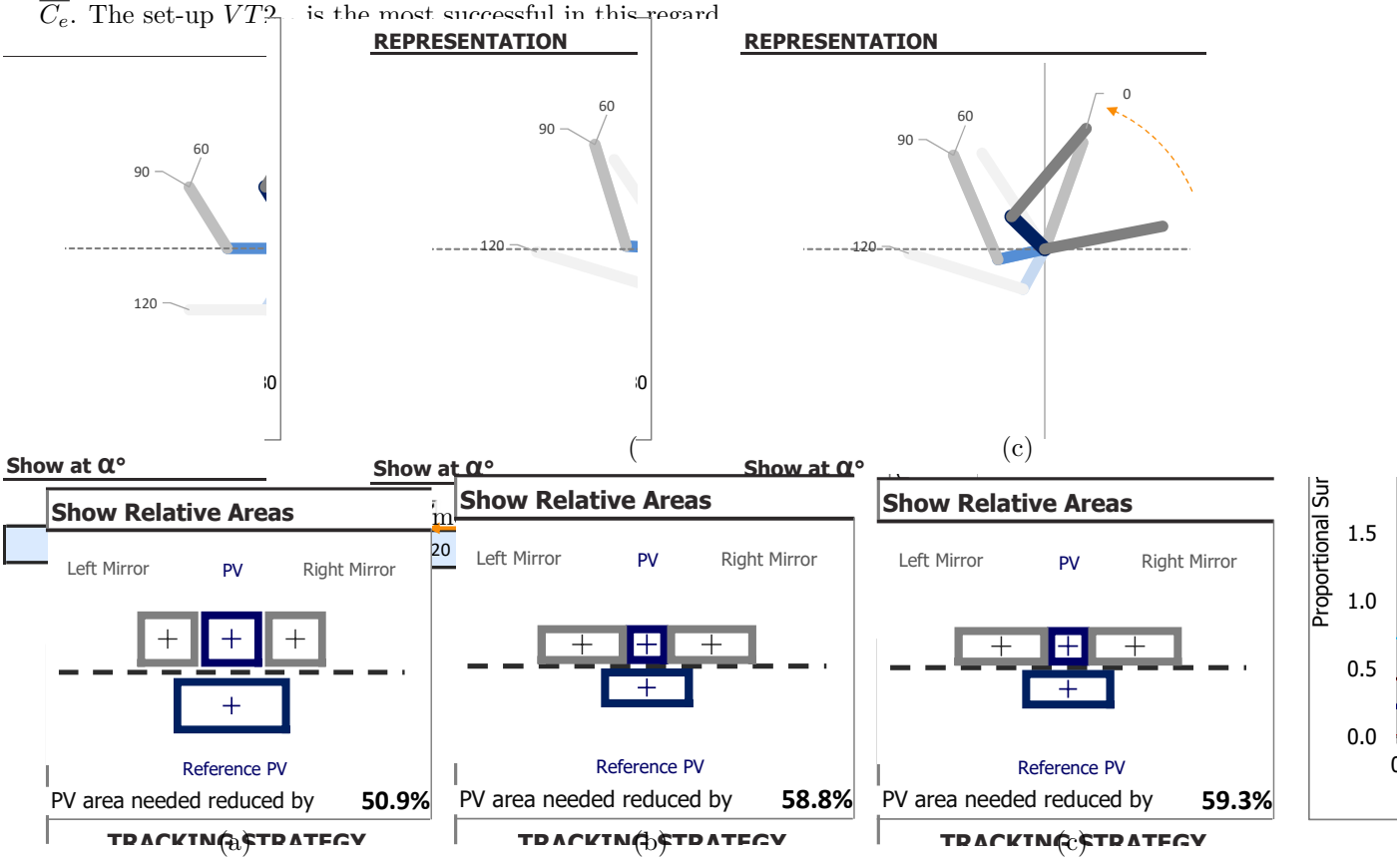

Figure 6.9: PV area reduction of (a) $VT2_i$, (b) $VT2_{VTD}$ and (c) $VT2_{ce}$.

Fig. 6.10 presents the optical performance charts, directly obtained from VTDesign, for the set-ups $VT2_i$ (6.10(a)–6.10(b)), $VT2_{VTD}$ (6.10(c)–6.10(d)) and $VT2_{ce}$ (6.10(e)–6.10(f)). A considerable difference, in terms of macro-optical phenomena, is revealed by these curves: in the set-up $VT2_i$ no ray reaches the PV surface after two reflections while this does happen in both $VT2_{VTD}$ and $VT2_{ce}$. Also, differently from $VT2_{VTD}$, the contributions after two reflections in $VT2_{ce}$ correspond only to the right mirror (CR_{LPV}). The difference between the curves CPV_e and CPV_0, for both $VT2_{VTD}$ and $VT2_{ce}$, reveal that there are shadows being generated over the PV surface in α ranges around the points when the V-Trough has adopted a new tracking position ($\alpha = 0°$, $\alpha = 60°$ and $\alpha = 120°$). It is also noticeable, in the curve CM_{PV}, how the mirror contributions present smoother transitions between the performance peaks in the set-up $VT2_{VTD}$.

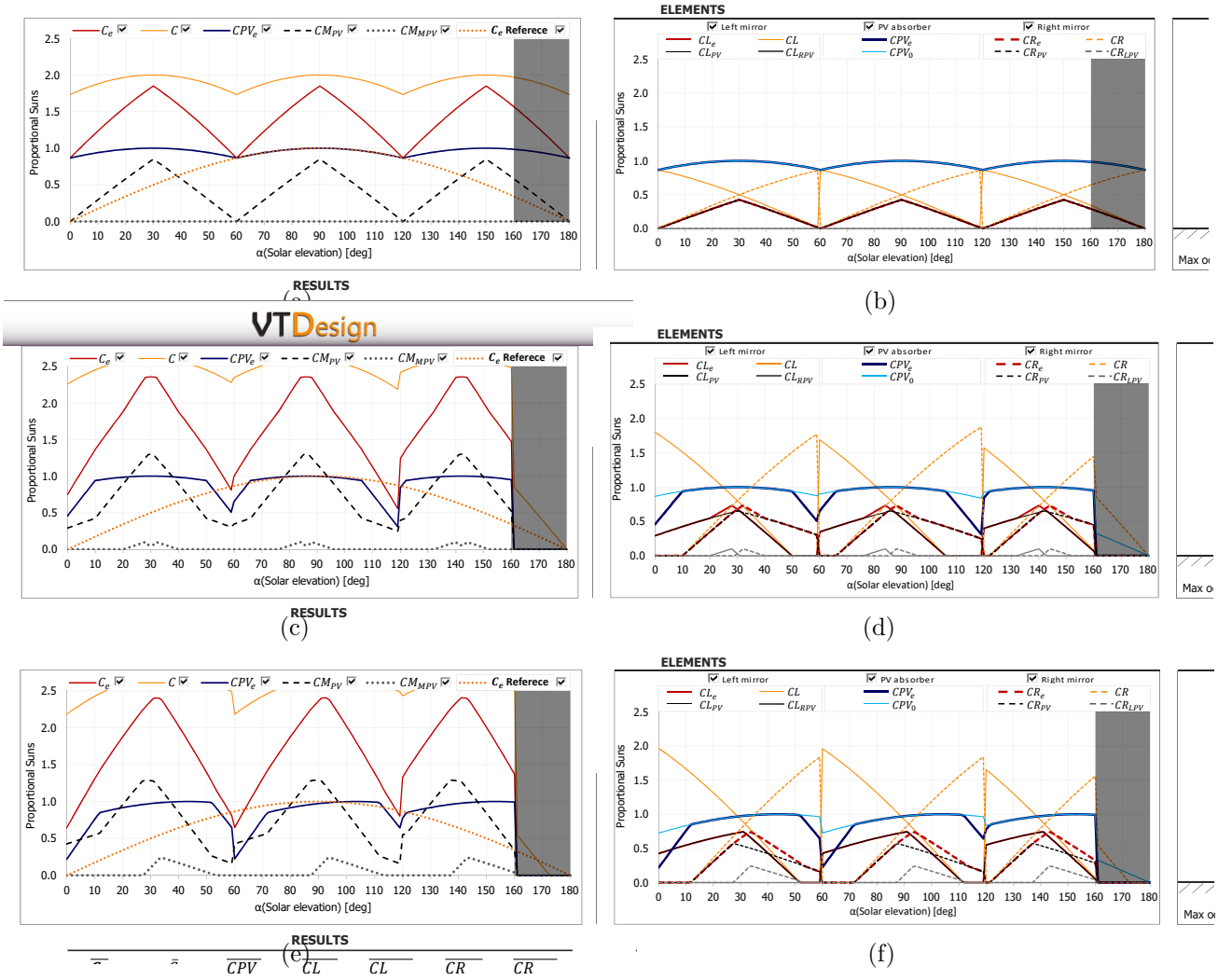

Figure 6.10: Optical performance curves of the set-ups (a)–(b) $VT2_i$, (c)–(d) $VT2_{VTD}$ and (e)–(f) $VT2_{ce}$.

Fig. 6.11(a) presents the preliminary CAD model of the fittest set-up achieved for the *Design Goal II* ($VT2_{VTD}$); obtained from the automatic integration between VTDesign and SolidWorks®. Fig. 6.11(b) illustrates the same geometrical set-up developed in a more detailed design and contextualized in the real scenario of the case study. The 80 solar cells, required by this set-up, are distributed in 4 rows and 20 columns of cells in the PV surface. This design was developed differently from the one shown for Goal I (Fig. 6.6(b)) in order to demonstrate how different detailed configurations can be used to implement a given V-Trough set-up.

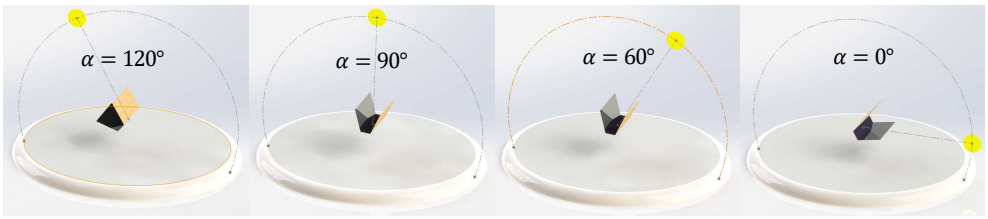

(a)

(b)

Figure 6.11: (a) Preliminary CAD model and (b) realistic rendering of the fittest set-up achieved for Goal II ($VT2_{VTD}$).

6.4 Design Goal III: Space

The goal is to minimize the space needed to allocate the device while fulfilling the energy need of $1495.4 Wh/day$. This goal was approached from both VTDesign and GA-WA. The following are the set-ups that resulted from the exploration with both tools (VTDesign and GA-WA):

- $VT3_i$: An intuitive set-up established as a starting point according to the *Design Goal III*.
- $VT3_{VTD}$: The fittest set-up, in terms of T_{sp}, achieved through the exploration with VTDesign.
- $VT3_{mdicoe}$: The fittest set-up achieved through the optimization with GA-WA by using the index MDI_{COE} as fitness function.
- $VT3_{tsp}$: The fittest set-up achieved through the optimization with GA-WA by using the index T_{sp} as fitness function.
- $VT3_{itsp}$: The fittest set-up achieved through the optimization with GA-WA by using the index T_{sp} as fitness function and with the first population distributed around the intuitive set-up $VT3_i$.

The geometrical parameters of the previous set-ups are presented in Table. 6.5. LL and LR are defined as proportions of LPV; ψL, ψR and β are given in [deg]; T_{sp} in $[m^2]$; $Cost$ in [USD] and E_{day} in $[Wh]$. The table also shows the performance results of each set-up in terms of the indicators and indices: $\overline{C_e}$, I_{COE}, MI_{COE}, T_{sp}, $Cost$, MDI_{COE} and E_{day}. The results in terms of T_{sp} are highlighted in the table because this is the most relevant indicator according to the *Design Goal III*. Also, the indices MI_{COE} and MDI_{COE} are calculated with the weights $W1 = 0.2$ and $W2 = 0.8$. Such weight prioritize the space implications over the monetary cost.

The intuitive set-up $VT3_i$ corresponds to a flat and horizontal panel with no mirrors in order to reduce the space required. The strategy for the exploration with VTDesign was to start iterating different variations of $VT3_i$ by identifying the changes that increased the Effective Concentration ($\overline{C_e}$) while maintaining a minimum mirror area.

Table 6.5: Results of the *Design Goal III*.

Geometrical set-up						Performance Indicators and Indices						
Set-up	LL	LR	ψL	ψR	β	$\overline{C_e}$	I_{COE}	MI_{COE}	T_{sp}	$Cost$	MDI_{COE}	E_{day}
$VT3_i$	0	0	-	-	[0,0,0]	0.691	1	1	**4.551**	3013.7	1	1497.6
$VT3_{VTD}$	0	0	-	-	[60,4,-52]	0.96	1.389	1.392	**3.277**	2175.7	1.388	1501.6
$VT3_{mdicoe}$	0	0	-	-	[89.98, -90.01, -90.03]	0.547	0.791	1382.8	**0.0026**	3819.5	1379.5	1501.2
$VT3_{tsp}$	0	0	-	-	[89.99, 90.01, -90]	0.55	0.795	3476.3	**0.001**	3787.3	3477.6	1497
$VT3_{itsp}$	0	0	-	-	[90.01, 89.99, -90]	0.55	0.795	3947.4	**0.0009**	3787.3	3948.8	1497

The fittest set-up achieved through VTDesign, in terms of the space required for the whole device, is $VT3_{VTD}$. As compared to the intuitive $VT3_i$, the tracking strategy of this set-up directly reduces the area footprint, by tilting the PV surface, and increases $\overline{C_e}$; which in turn allows to use only 135 solar cells as opposed to the 187 cells required for $VT3_i$. Accordingly, $VT3_{VTD}$ reduces the space required in 28% (see Fig. 6.12).

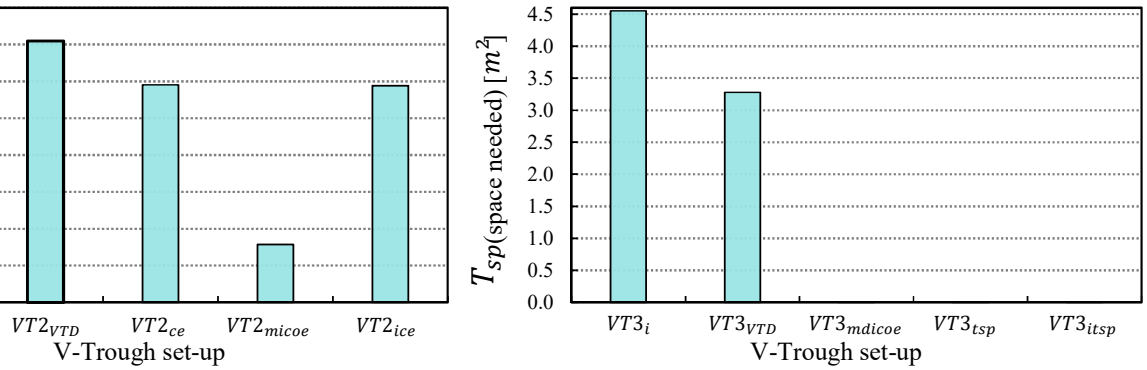

Figure 6.12: Results of the *Design Goal III* in terms of Space required.

For approaching this problem from GA-WA, the heuristic optimization algorithm was run in three different ways. The fittest set-ups obtained are: $VT3_{mdicoe}$, $VT3_{tsp}$ and $VT3_{itsp}$. While the fitness function T_{sp} directly addresses the goal here, the intention was to see if different set-ups resulted when MDI_{COE} was maximized; prioritizing space required with $W1 = 0.2$ and $W2 = 0.8$.

The three GA-WA results converged into virtually the same set-up, which is fundamentally superior to the intuitive $VT3_i$ and to even $VT3_{VTD}$. The three genetic set-ups evolved into eliminating both mirrors in order to reduce the space required, in the same way as intuition suggested. However, all genetic results found that the space could be minimized to virtually 0 if the panel was left vertical and then flipped in order to track the sun (see Fig. 6.13).

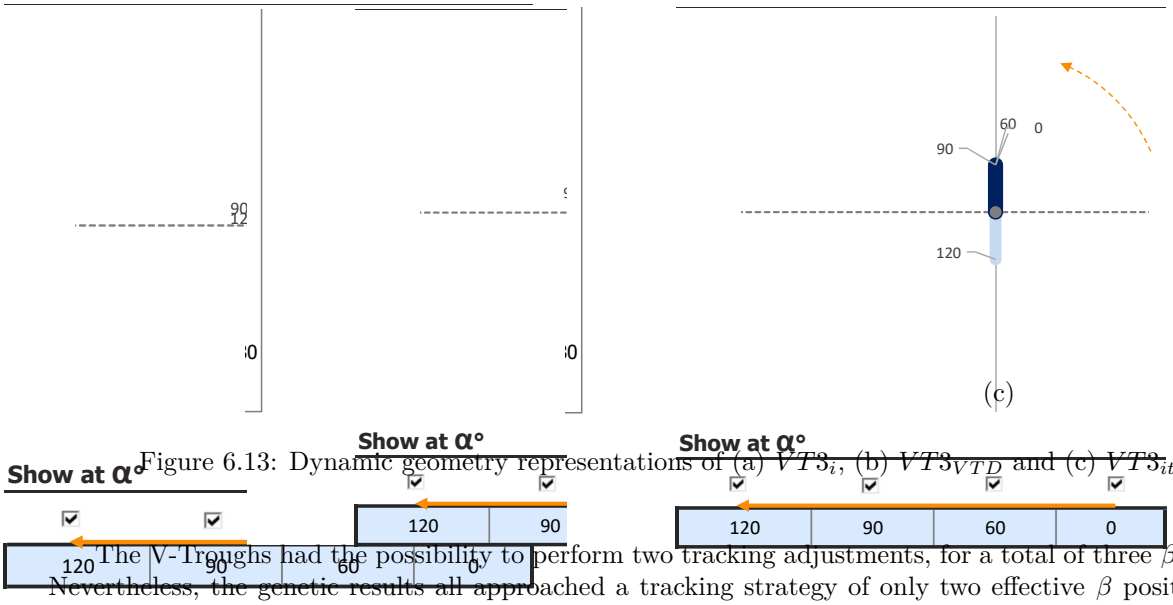

Figure 6.13: Dynamic geometry representations of (a) $VT3_i$, (b) $VT3_{VTD}$ and (c) $VT3_{itsp}$.

The V-Troughs had the possibility to perform two tracking adjustments, for a total of three β positions. Nevertheless, the genetic results all approached a tracking strategy of only two effective β positions, with the third one being almost equivalent to one of the other two; as can be inspected in Table. 6.5.

These results present a major divergence from the intuitive strategies explored and reveals how the GA-WA tool can "escape" from a particularly detrimental human bias. This is the case with $VT3_{itsp}$, which was initially biased around the parameters of $VT3_i$ but evolved into a superior strategy in terms of the fitness function used. $VT3_{itsp}$ achieved the lowest space needed to allocate the device. This set-up resulted in a space which is only 0.02% of the space with $VT3_i$ and 0.028% with $VT3_{VTD}$.

Fig. 6.13 illustrates the most relevant dynamic geometries, at $\alpha = 0°$, $\alpha = 60°$, $\alpha = 90°$ and $\alpha = 120°$, for the set-ups (a) $VT3_i$, (b) $VT3_{VTD}$ and (c) $VT3_{itsp}$. In these figures, two α values are linked to one same V-Trough illustration. This means that the V-Trough has maintained the same position for both solar elevations. Fig. 6.14 illustrates the PV area reduction, as compared to a reference flat and fixed solar panel, achieved by these same set-ups from calculations of $\overline{C_e}$. As expected, the PV area is not reduced in $VT3_i$ because it corresponds to the same geometrical disposition of the reference PV surface. The PV area was considerably reduced in $VT3_{VTD}$ by means of a two-step tracking strategy with no mirrors. On the other hand, since $VT3_{itsp}$ achieved a $\overline{C_e}$ which is less than the reference used, it actually increased the PV area required in a 25.7%. Accordingly, while the reference and intuitive set-up $VT3_i$ requires 187 solar cells to fulfill the energy need, $VT3_{itsp}$ requires 235 cells. Due to this fact, $VT3_{itsp}$ increases the material cost in 25.7% as compared to the reference.

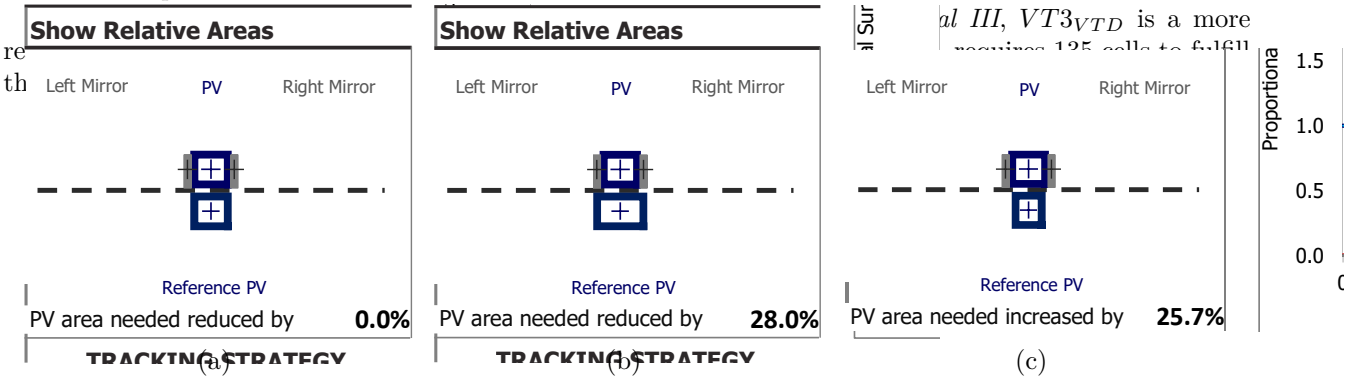

Figure 6.14: PV reduction of (a) $VT3_i$, (b) $VT3_{VTD}$ and (c) $VT3_{itsp}$.

Fig. 6.15 presents the optical performance charts, directly obtained from VTDesign, for the set-ups $VT3_i$ (6.15(a)–6.15(b)), $VT3_{VTD}$ (6.15(c)–6.15(d)) and $VT3_{itsp}$ (6.15(e)–6.15(f)). The optical performance curves of $VT3_i$ correspond to a flat horizontal PV surface without mirrors or tracking movements. As expected, there are no mirror contributions, nor shadows generated. The variation in the effective harvesting area,

proportional to C_e, corresponds only to the PV surface and varies according to the "cosine effect" as the solar elevation progresses. Similarly, $VT3_{VTD}$ achieves a smooth variation of C_e but it is distributed throughout three optical peaks as opposed to one.

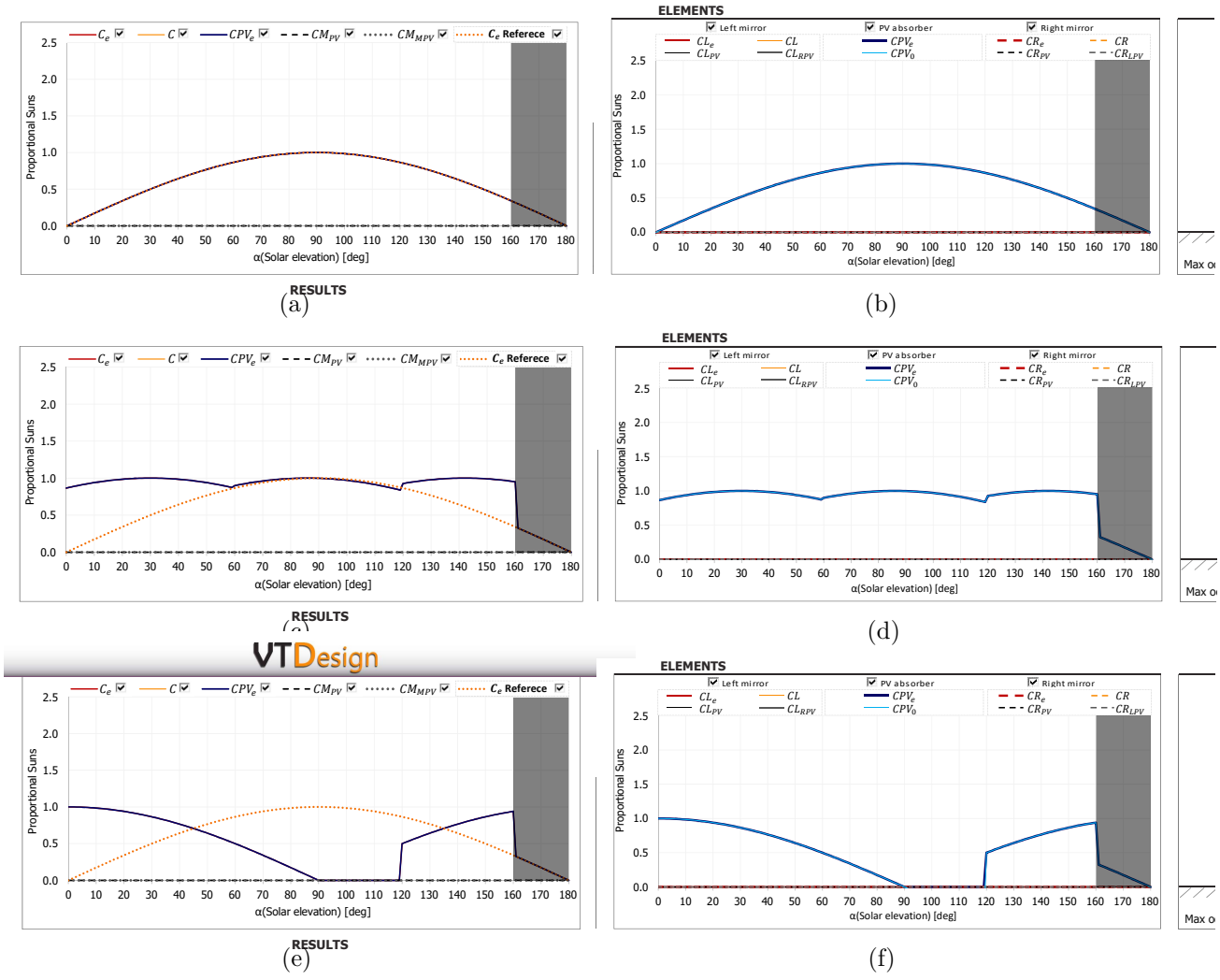

Figure 6.15: Optical performance curves of the set-ups (a)–(b) $VT3_i$, (c)–(d) $VT3_{VTD}$ and (e)–(f) $VT3_{itsp}$.

The optical behavior of $VT3_{itsp}$ is different in that there are two different peaks manifested in the curve C_e. The optical curves reveal that there is a shadow over the whole PV surface from $\alpha = 90°$ to $\alpha = 120°$. This can be explained from the fact that at $\alpha = 90°$, the solar rays are parallel to the PV surface and then reach the opposite surface of the device until it flips and faces the sunlight again.

Fig. 6.16(a) presents the preliminary CAD model of the fittest set-up achieved for the *Design Goal III* ($VT3_{itsp}$); obtained from the automatic integration between VTDesign and SolidWorks®. Fig. 6.16(b) illustrates the same geometrical set-up developed in a more detailed design and contextualized in the real scenario of the case study. The 235 solar cells, required by this set-up, are distributed in 5 rows and 47 columns of cells in the PV surface. This system evidently contrasts with the final solution presented for the *Design Goal I* (Fig. 6.6(b)) even though they generate almost the same daily energy. This difference illustrates how these devices can be tailored for specific scenarios and performance priorities.

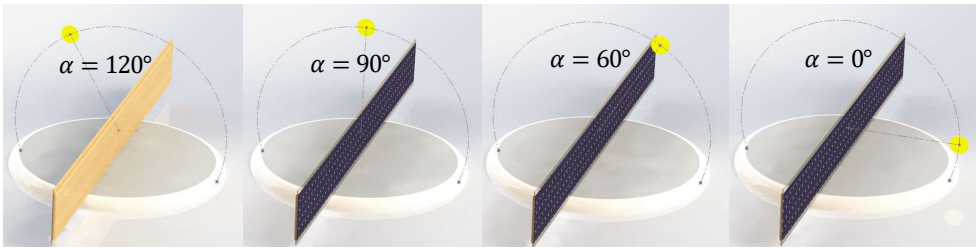

(a)

CaseStudy_3itsp_PreliminaryCAD

(b)

Figure 6.16: (a) Preliminary CAD model and (b) realistic rendering of the fittest set-up achieved for Goal III ($VT3_{itsp}$).

Remarkably, the average run-time for each of the GA-WA explorations in the case study, throughout the three Design Goals, was only 2 minutes and 36 seconds. These were run with the algorithms programmed in Python and in a conventional personal computer with 12GB RAM, 2.5GHz CPU and with Intel CORE i7. The heuristic optimization tool GA-WA "automatically" converged into similar solutions, or even superior in the case of the Design Goals I and III, as compared to the results achieved by a trained engineer interactively exploring V-Trough set-ups with VTDesign.

Chapter 7

General Analysis and Conclusions

This section represents the closing of the research project. First, the main findings are presented in the Conclusions. Then, the scientific and technological contributions of this project are delimited. Subsequently, the scientific publications, related to those contributions, are listed. Finally, further work is suggested.

7.1 Conclusions

The design concentration ratio of a V-Trough, which is the aperture area of the cavity over the PV area, is commonly used as an indicator of optical performance. This can be a misleading indicator for non-ideal situations, such as for asymmetrical set-ups or stepped tracking strategies. Through geometrical optics, it was found that several macro-optical phenomena can affect the effective harvesting area of a given V-Trough, such as blocked incident or reflected solar rays or rays which are reflected back out after one or two reflections. These phenomena depend on the V-Trough's geometrical parameters and the solar elevation. For instance, the optical analysis of a given V-Trough set-up in this research project, suggested that 36.2% of the rays that reached the device at the given solar elevation were blocked and, from the rays that did reach a useful surface, 2.2% were being reflected back out after being reflected twice. Therefore, for a more comprehensive assessment of the optical performance of a given V-Trough set-up, these macro-optical phenomena can be incorporated into an average effective concentration indicator; established in this research project as $\overline{C_e}$.

A new analytical model of the beam macro-optical phenomena in photovoltaic V-Troughs was proposed and experimentally validated against laser measurements in a testing platform. The linear response of 308 measurements, in function of the corresponding predictions drawn from the model, was by convention "extremely statistically significant". Both parametric and non-parametric analyzes were performed to test the significance of this regression and the resulting P-values were virtually equal to 0. This means that it is extremely unlikely that randomness alone could have been the causal reason for the observed correspondence between the model's predictions (X) and the experimental measurements (Y). Moreover, the linear model between these two variables was found to be statistically equivalent to an ideal model where $Y = X$. This can be argued from the fact that the difference between the observed linear slope and an ideal slope of 1 was found to have a significance of P-value = 0.90324. In terms of the observed Y-intercept and its difference from an ideal value of 0, the significance was of P-value = 0.96171. Therefore, it is very likely that the discrepancies between the observed linear model and the ideal response were due to randomness.

The residuals obtained from comparing the model's predictions X with the corresponding experimental measurements Y did not show a systematic behavior. This implies that no relevant macro-optical phenomena was ignored in the modeling framework, in terms of beam radiation. In order to assess the accuracy of the model, a 95% prediction interval was calculated with a Monte Carlo Bootstrapping method. The result implies that, if the model is applied to new data, it is expected that 95% of the times the real values would fall within an interval than would, in the worst case, underestimate a given optical entity in 3% of the PV length or overestimate it in a 4.1%. On average, the model's predictions lead to an Incident Concentration C that is 0.56% less than the same entity calculated from the experimental measurements. Also, the model's

predictions lead to an Effective Concentration C_e that is, on average, 0.31% greater than the experimentally calculated value.

The model achieved the established flexibility goals, namely the possibility of independently defining each of the main geometrical V-Trough parameters and to establish them as either fixed or as dynamic. The main geometrical parameters are the lengths and angular positions of the mirrors and the PV surface. This flexibility was tested in the experimental validation, where six V-Trough set-ups were defined from an unbiased random algorithm that assigned values to each of the main geometrical parameters and no systematic modeling errors were evidenced. The allowable ranges for these parameters are $[-\pi,\pi]$ for the inclination of the PV surface (β); $[-\pi/2,\pi/2]$ for the angular disposition of both mirrors (ψL and ψR); and $[0,\infty]$ for the length of each mirror (LL and LR) and the PV surface (LPV). No other analytical model found in the literature allows this level of geometrical flexibility with the level of optical detail achieved in this research project, in terms of the beam macro-optical phenomena involved.

Despite the geometrical simplicity of these devices, if each of the main geometrical parameter is discretized into only ten possible values and only two tracking movements are allowed, it was calculated that there are 10^{15} possible set-ups. Accordingly, the theoretical model was defined to be based on an analytical core partly because of an expected low computational demand that could enable its implementation on design-oriented tools. When the model was implemented in a proposed interactive tool, named VTDesign, the optical performance simulations were essentially in real-time, with no delay perceived between entering new parameters and the corresponding update of results. Hence, it is possible for a V-Trough designer to rapidly iterate and analyze in detail the optical performance consequences of different set-ups. Moreover, when the model was implemented in the proposed genetic algorithm, named GA-WA, the average run-time throughout the performed case study was only 2 minutes and 36 seconds in a conventional personal computer (12GB RAM, 2.5GHz CPU and with Intel CORE i7). Each run of the genetic algorithm involved 100 individuals, 100 generations and 160 solar elevations considered. Accordingly, every run of GA-WA implied, on average, 1.6E6 executions of the analytical model within the evolutionary process. This means that each execution of the analytical model, for a given solar elevation, took only an average of 9.75E-5 seconds. Correspondingly, the proposed model is considered to imply a computational demand which is sufficiently low for its successful practical implementation in design-oriented tools, such as interactive softwares and evolutionary optimization algorithms.

Some of the performance indicators and indices proposed, namely the *Cost of Materials* for a given energy need ($Cost$) and the three multi-objective indices (I_{COE}, MI_{COE} and MDI_{COE}), performed cost estimations based only in the area costs of the main materials involved. As long as the solar tracking is performed manually, or in a passive and low-cost manner, these indicators and indices are expected to reasonably account for the relation between the gain in effective harvesting area and the cost for additional support and mirror material. Nonetheless, since the level of tracking accuracy is not part of the cost considerations yet, a design exploration guided by these indicators and indices could be biased towards choosing perfect tracking, since this strategy achieves better cost-effectiveness and average effective concentration. These indicators and indices can hence provide a better support, in the definition of a given V-Trough's parameters, when the number of tracking steps is well established and the tracking strategy does not imply considerable costs as compared to the cost of materials.

The proposed interactive tool VTDesign was used to approach a constrained and personalized design scenario from three different performance perspectives (Design Goals): the minimization of cost in terms of materials for a given energy need; the maximization of daily energy harvested within constraints in space and the number of solar cells; and the minimization of the space required for the device for a given energy need. The design exploration was performed by interactively iterating the input geometrical parameters and analyzing the real-time performance simulations. The diagrams provided by VTDesign supported an intuitive understanding of the geometrical implications arising from the input parameters. Moreover, the numerical results shown in the VTDesign Dashboard provided the means for an objective comparison of successive set-ups. This enabled an effective and informed decision-making process that guided the design exploration towards three different set-ups; one for every design goal. As compared to the initial intuitive set-ups, the VTDesign solutions correspondingly achieved a reduction of the materials cost in 3.7%, an increase of the daily energy in 19.1% and a reduction of the space required in 28%. Furthermore, as compared to a reference flat and fixed horizontal solar panel, the VTDesign solutions correspondingly managed to achieve

a reduction of the materials cost in 41.8%, an increment of the daily energy in 142.7% and a reduction of the space required in 28%.

Not always the V-Trough set-up with the highest Index of Cost-Effectiveness (I_{COE}) results in the lowest cost in terms of materials. Solar cells are discrete units with discrete areas and, therefore, they can not always be arranged in a solar panel so as to precisely fulfill a given energy demand. This discretization effect was evidenced in the case study for the Design Goal I. The set-up 1_{VTD0} achieved a higher I_{COE} than 1_{VTD} but its cost was 8.3USD greater, corresponding to a 0.47%, because it was forced to generate $12.74Wh$ more than needed. However small, this effect was found to impact the selection decisions among similar set-ups.

The procedures presented in this research project allow to adjust Weibull distributions to a specific range and shape their function with a bias towards a desired mean. This capability is useful for controlling, with high detail and flexibility, semi-random processes. Randomness is critical in genetic algorithms to introduce variability and to favor a wider exploration of the solution space. The new genetic algorithm proposed, GA-WA, was shown to effectively make use of these Weibull procedures to control various heuristic processes that define: the number of individuals who mutate and by how much; the proportion of elites for every generation; the implementation of strategies to overcome stagnation; and the initialization of the first population with a bias around a pre-existing or intuitive value for any gene.

The parameters that control the heuristic processes of the genetic algorithms assessed were discretized into only three levels (0.1, 0.5 and 0.9) for a partial optimization. However, this optimization procedure managed to effectively improve the behavior towards convergence of the three genetic algorithms, namely the proposed GA-WA and the reference algorithms GAUniform and GAGauss. The optimized versions were more organized in their progression throughout the generations, converged to a narrower range and achieved, on average, a higher stagnation ceiling. For instance, the best combination of parameters in GA-WA, as compared to the combination with the worst performance, improved the mean highest fitness achieved per run in an 8.6% and the mean highest fitness achieved per generation in a 23.2%. The performed optimization allowed the three genetic algorithms to reach, on average, solutions with a higher fitness and with a higher reliability and stability in their results. Moreover, although the parameters were optimized with I_{COE} as fitness function, the algorithms performed equally well with the other fitness functions in the case study, namely $\overline{C_e}$, $Cost$, T_{sp}, MI_{COE} and MDI_{COE}.

The combination of the heuristic parameters of the genetic algorithms was found to have a highly significant effect, on the mean fittest I_{COE} achieved per run, in the algorithms GAUniform (P-value$=1.39*10^{-12}$), GAGauss (P-value$=4.15*10^{-13}$) and GA-WA (P-value$< 2.2*10^{-16}$). Furthermore, all heuristic parameters were found to independently have a significant effect, except for the *mean proportion of individuals to mutate* in elites (P-value$=0.077$) and in non-elites (P-value$=0.061$) for GA-WA. For the parameters *proportion of elites* and *probability of mutation in a given gene*, 0.1 was the value associated with the best performance in both GAUniform and GAGauss. Conversely, a value of 0.9 for these parameters was particularly detrimental because, too many elites or too much mutation, minimizes the genes exchange and the evolutionary process thus loses systematicity in its progress. Similarly, a 0.9 *mean proportion of elites* was the common denominator among the worst performing combinations for GA-WA. The optimized parameters for GA-WA resulted in a 0.1 *mean proportion of elites* (μn_e), among which a 0.5 mean proportion will mutate ($\mu pMut_e$) in a 0.5 magnitude factor ($fMut_e$); and a 0.9 *mean proportion of non-elites* defined to suffer mutations ($\mu pMut$) in a 0.1 magnitude factor ($fMut$). In other words, the best performance in GA-WA was obtained from a low proportion of elites with an intermediate occurrence of mutations and with half the magnitude of the average mutation of regular individuals; as well as a high occurrence of mutations in non-elites with a low mutation magnitude. Considering only the partially optimized configurations, GA-WA was found to have a significantly superior performance, on the mean fittest I_{COE} achieved per run, as compared to both reference algorithms GAUniform and GAGauss.

The three design goals in the case study were satisfactorily approached with GA-WA by using different fitness functions. As compared to a reference flat and fixed horizontal solar panel, the materials cost for a given energy need was reduced in 42.2% by using $Cost$ as the fitness function and with the first population distributed around intuitive values. The daily energy, with restrictions in space and the amount of solar cells, was increased in 133.4% by using $\overline{C_e}$ as the fitness function. Lastly, the occupied space needed to fulfill a given energy need was reduced in 99.98% by using T_{sp} as the fitness function and with the first population distributed around intuitive values. The solutions achieved through the interactive software, VTDesign, only

surpassed GA-WA in the energy maximization goal due to the more complex constraints which were not all directly considered by the used fitness functions in GA-WA.

Both VTDesign and GA-WA were found to be effective, efficient and flexible tools in the problem of defining the parameters of a given solar V-Trough in a personalized scenario. The intuition and the more holistic exploration of a trained engineer with VTDesign can be complemented with the broader and less biased heuristic evolutionary optimization of GA-WA. Both tools can be implemented in parallel, to compare different solutions, or in series by distributing the first GA-WA population around the results achieved with VTDesign. On the other hand, the GA-WA results can be then analyzed with VTDesign for a visual understanding of the set-ups and a further interactive exploration.

7.2 Scientific and Technological Contributions

As follows, the contributions to the state-of-the-art of this research project are described:

- A new theoretical model of the macro-optical phenomena of beam radiation in photovoltaic V-Troughs with manual tracking.
- A series of V-Trough performance indicators and indices for the design context: *Average Effective Concentration* ($\overline{C_e}$); *Cost of Materials* for a given energy need (*Cost*); *Horizontal Space* needed to fulfill an energy need (T_{sp}); and three multi-objective indices (I_{COE}, MI_{COE} and MDI_{COE}).
- A new interactive tool, VTDesign, intended to support the definition of a given V-Trough's parameters in a personalized household context. While the tool itself is a technological contribution, the underlying structure of the software and its assessment in a V-Trough case study constitute a theoretical contribution as well.
- A new heuristic tool, GA-WA, for optimizing a given V-Trough's parameters in a personalized household context. While the tool itself is a technological contribution, the new heuristic procedures proposed and their assessment in a V-Trough case study constitute a theoretical contribution as well. Moreover, GA-WA is a general purpose optimization tool that can be further studied for other design/engineering matters of the state-of-the-art.

7.3 Scientific Publications

Several scientific articles were generated and published during the development process of this research project.

Articles in International Journals:

- Andrés Arias-Rosales and Ricardo Mejía-Gutiérrez. Modelling and simulation of direct solar radiation for cost-effectiveness analysis of V-Trough photovoltaic devices. *International Journal on Interactive Design and Manufacturing (IJIDeM)*. Springer. Vol. 10, No. 03. p.p. 257–273, ISSN: 1955-2513, DOI: 10.1007/s12008-016-0333-4, 2016.
- Andrés Arias-Rosales and Ricardo Mejía-Gutiérrez. VTDesign: Implementation of a direct radiation model in an interactive software for designing V-Trough photovoltaic devices. *International Journal of Computer and Electrical Engineering (IJCEE)*. International Academy Publishing (IAP). Vol. 8. No. 05. p.p. 288–293, ISSN: 1793-8163, DOI: 10.17706/IJCEE.2016.8.5.288-293, 2016.

International conferences:

- Andrés Arias-Rosales and Ricardo Mejía-Gutiérrez. Modelling and simulation of direct solar radiation for the design of V-Trough devices with Tracking. *Proceedings of the International Virtual Concept Workshop on Major Trends in Product Design*. Bordeaux, France. ISBN: 978-2-954 8927-3-3, 17-18 March 2016.

- Andrés Arias-Rosales and Ricardo Mejía-Gutiérrez. VTDesign: Implementation of a direct radiation model in an interactive software for designing V-Trough photovoltaic devices. *3rd International Conference on Mechanical, Materials and Manufacturing (ICMMM)*. Savannah, U.S., 26-29 October 2016. (*)
- Andrés Arias-Rosales and Ricardo Mejía-Gutiérrez. Optimization of photovoltaic V-Trough concentrators through genetic algorithms based on the interactions with beam radiation. Accepted for publication and oral presentation in *SPIE Optical Engineering + Applications*, 2017.

(*) The oral presentation related to this conference obtained the **"Best Presentation Award"**, by the scientific conference committee.

7.4 Further Work

The proposed theoretical model, based on solar beam radiation, can be extended to consider the macro-optical phenomena related to diffuse radiation as well. Also, a model of temperature losses from the state-of-the-art can be included in the analytical modeling framework. Moreover, the solar irradiance can be treated as a variable in function of time as opposed to taking it as a constant daily average. For a more realistic guidance in the parameters definition process, these other modeling considerations can be included in the interactive tool VTDesign and in the algorithm of the heuristic optimization tool GA-WA. With this augmented model, there can also be a further experimental validation in a real case study with actual solar radiation. Even though the proposed model can already lead to useful design insights with possible industrial applications, this model is located in a wider research frame which is still under development. More research exploration and further broadening of the simulation scope are recommended in order to extend and empower its applicability in a real-life design exercises. Additionally, the GA-WA heuristic optimization tool demonstrated its effectiveness for V-Trough applications. However, GA-WA is a general purpose tool. Therefore, in further work, its performance can be explored for other design/engineering problems.

Nomenclature

Acronyms

CAD Computer Aided Design.

CI Confidence Interval.

CN Celestial North, relative to the celestial plane where the Earth's orbit is contained.

CNC Computer Numerical Control.

DF Defined Fixed; a given geometrical variable is defined as a fixed value entered by the user for a genetic algorithm.

DL Defined List; a given geometrical variable is defined as a list entered by the user for a genetic algorithm.

EHA Effective Harvesting Area.

GA Genetic Algorithm; plural (GAs).

GA-WA Genetic Algorithm - Weibull Arias; genetic algorithm.

GAGauss Genetic Algorithm Gaussian; genetic algorithm with random values defined from a Gaussian distribution

GAUniform Genetic Algorithm Uniform; genetic algorithm with random values defined from a Uniform distribution.

MC Monte Carlo.

N North, cardinal direction relative to the Earth's rotation axis.

PDF Probability Density Function; plural (PDFs).

PV Photovoltaic.

RD Random Dynamic; a given geometrical variable is defined as a random dynamic value, to be specified by a genetic algorithm, according to a user-defined list of α tracking points.

RF Random Fixed; a given geometrical variable is defined as a random fixed value to be specified by a genetic algorithm.

RRD Random Random Dynamic; a given geometrical variable is defined as a random dynamic value without a user-defined list of α tracking points for a genetic algorithm.

RRDsame Random Random Dynamic same; a given geometrical variable is defined in the same way as in RRD but, if there are several RRD-same variables, they will share the same α tracking points.

SE Standard Error of estimate.

Variables

α Angular solar elevation projected in a transverse plane with respect to the V-Trough geometry.

α_L Angle of longitudinal misalignment of the solar incidence measured from the normal to the PV surface.

α_c Ending point for the solar elevation range.

α_f Starting point for the solar elevation range.

β Inclination of the PV surface relative to the horizon and projected in a transverse plane with respect to the V-Trough geometry.

$\beta_{\alpha s}$ Step variation of α needed for every variation in β.

β_i Initial β inclination.

β_s Step variation of β every tracking movement.

Δb Delta between a given linear Y-intercept and a reference Y-intercept value.

Δm Delta between a given linear slope and a reference slope value.

δ Declination; angle between the incident solar rays and the plane containing the Earth's Equator.

η_{pv} Photovoltaic efficiency.

η_s Electric efficiency of the system.

μi Desired intuitive value for a gene; genetic algorithm heuristic parameter.

μMut Mean mutation magnitude for a gene in non-elites; genetic algorithm heuristic parameter.

μMut_e Mean mutation magnitude for a gene in elites; genetic algorithm heuristic parameter.

μn_e Mean proportion of elites; genetic algorithm heuristic parameter.

$\mu pMut$ Mean proportion of non-elites who will mutate; genetic algorithm heuristic parameter.

$\mu pMut_e$ Mean proportion of elites who will mutate; genetic algorithm heuristic parameter.

μ Mean value of a Weibull distribution.

$\overline{C_e}$ Average Effective Concentration index.

$\overline{CL_{PV}}$ Average Effective Concentration coming only from the left mirror after one reflection.

$\overline{CL_{RPV}}$ Average Effective Concentration coming only from the left mirror after two reflections.

$\overline{CPV_e}$ Average Effective Concentration coming only from the PV surface's direct contributions.

$\overline{CR_{LPV}}$ Average Effective Concentration coming only from the right mirror after two reflections.

$\overline{CR_{PV}}$ Average Effective Concentration coming only from the right mirror after one reflection.

$\overline{I}$ Average solar irradiance $[W/m^2]$.

ϕ Latitude; angular position measured from the plane containing the Earth's Equator.

ψL Left mirror's inclination measured from the normal to the PV surface.

ψR Right mirror's inclination measured from the normal to the PV surface.

ρ Index of reflection of the mirrors [0,1].

θ Angle of solar incidence with respect to a given surface.

A_{pvc} Area $[m^2]$ of a single solar cell.

aL Aperture length of the left mirror's Real Incidence.

aL_0 Aperture length of the left mirror's Geometrical Incidence.

aL_B Aperture length of the incident rays, heading towards the left mirror, that were blocked.

aL_e Length of the left mirror's Effective Aperture considering contributions after one and two reflections.

aL_{PVB} Aperture length of the rays reflected from the left mirror, heading towards the PV surface, that were blocked.

aL_{PV} Aperture length of the rays that manage to reach the PV surface after being reflected once from the left mirror.

aL_{RPV} Aperture length of the rays that manage to reach the PV surface after being reflected first from the left mirror and then from the right one.

aL_{RS} Aperture length of the shadow generated by the back part of the right mirror with respect to the rays reflected from the left mirror.

aL_{sp} linear space to the left of the tracking pivot.

aL_S Aperture length of the shadow generated by the left mirror.

aLL_{sp} linear space projected on the floor from the left mirror.

aLR_{sp} linear space projected on the floor from the right mirror.

aPV Aperture length of the PV surface's Real Incidence.

aPV_0 Aperture length of the PV surface's Geometrical Incidence.

aPV_B Aperture length of the incident rays, heading towards the PV surface, that were blocked.

aPV_e Length of the PV surface's Effective Aperture.

aPV_{sp} linear space projected on the floor from the PV surface.

aPV_S Aperture length of the shadow generated by the PV surface.

aR Aperture length of the right mirror's Real Incidence.

aR_0 Aperture length of the right mirror's Geometrical Incidence.

aR_B Aperture length of the incident rays, heading towards the right mirror, that were blocked.

aR_e Length of the right mirror's Effective Aperture considering contributions after one and two reflections.

aR_{LPV} Aperture length of the rays that manage to reach the PV surface after being reflected first from the right mirror and then from the left one.

aR_{LS} Aperture length of the shadow generated by the back part of the left mirror with respect to the rays reflected from the right mirror.

aR_{PVB} Aperture length of the rays reflected from the right mirror, heading towards the PV surface, that were blocked.

aR_{PV} Aperture length of the rays that manage to reach the PV surface after being reflected once from the right mirror.

aR_{sp} linear space to the right of the tracking pivot.

aR_S Aperture length of the shadow generated by the right mirror.

aT Aperture length of the total Real Incidence.

aT_0 Aperture length of the total Geometrical Incidence.

aT_e Length of the total Effective Aperture.

aT_{sp} Horizontal linear Space needed for the device to fulfill a given energy need.

C Incident Concentration index; ratio of the total Real Incidence over the PV surface's length.

c Weibull scale parameter.

C_e Effective Concentration index; ration between the total beam radiation, that reaches the PV surface, and the PV length.

CL Real Incidence Concentration of the left mirror.

CL_e Effective Concentration after both one and two reflections from the left mirror.

CM_{MPV} Effective Concentration coming from both mirrors after two reflections.

CM_{PV} Effective Concentration coming from both mirrors after one reflection.

CO_m Area cost $\left[\text{USD}/m^2\right]$ of the mirrors.

CO_{pv} Area cost $\left[\text{USD}/m^2\right]$ of the PV absorber.

CO_s Area cost $\left[\text{USD}/m^2\right]$ of the supporting structures.

$Cost$ Cost [USD] of Materials for a given energy need.

CPV_0 Geometrical Incidence Concentration relative only to the PV surface.

CR Real Incidence Concentration of the right mirror.

CR_e Effective Concentration after both one and two reflections from the right mirror.

D_{LR} Diagonal from the upper limit of the left mirror to the lower limit of the right one.

D_{RL} Diagonal from the upper limit of the right mirror to the lower limit of the left one.

$Depth$ PV surface's length measured in a longitudinal plane with respect to the V-Trough geometry.

E_{day} Daily energy need $[Wh]$.

f_{LR} Aperture length, normal to the rays of the first bounce, which starts from the vertex of the right mirror and ends in the projected length of the left mirror.

f_{RL} Aperture length, normal to the rays of the first bounce, which starts from the vertex of the left mirror and ends in the projected length of the right mirror.

$fMut_e$ Elite mutation factor relative to the non-elite mutation magnitude; genetic algorithm heuristic parameter.

$Gstuck$ No. of generations, without improvement, for stagnation; genetic algorithm heuristic parameter.

H_{sun} Hours of exposure to sunlight.

I_{COE} Index of Cost-Effectiveness.

iL Angle between the incident rays and left mirror.

iL_R Angle between the rays reflected from the left mirror and the surface of the right mirror.

iL_{PV} Angle between the rays reflected from the left mirror and the PV surface.

iL_{RPV} Angle between the PV surface and a ray that was first reflected by the left mirror and then by the right mirror.

iPV Angle between the incident rays and PV surface.

iR Angle between the incident rays and right mirror.

iR_L Angle between the rays reflected from the right mirror and the surface of the left mirror.

iR_{LPV} Angle between the PV surface and a ray that was first reflected by the right mirror and then by the left mirror.

iR_{PV} Angle between the rays reflected from the right mirror and the PV surface.

k Weibull shape parameter.

LL Left mirror's length measured in a transverse plane with respect to the V-Trough geometry.

LPV PV surface's length measured in a transverse plane with respect to the V-Trough geometry.

LR Right mirror's length measured in a transverse plane with respect to the V-Trough geometry.

m_{LR} Aperture length of the incoming rays which have access to the reflecting surface of the left mirror and which do not get directly reflected towards the PV surface.

m_{RL} Aperture length of the incoming rays which have access to the reflecting surface of the right mirror and which do not get directly reflected towards the PV surface.

MDI_{COE} Multi-Discrete-Index of Cost-Effectiveness.

MI_{COE} Multi-Index of Cost-Effectiveness.

Min Minimum allowed value for a given gene.

n_e Fixed proportion of elites; genetic algorithm heuristic parameter.

N_{pvc} Minimum number of solar cells required.

nG No. of generations; genetic algorithm heuristic parameter.

nP No. of individuals in the population; genetic algorithm heuristic parameter.

$p\mu$ Mean value of a Weibull distribution in proportion of the length of the range where most values are distributed.

p_{LR} Aperture length, over the left mirror, within which any ray reaching the reflective surface will be reflected towards the right mirror and then the PV surface.

p_L Aperture length, over the left mirror, within which any ray reaching the reflective surface will be reflected towards the PV surface.

p_{RL} Aperture length, over the right mirror, within which any ray reaching the reflective surface will be reflected towards the left mirror and then the PV surface.

p_R Aperture length, over the right mirror, within which any ray reaching the reflective surface will be reflected towards the PV surface.

$pMut$ Probability for any given gene to mutate; genetic algorithm heuristic parameter.

T_{sp} Horizontal Space $[m^2]$ needed for the device to fulfill a given energy need.

Top Maximum allowed value for a given gene.

$W1$ A weight assigned as the relative importance of monetary capital cost.

$W2$ A weight assigned as the relative importance of the space required.

References

Adger, W. N., Huq, S., Brown, K., Conway, D., and Hulme, M. (2003). Adaptation to climate change in the developing world. *Progress in development studies*, 3(3):179–195.

Arabali, A., Ghofrani, M., Etezadi-Amoli, M., Fadali, M. S., and Baghzouz, Y. (2013). Genetic-algorithm-based optimization approach for energy management. *IEEE Transactions on Power Delivery*, 28(1):162–170.

Arias-Rosales, A., Barrera-Velásquez, J., Osorio-Gómez, G., and Mejía-Gutiérrez, R. (2014). Designing a concentrating photovoltaic (cpv) system in adjunct with a silicon photovoltaic panel for a solar competition car. In *SPIE Sensing Technology+ Applications*, pages 91150W–91150W. International Society for Optics and Photonics.

Arias-Rosales, A. and Mejía-Gutiérrez, R. (2016). Modelling and simulation of direct solar radiation for cost-effectiveness analysis of v-trough photovoltaic devices. *International Journal on Interactive Design and Manufacturing (IJIDeM)*, 10(3):257–273.

Arriaga, J., Knight, J., and Russell, P. S. J. (2004). Modeling the propagation of light in photonic crystal fibers. *Physica D: Nonlinear Phenomena*, 189(1):100–106.

Assadi, M. K., Hanaei, H., Mohamed, N. M., Saidur, R., Bakhoda, S., Bashiri, R., and Moayedfar, M. (2016). Enhancing the efficiency of luminescent solar concentrators (lscs). *Applied Physics A*, 9(122):1–12.

Bahaidarah, H. M., Tanweer, B., Gandhidasan, P., and Rehman, S. (2015). A combined optical, thermal and electrical performance study of a v-trough pv system–experimental and analytical investigations. *Energies*, 8(4):2803–2827.

Bannerot, R. B. and Howell, J. R. (1979). Predicted daily and yearly average radiative performance of optimal trapezoidal groove solar energy collectors. *Solar energy*, 22(3):229–234.

Bione, J., Vilela, O., and Fraidenraich, N. (2004). Comparison of the performance of pv water pumping systems driven by fixed, tracking and v-trough generators. *Solar Energy*, 76(6):703–711.

Bojić, M., Marjanović, N., Miletić, I., and Bojić, L. (2015). Comparison of optical performances of sea-shell trough solar concentrators. *Energy and Buildings*, 98:144–150.

Bowden, G., Barker, P., Shestopal, V., and Twidell, J. (1983). The weibull distribution function and wind power statistics. *Wind Engineering*, 7:85–98.

Brest, J., Greiner, S., Boskovic, B., Mernik, M., and Zumer, V. (2006). Self-adapting control parameters in differential evolution: A comparative study on numerical benchmark problems. *IEEE transactions on evolutionary computation*, 10(6):646–657.

Burkhard, D. G., Strobel, G. L., and Burkhard, D. R. (1978). Flat-sided rectilinear trough as a solar concentrator: an analytical study. *Applied Optics*, 17(12):1870–1883.

Calderón-Garcidueñas, L., Kulesza, R. J., Doty, R. L., D'angiulli, A., and Torres-Jardón, R. (2015). Megacities air pollution problems: Mexico city metropolitan area critical issues on the central nervous system pediatric impact. *Environmental research*, 137:157–169.

Caton, P. (2014). Design of rural photovoltaic water pumping systems and the potential of manual array tracking for a west-african village. *Solar Energy*, 103:288–302.

Chen, J., Li, X., Nilson, T., and Strahler, A. (2000). Recent advances in geometrical optical modelling and its applications. *Remote Sensing Reviews*, 18(2-4):227–262.

Chen, Y.-M., Lee, C.-H., and Wu, H.-C. (2005). Calculation of the optimum installation angle for fixed solar-cell panels based on the genetic algorithm and the simulated-annealing method. *IEEE Transactions on Energy Conversion*, 20(2):467–473.

Chiam, H. (1981). Planar concentrators for flat-plate solar collectors. *Solar Energy*, 26(6):503–509.

Chiam, H. (1982). Bi-yearly adjusted v-trough concentrators. *Solar Energy*, 28(5):407–412.

Coit, D. W. and Smith, A. E. (2002). Genetic algorithm to maximize a lower-bound for system time-to-failure with uncertain component weibull parameters. *Computers & Industrial Engineering*, 41(4):423–440.

Collares-Pereira, M. and Rabl, A. (1979). Simple procedure for predicting long term average performance of nonconcentrating and of concentrating solar collectors. *Solar Energy*, 23(3):235–253.

Compagnon, D. R. (1997). Radiance: a simulation tool for daylighting systems. *The Martin Centre for Architectural and Urban Studies University of Cambridge Department of Architecture*.

Cook, J., Nuccitelli, D., Skuce, A., Jacobs, P., Painting, R., Honeycutt, R., Green, S. A., Lewandowsky, S., Richardson, M., and Way, R. G. (2014). Reply to 'quantifying the consensus on anthropogenic global warming in the scientific literature: A re-analysis'. *Energy Policy*, 73:706–708.

Cotter, J. (2005). Raysim 6.0: a free geometrical ray tracing program for silicon solar cells. In *Conference Record of the Thirty-first IEEE Photovoltaic Specialists Conference, 2005.*, pages 1165–1168. FL, USA, IEEE.

D'Amelio, M., Garrone, P., and Piscitello, L. (2016). Can multinational enterprises light up developing countries?: Evidences from the access to electricity in sub-saharan africa. *World Development*, 88:12–32.

De La Tour, A., Glachant, M., and Ménière, Y. (2011). Innovation and international technology transfer: The case of the chinese photovoltaic industry. *Energy Policy*, 39(2):761–770.

Deb, K., Pratap, A., Agarwal, S., and Meyarivan, T. (2002). A fast and elitist multiobjective genetic algorithm: Nsga-ii. *IEEE transactions on evolutionary computation*, 6(2):182–197.

Dinno, A. (2015). Nonparametric pairwise multiple comparisons in independent groups using dunn's test. *Stata Journal*.

Dorigo, M., Birattari, M., and Stützle, T. (2010). *Metaheuristic*, pages 662–662. Springer US, Boston, MA.

Duffie, J. A. and Beckman, W. A. (2013). *Solar engineering of thermal processes*, volume 3. Wiley New York.

Dunlop, S. (2008). *A Dictionary of Weather (2 ed.)*. Oxford University Press.

Eldin, S. S., Abd-Elhady, M., and Kandil, H. (2016). Feasibility of solar tracking systems for pv panels in hot and cold regions. *Renewable Energy*, 85:228–233.

Eremia, M., Liu, C.-C., and Edris, A.-A. (2016). *Advanced Solutions in Power Systems: HVDC, FACTS, and Artificial Intelligence*. John Wiley & Sons.

Famoso, F., Lanzafame, R., Maenza, S., and Scandura, P. F. (2015). Performance comparison between low concentration photovoltaic and fixed angle pv systems. *Energy Procedia*, 81:516–525.

Fischer, X. and Coutellier, D. (2006). *Research in interactive design: Proceedings of virtual concept 2005*. Paris, France, Springer-Verlag.

Fischer, X. and Nadeau, J.-P. (2011). Interactive design: Then and now. In *Research in Interactive Design Vol. 3*, pages 1–5. Paris, France, Springer-Verlag.

Foss, A. R. (2015). Breaking the cycle: Changing alberta in the present to save the future. *Earth Common Journal*, 5(1):23–33.

Fraidenraich, N. (1992). Analytic solutions for the optical properties of v-trough concentrators. *Applied optics*, 31(1):131–139.

Fraidenraich, N. (1998). Design procedure of v-trough cavities for photovoltaic systems. *Progress in photovoltaics: Research and Applications*, 6(1):43–54.

Fraunhofer Institute for Solar Energy Systems, ISE (2016). PHOTOVOLTAICS REPORT. Technical report, Fraunhofer ISE.

Freeman, J., Whitmore, J., Kaffine, L., Blair, N., and Dobos, A. P. (2013). System advisor model: Flat plate photovoltaic performance modeling validation report. Technical report, National Renewable Energy Laboratory (NREL), Golden, CO.

French, M. J. (2002). *Insight, design principles and systematic invention*, pages 19–34. Springer London, London.

Garg, H. and Hrishikesan, D. (1988). Enhancement of solar energy on flat-plate collector by plane booster mirrors. *Solar Energy*, 40(4):295–307.

Gotelli, N. and Ellison, A. (2013). *A Primer of Ecological Statistics*. Macmillan Education.

Grynberg, G., Aspect, A., and Fabre, C. (2010). *Introduction to quantum optics: from the semi-classical approach to quantized light*. Cambridge university press.

Gupta, B. P. and Anderson, J. V. (1991). Solar detoxification of hazardous waste-an overview of the us department of energy program. *Solar energy materials*, 24(1):40–61.

Ha, S. M., Choi, D., Han, M., and Lee, J. S. (2017). Optical design of a static solar concentrator using fresnel lenses. *Journal of Mechanical Science and Technology*, 2(31):949–958.

Hamming, R. (2012). *Numerical methods for scientists and engineers*. Courier Corporation.

He, G. and Victor, D. G. (2017). Experiences and lessons from china's success in providing electricity for all. *Resources, Conservation and Recycling*, 122:335–338.

Herington, M., van de Fliert, E., Smart, S., Greig, C., and Lant, P. (2017). Rural energy planning remains out-of-step with contemporary paradigms of energy access and development. *Renewable and Sustainable Energy Reviews*, 67:1412–1419.

Hermawanto, D. (2013). Genetic algorithm for solving simple mathematical equality problem. *arXiv preprint arXiv:1308.4675*.

Hermenean, I., Visa, I., and Diaconescu, D. (2009). On the geometric modelling of a concentrating pv-mirror system. *Bulletin of the Transilvania University of Braşov*, 2:51.

Hilbert, R., Janiga, G., Baron, R., and Thévenin, D. (2006). Multi-objective shape optimization of a heat exchanger using parallel genetic algorithms. *International Journal of Heat and Mass Transfer*, 49(15):2567–2577.

Hollands, K. (1971). A concentrator for thin-film solar cells. *Solar Energy*, 13(2):149–163.

Holzbecher, E. (2012). *Fundamentals of Modeling, Principles and MATLABÂ®*, pages 35–56. Springer Berlin Heidelberg, Berlin, Heidelberg.

Horvath, I. (2008). Differences between'research in design context'and'design inclusive research'in the domain of industrial design engineering. *Journal of Design Research*, 7(1):61–83.

Imre, H. (2007). Comparison of three methodological approaches of design research. *Guidelines for a Decision Support Method Adapted to NPD Processes*.

Jaaz, A. H., Hasan, H. A., Sopian, K., Ruslan, M. H. B. H., and Zaidi, S. H. (2017). Design and development of compound parabolic concentrating for photovoltaic solar collector. *Renewable and Sustainable Energy Reviews*, 76:1108–1121.

Jiang, B., Ravindran, B., and Cho, H. (2013). Probability-based prediction and sleep scheduling for energy-efficient target tracking in sensor networks. *IEEE Transactions on Mobile Computing*, 12(4):735–747.

Johnson, T., Mol, A. P., Zhang, L., and Yang, S. (2017). Living under the dome: Individual strategies against air pollution in beijing. *Habitat International*, 59:110–117.

Karathanassis, I., Papanicolaou, E., Belessiotis, V., and Bergeles, G. (2017). Design and experimental evaluation of a parabolic-trough concentrating photovoltaic/thermal (cpvt) system with high-efficiency cooling. *Renewable Energy*, 101:467–483.

Kelly, N. A. and Gibson, T. L. (2009). Improved photovoltaic energy output for cloudy conditions with a solar tracking system. *Solar Energy*, 83(11):2092–2102.

Khlaichom, P. and Sonthipermpoon, K. (2006). Optimization of solar tracking system based on genetic algorithms.

Kostić, L. T., Pavlović, T., and Pavlović, Z. (2010). Optimal design of orientation of pv/t collector with reflectors. *Applied Energy*, 87(10):3023–3029.

Kowalczewski, P. and Andreani, L. C. (2015). Towards the efficiency limits of silicon solar cells: How thin is too thin? *Solar Energy Materials and Solar Cells*, 143:260–268.

Kumar, B. S. and Sudhakar, K. (2015). Performance evaluation of 10 mw grid connected solar photovoltaic power plant in india. *Energy Reports*, 1:184–192.

Kummu, M. and Varis, O. (2011). The world by latitudes: a global analysis of human population, development level and environment across the north–south axis over the past half century. *Applied geography*, 31(2):495–507.

Le Roux, W. (2016). Optimum tilt and azimuth angles for fixed solar collectors in south africa using measured data. *Renewable Energy*, 96:603–612.

Lee, C.-Y. and Yao, X. (2004). Evolutionary programming using mutations based on the lévy probability distribution. *IEEE Transactions on Evolutionary Computation*, 8(1):1–13.

León, N., Aguayo, H., García, H., and Anaya, A. (2011). Computer aided optimization/innovation of passive tracking solar concentration fresnel lens. *Building Innovation Pipelines through Computer-Aided Innovation*, pages 57–70.

Li, D., editor (2015a). *Analytical Modeling*, pages 64–64. Springer New York, New York, NY.

Li, D., editor (2015b). *Behavioral Model*, pages 94–94. Springer New York, New York, NY.

Lins, I. D., Droguett, E. L., das Chagas Moura, M., Zio, E., and Jacinto, C. M. (2015). Computing confidence and prediction intervals of industrial equipment degradation by bootstrapped support vector regression. *Reliability Engineering & System Safety*, 137:120–128.

Lo, C. K., Lim, Y. S., and Rahman, F. A. (2015). New integrated simulation tool for the optimum design of bifacial solar panel with reflectors on a specific site. *Renewable Energy*, 81:293–307.

López, D. (2015). Análisis de los aspectos tecnológicos de la fabricación de celdas fotovoltaicas de silicio cristalino en la perspectiva de su producción en uruguay.

Lubitz, W. D. (2011). Effect of manual tilt adjustments on incident irradiance on fixed and tracking solar panels. *Applied energy*, 88(5):1710–1719.

Lueking, A. D. and Cole, M. W. (2017). Energy and mass balances related to climate change and remediation. *Science of The Total Environment*.

Maatallah, T., El Alimi, S., and Nassrallah, S. B. (2011). Performance modeling and investigation of fixed, single and dual-axis tracking photovoltaic panel in monastir city, tunisia. *Renewable and Sustainable Energy Reviews*, 15(8):4053–4066.

Magalhães-Mendes, J. (2013). A comparative study of crossover operators for genetic algorithms to solve the job shop scheduling problem. *WSEAS transactions on computers*, 12(4):164–173.

Maiti, S., Sarmah, N., Bapat, P., and Mallick, T. K. (2012). Optical analysis of a photovoltaic v-trough system installed in western india. *Applied optics*, 51(36):8606–8614.

Mannan, K. and Bannerot, R. (1978). Optimal geometries for one-and two-faced symmetric side-wall booster mirrors. *Solar Energy*, 21(5):385–391.

Martin, A. P., Naylor, G. J., and Palumbi, S. R. (1992). Rates of mitochondrial dna evolution in sharks are slow compared with mammals. *Nature*, 357(6374):153.

McDaniels, D., Lowndes, D., Mathew, H., Reynolds, J., and Gray, R. (1975). Enhanced solar energy collection using reflector-solar thermal collector combinations. *Solar energy*, 17(5):277–283.

McNeal, K. S., Miller, H. R., and Herbert, B. E. (2008). The effect of using inquiry and multiple representations on introductory geology students' conceptual model development of coastal eutrophication. *Journal of Geoscience Education*, 56(3):201–211.

Miles, R., Hynes, K., and Forbes, I. (2005). Photovoltaic solar cells: An overview of state-of-the-art cell development and environmental issues. *Progress in Crystal Growth and Characterization of Materials*, 51(1):1–42.

Ministerio de Ambiente, Vivienda y Desarrollo Territorial, Ministerio de Minas y Energía (2005). Atlas de Radiación Solar de Colombia. Technical report, Ministerio de Ambiente, Vivienda y Desarrollo Territorial, Ministerio de Minas y Energía.

MIT (2015). *The Future of Solar Energy-AN INTERDISCIPLINARY MIT STUDY*. MIT, Cambridge, MA. USA.

Mousazadeh, H., Keyhani, A., Javadi, A., Mobli, H., Abrinia, K., and Sharifi, A. (2009). A review of principle and sun-tracking methods for maximizing solar systems output. *Renewable and sustainable energy reviews*, 13(8):1800–1818.

Neth, H. and Gigerenzer, G. (2015). Heuristics: Tools for an uncertain world. *Emerging trends in the social and behavioral sciences: An interdisciplinary, searchable, and linkable resource*.

O'Kane, S. E., Sarma, J., and Allsopp, D. W. (2014). A quasi-analytic modal expansion technique for modeling light emission from nanorod leds. *Quantum Electronics, IEEE Journal of*, 50(9):774–781.

Otte, P. P. (2013). Solar cookers in developing countries–what is their key to success? *Energy Policy*, 63:375–381.

Oxford University (2017). *Oxford English Dictionary*. Oxford University Press.

Panos, E., Densing, M., and Volkart, K. (2016). Access to electricity in the world energy council's global energy scenarios: An outlook for developing regions until 2030. *Energy Strategy Reviews*, 9:28–49.

Pearl, J. (1984). *Heuristics: Intelligent search strategies for computer problem solving*. Addison-Wesley Pub. Co., Inc.,Reading, MA.

Pedrotti, L. S. (2012). *Module 1.3: Basic geometrical optics*. USA, SPIE Press.

Pei, G., Li, G., Su, Y., Ji, J., Riffat, S., and Zheng, H. (2012). Preliminary ray tracing and experimental study on the effect of mirror coating on the optical efficiency of a solid dielectric compound parabolic concentrator. *Energies*, 5(9):3627–3639.

Penttilä, A. and Lumme, K. (2009). The effect of the properties of porous media on light scattering. *Journal of Quantitative Spectroscopy and Radiative Transfer*, 110(18):1993–2001.

Platt, U., Pfeilsticker, K., and Vollmer, M. (2007). *Radiation and Optics in the Atmosphere*, pages 1165–1203. Springer New York, New York, NY.

Pucar, M. and Despic, A. (2002). The enhancement of energy gain of solar collectors and photovoltaic panels by the reflection of solar beams. *Energy*, 27(3):205–223.

Puzzolo, E., Pope, D., Stanistreet, D., Rehfuess, E. A., and Bruce, N. G. (2016). Clean fuels for resource-poor settings: A systematic review of barriers and enablers to adoption and sustained use. *Environmental research*, 146:218–234.

Qureshi, T. M., Ullah, K., and Arentsen, M. J. (2017). Factors responsible for solar pv adoption at household level: A case of lahore, pakistan. *Renewable and Sustainable Energy Reviews*, 78:754–763.

Rahimi, M., Banybayat, M., Tagheie, Y., and Valeh-e Sheyda, P. (2015). An insight on advantage of hybrid sun–wind-tracking over sun-tracking pv system. *Energy Conversion and Management*, 105:294–302.

Randall, M. (1995). The future and applications of genetic algorithms. In *Proceedings of the Electronic Directions to the Year 2000 Conference*, pages 471–475. IEEE Computer Society Press.

Reis, F., Brito, M., Corregidor, V., Wemans, J., and Sorasio, G. (2010). Modeling the performance of low concentration photovoltaic systems. *Solar Energy Materials and Solar Cells*, 94(7):1222–1226.

Reis, H. T. and Judd, C. M. (2000). *Handbook of research methods in social and personality psychology*. Cambridge University Press.

Roupec, J. (2011). Advanced genetic algorithms for engineering design problems. *Engineering Mechanics*, 17(5-6):407–417.

Salman, K. A. (2017). Effect of surface texturing processes on the performance of crystalline silicon solar cell. *Solar Energy*, 147:228–231.

Sampaio, P. G. V. and González, M. O. A. (2017). Photovoltaic solar energy: Conceptual framework. *Renewable and Sustainable Energy Reviews*, 74:590–601.

Sangani, C. and Solanki, C. (2007). Experimental evaluation of v-trough (2 suns) pv concentrator system using commercial pv modules. *Solar energy materials and solar cells*, 91(6):453–459.

Savio, G., Concheri, G., and Meneghello, R. (2013). Progressive lens design by discrete shape modelling techniques. *International Journal on Interactive Design and Manufacturing (IJIDeM)*, 7(3):135–146.

Seitel, S. C. (1975). Collector performance enhancement with flat reflectors. *Solar Energy*, 17(5):291–295.

Selçuk, M. K. (1979). Analysis, development and testing of a fixed tilt solar collector employing reversible vee-trough reflectors and vacuum tube receivers. *Solar Energy*, 22(5):413–426.

Shaviv, E. (1999). Design tools for bio-climatic and passive solar buildings. *Solar energy*, 67(4):189–204.

Sheng, Y., Shi, Y., Wang, L., and Narasimhan, S. G. (2013). A practical analytic model for the radiosity of translucent scenes. In *Proceedings of the ACM SIGGRAPH Symposium on Interactive 3D Graphics and Games*, pages 63–70. New York, USA, The Association for Computing Machinery, Inc.

Shiffman, D., Fry, S., and Marsh, Z. (2012). *The nature of code*. D. Shiffman.

Shyu, C.-W. (2014). Ensuring access to electricity and minimum basic electricity needs as a goal for the post-mdg development agenda after 2015. *Energy for Sustainable Development*, 19:29–38.

Sindhu, S., Nehra, V., and Luthra, S. (2016). Identification and analysis of barriers in implementation of solar energy in indian rural sector using integrated ism and fuzzy micmac approach. *Renewable and Sustainable Energy Reviews*, 62:70–88.

Su, Y., Pei, G., Riffat, S. B., and Huang, H. (2012). Radiance/pmap simulation of a novel lens-walled compound parabolic concentrator (lens-walled cpc). *Energy Procedia*, 14:572–577.

Sun, Y., Wang, Y., Zhu, L., Huang, Q., and Xiang, H. (2016). Simulation study of a linear concentrating photovoltaic receiver with direct liquid-immersed solar cells. *Solar Energy*, 124:1–14.

Taha, I. S. and Eldighidy, S. M. (1980). Effect of off-south orientation on optimum conditions for maximum solar energy absorbed by flat plate collector augmented by plane reflector. *Solar Energy*, 25(4):373–379.

Tang, R. and Liu, X. (2010). Installation design of solar panels with seasonal adjustment of tilt-angles. In *Power and Energy Engineering Conference (APPEEC), 2010 Asia-Pacific*, pages 1–4. IEEE.

Tang, R. and Liu, X. (2011). Optical performance and design optimization of v-trough concentrators for photovoltaic applications. *Solar Energy*, 85(9):2154–2166.

Taylor, A. E. (2000). Pasadena, USA, Rensselaer Polytechnic Institute.

Tina, G. and Scandura, P. (2012). Case study of a grid connected with a battery photovoltaic system: V-trough concentration vs. single-axis tracking. *Energy Conversion and Management*, 64:569–578.

Turner, L. (2001). Making the most of sunshine–a handbook of solar energy for the common man.

Velzel, C. (2014). *Geometrical Optics*, pages 1–24. Springer Netherlands, Dordrecht.

Vergnano, A., Berselli, G., and Pellicciari, M. (2015). Parametric virtual concepts in the early design of mechanical systems: a case study application. *International Journal on Interactive Design and Manufacturing (IJIDeM)*, in press:1–10.

Wang, C., Winston, R., Zhang, W., Pelka, D., and Carter, S. (2011). Size-and structure-dependent efficiency enhancement for luminescent solar concentrators. *Journal of Photonics for Energy*, 1(1):015502–015502.

Wang, M., Gu, X., Ma, P., Zhang, W., Yu, D., Chang, P., Chen, X., and Li, D. (2017). Microstructured superhydrophobic anti-reflection films for performance improvement of photovoltaic devices. *Materials Research Bulletin*, 91:208–213.

Wong, L. and Chow, W. (2001). Solar radiation model. *Applied Energy*, 69(3):191–224.

Yew, T.-K., Chong, K.-K., and Lim, B.-H. (2015). Performance study of crossed compound parabolic concentrator as secondary optics in non-imaging dish concentrator for the application of dense-array concentrator photovoltaic system. *Solar Energy*, 120:296–309.

Yu, X., Su, Y., Zheng, H., and Riffat, S. (2014). A study on use of miniature dielectric compound parabolic concentrator (dcpc) for daylighting control application. *Building and Environment*, 74:75–85.

Zhao, X., Gao, X.-S., and Hu, Z.-C. (2007). Evolutionary programming based on non-uniform mutation. *Applied Mathematics and Computation*, 192(1):1–11.